AD NUMBER

AD805884

LIMITATION CHANGES

TO:

Approved for public release; distribution is unlimited.

FROM:

**Distribution authorized to U.S. Gov't. agencies and their contractors;
Administrative/Operational Use; JAN 1967. Other requests shall be referred to Air Force Rocket Propulsion Lab., Edwards AFB, CA.**

AUTHORITY

AFRPL ltr 20 Dec 1971

AFRPL - TR-66-331
VOLUME II

COPY NO. 33

FINAL REPORT

156 INCH FIBERGLASS CASE LITVC MOTOR PROGRAM (U)

THIOKOL CHEMICAL CORPORATION
WASATCH DIVISION

TECHNICAL REPORT NO. AFRPL-TR-66-331

VOLUME II
NOZZLE DESIGN ANALYSIS

JANUARY 1967

PREPARED FOR

HEADQUARTERS, SPACE SYSTEMS DIVISION
AIR FORCE SYSTEMS COMMAND
UNITED STATES AIR FORCE
LOS ANGELES, CALIFORNIA 90045

5

DISCLAIMER NOTICE

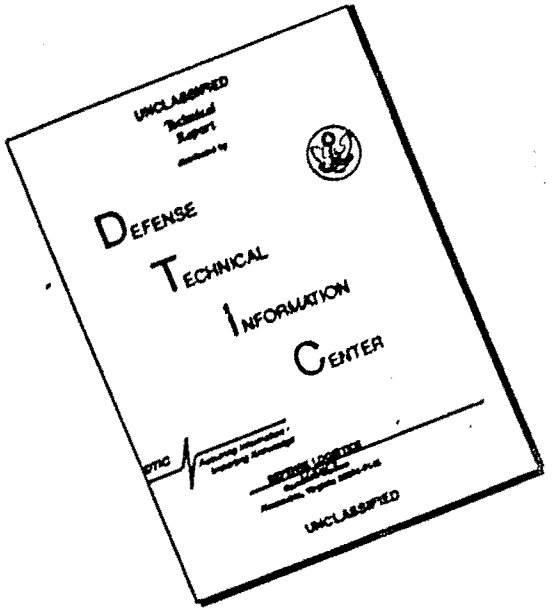

THIS DOCUMENT IS BEST QUALITY AVAILABLE. THE COPY FURNISHED TO DTIC CONTAINED A SIGNIFICANT NUMBER OF PAGES WHICH DO NOT REPRODUCE LEGIBLY.

AFRPL-TR-66-331
Volume II

Copy No.

FINAL REPORT

156 INCH FIBERGLASS CASE LITVC MOTOR PROGRAM (U)

THIOKOL CHEMICAL CORPORATION
WASATCH DIVISION

TECHNICAL REPORT NO. AFRPL-TR-66-331

VOLUME II

NOZZLE DESIGN ANALYSIS

January 1967

Approved by

W. G. Ramroth

W. G. Ramroth, Manager
Large Space Booster
Project Engineering

Approved by

C. G. Kennedy

C. G. Kennedy, Manager
Space Booster Development

Publications No. 167-11000

FOREWORD

This Final Technical Engineering Report covers the work performed under Contract AF 04(695)-773, "156-7 Fiberglass Case Liquid Injection Thrust Vector Control Motor Program". The program motor, designated by the Air Force as the 156-7 rocket motor, is identified for inhouse processing as the TU-393 rocket motor.

This program was conducted under the overall direction of Col H. W. Robbins of SSD, with technical direction by the Air Force Rocket Propulsion Laboratory (AFRPL). Mr. Carver G. Kennedy, Manager Space Booster Development, was the Wasatch Division Program Manager and Mr. W. G. Ramroth, Manager Large Space Booster Project Engineering was the Project Engineer.

This technical report has been reviewed and is approved.

Mr. R. Felix
Senior Project Engineer (RPMMS)
AFRPL, Edwards, California

ABSTRACT

The 156 in. diameter case LITVC motor program was conducted by the Wasatch Division, Thiokol Chemical Corporation for the Air Force Space Systems Division with technical direction by the Air Force Rocket Propulsion Laboratory. The two major objectives were (1) the design and fabrication of a flightweight 156 in. diameter monolithic solid propellant motor utilizing a fiberglass reinforced plastic monolithic case, a 34 to 1 expansion ratio submerged fixed nozzle, and a N_2O_4 LITVC system; and (2) the demonstration static test of the motor in a simulated altitude environment to provide meaningful LITVC data in a high expansion ratio nozzle. Both objectives were successfully attained. The program was culminated on 13 May 1966 with a static test of the motor utilizing a 10 ft diameter by 82 ft long diffuser for altitude simulation. The motor had a mass fraction in excess of 0.90 and operated for 110 sec at an average thrust level of approximately 325,000 lb. The static test was successful and all motor components were intact and in good condition at the completion of the firing. Two abnormalities occurred during the firing. At approximately 0 sec, a burnthrough occurred in the diffuser tube approximately four feet aft of the nozzle exit plane, apparently due to high localized erosion of the ablative insulation on the inside diameter. The diffuser continued to operate throughout the test although at a lower simulated altitude. A malfunction of the pressure regulating subsystem portion of the LITVC system caused a degradation of injectant pressure during the firing and subsequent degradation of the LITVC performance. Post-test inspection of the motor and components revealed that internal insulation, nozzle design, and case design were satisfactory and the motor had functioned as expected. The static test demonstrated attainment of all program objectives. After post-test analysis of the fired motor and components, the fired case was hydroburst tested to obtain additional data on fiberglass case design. The case burst at 963 psig, very near the design ultimate pressure of 970 psig. This hydroburst, performed under a supplemental agreement to the contract, demonstrated the validity of the design and fabrication techniques used for this case.

REPORT OUTLINE

VOLUME I MOTOR DESIGN AND FABRICATION

Book 1

I Program Summary and Design Criteria
II Insulation and Liner
III Case Design and Fabrication
IV Grain Design and Fabrication
V Igniter Design, Fabrication and Support Testing
VI Nozzle Design and Fabrication

Book 2

VII LITVC System Design, Fabrication, and Support Testing
VIII Diffuser Design and Fabrication
IX Motor Assembly
X Tooling Design and Fabrication
XI System Support

VOLUME II NOZZLE DESIGN ANALYSIS

I Introduction
II Nozzle Design and Fabrication
III Loads and Analysis Summary
IV Design Analysis
V Weight Analysis
VI List of References

VOLUME III STATIC TEST REPORT

Book 1

I Introduction
II Test Objectives
III Test Results and Summary
IV Conclusions
V Motor Case
VI Insulation and Liner
VII Ballistics

Book 2

VIII Nozzle
IX LITVC System
X Ignition System
XI Diffuser
XII Quench System
XIII Instrumentation
XIV Chronological Assembly in Test Area
XV Conclusions and Recommendations

VOLUME IV APPENDICES

Appendix I Test Plan for Verification of Liner and Insulation Bonds for TU-393 Motor
Appendix II Test Plan for TU-393 Rocket Motor Case Hydrotest
Appendix III Test Plan for TU-393 Rocket Motor Case No. 2 Hydrotest
Appendix IV Stress Analysis of Thiokol TU-393 Motor
Appendix V Stress Analysis of the 156-7 (TU-393.01) Propellant Grain
Appendix VI LITVC Integrated Systems Test Report
Appendix VII Hydroburst Test Report
Appendix VIII Documentation

TABLE OF CONTENTS

TABLE OF CONTENTS (Cont)

LIST OF ILLUSTRATIONS

LIST OF ILLUSTRATIONS (Cont)

LIST OF ILLUSTRATIONS (Cont)

LIST OF ILLUSTRATIONS (Cont)

LIST OF ILLUSTRATIONS (Cont)

SECTION I

INTRODUCTION

Detailed design analyses were conducted on the 156-7 nozzle for the 156 Inch Demonstration Motor. The nozzle presented in this report complies with the requirements of Exhibit "A" to Contract AF 04(695)-773 and will provide a reliable performance.

The detailed analyses that were conducted include an aerodynamic analysis, a thermal analysis, and a structural analysis.

This section presents the results of these analyses for the design of the 156-7 nozzle.

Maximum use of recent developments in analytical techniques and test results from recent firings (such as Thiokol's TU-402, TU-412, TU-454, TU-455, and SURVEYOR and UTC's 1205-3 Motor) was made in the design of this nozzle. Analyses indicate that design objectives were met and that the 156-7 nozzle design should perform successfully.

SECTION II

NOZZLE DESIGN AND FABRICATION

The nozzle concept selected for the 156-7 156 in. rocket motor is a semisubmerged, fixed, contoured, ablative plastic nozzle for an upper stage application and utilizes liquid injection of nitrogen tetroxide for thrust vector control. The nozzle has been analyzed for both flight and static test conditions; these analyses are presented later in this section.

Nozzle liner and insulation thickness was based on heat transfer and erosion analyses and a thorough evaluation of test and manufacturing data. The structural member thicknesses were determined from a comprehensive structural analysis. In all cases, compatibility, ease of fabrication, cost, availability, and the properties and past performance of each material were carefully considered before making a material selection. The materials chosen for this nozzle, (graphite cloth phenolic, carbon cloth phenolic, silica cloth phenolic, and glass cloth phenolic) are all in common use in the industry and have proven reliable as used in the appropriate design application.

Other nozzle designs considered especially pertinent to the 156-7 nozzle design were the submerged structures of the Wing VI Stage II MINUTEMAN and SURVEYOR, the submerged noses of the TU-454 and TU-455 motors, and the exit cone structure of the TITAN III 120 in. motor. Available material data obtained by all contractors (primarily Thiokol and Lockheed) in the 623A program were carefully analyzed. Properties of the various materials are presented in Figures 1 thru 3.

Material	Graphite Cloth Tape Phenolic	Carbon Cloth Tape Phenolic	Silica Cloth Tape Phenolic	181 Glass Cloth Tape Phenolic E-Glass	341 and 143 Glass Broad Cloth Phenolic E-Glass	143 Glass Cloth Epoxy Broad Cloth E-Glass	181 Glass Cloth Epoxy Tape Wrap E-Glass	20 End S-HTS Glass Filament - Epoxy
Ultimate Flexural (psi)	15,000	25,000	25,000	45,000	75,000	110,000	65,000	75,000
Flexural Modulus (psi x 10^6)	1.2	1.8	2.6	2.5	4.5	5.0	3.2	8.10
Ultimate Tensile (psi)	12,000	12,000	12,000	38,000	75,000	85,000	45,000	75,000
Tensile Modulus (psi x 10^6)	1.75	2.0	2.3	2.62	5.39	4.58	3.30	8.10
Compressive Strength (psi)	15,000	25,800	25,800	35,000	45,000	60,000	45,000	75,000
Compression Modulus (psi x 10^6)	2.00	2.00	2.50	2.94	4.91	5.12	3.29	8.10
Specific Gravity	1.50	1.54	1.74	1.94	1.94	1.94	1.94	1.94
Barcol Hardness	37	72	73	NR	74	78	NR	NR
Specific Heat	0.26	0.25	0.24	0.22	0.20	NR	NR	NR
Thermal Conductivity (Btu/in./sq ft/hr/°F)	6.0	3.17	2.1	1.37	1.92	NR	NR	NR
Tape Breaking Strength (lb)	45 (min)	50 (min)	50	NR	NR	NR	NR	NR
Organic Resin Solids (percent)	34 ± 3	34 ± 3	34 ± 3	34 ± 3	NR	36 max	36 max	36 max
Volatile Range (percent)	3 - 8 ± 1	3 - 8 ± 1	2.2 max	NR	3.5	2.0 max	2.0 max	2.0 max
Percent Flow (percent)	5 - 15	5 - 15	5 - 15	NR	NR	NR	NR	NR
Component Use	Inlet Throat	Exit Cone	Exit Cone Structural Insulation	End Ring Substructure	Submerged Structural Shell	Face Sheets	Fwd Ring Sandwich	End Ring Sandwich Face Sheets

NOTE: NR - Not reported

Figure 1. Physical Properties of Plastic Laminates at Room Temperature (Warp Direction, 0°)

	18 Percent Nickel Steel	5052-Sheet Aluminum
Tension, ultimate (psi)	210,000	31,000
Tension, yield (psi)	200,000	21,000
Compression, ultimate (psi)	210,000	31,000
Compression, yield (psi)	200,000	20,000
Shear, ultimate (psi)	120,000	19,000
Modulus of Elasticity (psi)	27×10^6	10.1×10^6
Density (lb/cu in.)	0.293	0.097
Thermal Conductivity, (BTU/ft-hr-°F)	--	110.0
Specific Heat	--	0.23
Component Use	Flange Injector Ring	Sandwich Core

Figure 2. Metal Material Properties at Room Temperature

Aluminum Honeycomb - 5052 Aluminum

1/4 in. Cell - 5052 Aluminum - 0.0025 in. Thick

Density - 5.2 lb/cu ft

Compression

Stress - 480 psi

E_c (modulus) - 116,000 psi

Crush Strength - 326 psi

Shear

	L Direction	W Direction
Strength (psi)	360	210
Modulus, G_c (psi)	61,000	30,500

Bolt-EWB 26-12 - Nozzle-Case Attachment

Tensile Ultimate (psi)	220,000
Shear Ultimate (psi)	128,000
Modulus of Elasticity (psi)	29×10^6
Poisson's Ratio	0.30

Figure 3. Properties of Aluminum Honeycomb and Attach Bolts

1. DESIGN

The 156-7 nozzle incorporates a fiberglass-steel-aluminum sandwich structural shell from the inlet to the exit plane with reinforced plastic insulation liners. The nozzle divergent section is contoured to provide a higher performance than is obtainable with a cone of equal length (133.3 in.) and expansion ratio (34:1). The nozzle is submerged 48.8 percent of its nose to exit length. The depth of submergence was based on the case pole piece opening (67.87 in. diameter) and the location of the injector ports (ϵ = 13.1:1).

Figure 4 shows the nozzle design with the selected insulation and structural materials. The weight summary is presented in Section V.

a. Submerged Assembly--The submerged assembly consists of a structural member and the necessary erosive and insulative barriers as shown in Figures 5 and 6. The submerged structural cone is fabricated from glass cloth phenolic selected because of its compatibility with reinforced plastic insulation, ease of fabrication, adaptability to design improvement, low cost, availability, and successful use in the SURVEYOR nozzle.

The SURVEYOR retro-rocket uses a nozzle submerged to half its length with a similar structural shell. This nozzle, with a throat diameter of 3.5 in. and an expansion ratio of 53:1 was successfully static tested 25 times, 13 under simulated vacuum conditions at AEDC.

The structural cone for the 156-7 nozzle is subjected to an axial compressive load with internal and external pressure distribution. It was analyzed using

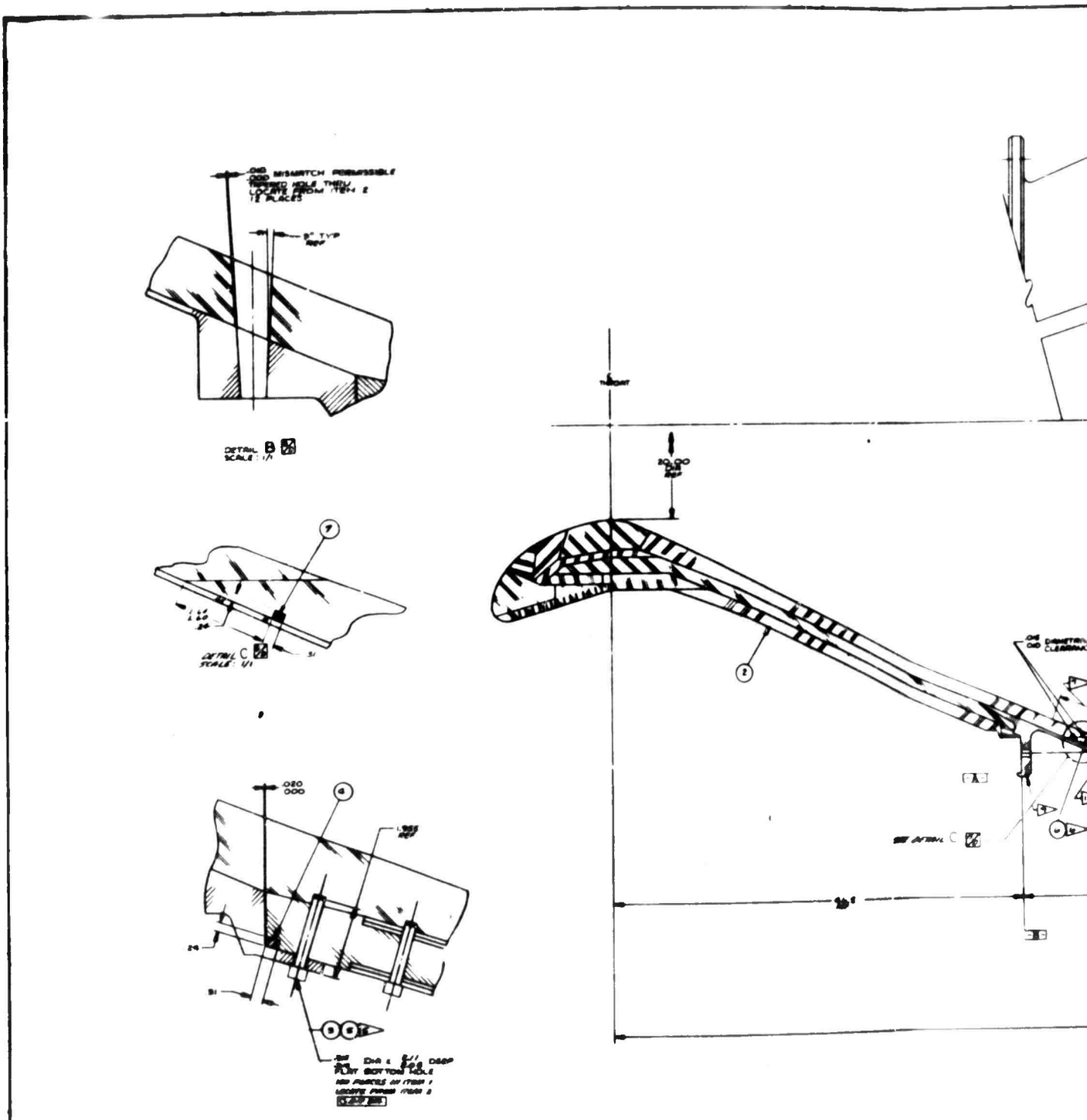

A

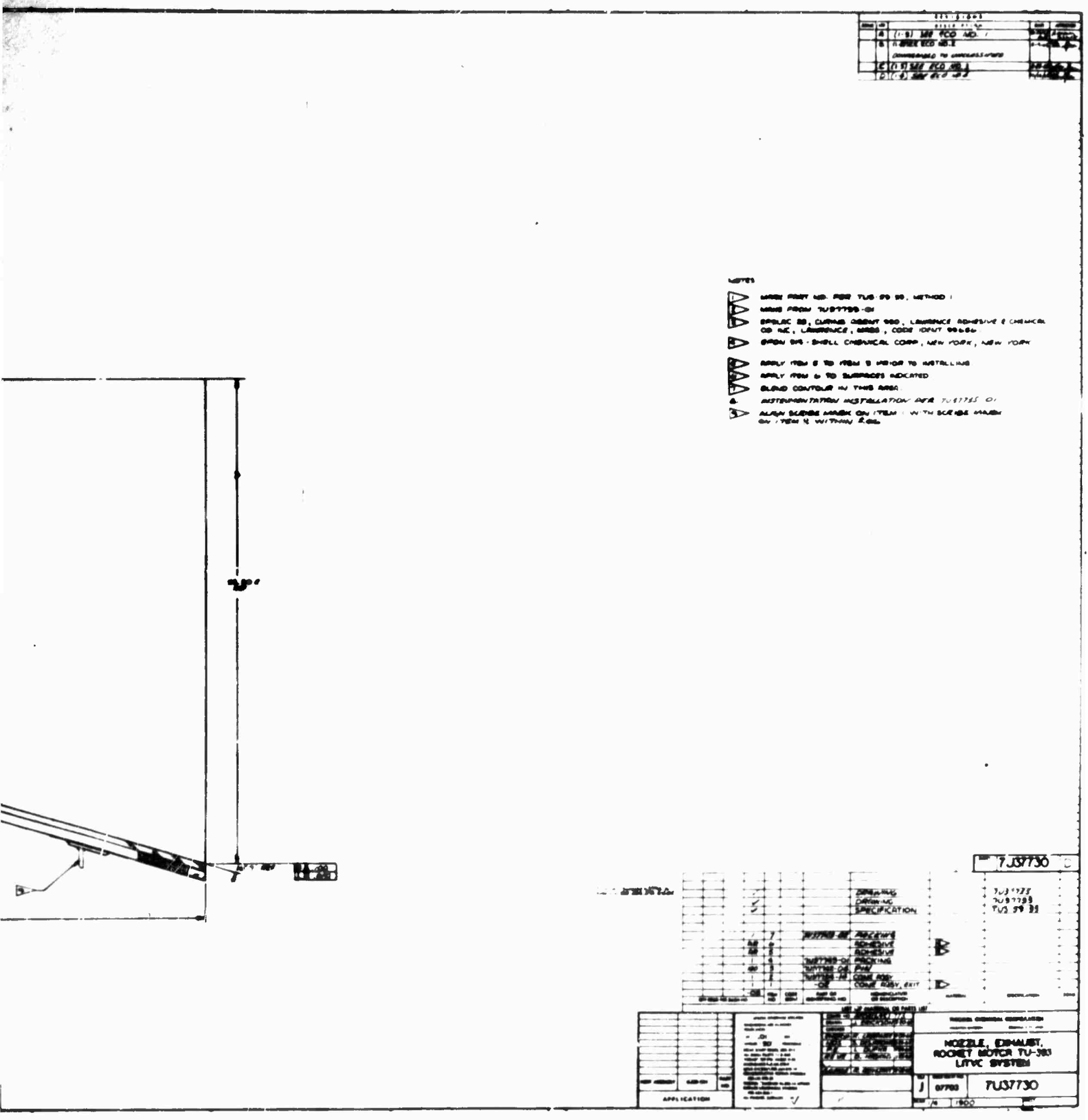

Figure 4. 156-7 Nozzle

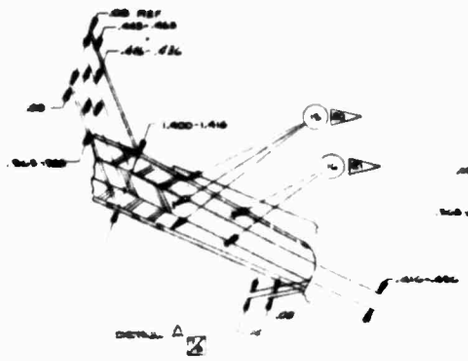

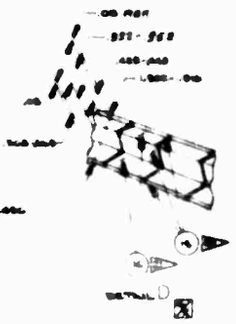

BASIC COORDINATES	
X	W

BASIC COORDINATES	
X	W

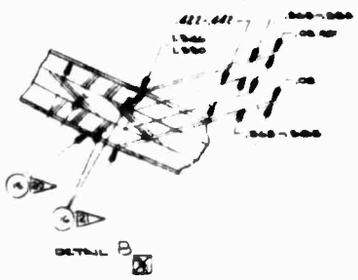

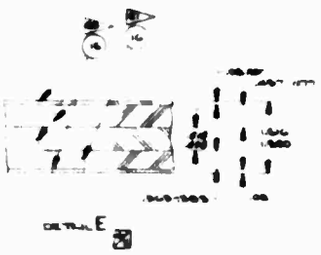

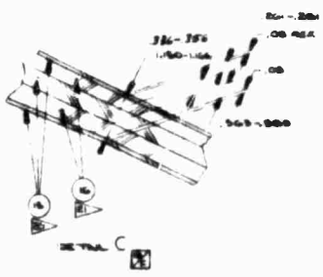

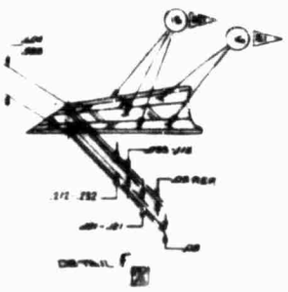

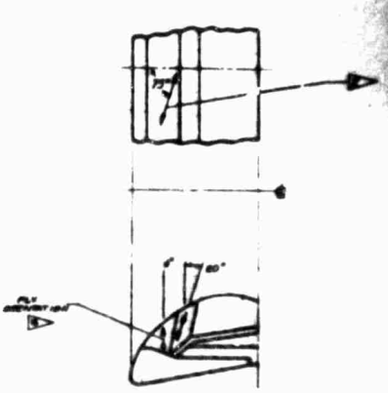

PLY ORIENTATION

A

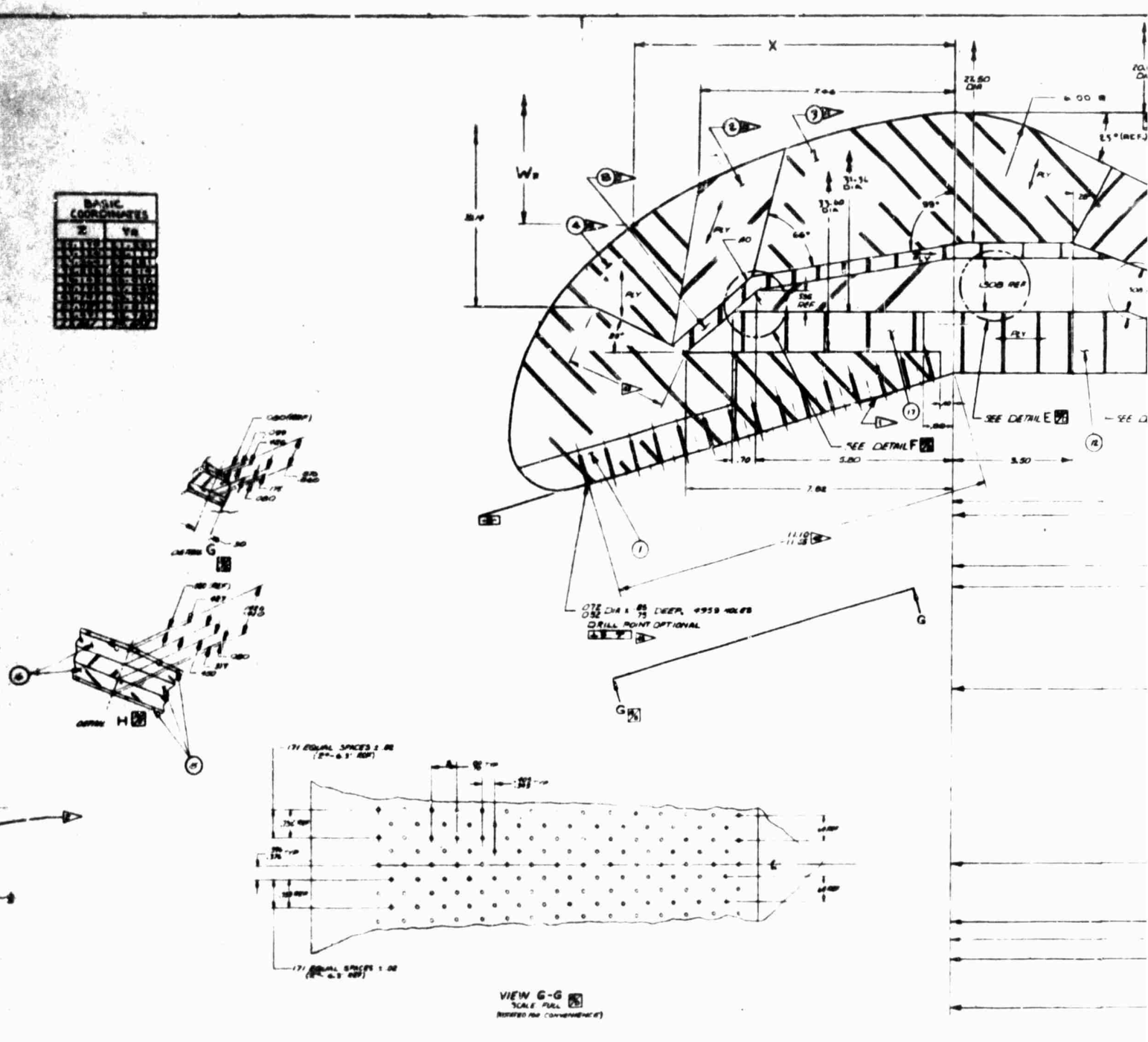

BASIC COORDINATES	
X	W_B

7U37134

3

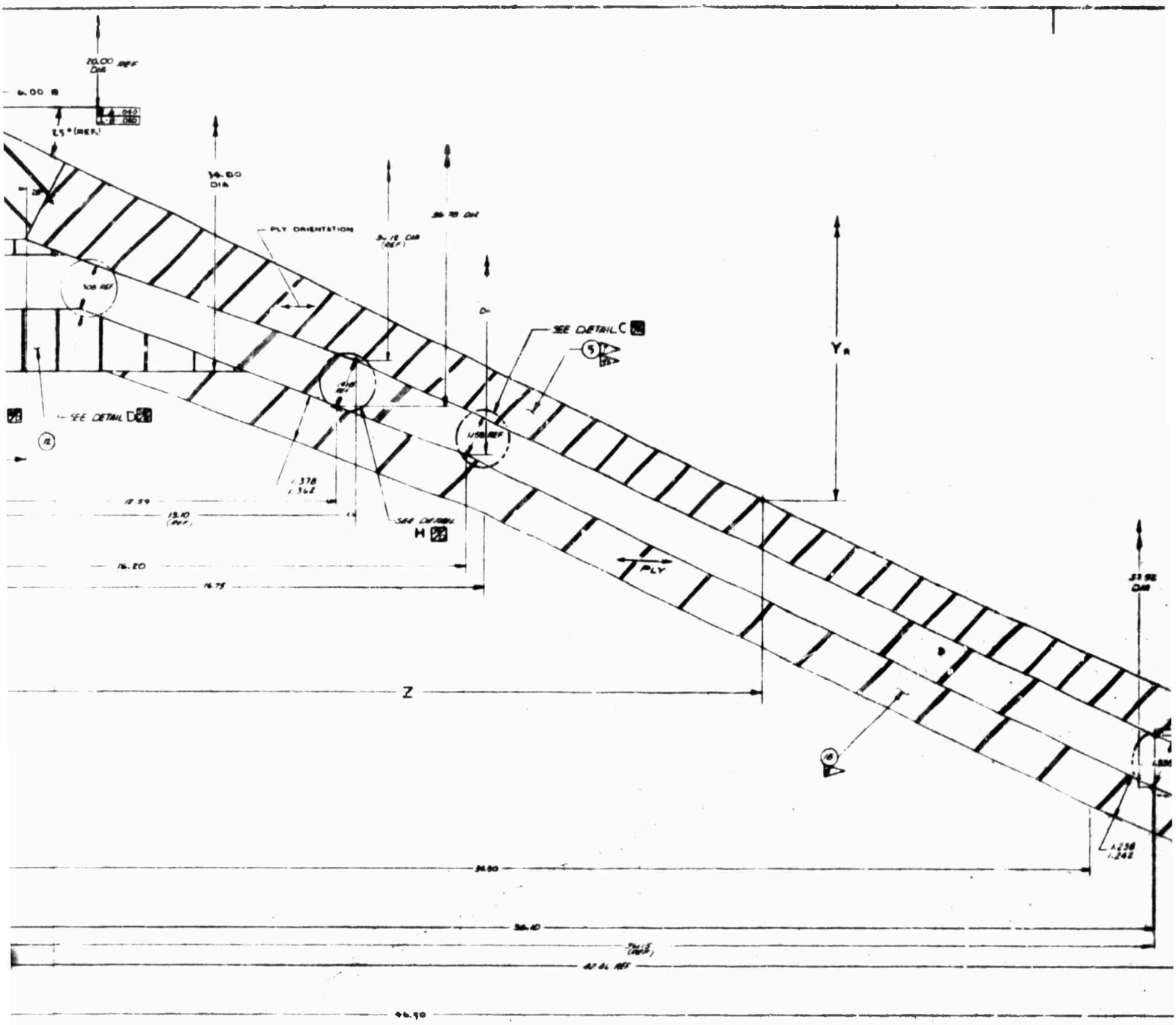

TU37734

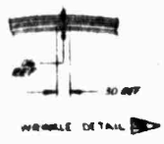

NOTES (CONT)

DELETED

DELETED

DELETED

DELETED

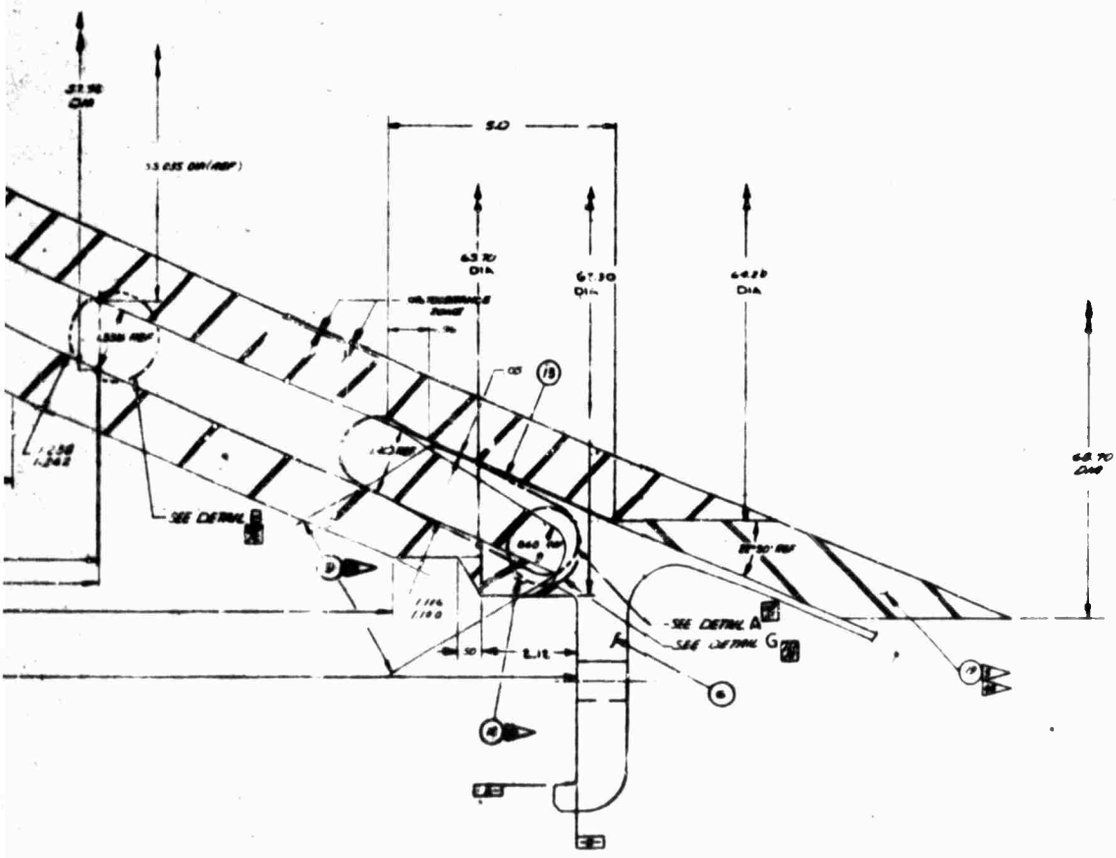

D

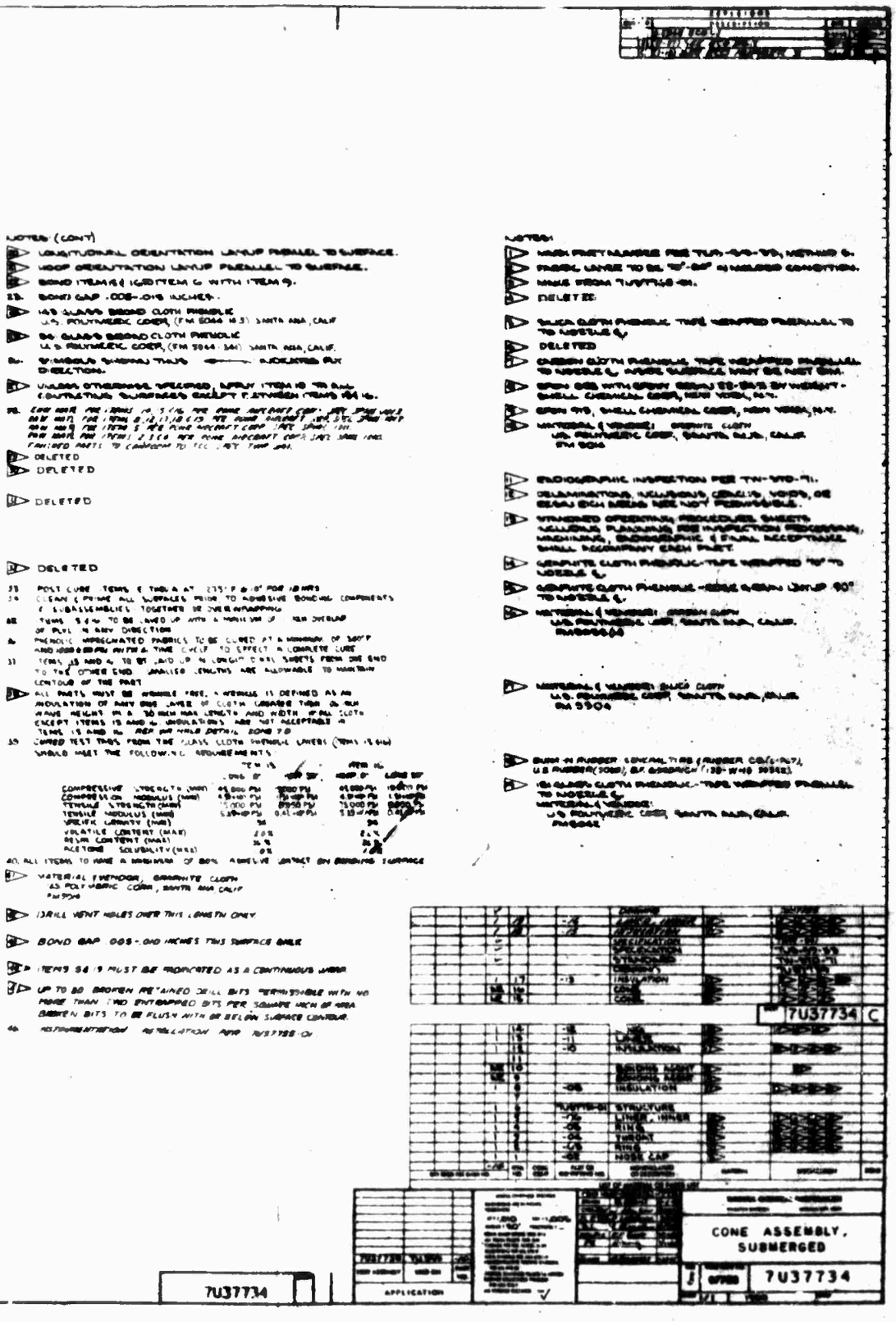

Figure 5. 156-7 Nozzle Submerged Cone Assembly

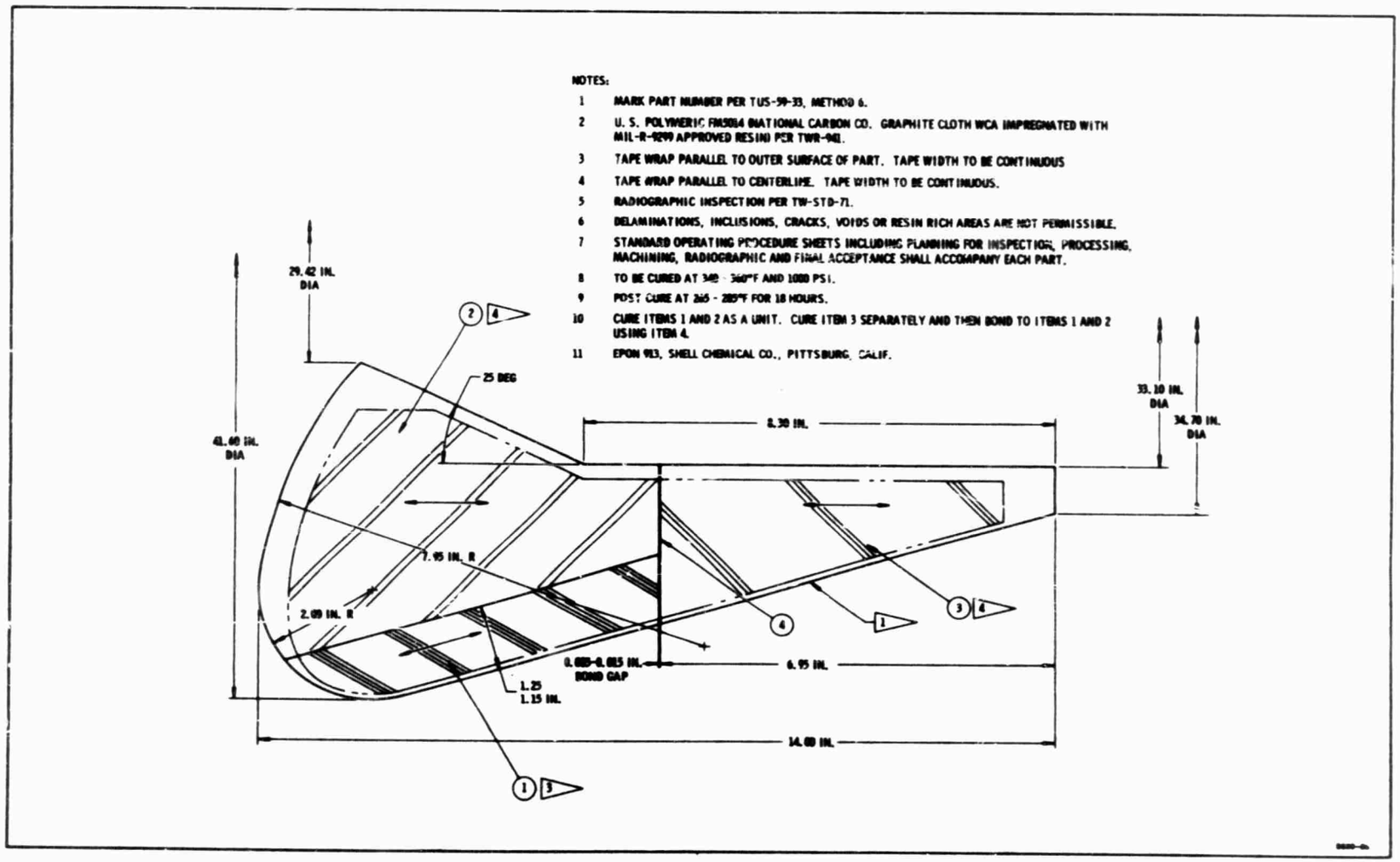

Figure 6. 156-7 Nozzle Nose Inlet Cap Blank

acceptable buckling and local crippling criteria for monocoque truncated cones (the critical buckling pressure is 1,088 psi). The glass cloth phenolic composite structure is composed of two layers of hoop oriented broadcloth laid up parallel to the surface and three layers of longitudinally oriented cloth, also laid up parallel to the surface. This combination is stronger in the hoop direction for the critical external pressure with no large degradation of the longitudinal strength for the axial blowout load and provides the lowest weight design. Figure 7 presents the complete structural shell.

The nose and throat region are formed by graphite cloth phenolic. This fabric is laid up and cured in a ply orientation that exposes ply edges to the gas stream as much as possible, thereby maximizing erosion resistance. Graphite cloth is used in regions where erosion is high because of its reliable and reproducible past performance as an erosion barrier. Silica cloth phenolic was chosen as insulation beneath the graphite cloth in the throat region due to its effective low thermal conductivity and wide acceptance as a thermal heat barrier. The outside diameter of the supporting structure is silica cloth phenolic. This material extends aft on the chamber side of the submerged portion and is the sole insulating material between the supporting structure and the motor environment in this low velocity region where heating is due almost entirely to radiation.

The forward exit cone liner from an expansion ratio of 1.33:1 to 10.33:1 is carbon cloth phenolic tape. Graphite cloth is used in the

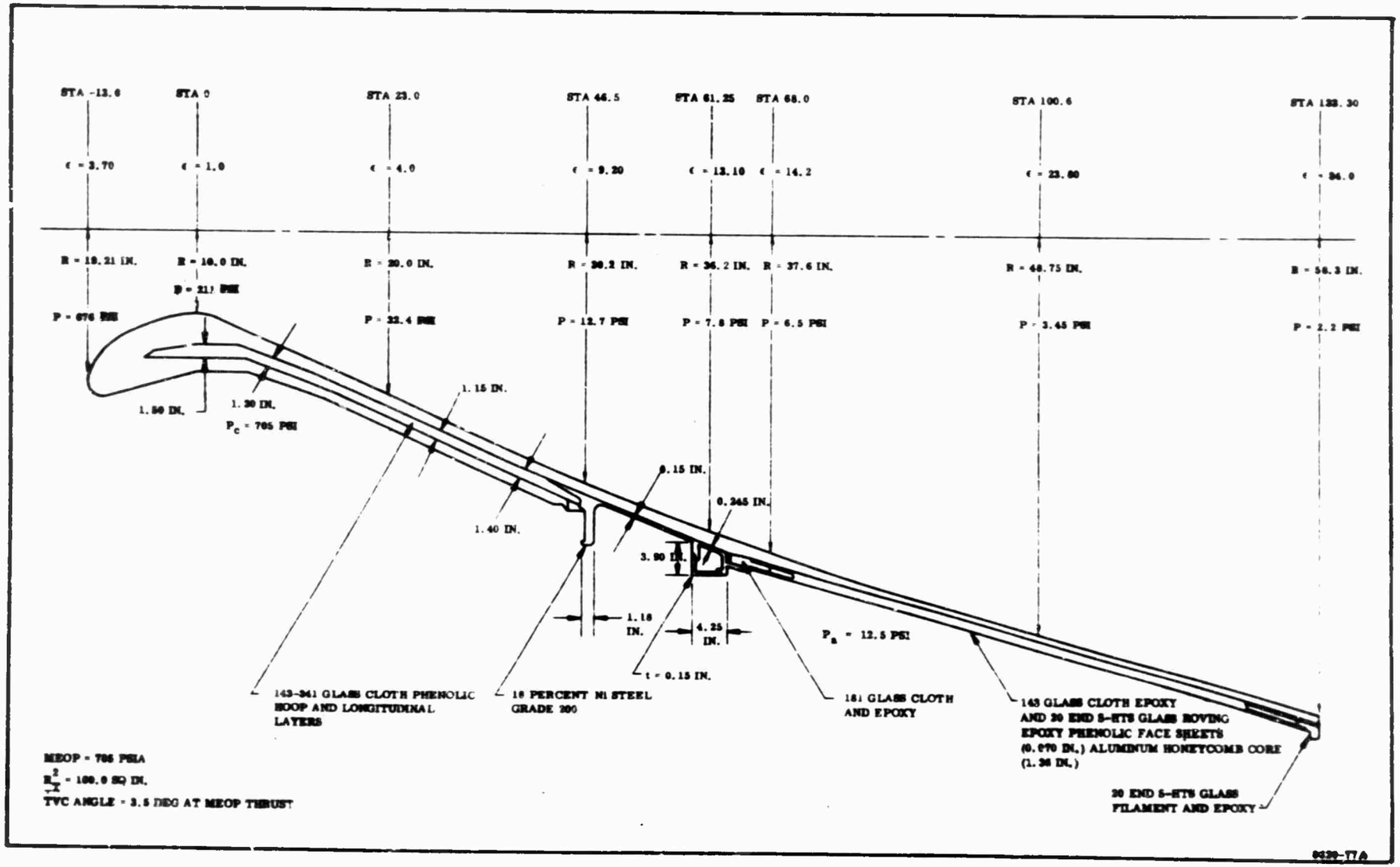

Figure 7. Structural Shell Upper Stage Nozzle

critical region of the inlet and throat, but carbon cloth has been substituted in the less critical upper exit cone region because of its lower cost.

b. Flange and Injector Ring Pad--The flange shell (Figure 8) and injector ring (Figure 6), are machined from one ring forging of maraging 18 percent nickel steel and bolted together. Maraging 18 percent nickel steel, grade 200 Kpsi, was select because of the requirements for the highest strength material available coupled with ease of fabrication, low cost, and schedule compatibility. The flange shell is the connecting structure between the case aluminum pole piece, the submerged cone, and the exit cone, and is subjected to axial and lateral loads, transverse bending, pressure distribution, concentrated bolt loads, and discontinuity bending and shear loads. The injector ring primarily provides the support area for attaching the LITVC system components.

Other materials considered for this application were aluminum, titanium, and beryllium. Aluminum and titanium were rejected because of cost and schedule compatibility; beryllium forgings of this magnitude do not exist.

c. Exit Cone Assembly--The exit cone assembly (Figure 9) is comprised of a liner and structural shell. The liner is silica cloth phenolic tape wrapped parallel to the nozzle centerline and extends from an expansion ratio of 10.33:1 to the exit plane. The compatibility of silica cloth phenolic with nitrogen tetroxide injectant has been demonstrated in the TITAN III program. Erosion near the injectors is a function of the TVC duty cycle requirement (i.e., injectant mass flow rate and total mass flow) and injector location. Under the most extreme conditions of injection (all the injectant flowing from one port) which might occur during firing,

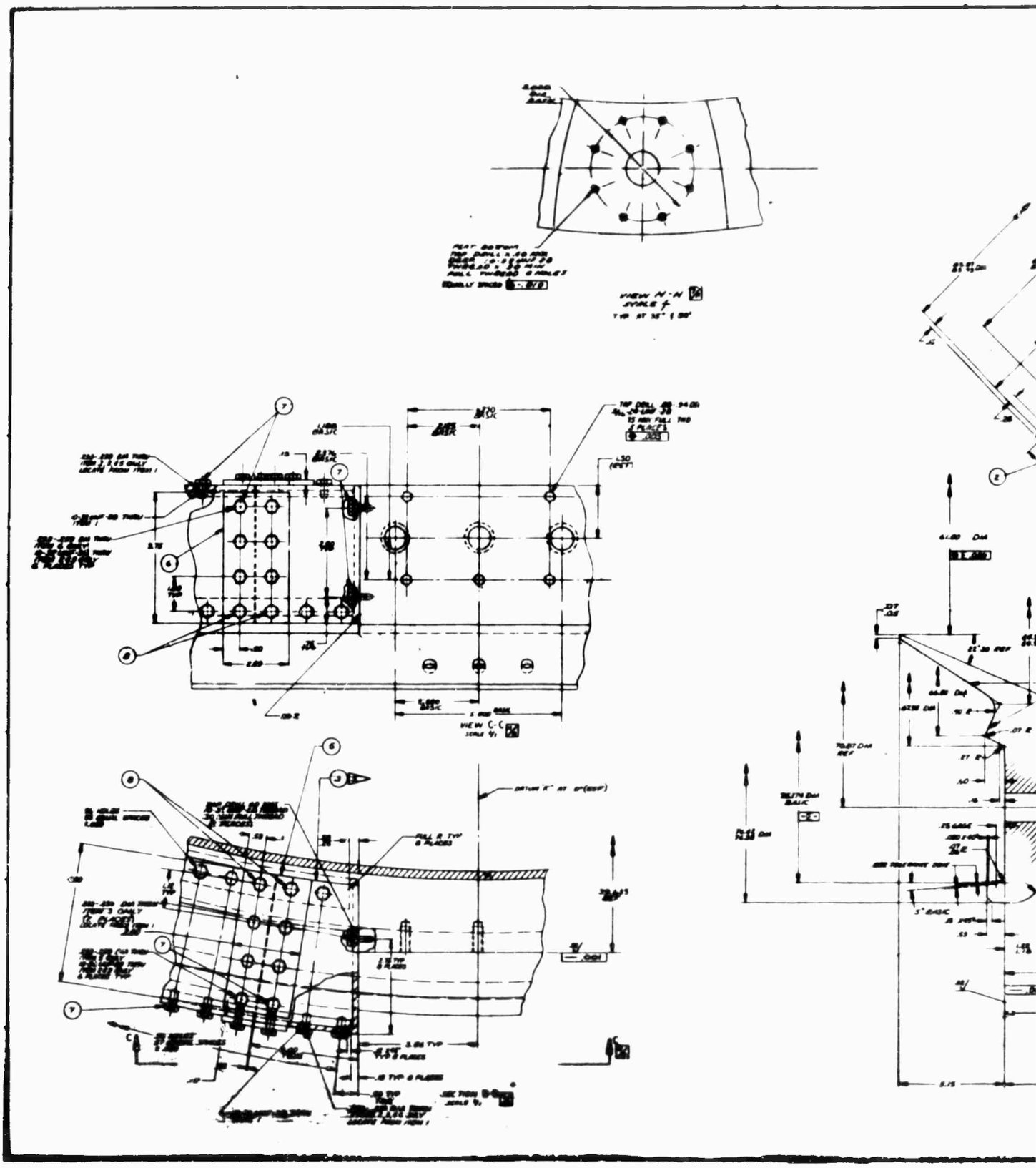

A

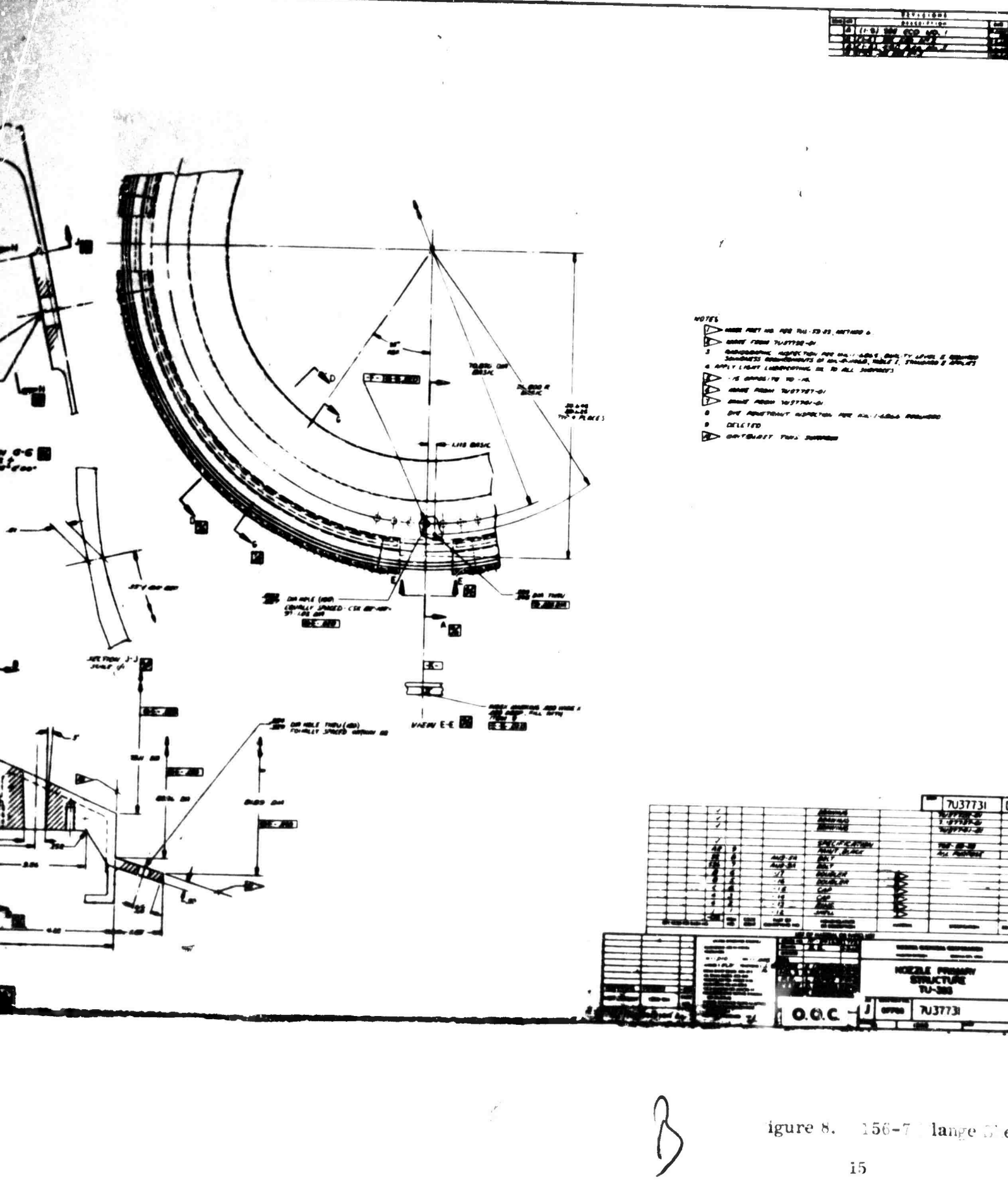

Figure 8. 156-7 flange 3' e

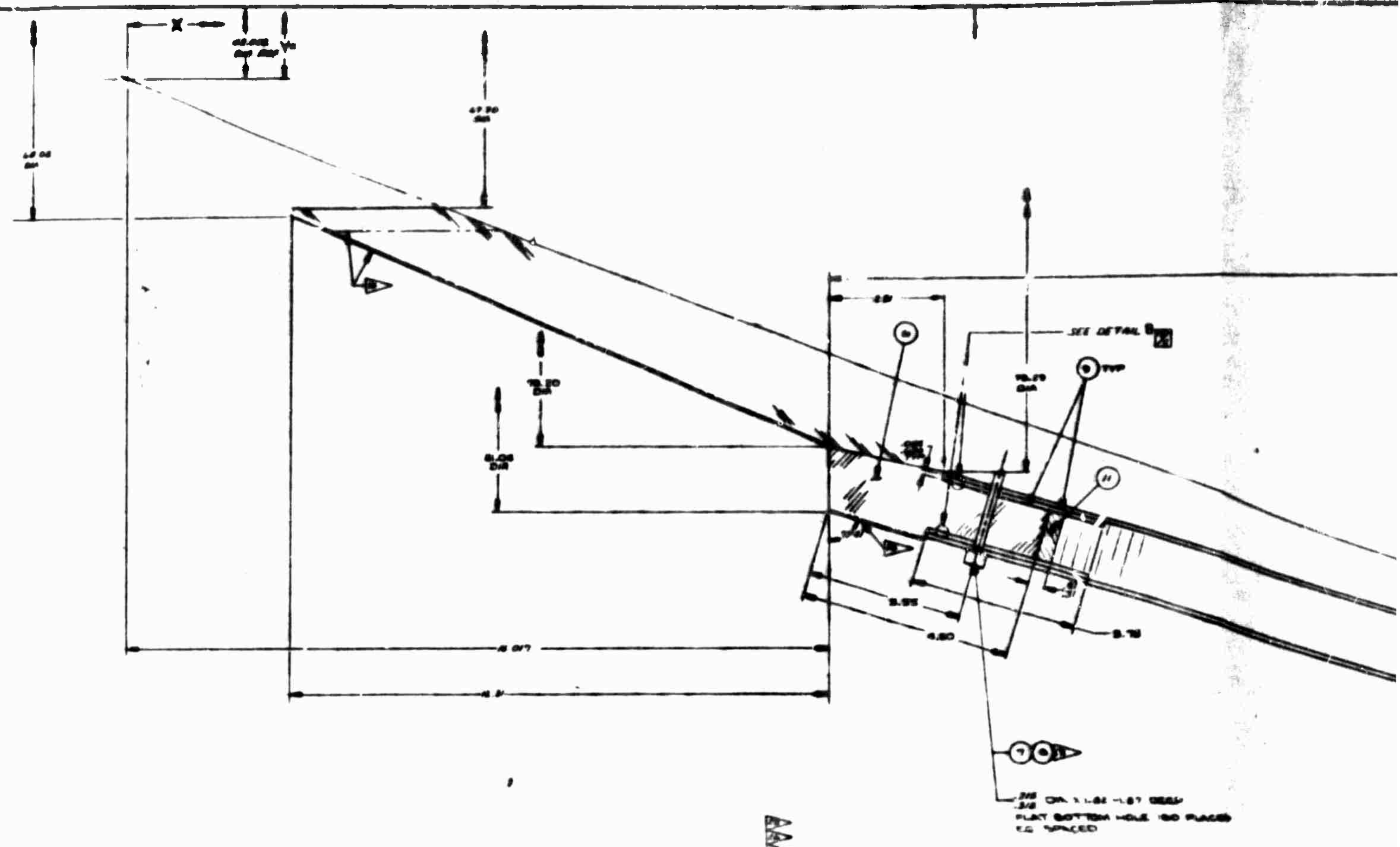

BASIC COORDINATES	
X	Y_n
0.000	31.011
4.500	[illegible]
[illegible]	[illegible]
[illegible]	[illegible]
[illegible]	[illegible]
[illegible]	[illegible]
[illegible]	[illegible]
[illegible]	[illegible]
[illegible]	[illegible]
[illegible]	[illegible]
[illegible]	[illegible]
[illegible]	[illegible]

TANGENT POINT — STRAIGHT TAPER

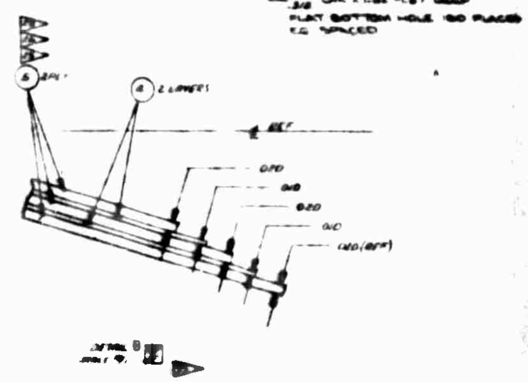

7U37733 C

A

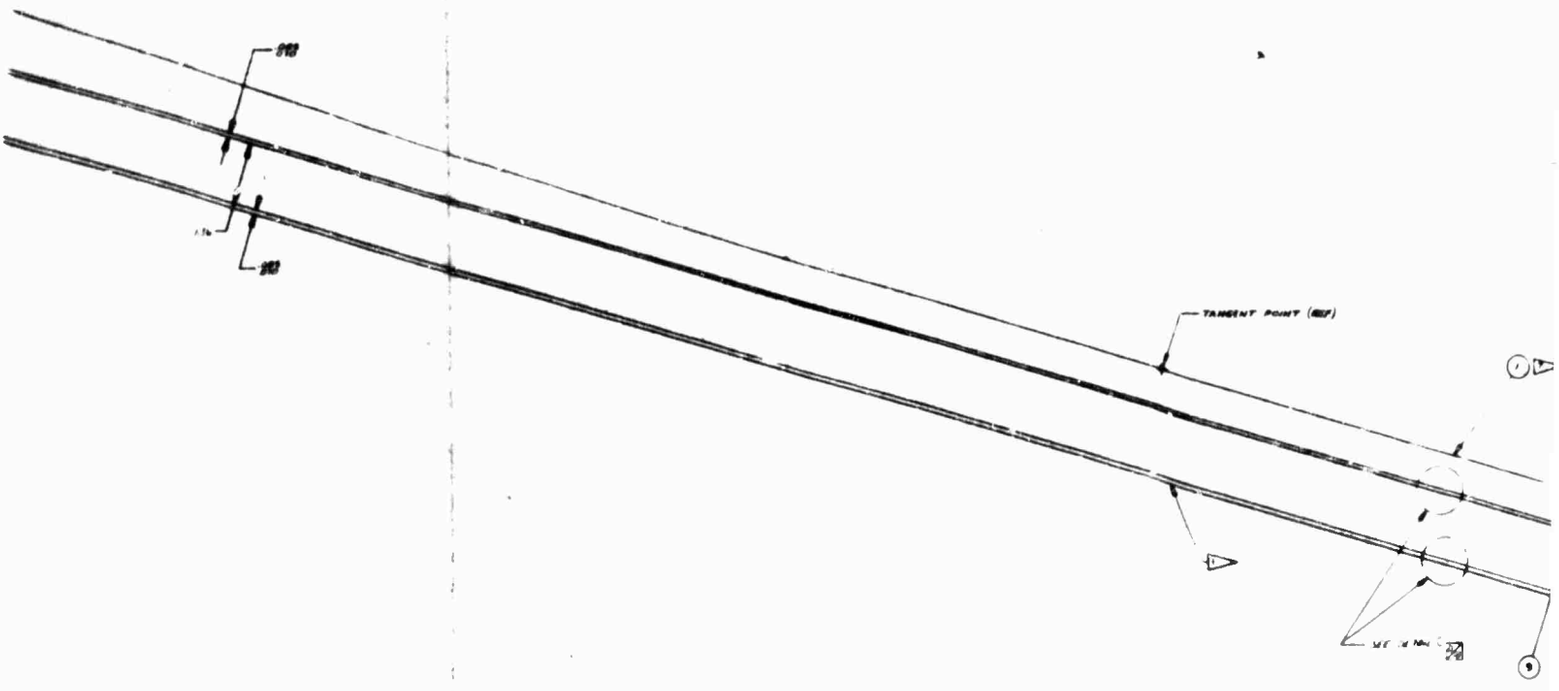
TANGENT POINT (BCF)

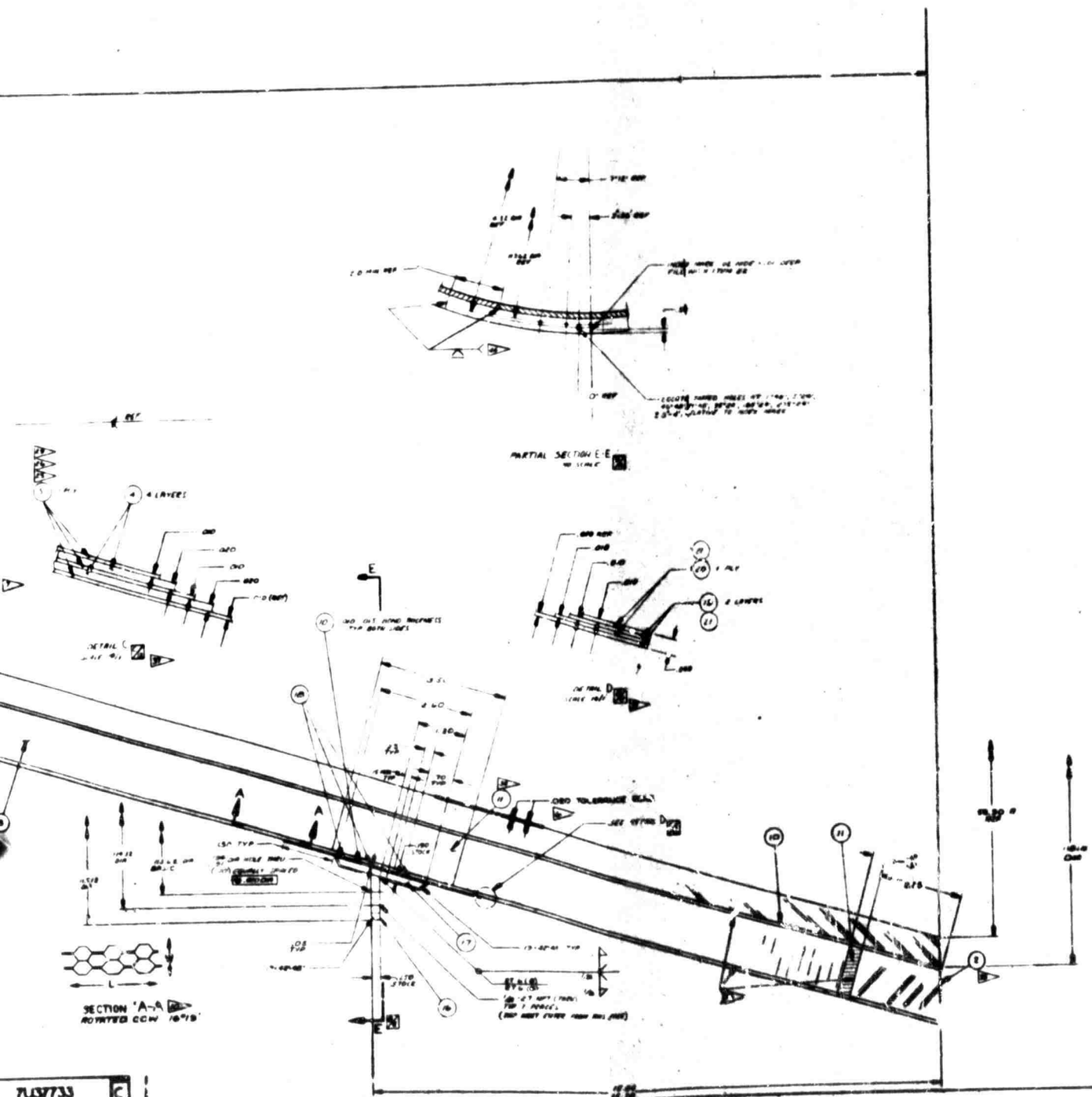

7U37733 C

C

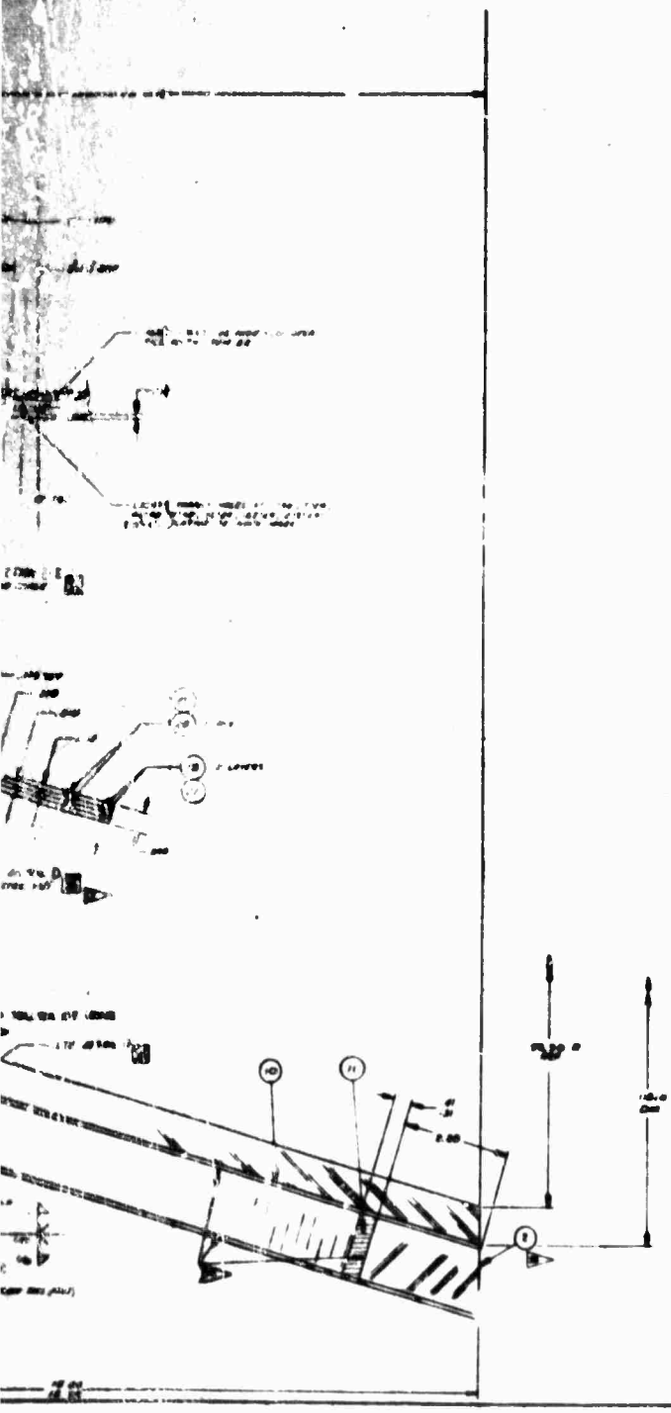

Figure [illegible] Nozzl

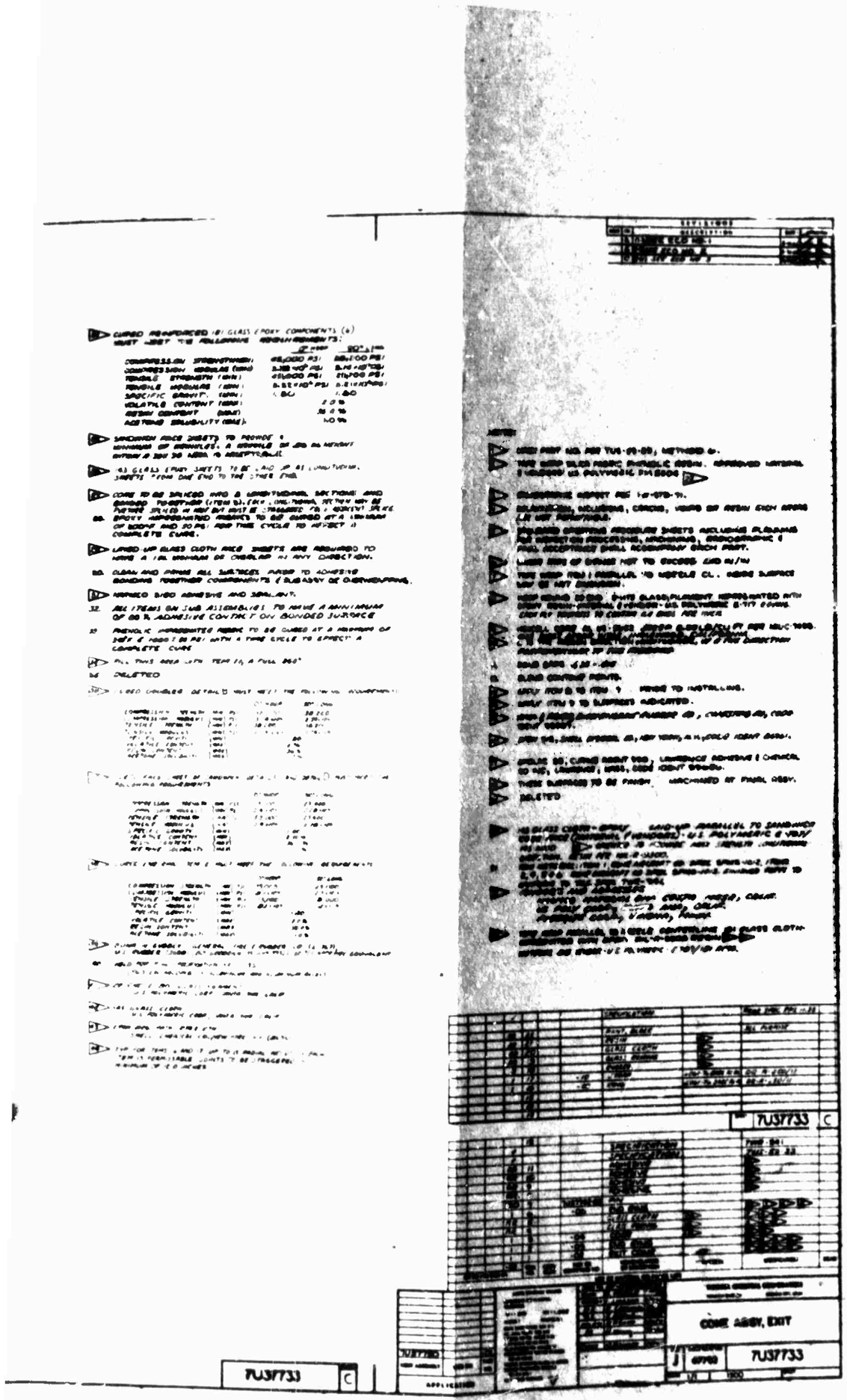

Figure [illegible] Nozzle Exit Cone Assembly

approximately 0.150 in. of material could be lost. Erosion in the port region during periods of no TVC is not anticipated because of the high expansion ratio at which the injectors are located.

The design erosion rate in quadrants having no injection ports was 1.65 mils/sec and the corresponding rate used to size material required in the port regions was 2.65 mils/sec. The resulting liner thickness is not necessary in quadrants having no injection ports; however, this thickness has been maintained constant around the circumference for ease of fabrication.

The exit cone structural shell is a sandwich structure consisting of a 5052 aluminum honeycomb core with 143 glass cloth parallel to the surface and 20 S-HTS glass roving epoxy sheets. Use of this sandwich type structure on the TITAN III-C solid propellant nozzles indicate the current state-of-the-art for this lightweight rigid structure. State-of-the-art glass cloth facings are used for weight reduction on this nozzle in lieu of the stainless steel facings used on the TITAN III-C solid propellant nozzles.

This honeycomb shell provides the rigidity required to support the asymmetric LITVC pressure distribution, the external pressure loads, and the acceleration loads. The selection is based on the results of a comprehensive engineering study of high expansion ratio nozzles (Reference 7).

2. METHOD OF FABRICATION

Methods of fabrication have been carefully considered in the design of the 156-7 nozzle. The chosen methods allow the parts to be processed separately, yet still provide a reliable nozzle with structural and insulative integrity. No one unit

can delay the manufacturing time cycle excessively. A flow chart of the fabrication steps for this nozzle is shown in Figure 10.

The inlet rings and the throat section graphite cloth phenolic are processed in three ring blocks. The upstream block is an edge grain layup at an upstream angle of 90 deg to the nozzle centerline. The middle block and the throat block are tape wrapped at a downstream angle of 70 degrees. This concept has been successfully tested on the TU-454 and TU-455 motors. The silica cloth phenolic backup insulation is tape wrapped parallel to the centerline on a separate mandrel and bonded to the inlet and throat rings.

The carbon cloth phenolic of the forward exit cone liner is wrapped parallel to the nozzle centerline and cured on a mandrel. The steel flange and the structural glass, consisting of two layers of hoop oriented glass cloth laid up parallel to the surface and three layers of longitudinally oriented glass layup, are then applied.

The silica cloth submerged OD insulation is tape wrapped, parallel to centerline, fabricated separately and bonded in place. The graphite cloth phenolic nose cap is composed of three separate rings. The forward section inner ring is tape wrapped parallel to centerline with an overwrap parallel to the backside surface for the outer ring. The aft section is tape wrapped parallel to centerline.

The exit cone structural shell will be processed on the outside of the cured exit cone liner. The exit cone liner is silica cloth phenolic tape wrapped parallel to the nozzle centerline. The aluminum honeycomb core will be spliced into 8 longitudinal segments to provide for ease of fabrication. A forward end block of glass cloth attaches the exit cone structural shell to the steel flange shell. A block

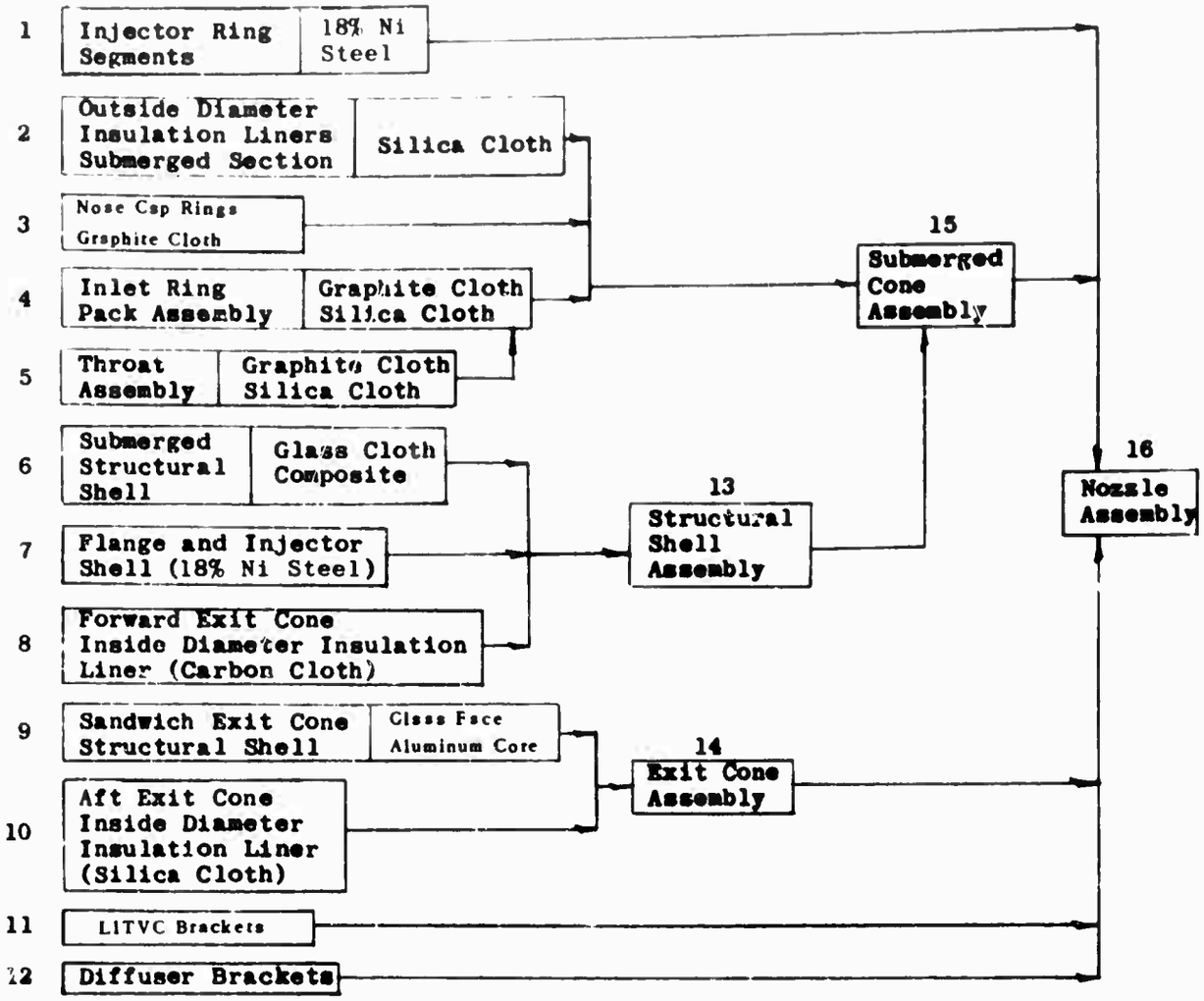

Figure 10. 156-7 Nozzle Fabrication Flow Chart

of glass roving epoxy tape wrapped parallel to the centerline provides an end ring stiffener at the exit plane.

3. DESIGN CRITERIA

Consideration was given to the criteria outlined in the following paragraph in the design of the 156-7 nozzle.

The nozzle must be a flightweight submerged nozzle. Nozzle parts exposed to gas flow shall be of ablative plastic.

The nozzle shall be capable of liquid injection thrust vector control (LITVC).

The minimum structural safety factor will be 1.25. An analysis consisting of the following factors shall be performed.

1. Aerodynamic, heat transfer and stress analysis of the submerged portion, throat, and exit cone.
2. Aerodynamic, heat transfer and stress analysis of the interaction of secondary fluid injectant with the local materials in this area.
3. Vibration loads and exit cone deflection data from previous firings.
4. Prediction of erosion profile, char layer, and temperature isotherms.

External design considerations shall be based on the following parameters.

1. Dynamic pressure (maximum) of 1,000 psf.
2. Thrust misalignment (maximum) of 0.5 degrees.
3. Staging angle of attach (maximum) of ± 5 degrees.
4. No wind shear.

Materials and fabrication techniques shall be within current industrial experience and design.

The nozzle design shall incorporate a nozzle expansion ratio compatible with the exit cone diameter limit of 149 inches.

In addition to the above criteria, the following specific requirements were used.

1. Motor Requirements

Web Time

	Average	Maximum	MEOP
Chamber Pressure (psi)	550	625	705*
Burn Time (sec)		107	

*Reference Figure 11.

	Average	Maximum	MEOP
Thrust (lb) (Vacuum)	342,000	400,000	442,000*

Action Time, t_a (sec) 110.0

Shock - Vibration

Radial Shock at Ignition

Submerged Section	$\pm$ 60g's for 0.25×10^{-3} sec
Flange and Steel Shell	$\pm$ 30g's for 0.25×10^{-3} sec
Exit Section	$\pm$ 60g's for 0.25×10^{-3} sec

Shock Load	**3 g's axially**
Vibration Load	**1.5g's laterally**
Acceleration	**8.0g's axial, 5.0g's lateral**

2. **Thrust Vector Control Requirements**

Maximum TVC Angle (Pitch or Yaw)	**3.5 deg**
Includes 2.0 deg (AF requirement) + 0.50 deg (Misalignment) + 1.0 deg (for LITVC Performance Band at MEOP = 705 psi)	
Injector Port Diameter (in.)	**0.70**
Injectant Pressure (psi)	**750**
Injector Ports/Quadrant	**3**
Maximum Port Mass Flow (lbm/sec)	**16.84 lbm/sec**

* Reference Figure 12.

Injectant Fluid	Nitrogen Tetroxide (N_2O_4)

3. Nozzle Requirements

Weight (lb)	5,400 (nominal target)
Throat Diameter - Initial (in.)	20.0
Expansion Ratio	34.0:1
Configuration	Fixed Submerged Upper Stage, Contour Exit Cone. Designed for Static Test at Utah and Flight Test
Area Ratio Locations	
Case Boss	9.20:1
LITVC Port	13.10:1

4. Propellant Requirements

Formulation	TP-H8163
Composition	16 Al/69 AP/HB
Temperature, Chamber	5,780°F
Configuration	Modified Slotted CP

5. Structural Requirements

Stress

Steel F.S. (min) = 1.25 at Yield Allowable

Glass F.S. (min) = 1.50 at Ultimate Strength

Insulation

Maintain at least minimum thickness as required by thermodynamic analysis

Maintain room temperature on structural glass of submerged cone

Deformation

Throat = 10.0 (0.40 percent) = 0.040 in. Radial Growth

Exit Cone = 58.3 (0.50 percent) = 0.292 in. Radial Growth

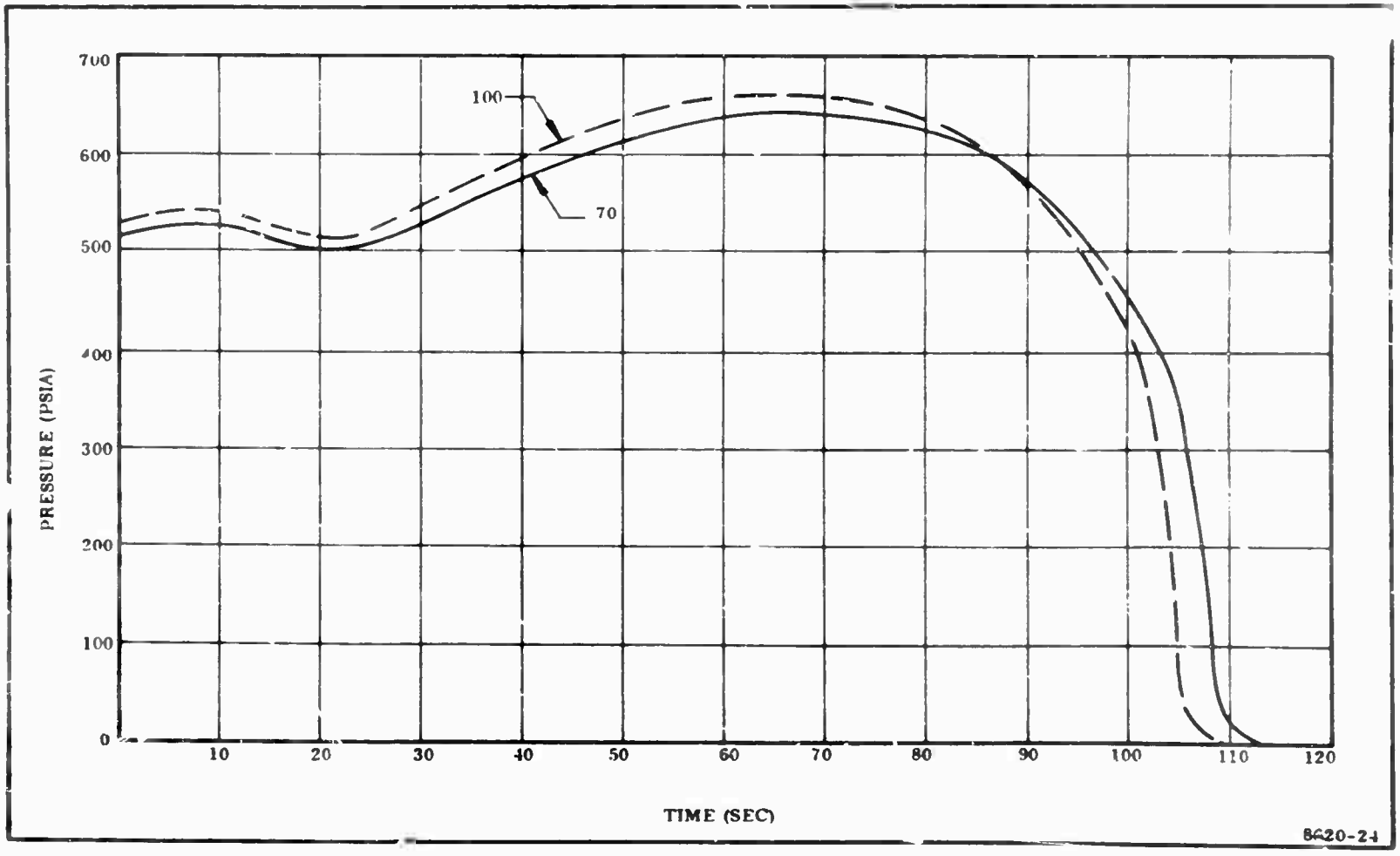

Figure 11. Pressure vs Time Curves for 156-7 Motor (70 and 100° F)

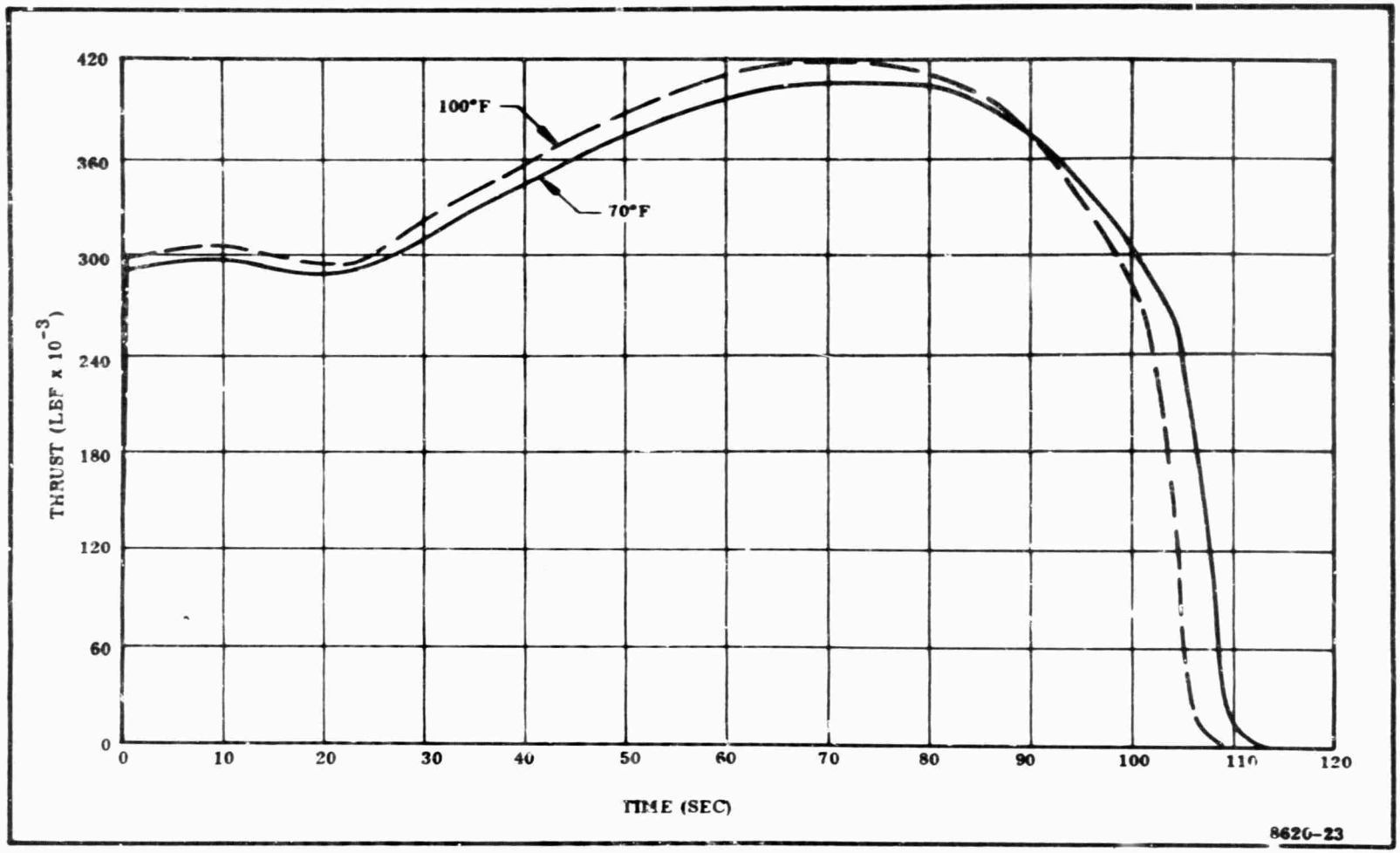

Figure 12. Vacuum Thrust vs Time Curves for 156-7 Motor (70 and 100° F)

SECTION III

LOADS AND ANALYSIS SUMMARY

1. LOADS

The two major loading conditions, static and flight tests, receive the forces through (1) the pressure distribution on the inside and outside nozzle walls, (2) by shock and vibration, and (3) by acceleration loads in the axial and laterla directions. Typical static test condition loads are graphically presented in Figure 13.

Temperature gradients will exist on all surfaces of the nozzle, except the external wall from flange to diffuser, and will contribute to the total stress and deformation at critical design sections.

The nozzle wall pressure and resulting axial load are presented in Figures 14 and 15. The wall pressure due to secondary injection, the transverse shear, and the bending moments are shown in Figures 16 through 22. The injector ring loads from the mounting of the TVC system and acceleration loads are presented in Figures 23 through 27.

The analysis and evaluation to obtain the above loading conditions are presented in detail in Section IV-1. The design condition for the static and flight test loadings are listed in Figure 28.

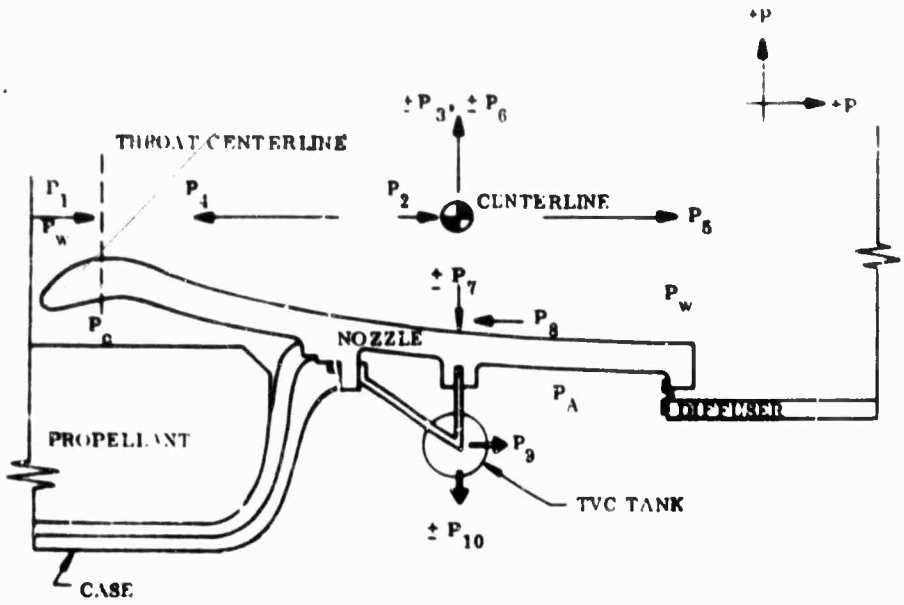

SYMBOLS

P_1 - AXIAL PRESSURE LOAD ON THE NOZZLE FROM THROAT TO SEAL O-RING AT CASE BOSS (VARIES WITH NOZZLE EROSION)

P_2 - AXIAL ACCELERATION LOAD AT NOZZLE CENTER OF GRAVITY

P_3 - ± LATERAL ACCELERATION LOAD AT NOZZLE CENTER OF GRAVITY

P_4 - NOZZLE INTERNAL WALL PRESSURE LOAD ON THE NOZZLE FROM THROAT TO DIFFUSER ATTACHMENT (VARIES WITH NOZZLE EROSION)

P_5 - AMBIENT PRESSURE LOAD ON THE NOZZLE OUTSIDE DIAMETER FROM THE CASE BOSS TO THE DIFFUSER ATTACHMENT

P_6 - ± LATERAL LOAD DUE TO THRUST MISALIGNMENT AT CENTROID OF SUBMERGED NOZZLE SUBASSEMBLY

P_7 - ± LATERAL LOAD DUE TO SECONDARY INJECTION (DIRECTION OF LOAD DEPENDS ON PORT LOCATION)

P_8 - AXIAL LOAD FROM SECONDARY INJECTION

P_9 - ± LATERAL ACCELERATION LOAD AT SITVC TANK CENTER OF GRAVITY

P_{10} - AXIAL ACCELERATION LOAD AT SITVC TANK CENTER OF GRAVITY

P_w - VARIABLE NOZZLE WALL PRESSURE DEPENDENT ON GAS MACH NUMBER

P_c - CHAMBER PRESSURE

P_A - AMBIENT PRESSURE AT UTAH CONDITIONS

8620-10

Figure 13. Static Test Loads at Utah Conditions

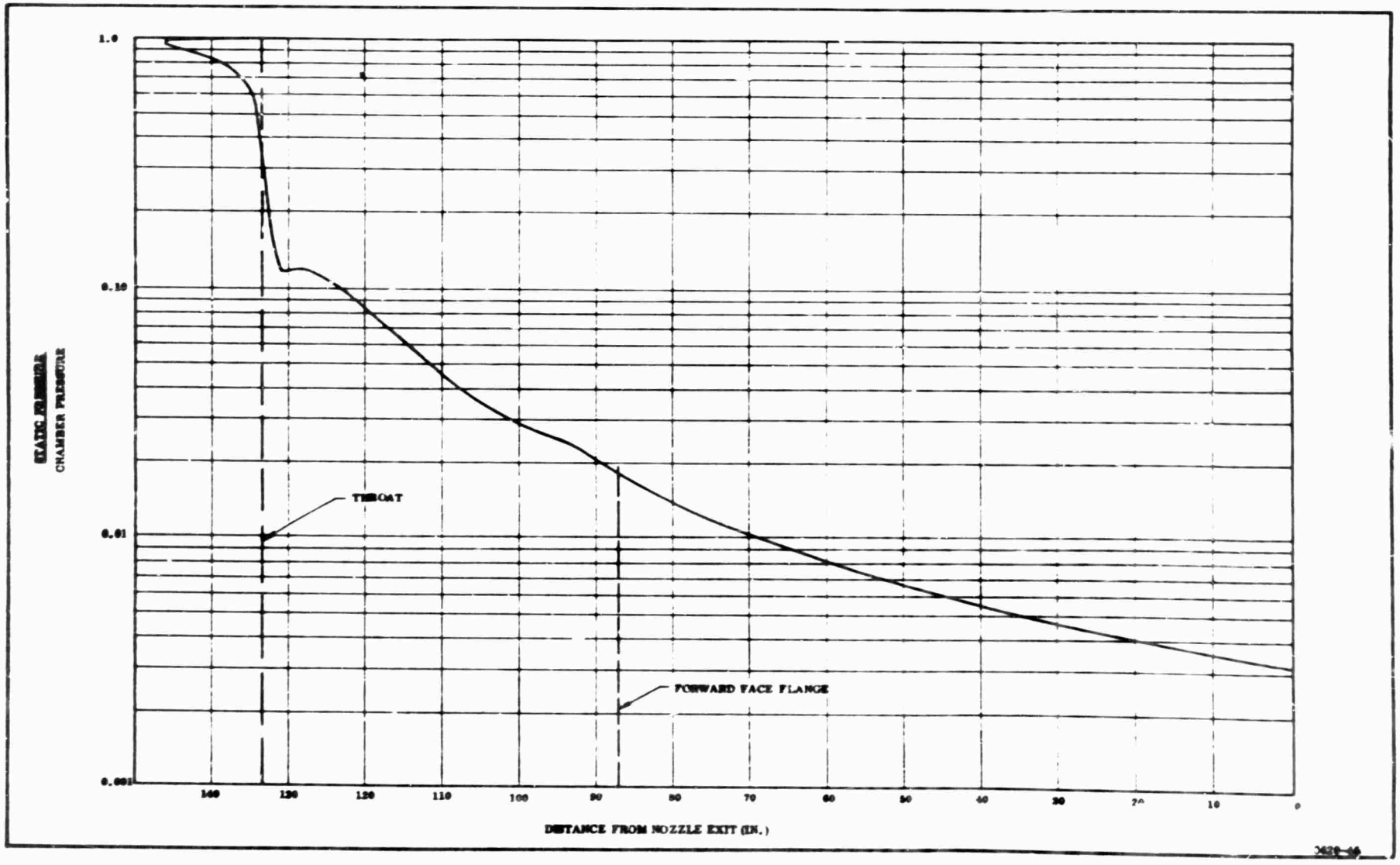

Figure 14. 156-7 Nozzle Internal Pressure Distribution

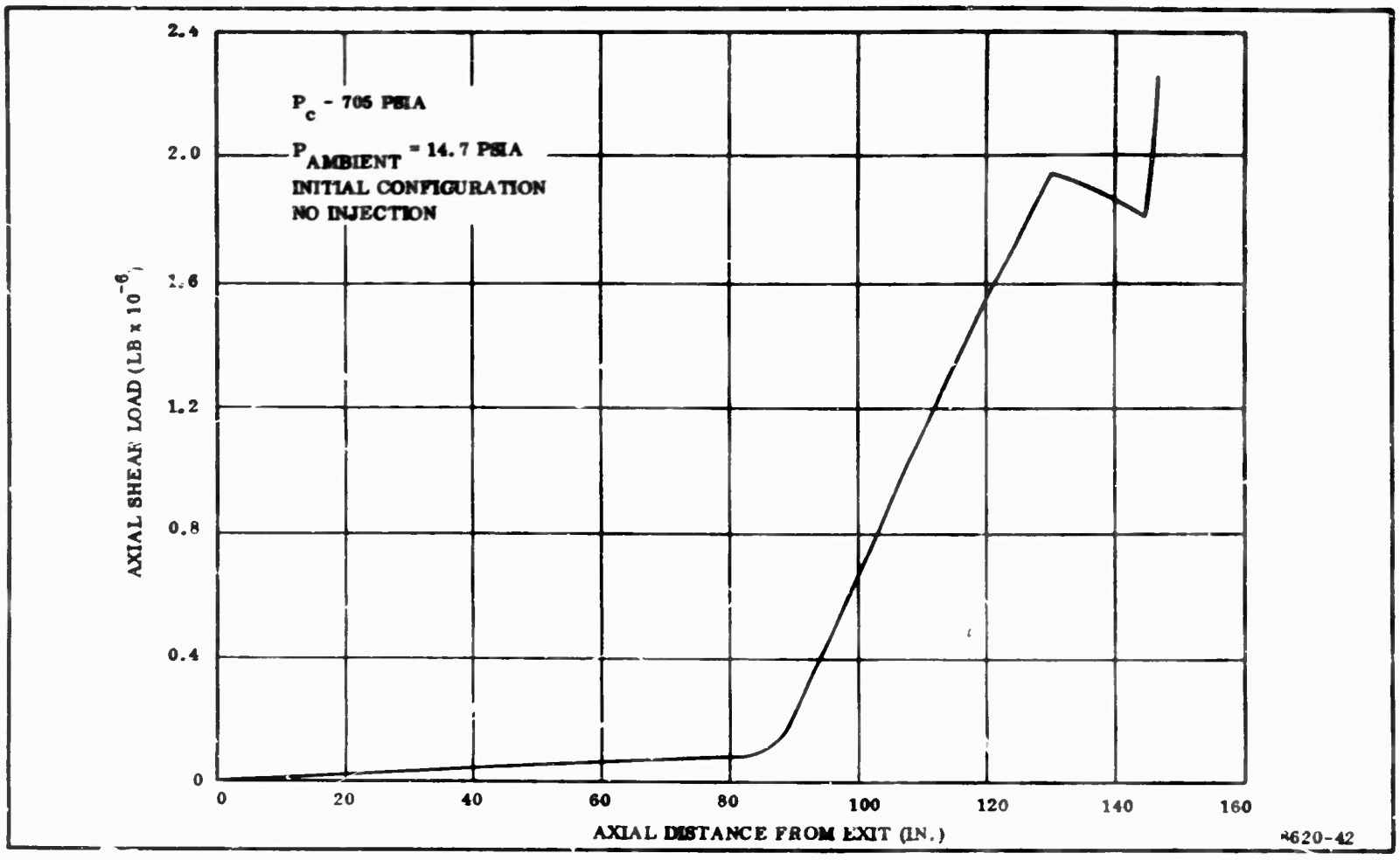

Figure 15. 156-7 Nozzle Axial Shear Load Distribution

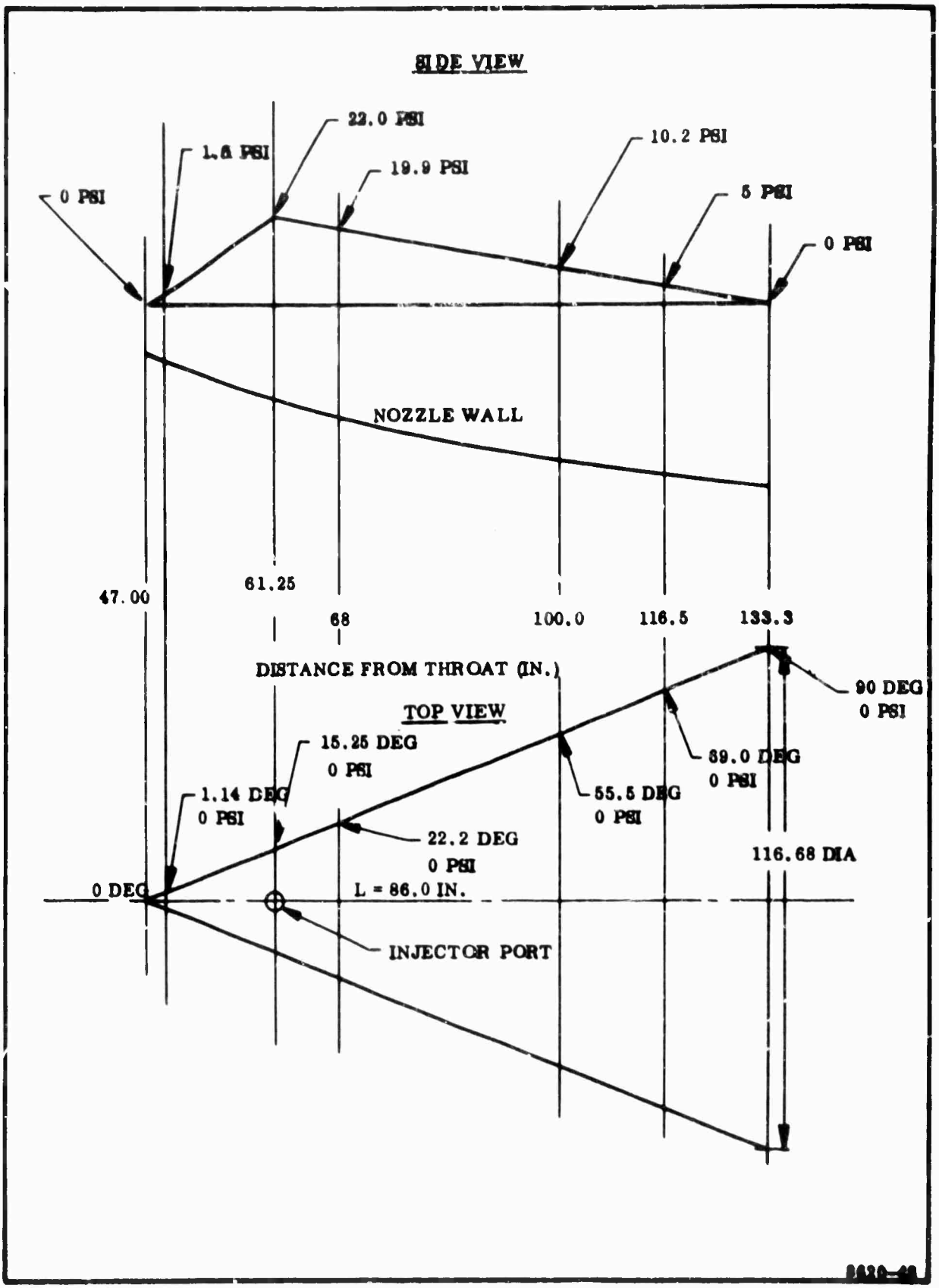

Figure 16. Pressure Distribution During Secondary Injection

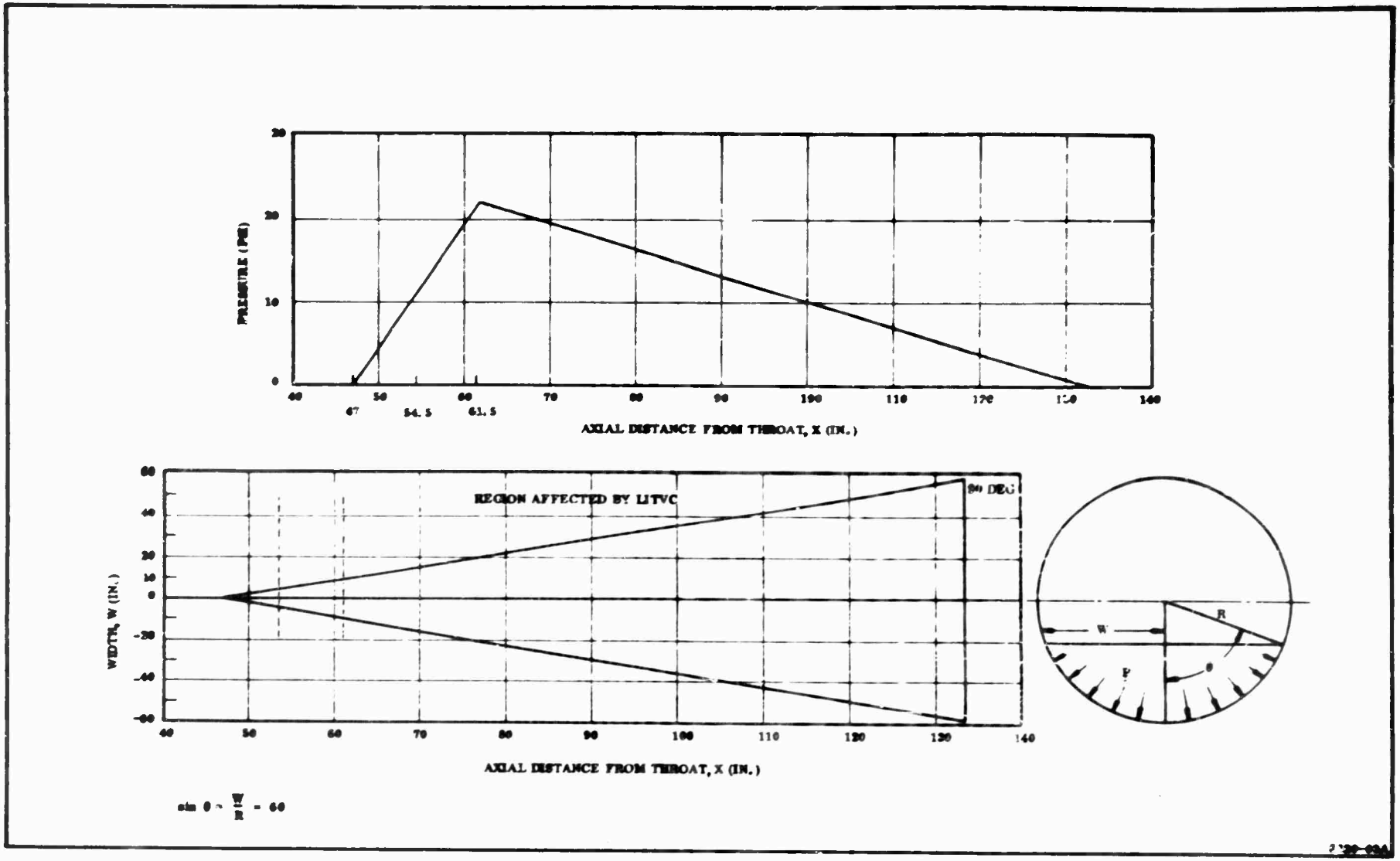

Figure 17. 156-7 Nozzle Axial Pressure Distribution Due to LITVC

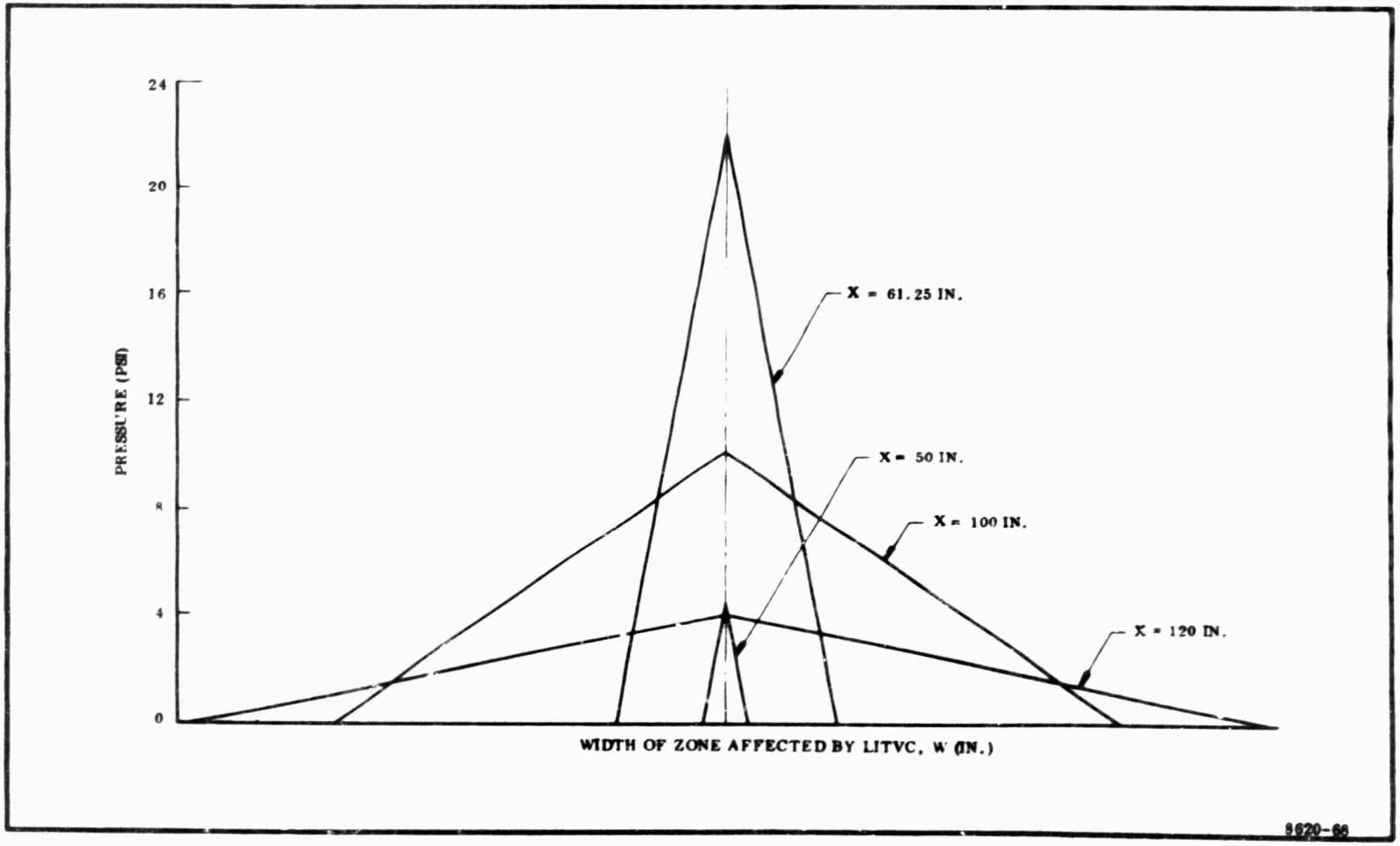

Figure 18. 156-7 Pressure Distribution Due to LITVC

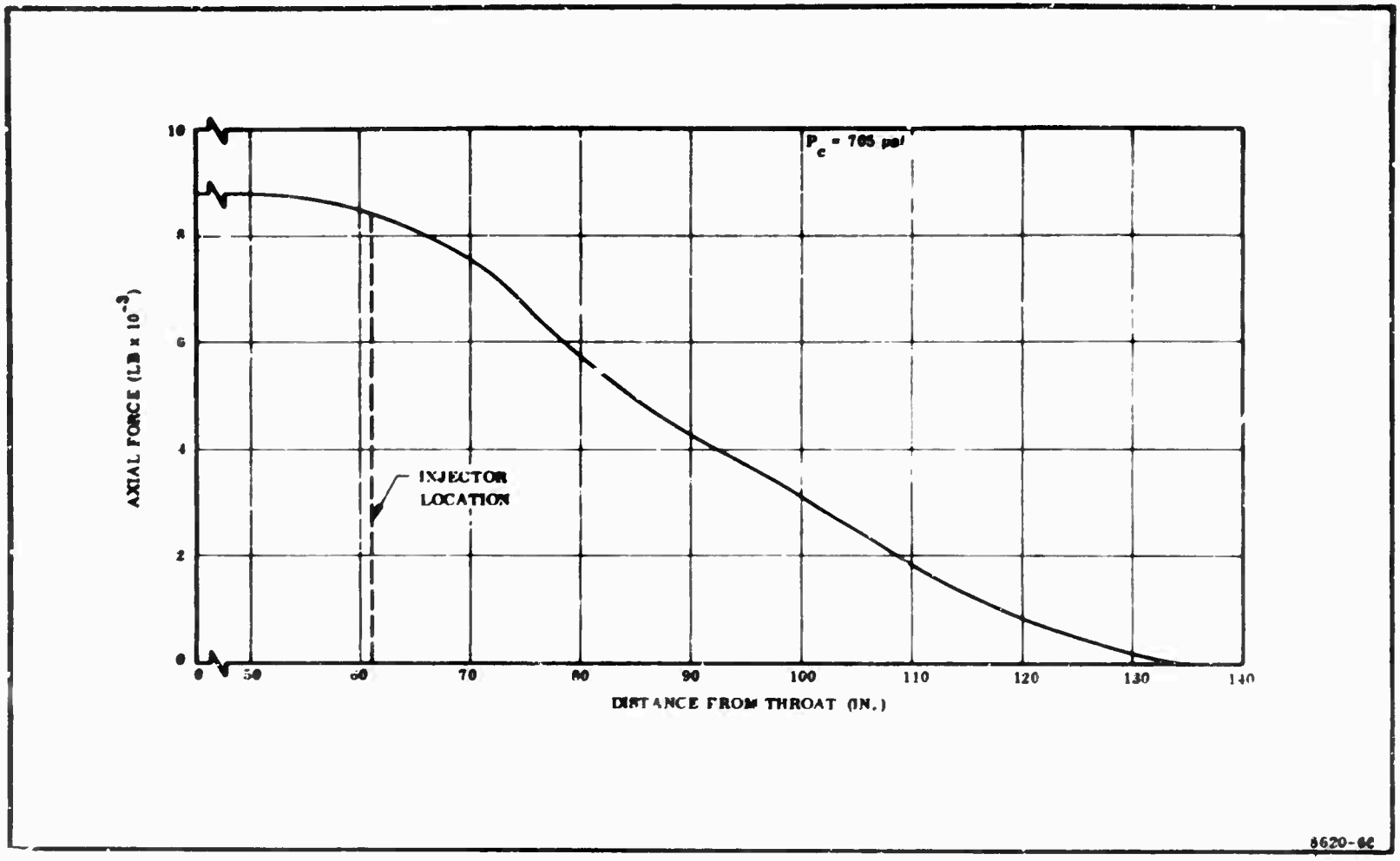

Figure 19. Axial Shear Force Due to LITVC (3.5 Deg Thrust Vector)

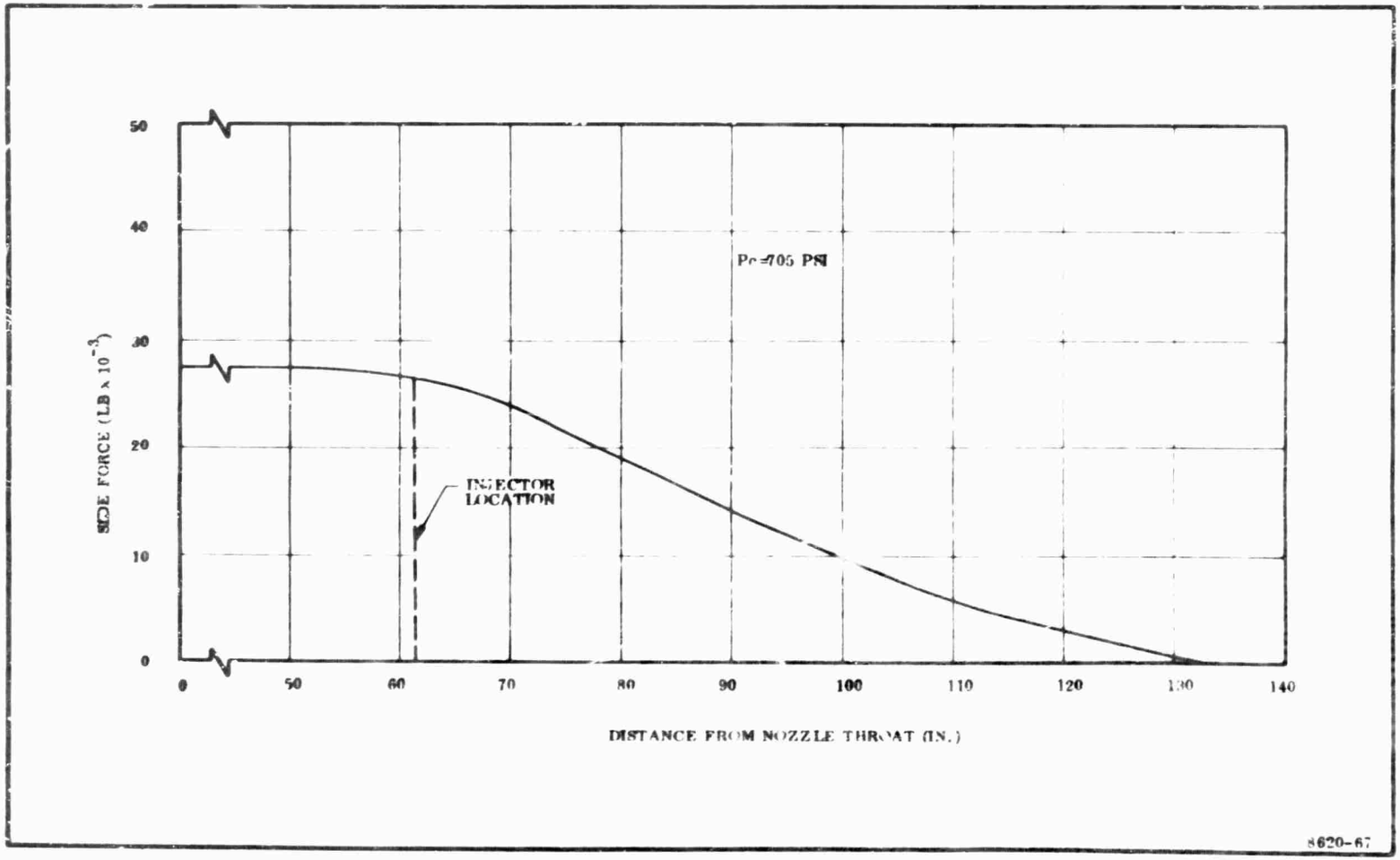

Figure 20. Transverse Shear Load Due to LITVC (3.5 Deg Thrust Vector)

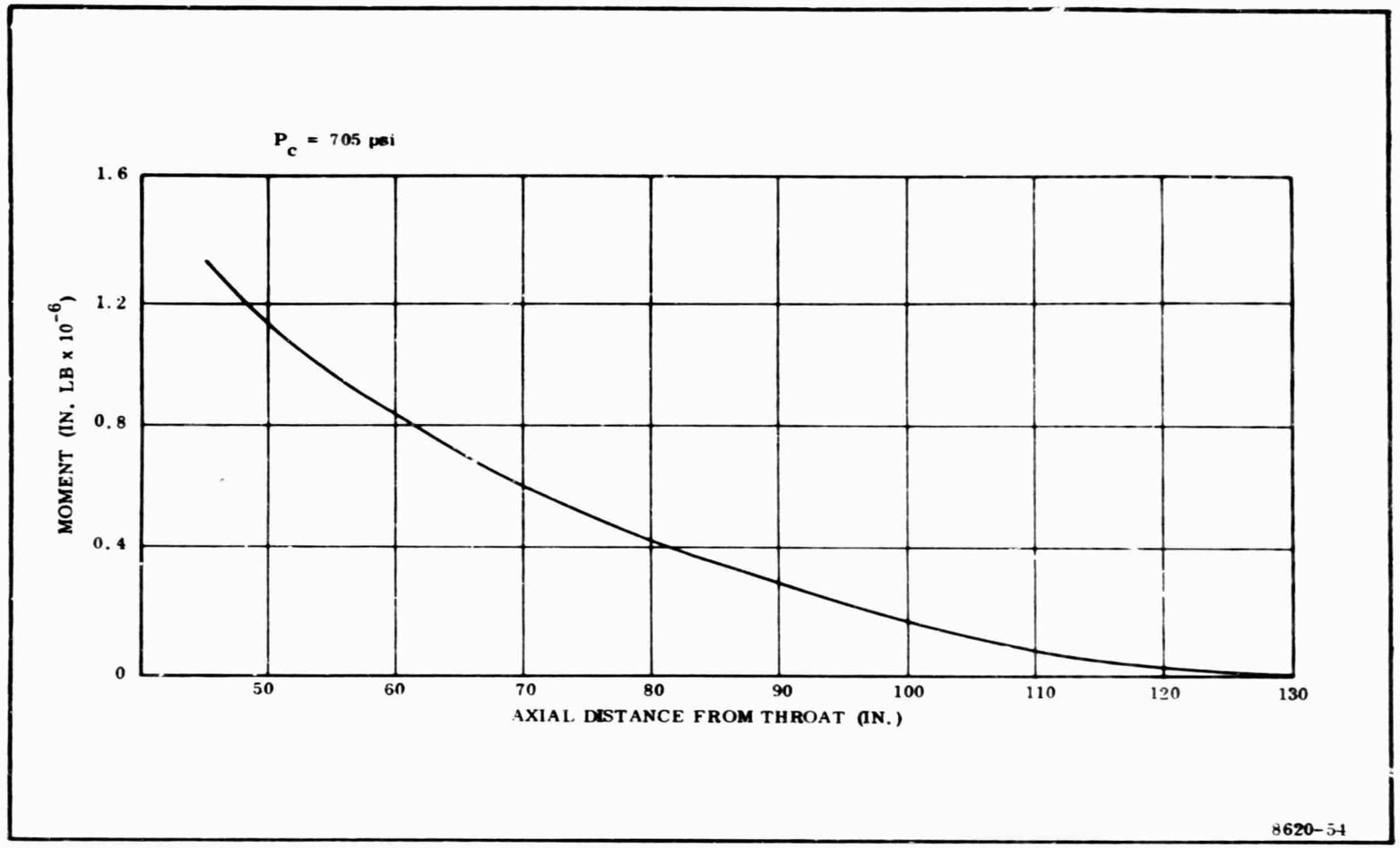

Figure 21. 156-7 Moment Distribution Due to Side Load

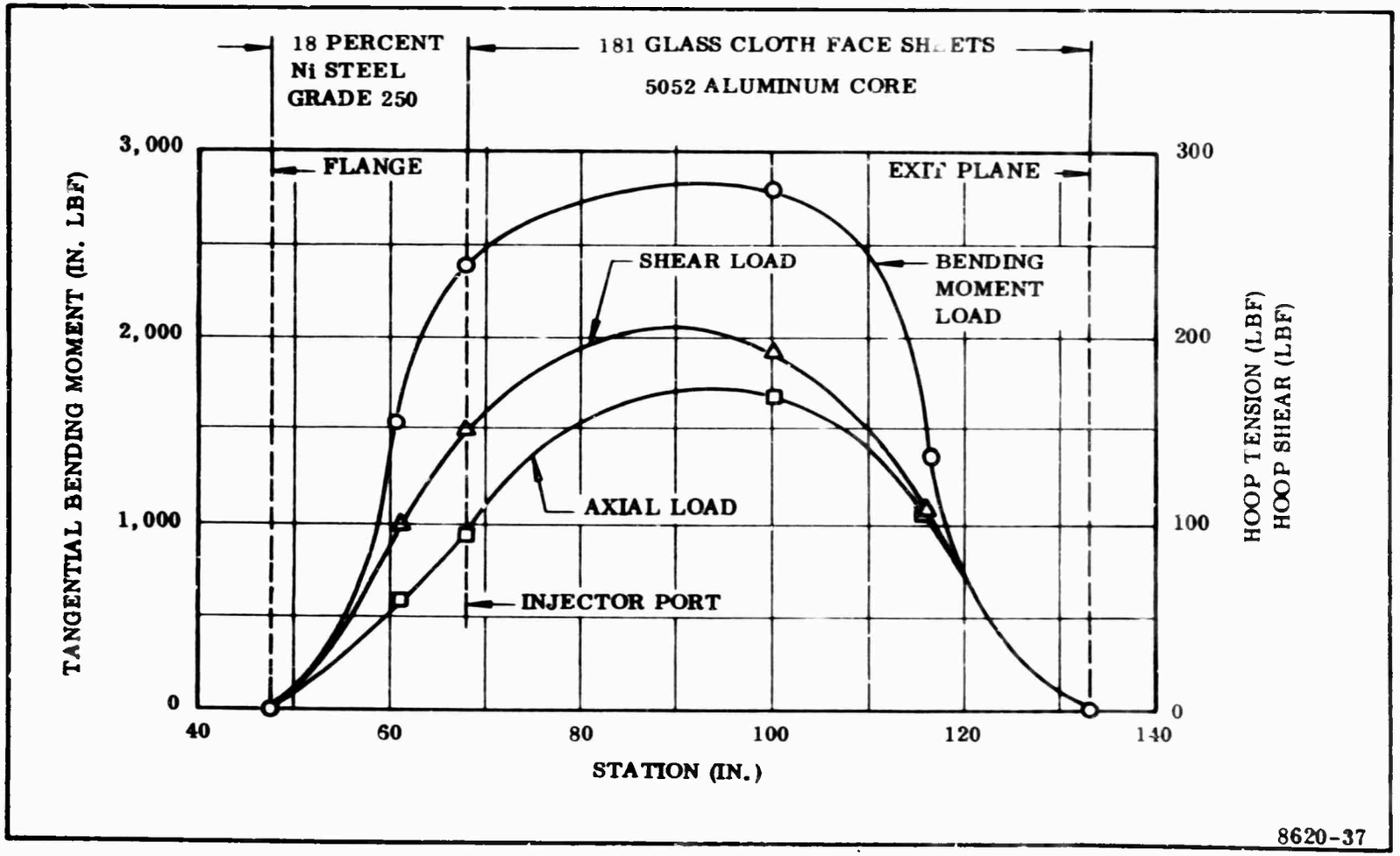

Figure 22. LITVC Tangential Moment vs Station in the Exit Cone

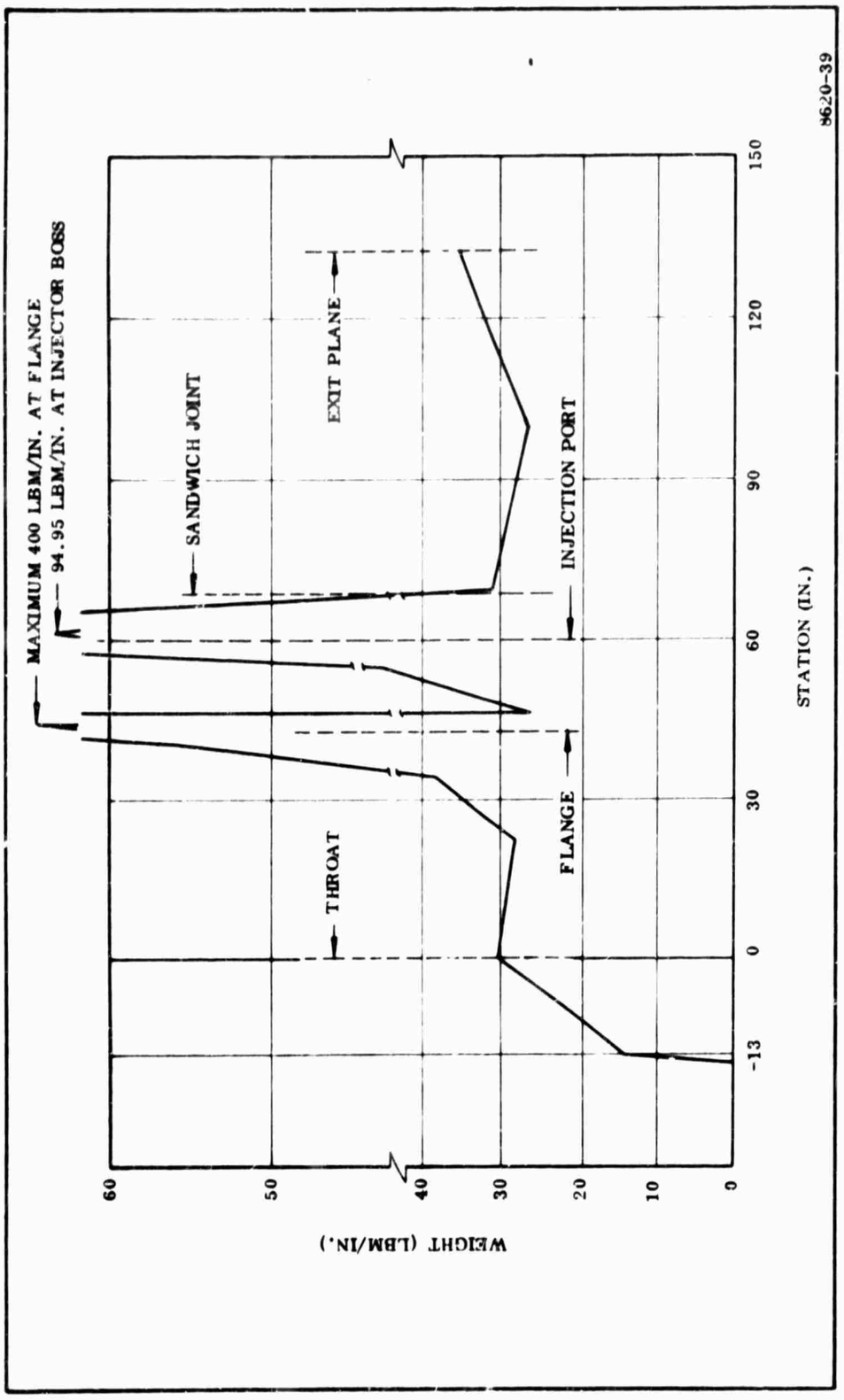

Figure 23. Weight Per Inch vs Station

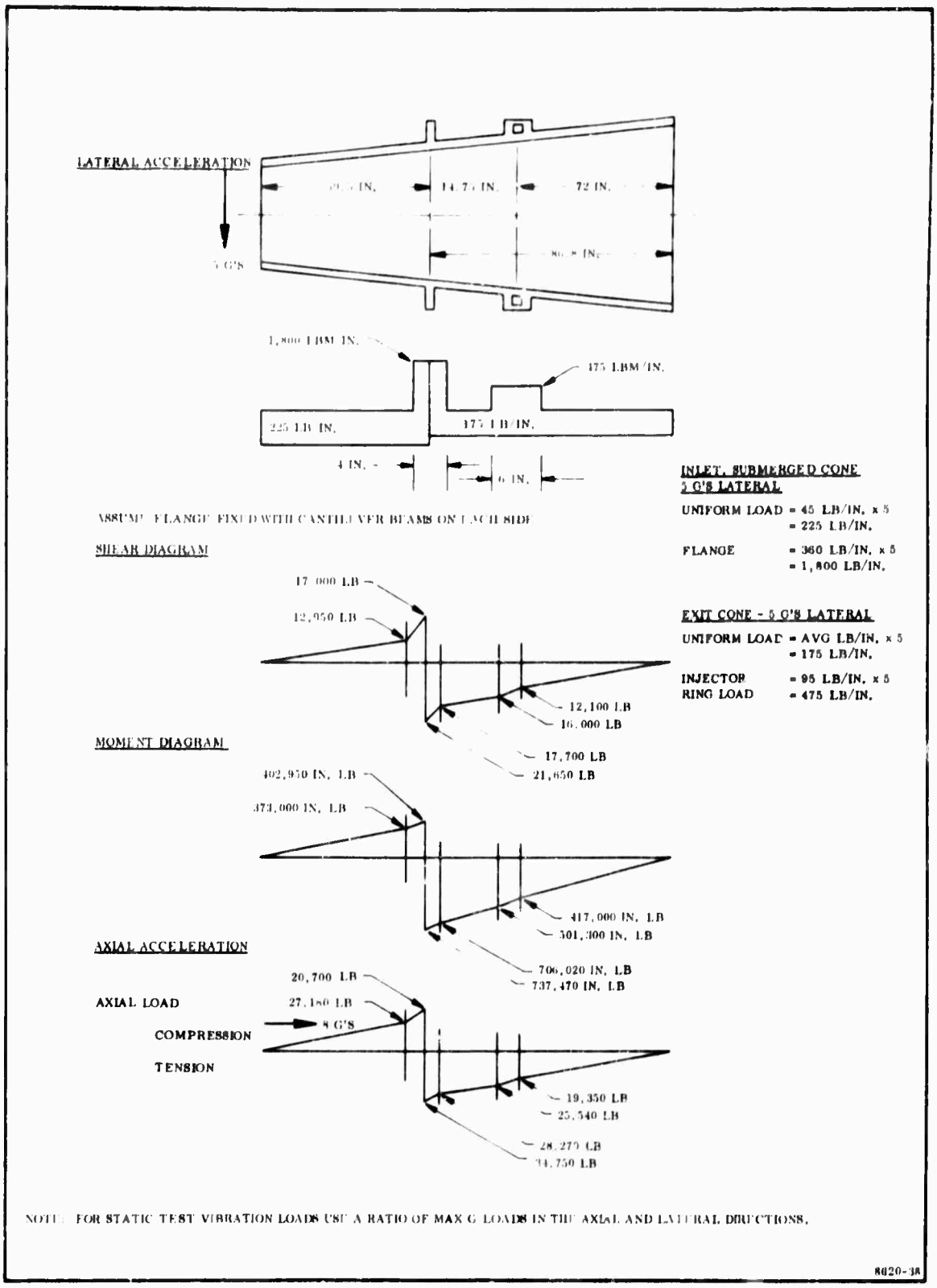

Figure 24. Flight Test Acceleration Loads

THE HEAVIEST TANK WEIGHS 700 LB (N_2O_4 TANK WET WEIGHT). FOR FLIGHT TEST CONDITIONS, 5 G'S AXIAL AND 5 G'S LATERAL ARE CONSIDERED WITH 5 G'S AXIAL AND 1.5 G'S LATERAL USED FOR STATIC TEST. THE TANKS ARE SUPPORTED AS SHOWN BELOW, 180 DEG APART.

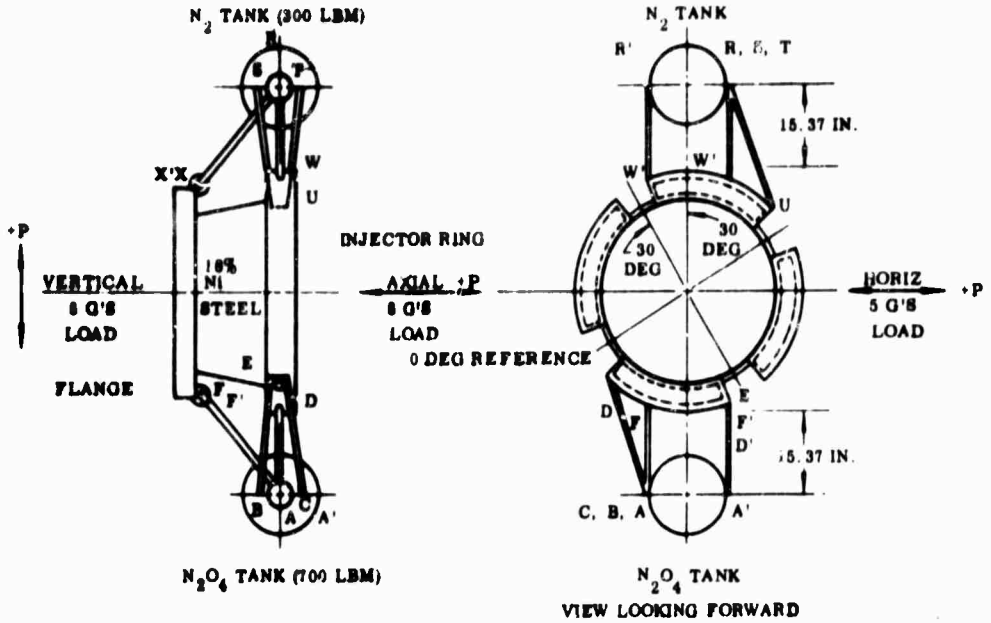

LOAD CONDITION			N_2O_4 TANK STRUTS						
AXIAL	VERT	HORIZ	AD	A'D'	BE	CE	AF	A'F'	
+5.0	+5.0	+5.0	-12,176	-6,123	+3,496	+3,496	+5,191	+5,191	
+5.0	-5.0	+5.0	- 8,663	-2,623	+3,496	+3,496	+5,191	+5,191	
+5.0	-5.0	-5.0	+ 3,437	-2,623	-3,496	-3,496	+5,191	+5,191	
+5.0	+5.0	-5.0	- 63	-6,123	-3,496	-3,496	+5,191	+5,191	
-5.0	-5.0	-5.0	+10,533	+4,490	-3,496	-3,496	-3,240	-3,240	

LOAD CONDITION			N_2 TANK STRUTS						
AXIAL	VERT	HORIZ	RW	R'W'	RU	TU	RX	R'X'	
+5.0	+5.0	-5.0	-4,787	-2,291	-1,442	-1,442	+2,172	+2,172	
-5.0	-5.0	+5.0	+4,106	+1,890	+1,442	+1,442	-1,358	-1,358	
+5.0	+5.0	+5.0	+1,382	-1,173	-1,442	-1,442	+2,172	+2,172	

NOTES:

1. UNDERLINED LOADS ARE MAXIMUM TENSION AND COMPRESSION FORCES
2. + STRUT LOAD IS IN TENSION
3. -STRUT LOAD IS IN COMPRESSION

8620-41A

Figure 25. LITVC Tank Strut and Nozzle Loads (Flight Test Condition)

TO SIZE THE INJECTOR RING FOR THE TANK LOADS THE STRUT LOADS WERE SIMULATED BY A TANGENTIAL BENDING MOMENT, RADIAL LOAD AND HORIZONTAL LOAD IMMEDIATELY UNDER THE TANK ON ITS CENTERLINE. THE RESULTING CONSERVATIVE APPROXIMATION OF THE TANK LOADS ON THE NOZZLE ARE ILLUSTRATED BELOW. SINCE THE LOADS AT 0 DEG DO NOT AFFECT THE STRESS AND DEFLECTION AT 180 DEG THE MAXIMUM CASE IS SHOWN FOR EACH TANK.

MOMENT, RADIAL, TANGENTIAL LOADS

LOAD AT T

F_1 = 300 LB (5 G'S) = 1,500 LB

F_3 = 2(1,173) = 2,346 LB

M_1 = 1,500 LB (15.37)
= 23,000 IN. LB

LOAD AT Z

F_2 = 700 LB (5 G'S)
= 3,500 LB.

F_4 = 2(6,123) = 12,246 LB

M_2 = 3,500 LB (15.37)
= 53,700 IN. LB

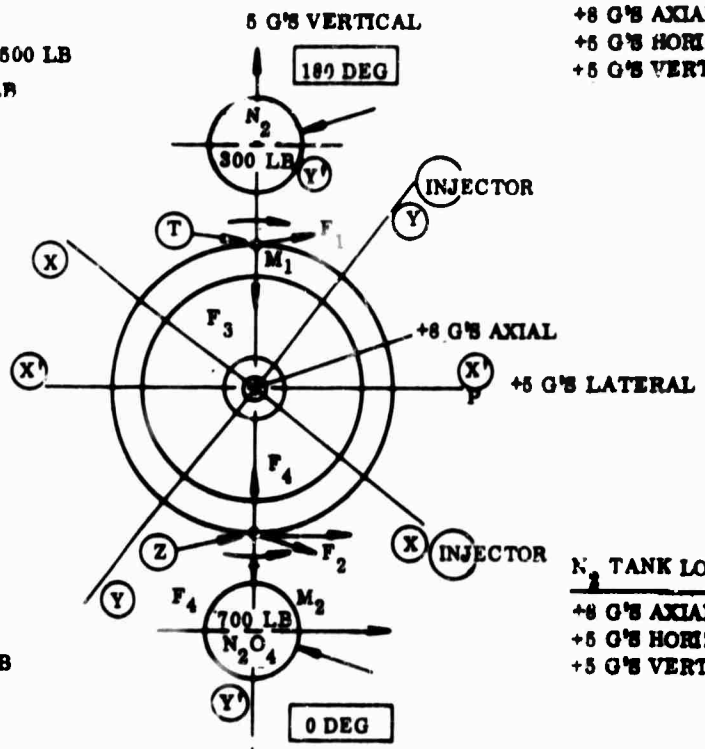

N_2O_4 LOAD CONDITION

+8 G'S AXIAL
+5 G'S HORIZONTAL
+5 G'S VERTICAL

N_2 TANK LOAD CONDITION

+8 G'S AXIAL
+5 G'S HORIZONTAL
+5 G'S VERTICAL

FLIGHT TEST CONDITION*

*FOR STATIC TEST CONDITION USE A RATIO TIMES FLIGHT TEST CONDITION

9216-6

Figure 26. Simulated Tank Loads on Igniter Ring

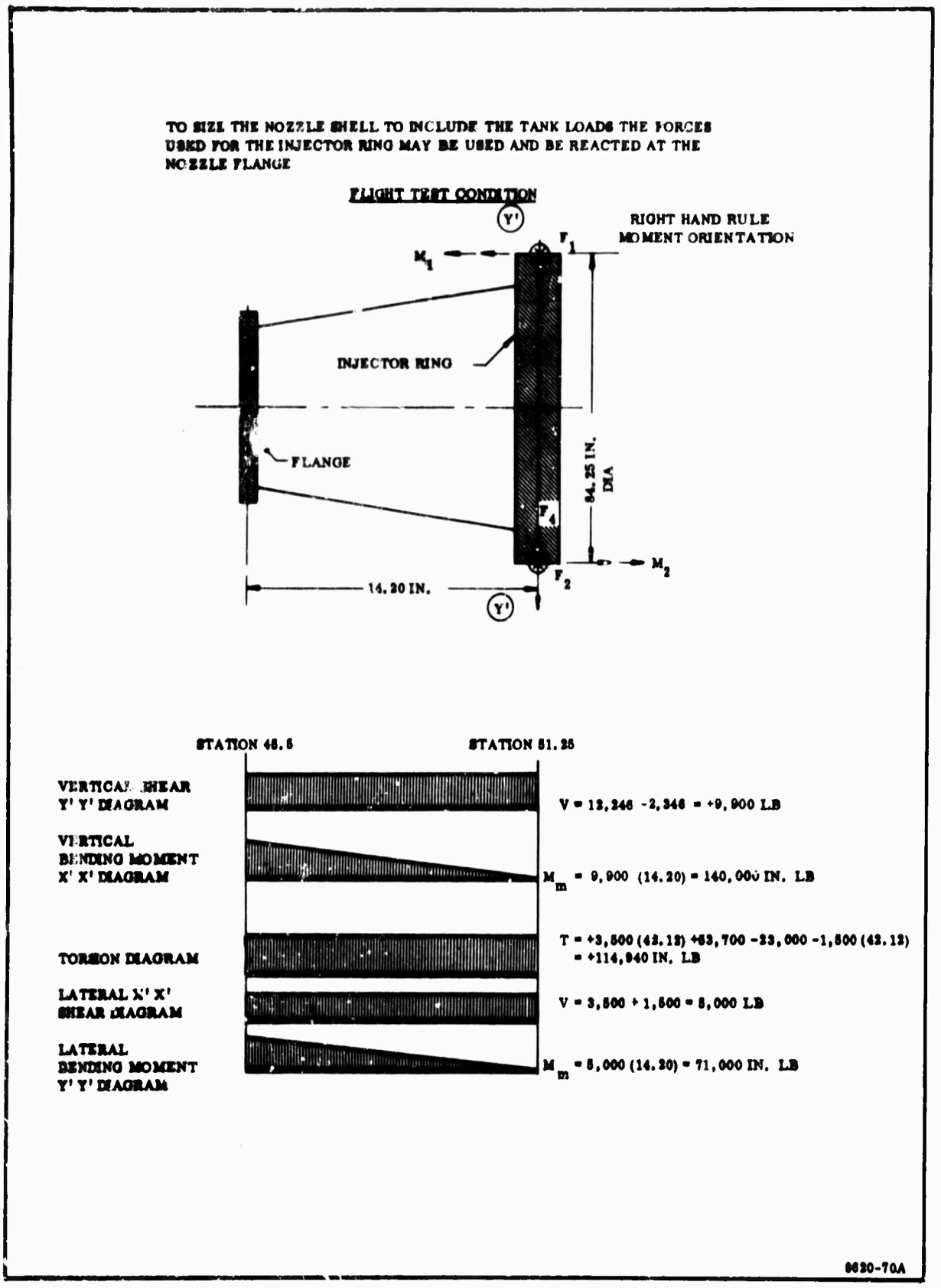

Figure 27. Simulated Tank Loads on Flange Shell

Static Test at Utah Conditions

Internal Motor Pressure	MEOP (psi) = 705
LITVC Pressure Distribution	3.5 deg TVC at MEOP thrust
Radial Shock Loads (at ignition)	
Submerged Section	$\pm$ 60 g's for 0.25×10^{-3} sec
Flange and Injector Shell	$\pm$ 30 g's for 0.25×10^{-3} sec
Exit Section	$\pm$ 60 g's for 0.25×10^{-3} sec
Shock Load	3 g's axial
Vibration Load	1.5 g's lateral
Ambient Pressure on Nozzle and Diffuser OD	12.5 psi
LITVC System Support	

Flight Conditions for Upper Stage Motor

Internal Motor Pressure	MEOP = 705 psi
LITVC Pressure Distribution	3.5 deg TVC at MEOP thrust
Radial Shock Loads (at ignition)	
Submerged Section	$\pm$ 60 g's for 0.25×10^{-3} sec
Flange and Injector Shell	$\pm$ 30 g's for 0.25×10^{-3} sec
Exit Section	$\pm$ 60 g's for 0.25×10^{-3} sec
Acceleration Loads	8.0 g's axial
	5.0 g's lateral
Dynamic Pressure on Nozzle OD (Staging and base pressures not considered)	6.94 psi
LITVC System Support	

Figure 28. Design Conditions

2. ANALYSIS

Key areas in the nozzle have been analyzed to determine maximum stresses and deformations using the ultimate loads and calculated temperature distributions throughout the nozzle (See Section IV-3). A summary of this analysis is presented in Figure 29, which presents the type of stress at various nozzle sections with the corresponding factor of safety and calculated deformation. A minimum factor of safety of 1.25 is maintained throughout the nozzle. A percent deformation band ($\Delta R/R$) is allowed along the length of the nozzle with 0.4 percent at the throat and 0.5 percent at the exit plane.

The nozzle wall, from the start of the hyperbolic spiral inlet through the throat to the exit cone, is subjected to erosion and charring of the reinforced plastic liner. The insulation and erosion liner design provides a sufficient material thickness to maintain the structural glass cone at room temperature and provides a sufficient material thickness for erosion in the throat and exit cone (Figures 30 and 31).

SECTION	STRESS	FACTOR OF SAFETY	DEFLECTION (IN.)	DEFLECTION PERCENT RADIUS	REFER TO PAGE
THERMAL-MECHANICAL ANALYSIS					108
Station 0.0 (throat)	Hoop	Ref. Fig	-0.0058	-0.0 [illegible]	--
NOZZLE FLANGE-CASE INTERFACE	Shear Lip	+1.27 Steel	+0.106	+0.320	112
SUBMERGED STRUCTURAL SHELL	Column Buckling	+1.91 Glass	-0.083	-0.24	125
Station 6.0	Local Hoop	+1.66 Glass	-0.067	-0.58	--
	Local Buckling	+4.03 Glass	--	--	--
Station 43.40	Local Buckling	+1.54 Glass	--	--	--
	Local Hoop	+1.93 Glass	-0.140	-0.44	--
FLANGE SHELL	Column Buckling	+ High Steel		--	137
Station 47.6	Local Buckling	+ High Steel	--	--	--
Station 54.5	Local Hoop	+ 1.60 Steel	--	--	--
	Local Stress Long.	+ High Steel	--	--	--
Station 61.25	Local Buckling	+ High Steel	--	--	--
	Local Stress Long.	+1.30 Steel	+0.103	+0.27	--
EXIT CONE SHELL	Column Buckling	+ High Glass	--	--	151
Station 65.06	Local Buckling	+ High Glass	--	--	--
	Local Hoop Stress	+2.11 Glass	+0.022	+0.07	--
Station 100.60	Local Buckling	+ High Glass	--	--	--
	Local Hoop Stress	+1.68 Glass	+0.039	+0.08	--
Station 130.30	Local Buckling	+4.45 Glass	-0.068	-0.12	--
FLANGE SHELL-EXIT CONE INTERFACE	Long. Bending	+ High	--	--	170
INJECTOR-[illegible] SUPPORT RING	Hoop Bending	+ High Steel	-0.011	+0.03	176
ATTACHMENTS					--
Injector Ring					--
Screws	Shear	+1.95	--	--	187
Sandwich and Liner					190
Pin A	Bending	+1.31	--	--	--
Pin B	Bending	+2.44	--	--	--
Case Bolts	Shear-tension	+1.29	--	--	197
Diffuser Screws	Shear	NA	--	--	197
Nitrogen Tetroxide Tank Attachments					197
Strut AF, A'F'	Tension, Shear	See Sect	--	--	--
Strut AD	Tension, Shea	+2.44	--	--	--
Strut A'D'	Tension, Shear	+1.27	--	--	--
Strut BE, CE	Tension, Shear	+2.75	--	--	--
Nitrogen Tank Attachment					211
Strut RX, R'X'	Tension, Shear	+1.25 Min	--	--	--
Strut RW	Tension, Shear	+1.25 Min	--	--	--
Strut R'W'	Tension, Shear	+1.25 Min	--	--	--
Strut SU, TU	Tension, Shear	+1.25 Min By Inspection	--	--	--
Injector Bolts	Shear, Tension Load	NA	--	--	211

Figure 29. Structural Analysis Summary

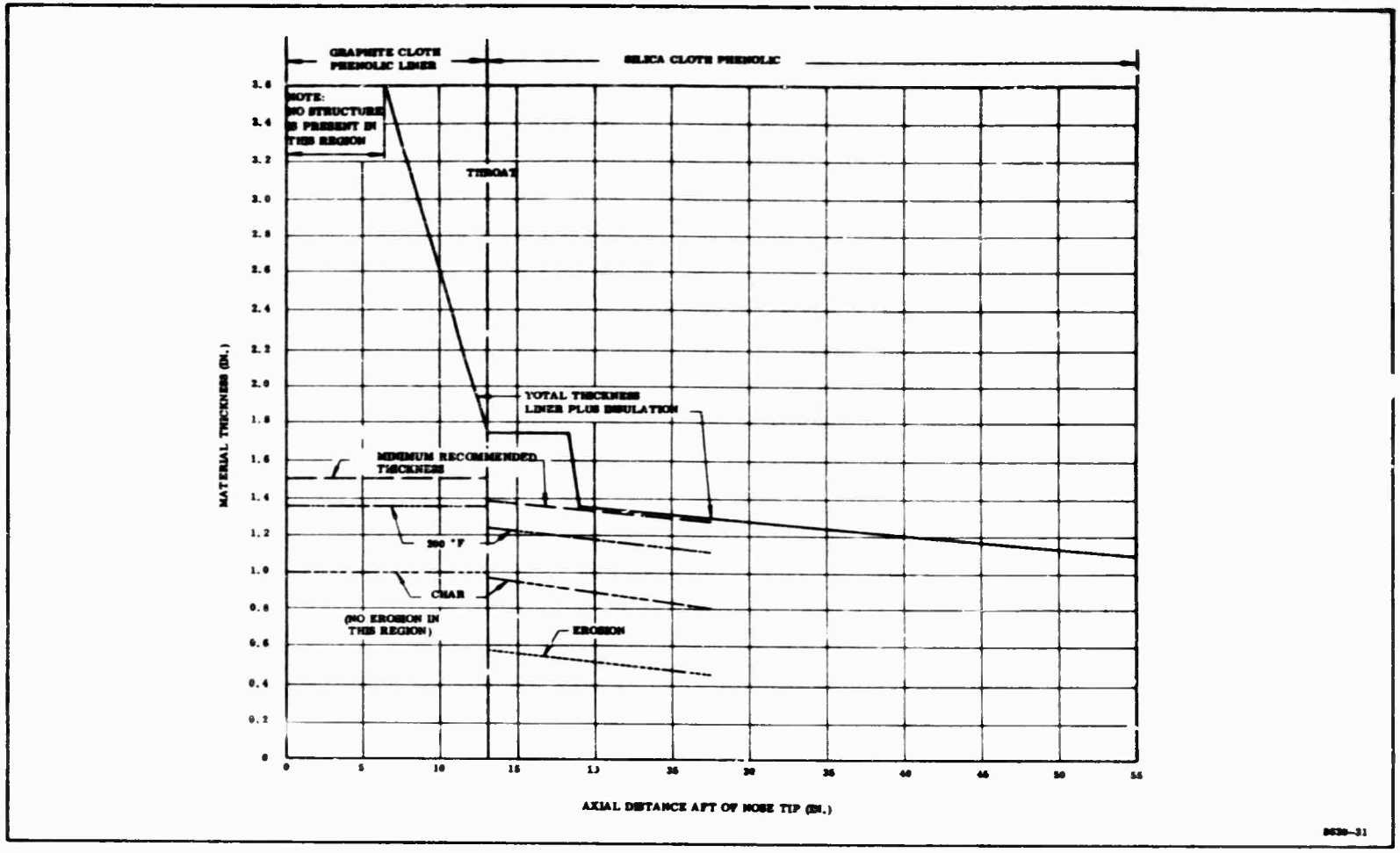

Figure 30. 156-7 Chamber Side of Nozzle Erosion and Char Prediction

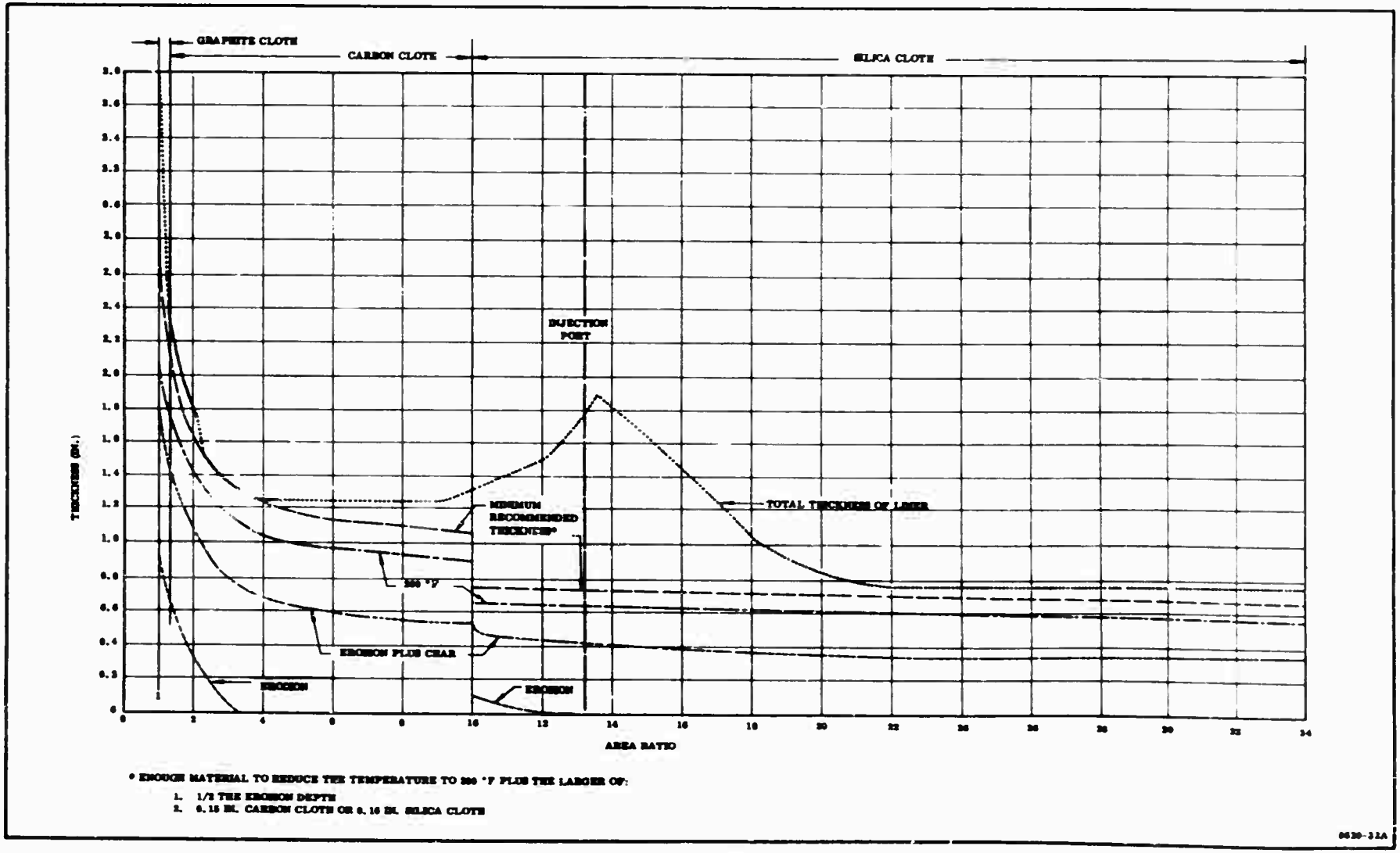

Figure 31. 156-7 Nozzle Exit (Inside Wall) Erosion and Char Prediction

SECTION IV

DESIGN ANALYSES

The nozzle must be analyzed gas dynamically, thermodynamically, and structurally to finalize design details prior to release for fabrication. These analyses are based on the design criteria, materials and their fabrication capabilities, and the static and flight test loadings.

The gas dynamic analysis establishes the submerged nose and exit cone contours, the static and flight test loadings, and the heat transfer coefficients at various stations throughout the nozzle.

The final temperature distribution and insulation thicknesses are determined from the thermodynamic analysis with the use of the above mentioned heat transfer coefficients.

The structural analysis certifies the integrity of the nozzle design and TVC system support structures with the loads and temperature distribution determined from the gas dynamic and thermodynamic analyses respectively.

1. AERODYNAMIC ANALYSIS

A gas dynamic analysis of the fixed, submerged, 156-7 nozzle was conducted to design the contour of the inlet, throat and exit cone sections necessary to develop flow conditions throughout the nozzle that will uniformly accelerate the motor exhaust gases.

The analysis included the following areas: (1) selection and analysis of the exit cone contour, (2) determination of the configuration for the subsonic portion of

the nozzle (inlet and throat approach), and (3) nozzle aerodynamic loads affecting the nozzle structure. The following motor criteria were used in the analysis.

1. Motor web time = 107 seconds
2. Motor operating pressure = 550 psia
3. Propellant = TP-H8163

The initial throat diameter is 20.0 inches. For this design study the nozzle throat erosion rate was calculated to be 11.5 mils/sec based on the simplified Bartz heat transfer analysis. This throat erosion rate was held constant.

a. Exit Cone--The analysis considered the exit cone contour and the Mach number and heat transfer coefficient to assist in the thermodynamic analysis.

(1) Contour--The internal nozzle contour of the 156-7 nozzle was designed using a Thiokol computer program with the method of characteristics, a solution using a set of hyperbolic partial differential equations.

The boundary conditions around the region of integration are determined by the following assumptions.

1. A three-dimensional point-source flow exists from some point in the nozzle to the point of inflection of the nozzle.
2. The three-dimensional point source is considered to be a distance r* from the sonic surface for which M = 1.
3. The specific heat ratio is constant in the flow field.

4. The flow is axially symmetric, nonviscous, irrotational, and isentropic.

In addition, the direction of the streamline at the inflection point is specified and Prandtl-Meyer flow is assumed along the point-source boundary. The contour is determined by the condition that the slope of the contour at some computed point must be equal to the slope of the streamline at that point.

The variables in the contour optimization are initial divergence angle, length, and expansion ratio. The expansion ratio and length were determined during the preliminary tradeoff studies.

This envelope-contour required to meet the RFP performance requirements was determined as part of the overall motor configuration selection. This selection involved a tradeoff of nozzle weight, motor thrust, and envelope.

The only remaining independent variable for contour optimization was initial divergence angle. A series of contours was developed and the performance maximized with initial divergence angle. The performance is calculated by a series of empirical efficiency curves on each of the primary variables.

The selected contour has an initial divergence angle of 25 degrees. The contour wall turns back to an exit angle of 13 deg within a throat to exit length of 13.5 throat radii. An external arc equal to 0.6 throat radii blends the throat into the initial divergence angle. This small arc minimizes weight of the blending section while providing for smooth transitory flow.

(2) Mach Number and Heat Transfer Coefficient--The exit contour Mach number and heat transfer coefficient were calculated from a characteristics net in

the exit. This calculation also developed the wall pressure profile for the load calculation. The exit cone Mach number variation is shown in Figure 32. The heat transfer coefficient variation in the exit cone is shown in Figure 33.

The subsonic Mach number variation was developed from the nose design analysis presented in the next section. The subsonic Mach number for the four burning times considered in the design analysis is presented in Figure 34.

The heat transfer coefficient profile corresponding to the Mach number profile is presented in Figure 35. Eroded configuration data were developed during the nose design and are included here. Eroded exit cone data were not necessary for design but will be presented in the final design report.

b. Nose Contour--An aerodynamic study was conducted to design the contour of the entrance section or nose of the submerged nozzle for the 156-7 motor and to develop the flow conditions throughout the nozzle and motor. The objective of the design study was to design a minimum size, acceptable performance, nozzle inlet contour to operate with the motor criteria.

The nose of a submerged nozzle must provide a uniform transition of the propellant combustion products from the motor to the nozzle throat. A uniform transition is required to:

1. Assure a predictable throat erosion rate;
2. Assure a high nozzle discharge coefficient;
3. Provide uniform nozzle nose erosion such that conditions 1) and 2) will be fulfilled throughout motor burning time.

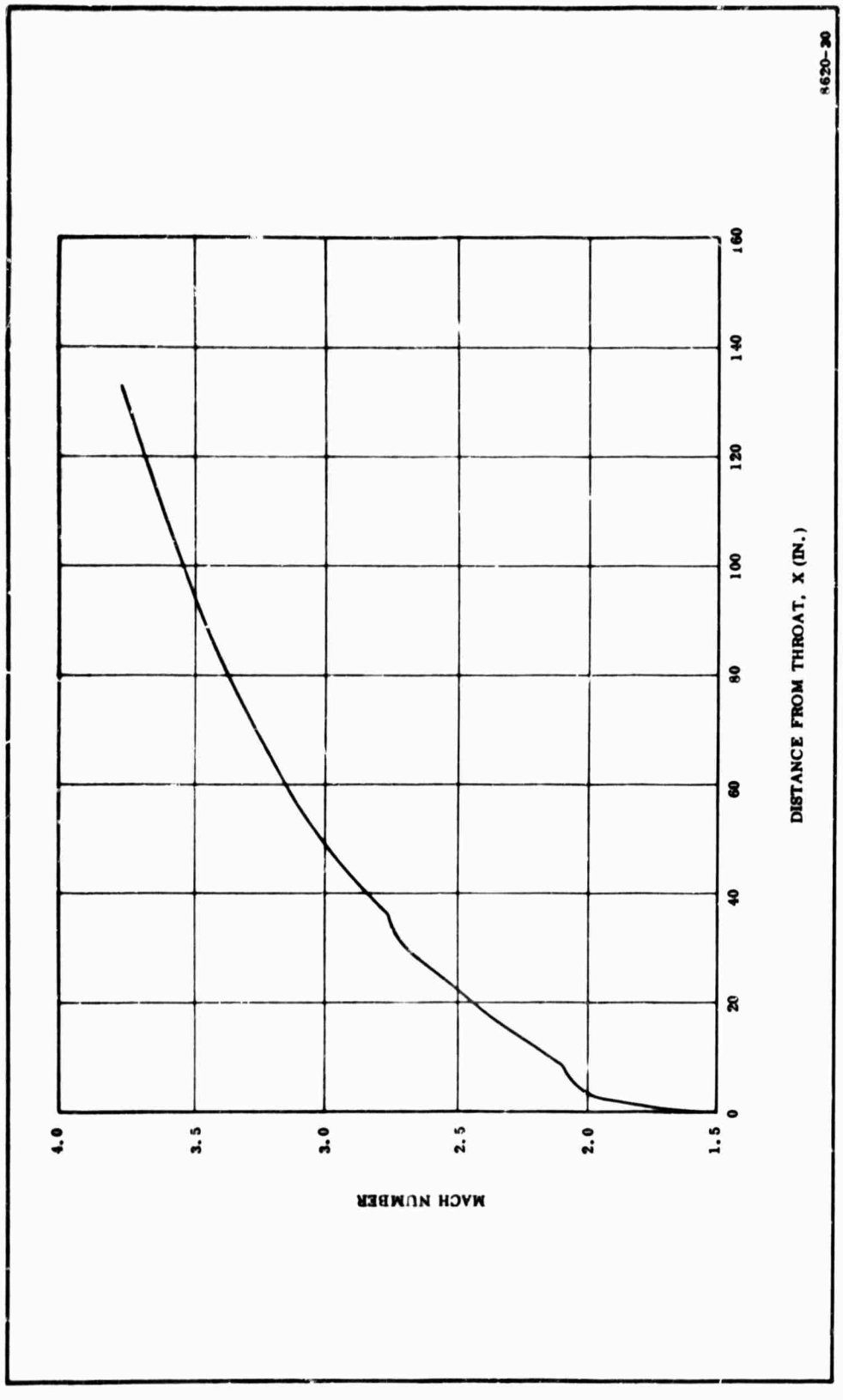

Figure 32. 156-7 Exit Cone Mach Number Profile

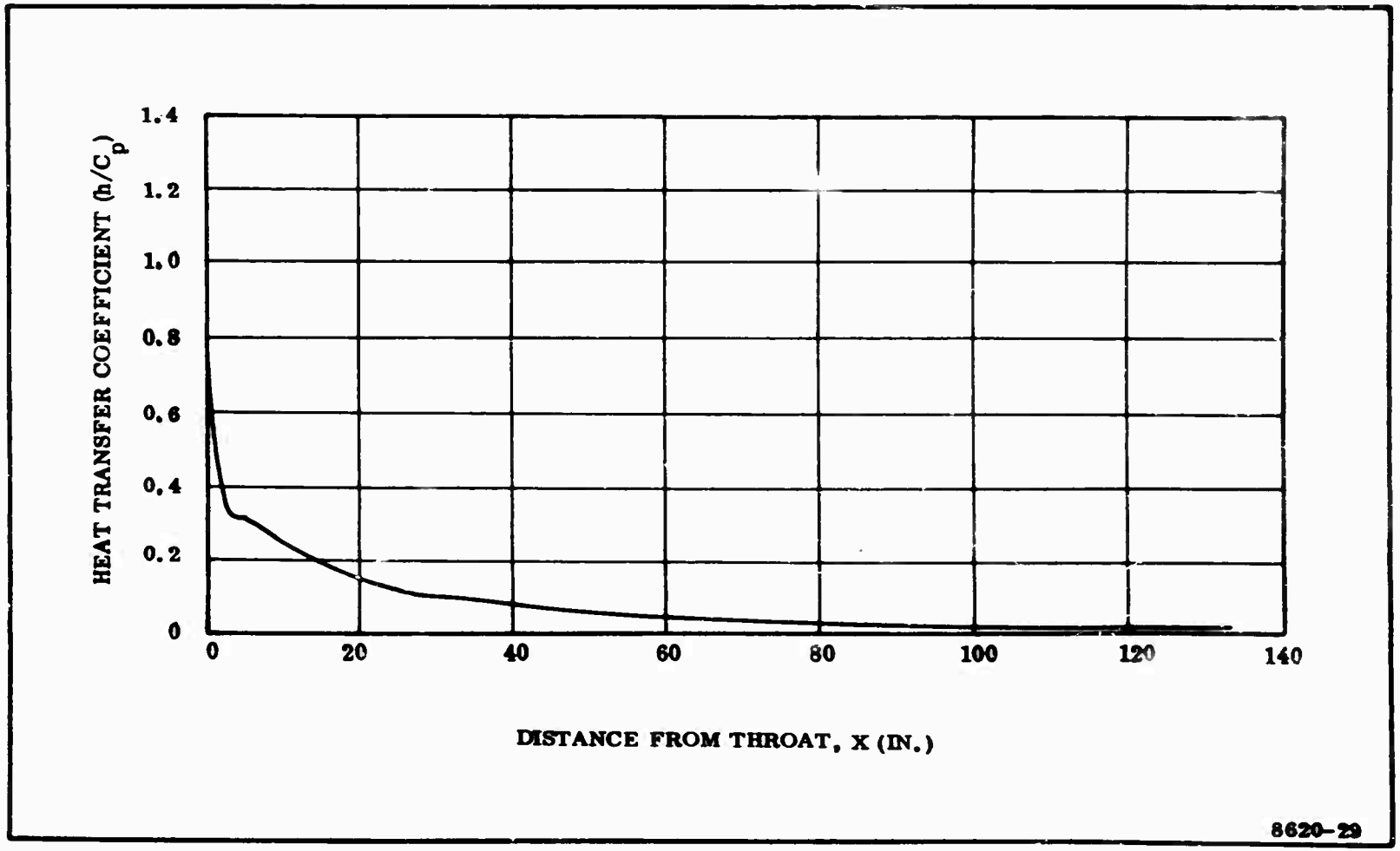

Figure 33. 156-7 Exit Cone Heat Transfer Coefficient Variation

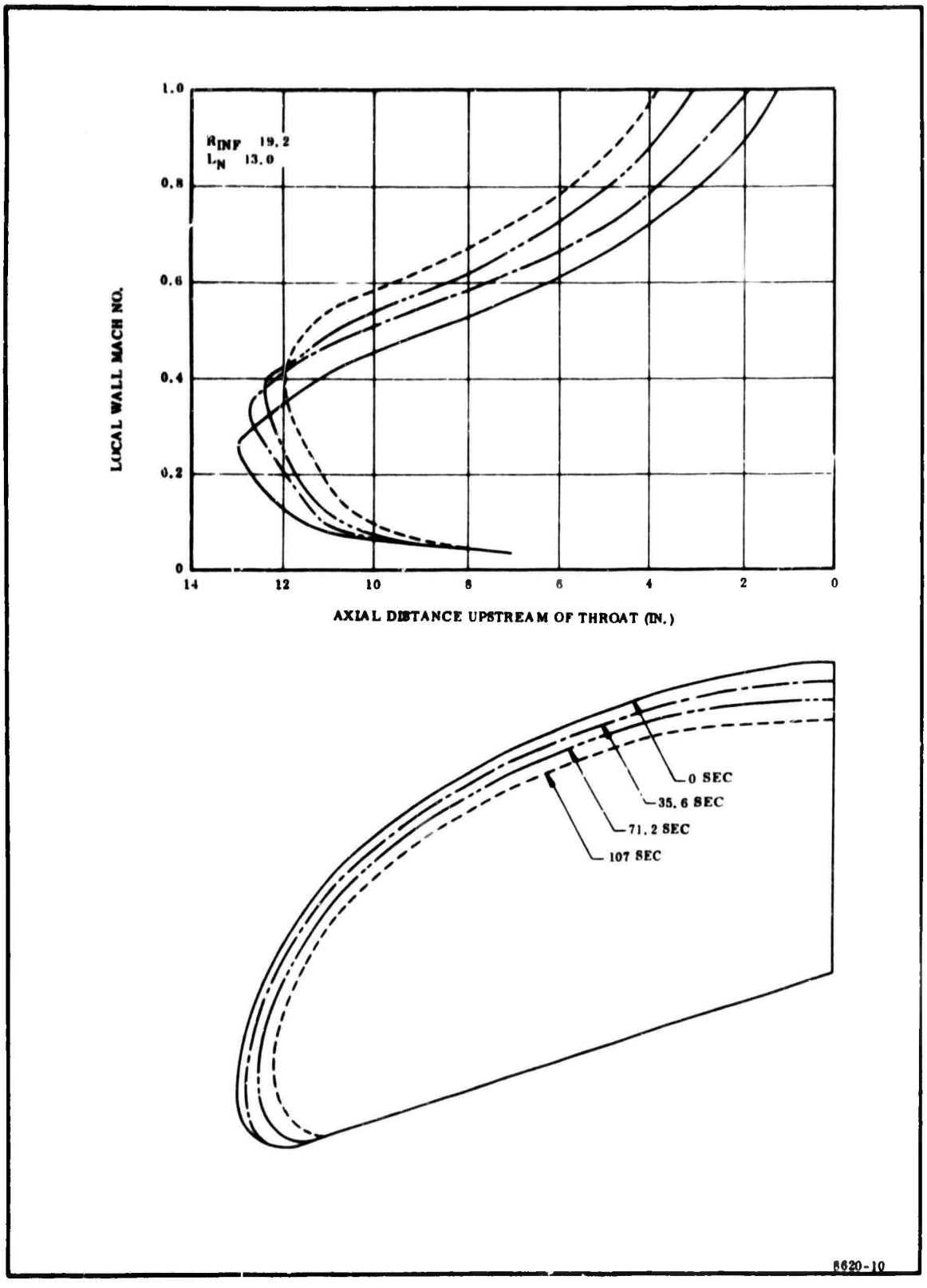

Figure 34. 156-7 Local Wall Mach Number vs Axial Location in Nozzle (R_{INF} = 19.2 In. ; L_N = 13.0 In.)

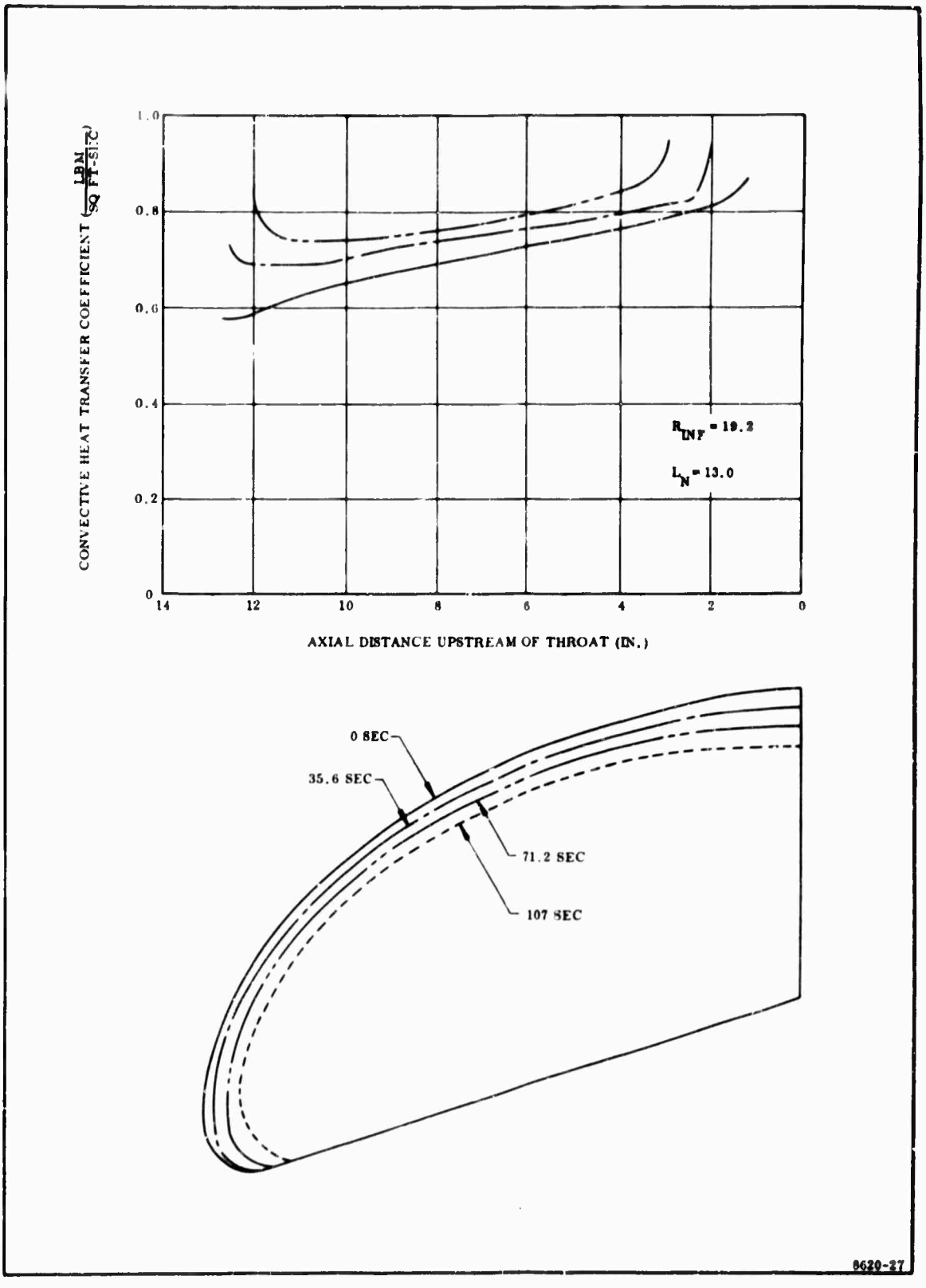

Figure 35. 156-7 Convective Heat Transfer Coefficient vs Axial Location in Nozzle (R_{INF} = 19.2 In.; L_N = 13.0 In.)

A minimum size nose, compatible with the above conditions is also required to aid in providing a minimum cost and weight nozzle.

Design studies conducted by Thiokol have indicated that the design objectives can be attained using a hyperbolic spiral for the contour of the nozzle nose. This hyperbolic spiral is blended into the throat by a circular arc (Figure 36). The length of the nozzle nose from the nose tip to the throat (L_N) and the width of the nozzle nose from the nozzle centerline to the nose tip must be determined for each nozzle application (R_{INF}), however.

Previous detailed design analyses of submerged nozzles using graphite cloth in the throat region indicated that the minimum nose length required was given approximately by the expression:

$$L_N = 1.1\, R_T + \epsilon'_t\, (t_w)$$

where

L_N = length of nose from tip to throat (in.)

R_T = nozzle throat radius (in.)

ϵ'_t = erosion rate at the throat (in./sec)

t_w = motor web time (sec)

and the minimum radius from the nozzle centerline to the nose tip was approximated by:

$$R_{INF} = 1.6\, (R_T + \epsilon'_t\, t_w)$$

Using these approximate relationships, the nose length for the 156-7 nozzle was determined to be approximately 12.0 in. and the radius from the nozzle centerline to the nose tip was determined to be 18.57 inches.

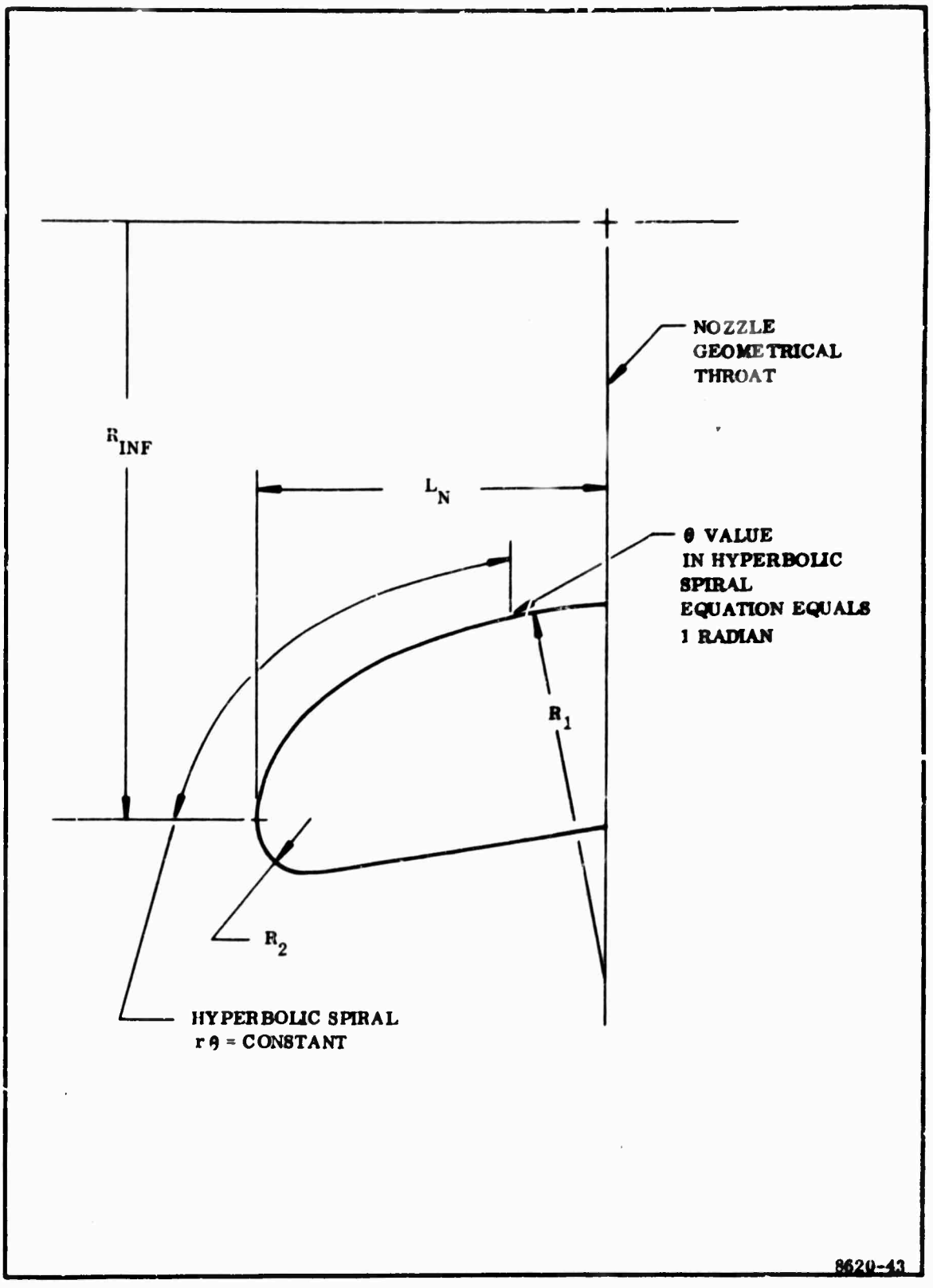

Figure 36. Hyperbolic Spiral Description

Two nozzle nose contours were evaluated simultaneously using longer nose lengths and larger nose tip radii. The complete analysis matrix is shown in Figure 37.

Results of the analysis on the nose contour 12.0 in. long with a radius from the nozzle centerline to the nose tip of 18.57 in. are shown in Figures 38 and 39 Figure 38 shows the variation of the Mach number along the nozzle nose at 0 sec, 35.6 sec (1/3 web), 71.2 sec (2/3 web), and 107 sec (web time). These Mach number profiles were calculated using the axisymmetric potential flow solution. The zero sec Mach number profile was calculated using the initial propellant configuration and the uneroded nozzle geometry. The 35.6 sec configuration shown in Figure 38 was determined using the convective heat transfer coefficient determined for the zero sec flow conditions shown in Figure 39. The material erosion rates determined from the convective heat transfer coefficients calculated for the zero sec flow condition were extrapolated for 35.6 sec to determine the total erosion depth. A new Mach profile and heat transfer coefficient variation along the nozzle nose were then calculated for the 35.6 sec eroded configuration and extrapolated to 71.2 seconds. The process was then repeated to obtain the flow properties at motor web time (107 sec).

Examination of Figures 38 and 39 indicates the following conclusions.

1. The flow Mach number along the backside of the nozzle nose is low ($M < 0.10$).
2. At zero sec the flow is smoothly accelerated about the nozzle nose tip at low Mach number ($M \approx 0.30$).

CONFIGURATION	NOSE LENGTH (IN.)	RADIUS FROM NOZZLE CENTERLINE TO NOSE TIP (IN.)
1	12.00	18.57
2	13.00	19.20
3	13.80	19.80

Figure 37. Analysis Matrix

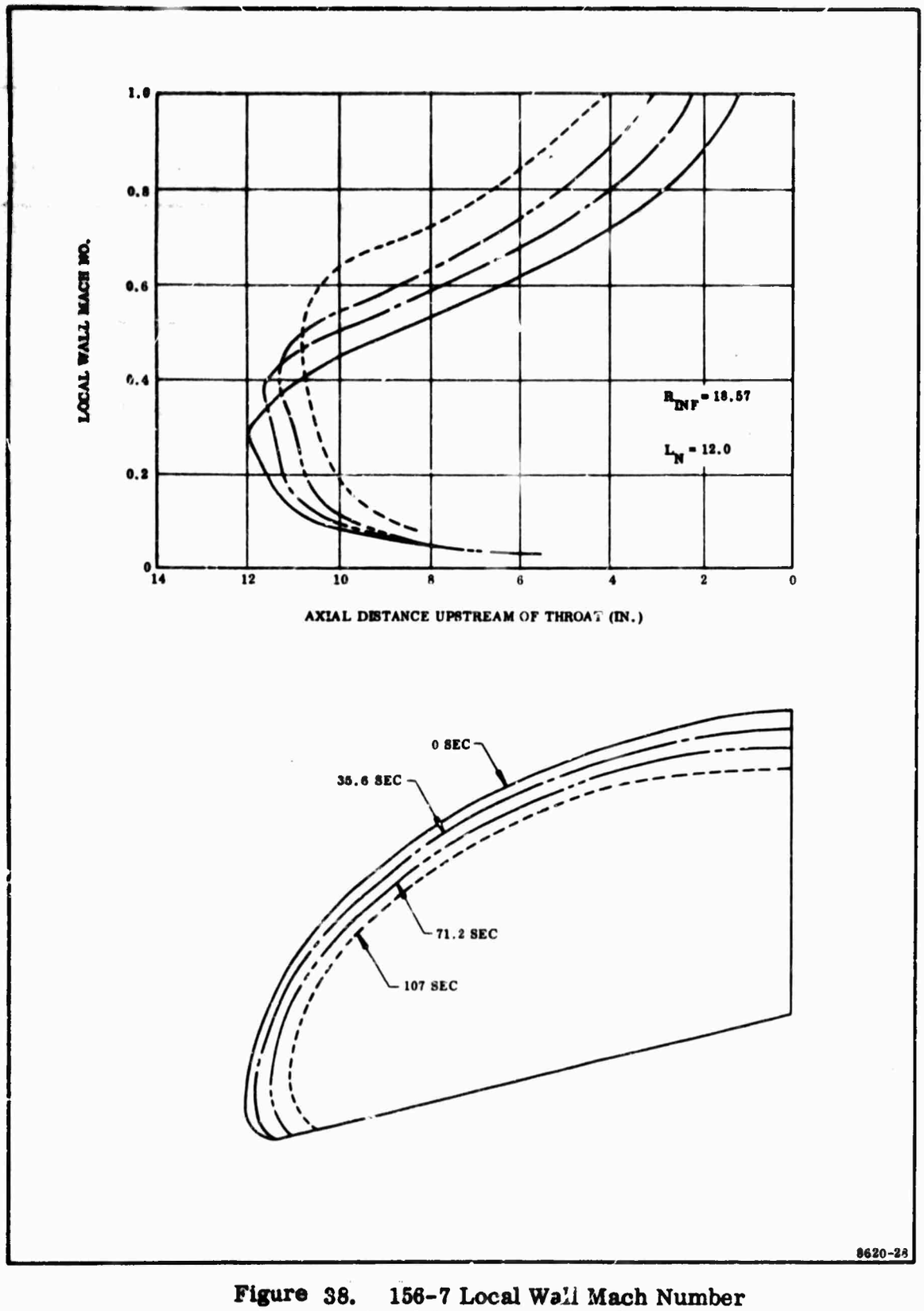

Figure 38. 156-7 Local Wall Mach Number vs Axial Location in Nozzle (R_{INF} = 18.57 In.; L_N = 12.0 In.)

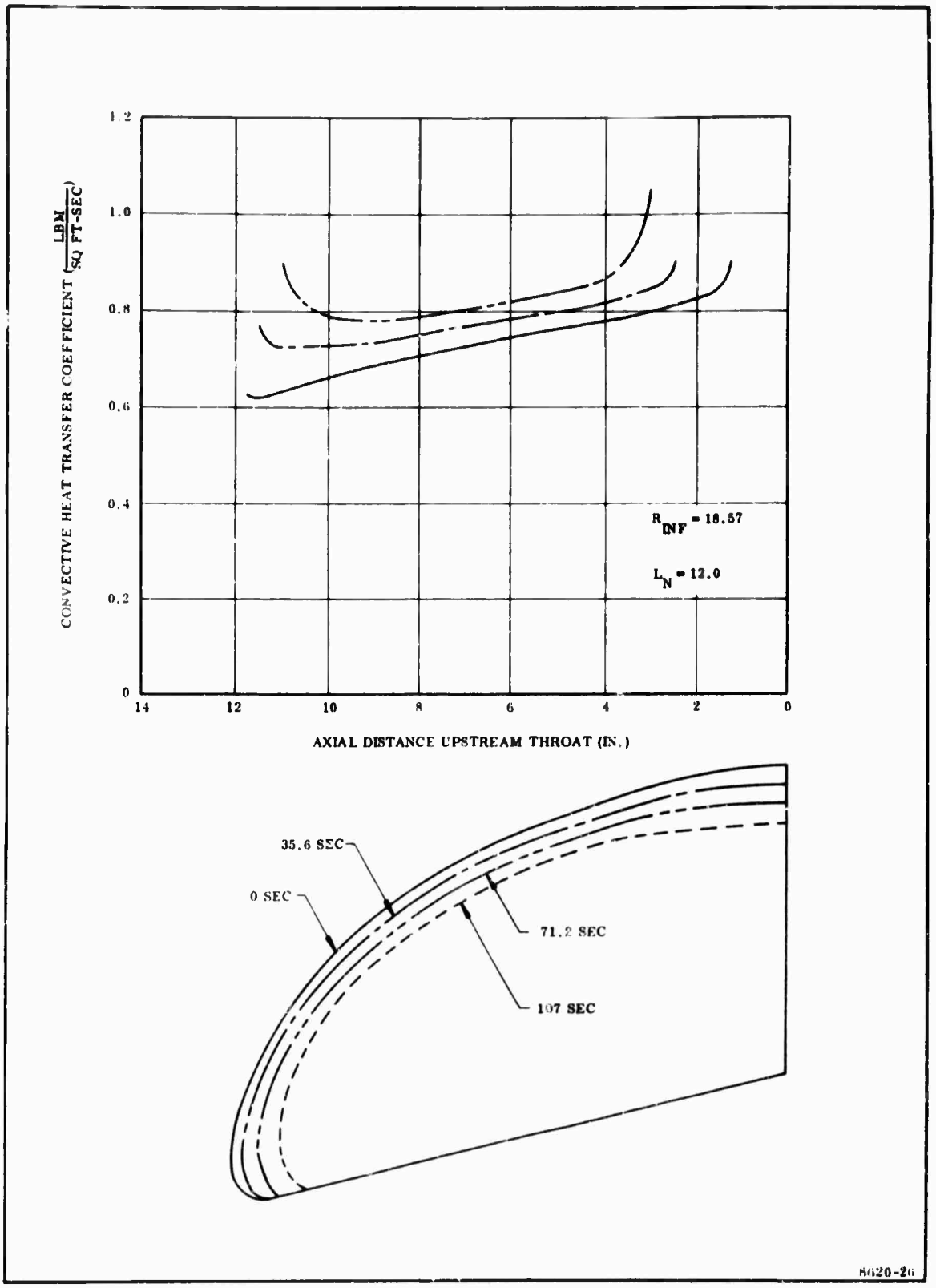

Figure 39. 156-7 Convective Heat Transfer Coefficient vs Axial Location in Nozzle (R_{INF} = 18.57 In.; L_N = 12.0 In.)

The flow then accelerates uniformly along the wall to a point approximately 1 in. upstream of the geometrical throat at which time it reaches Mach 1.

3. As motor burning progresses, the Mach number around the tip of the nozzle increases and the point at which sonic velocity is reached moves upstream along the nozzle nose.
4. At 107 sec of motor burning, the flow Mach number at the nose tip is high (M = 0.5).
5. The average convective heat transfer coefficient in the nozzle throat area is approximately 1.00. This value of heat transfer coefficient will produce a throat erosion rate of 10.3 mils per second. For this analysis, however, the throat erosion rate of 11.5 mils/sec was used to assure reliability of the design.

The Mach number variation along the 13.0 in. long nose is shown in Figure 34. These Mach numbers also were determined using the axisymmetric potential flow analysis. The convective heat transfer coefficient variation along this nose design is shown in Figure 35.

Comparison of the Mach number variations produced by this nose design during motor operation with those of the 12.0 in. nose (Figure 38) indicates that

the larger nose reduces the flow Mach number at the tip of the nose. In this area of motor web time the Mach number is reduced from approximately 0.6 to 0.4.

The average convective heat transfer coefficient in the throat of the 13.0 in. long nozzle is reduced from that calculated in the 12.0 in. long nozzle. The average value is approximately 0.95 which will result in a throat erosion rate of 9.75 mils/sec compared to 10.5 mils/sec in the 12.0 in. long design.

The Mach number and convective heat transfer coefficient variations along the 13.8 in. long nose design are shown in Figures 40 and 41. The flow is again smoothly accelerated around the nose into the throat. This nose does not significantly reduce the Mach number at the nose tip from that produced in the 13.0 in. long nose. The throat convective heat transfer coefficient is reduced, however, to an average value of approximately 0.9 over motor burn time, which would result in a throat erosion rate of 9.0 mils per second.

The nose contour recommended for the 156-7 nozzle is 13.0 in. long with a radius from the nozzle centerline to the nose tip of 19.2 inches. This contour was selected in the following manner.

The three designs subjected to detailed analysis all produced a smooth acceleration of flow from the backside of the nozzle nose, around the nose tip to the nozzle throat. The 12.0 in. long nose, because of nozzle erosion, produces a high flow Mach number about the tip of the nozzle nose, at motor web time. This high acceleration will result in thinning of the boundary layer with significant increases in nose heating and erosion. This effect is undesirable. The 13.0 in.

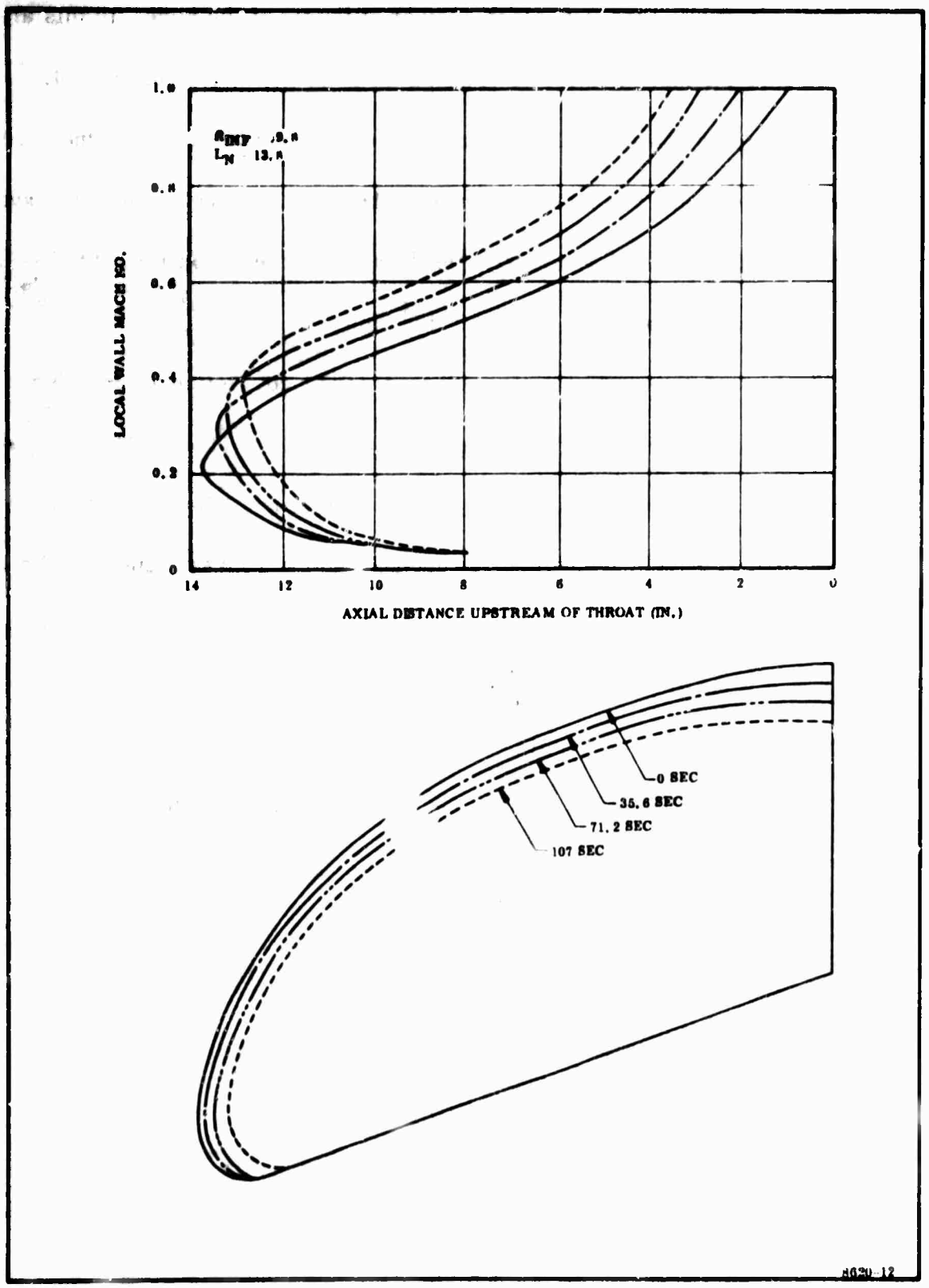

Figure 40. 156-7 Local Wall Mach Number vs Axial Location in Nozzle (R_{INF} = 19.8 In.; L_N = 13.8 In.)

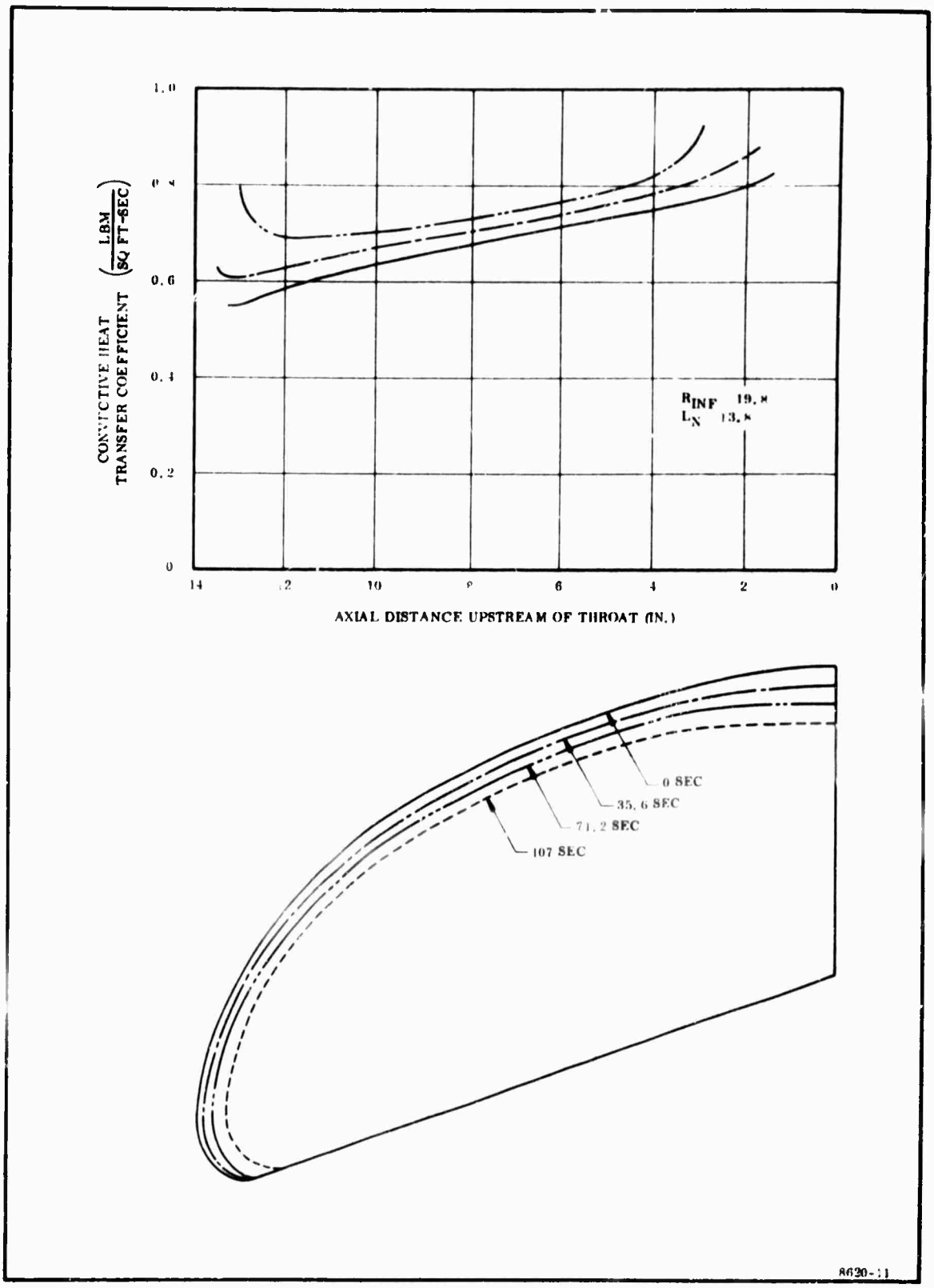

Figure 41. 156-7 Convective Heat Transfer Coefficient vs Axial Location in Nozzle (R_{INF} = 19. 8 In. ; L_N = 13. 8 In.)

long nose reduces this Mach number of turning on the nose tip approximately 20 percent from 0.50 to 0.40.

The Mach number on the nose tip of the 13.8 in. nose is not significantly changed from the 13.0 in. nose. Although the nozzle throat erosion rate would be reduced to 9.0 mils/sec, in the 13.8 in. nose from the 9.75 mils/sec rate obtained with the 13.0 in. nose, this change was not considered significant enough to warrant the increased nose size.

Therefore, because of the desirable nose tip flow properties on the 13.0 in. long nose compared to the 12.0 in. nose, the 13.0 in. nose contour was selected.

c. Aerodynamic Nozzle Loads--To assist with the structural analysis of the 156-7 nozzle, the following items were developed.

1. Internal wall pressure.
2. Axial blowout load.
3. LITVC wall pressure, transverse shear, and longitudinal bending moment.
4. Injector reaction ring load.

Figures illustrating these loads are in Section III. The analysis used to obtain these loads is explained in the following paragraphs.

(1) Wall Pressure--The internal pressure distribution is shown in Figure 14. Pressures in the subsonic region were determined using a subsonic potential flow solution programed for the IBM 7040 computer and were developed as part of the nose design. The wall pressures in the supersonic flow region were calculated

using an axisymmetric method of characteristics program. Ambient sea level pressures were assumed acting on the external surface.

(2) Axial Load--The loads acting on the nozzle were determined by integrating the internal and external wall pressures. Since the pressures are assumed to be axisymmetric in the undisturbed stream, the resultant load acting on the nozzle without liquid injection will be in the axial direction. The following equation was used to determine the axial load·

$$F_A = \int_0^{2\pi} \int_{r_1}^{r_2} Pr d\theta \, dr$$

Integration of these pressures was performed from the exit forward to the nose in incremental steps such that the axial load acting aft of any given point along the nozzle axis can be determined. This axial load vs axial location is plotted in Figure 15.

(3) LITVC Wall Pressure--The nozzle loading due to liquid injection consists of the wall pressure load and the reaction load due to the momentum of the injected liquid.

Limited data are available for determining the wall pressure distribution due to N_2O_4 injection. However, the peak pressure due to injection was determined using a method developed under Contract No. AF 04(611)-9960 (See Reference 27). This pressure was assumed to act at the injection port and the pressures were assumed to vary as shown in Figures 17 and 18. The region affected by these pressures was established using data presented in Reference 28. These data also indicated that the assumption of linear pressure variations is adequate for predicting

the structural design loads. Integration of the pressures shown in Figures 17 and 18 was performed to establish the axial and transverse loading along the nozzle axis. These loads are presented in Figures 19 and 20 respectively. The bending moment distribution due to the side load is presented in Figure 21 This curve was obtained through evaluation of the moment integral at various axial locations.

(4) Injector Ring Load--The reaction load due to the momentum of the injected liquid can be written as:

$$F_R = \dot{m} V_j + (P_j - P_g) A_j$$

where:

$\dot{m}$ = mass of injectant per port = 16.8 lb/sec

V = velocity of injection, ft/sec

P_j = static pressure of injectant, psia

P_g = static pressure of gases at injection port, psia

A_j = area of injection port = 0.0029 sq ft

The velocity (V_1) was calculated using the following equation:

$$V_j = \dot{m}/C_D \quad \rho A$$

where:

ρ = fluid density, lbm/cu ft

C_D = discharge coefficient = 0.7

The calculated reaction load was 420 lb per quadrant.

2. HEAT TRANSFER AND EROSION ANALYSIS

The thermal analysis insures that adequate material is provided to allow for anticipated losses (erosion-corrosion) with enough material remaining to adequately insulate the structural parts during firing. A list of thermal and erosion analysis definitions is presented in Figure 42.

A newly developed, two-dimensional, axisymmetric, computer program which determines temperature response in ablating, charring materials was used in the analysis (Reference 23). Boundary conditions and other input required by this program are described below and are followed by a sample analysis in the throat region.

The transient temperature response of the insulation and nozzle parts is a function of the thermal properties of the material and the internal environment to which the part is subjected. The thermal properties are usually published values obtained from vendors and laboratory tests. The motor internal thermal environment is theoretically determined by the methods outlined below.

a. Definition of Motor Internal Thermal Environment--The internal thermal environment of the motor is dependent on propellant composition and pressure at which combustion occurs. With these two parameters fixed, the combustion temperature, the enthalpy, the equilibrium composition of the combustion products, and the motor performance are calculated by the IBM 7040 computer. The program used expands the gases isentropically through the nozzle and calculates the static enthalpy of the gas at prescribed locations in the nozzle. From this information

A	=	Condensed particle cross sectional area (sq cm)
A/A^*	=	Nozzle expansion ratio
C^*	=	Characteristic gas velocity (ft/sec)
C_H	=	Convective heat transfer coefficient based on enthalpy differences (lb/sq ft-sec)
D_t	=	Nozzle throat diameter (ft or in.)
g	=	Acceleration due to gravity (ft/sec^2)
i_r	=	Recovery enthalpy (Btu/lb)
i_s	=	Static enthalpy (Btu/lb)
i_t	=	Total (stagnation) enthalpy (Btu/lb)
i_w	=	Static enthalpy of the gases on the wall side of the boundary layer (Btu/lb)
L	=	Mean radiation beam length (cm)
L_e	=	Lewis number (dimensionless)
$\dot{m}$	=	Erosion rate (lb/sq ft-sec)
N	=	Particle number density (number/cu cm)
N_{r_f}	=	Recovery factor (dimensionless, the cube root of the Prandtl number)
r_c	=	Throat radius of curvature (ft)
P_c	=	Chamber pressure (psfa or psia)
P_r	=	Prandtl number (cp/k) (dimensionless)
q	=	Heat flux (Btu/ft^2-sec)
St	=	Stanton number (dimensionless)

Figure 42. Thermal and Erosion Analysis Definitions

T_g = Gas temperature

T_w = Wall temperature

α_g = Gas absorptivity

β = Blowing parameter (dimensionless)

ϵ_g = Gas emissivity

$\epsilon_{w'}$ = Effective wall emissivity

μ = Viscosity (lb/ -sec)

ρ = Gas density

σ = Boltzman's constant $\left[(0.476 \times 10^{-12} \text{ Btu/sq ft-sec } (^\circ R)^4)\right]$

ϕ = Dimensionless factor accounting for variation of gas density and gas viscosity across the boundary layer

SUBSCRIPTS

c = Chamber conditions or curvature

e = Boundary layer edge

DL = Diffusion limited

g = Gas

t = Throat

T = Total

RL = Rate limited

w = Wall

Figure 42. Thermal and Erosion Analysis Definitions (Cont)

and a suitable recovery factor (a function of the Prandtl number), the recovery enthalpy may be determined from the following relationship:

$$i_r = N_{r_f}(i_T - i_S) + i_S$$

where:

i_r = recovery enthalpy (Btu/lb)

N_{r_f} = recovery factor (dimensionless, the cube root of the Prandtl number)

i_T = total (stagnation) enthalpy (Btu/lb)

i_S = static enthalpy (Btu/lb)

The recovery enthalpy represents the potential heat available for transmission across the boundary layer to the wall. Recovery enthalpy, as well as static enthalpy, is plotted as a function of area ratio in Figure 43.

To determine the amount of heat actually transmitted across the boundary layer (by convection), the enthalpy on the wall side of the boundary layer must also be known. This is obtained by a second computer program which calculates equilibrium composition and enthalpy as a function of temperature and pressure. Computation by this program considers the effect on wall enthalpy of mass added at the surface by diffusion through the boundary layer, percolation of pyrolysis gases through the char, char consumption at the surface, and particle impingement on the surface (if the impingement rate is known). Wall enthalpy as a function of these parameters is the output on punched cards that becomes input for the ablation and char heat transfer program. From these data and the recovery enthalpy, the enthalpy difference across the boundary layer at any instantaneous set of conditions may be

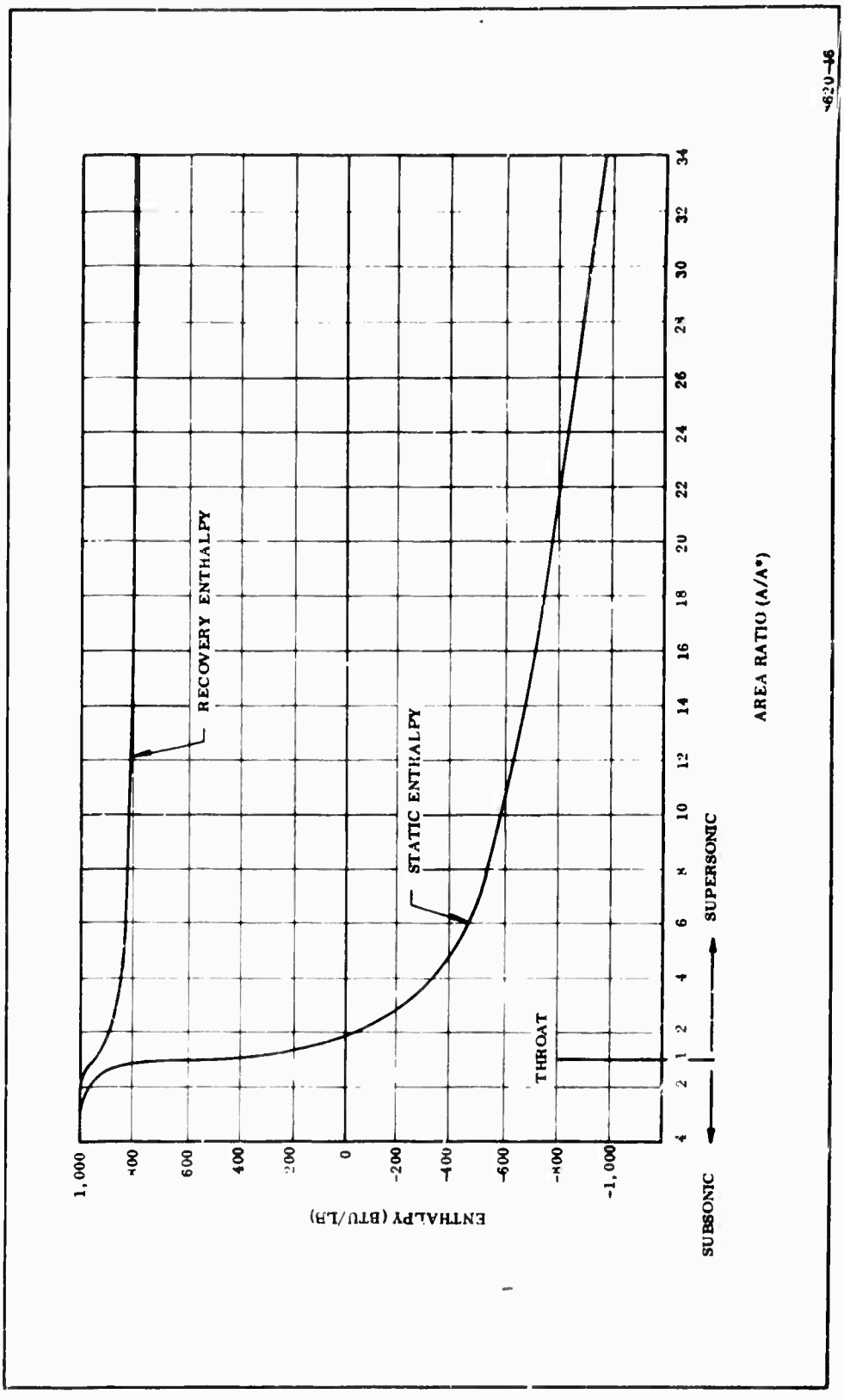

Figure 43. Exhaust Gas Enthalpy vs Area Ratio

determined by the computer. This information, as well as the convective heat transfer coefficient, is needed to evaluate convective heat flux.

The simplified Bartz (Reference 21) equation is used to calculate the convective heat transfer coefficient:

$$C_H = \frac{0.026}{(D_t)^{0.2}(A/A^*)^{0.9}} \left(\frac{(\mu)^{0.2}}{(P_r)^{0.6}}\right)_0 \left(\frac{P_{cg}}{C^*}\right)_0^{0.8} \left(\frac{D_t}{r_c}\right)^{0.1} \phi$$

where:

C_H = heat transfer coefficient based on enthalpy difference (lb/sq ft/sec)

0.026 = a correlation constant derived by Bartz from turbulent boundary laver analyses

D_t = nozzle throat diameter (ft)

(A/A^*) = expansion ratio at the nozzle location under consideration

μ = viscosity at stagnation conditions (lb/ft-sec)

P_r = Prandtl number ($\mu c_p/k$) (dimensionless)

P_c = chamber pressure (psfa)

g = acceleration due to gravity (ft/sec^2)

C^* = characteristic gas velocity (ft/sec)

r_c = throat radius of curvature (ft)

ϕ = dimensionless factor accounting for variation of ρ (gas density) and μ (gas viscosity) across the boundary layer

Transport properties appearing in the Bartz equation are evaluated by a computer program based on the kinetic theory of gases. The latest thermochemical data are used in this program and their predictions compare well with available experimental data. Pertinent transport properties are plotted as a function of temperature in Figures 44 and 45.

Heat transfer coefficients as a function of wall temperature and nozzle expansion ratio are shown in Figure 46.

Having obtained the foregoing information, the convective heat flux may be calculated according to the following equation:

$$q_{conv} = C_H (i_r - i_w)$$

where:

C_H = convective heat transfer coefficient (lb/sq ft-sec)

i_r = recovery enthalpy of the combustion gases (Btu/lb)

i_w = static enthalpy of the gases on the wall side of the boundary layer (Btu/lb)

Conventional techniques are used to determine the net radiant heat flux to the wall. The net radiant heat flux may be expressed as:

$$q_{rad} = \epsilon_w' \sigma (\epsilon_g T_g^4 - \alpha_g T_w^4)$$

where:

ϵ_w' = effective wall emissivity

ϵ_g = gas emissivity

α_g = gas absorptivity

T_g = temperature of the gas (°R)

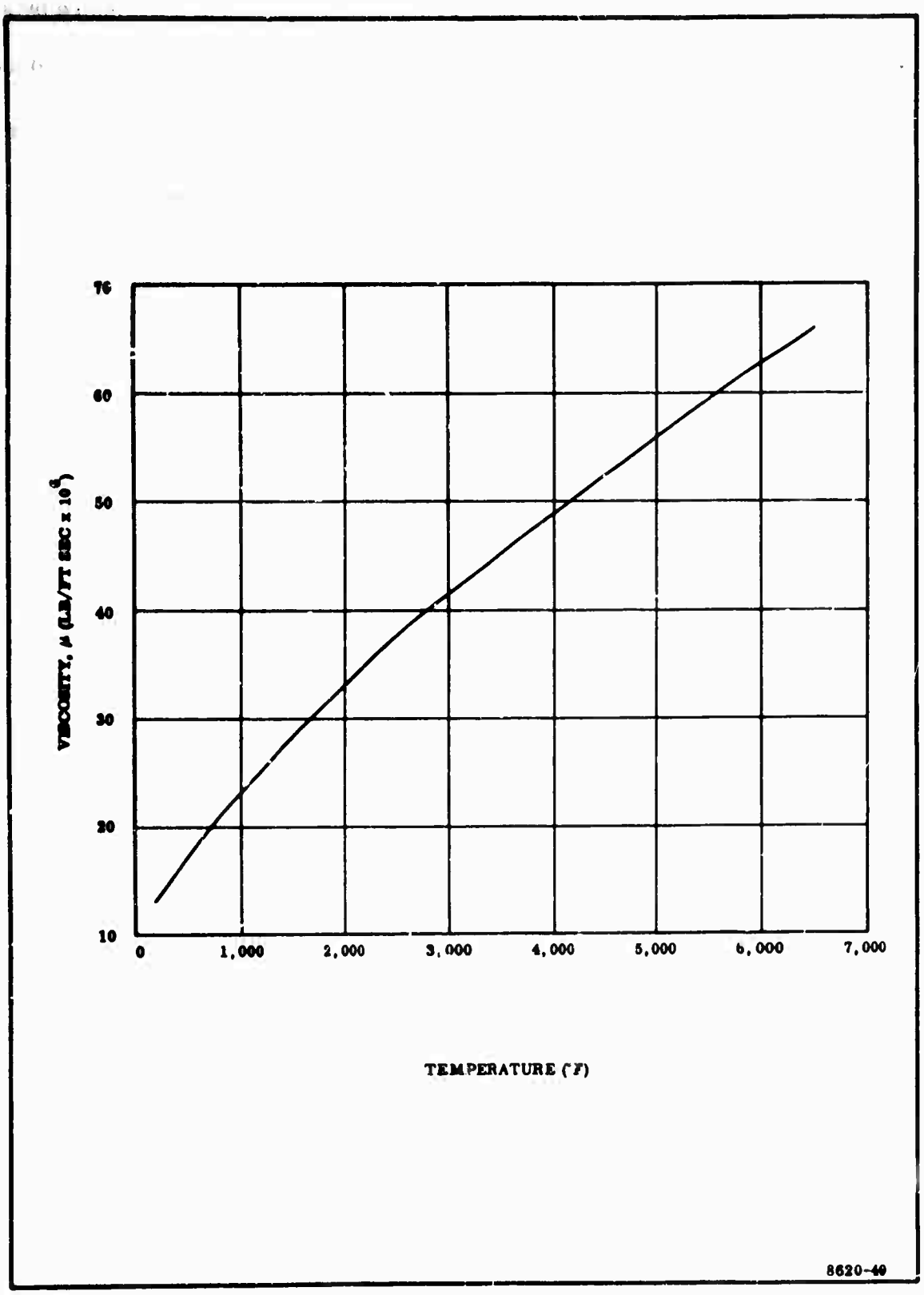

Figure 44. Viscosity of Combustion Products
(Evaluated at 1,000 psi)

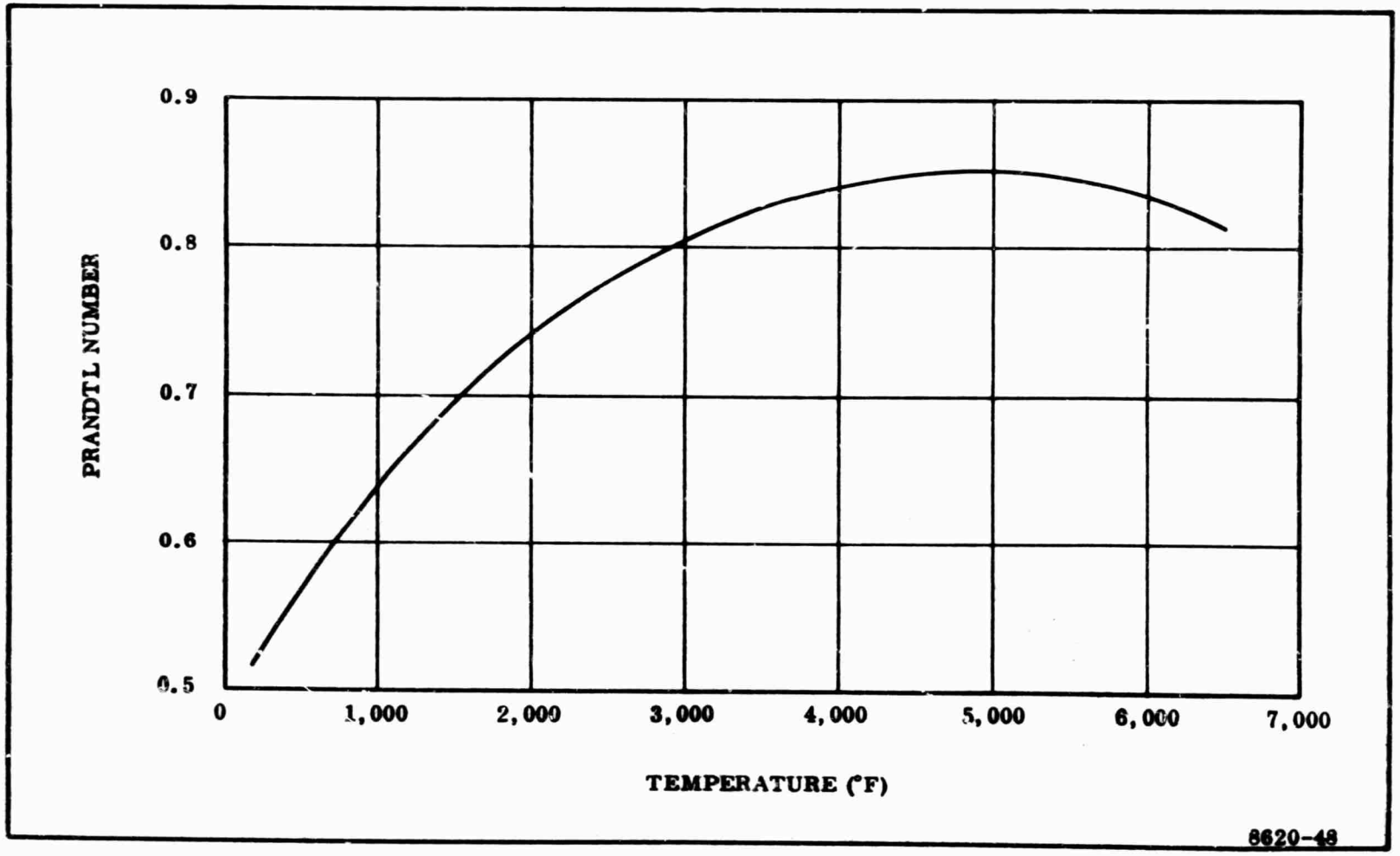

Figure 45. Prandtl Number of Combustion Products (Evaluated at 1,000 psi)

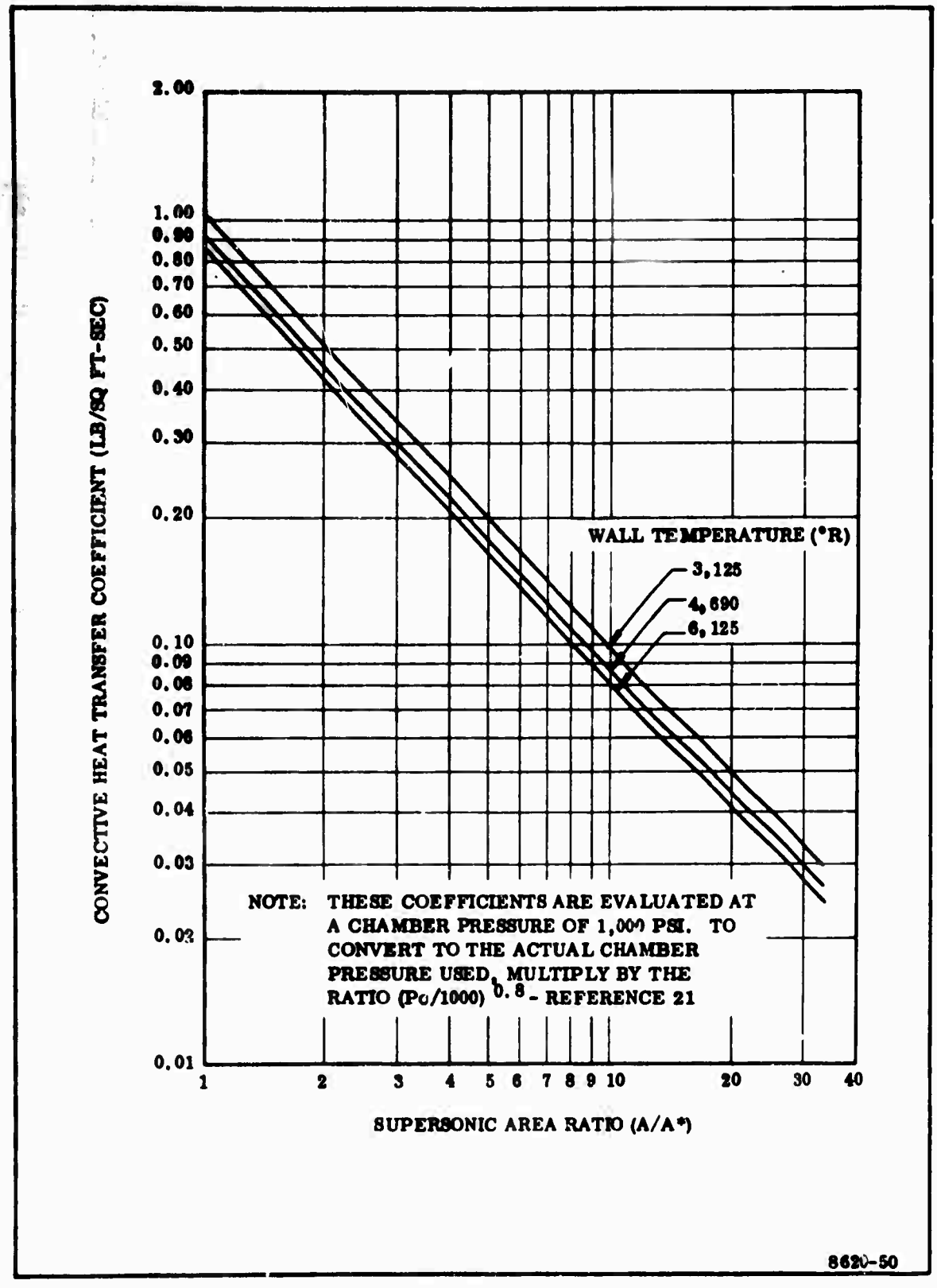

Figure 46. Convective Heat Transfer Coefficient vs Area Ratio

T_w = temperature of the wall (°R)

σ = Boltzman's constant

Gas temperature (T_g) is shown as a function of nozzle expansion ratio in Figure 47.

The emissivity (absorptivity of a particle laden gas at any particular temperature) (Reference 22) may be expressed as:

$$\epsilon_g = \alpha_g = 1 - e^{-NAL}$$

where:

N = particle number density (number/cu cm)

A = condensed particle cross sectional area (cu cm)

L = mean radiation beam length (cm)

The effective wall emissivity is determined from available material data and/or from experiment.

b. Insulation Performance--The computer program used in the thermal analysis is an explicit, finite difference solution for the transient temperature response in a one-dimensional, axisymmetric body, which can experience decomposition in depth. The ablating surface boundary condition is one of general convective-radiative heating with coupled mass transfer, assuming unity Lewis number.

The program uses a three component model for the thermal decomposition of the reinforced plastic. The plastic is assumed to consist of two components which decompose separately; the reinforcement is the third decomposing component.

The heat transfer coefficient used to calculate the surface heating rate is corrected for surface transpiration of the gases from the decomposing

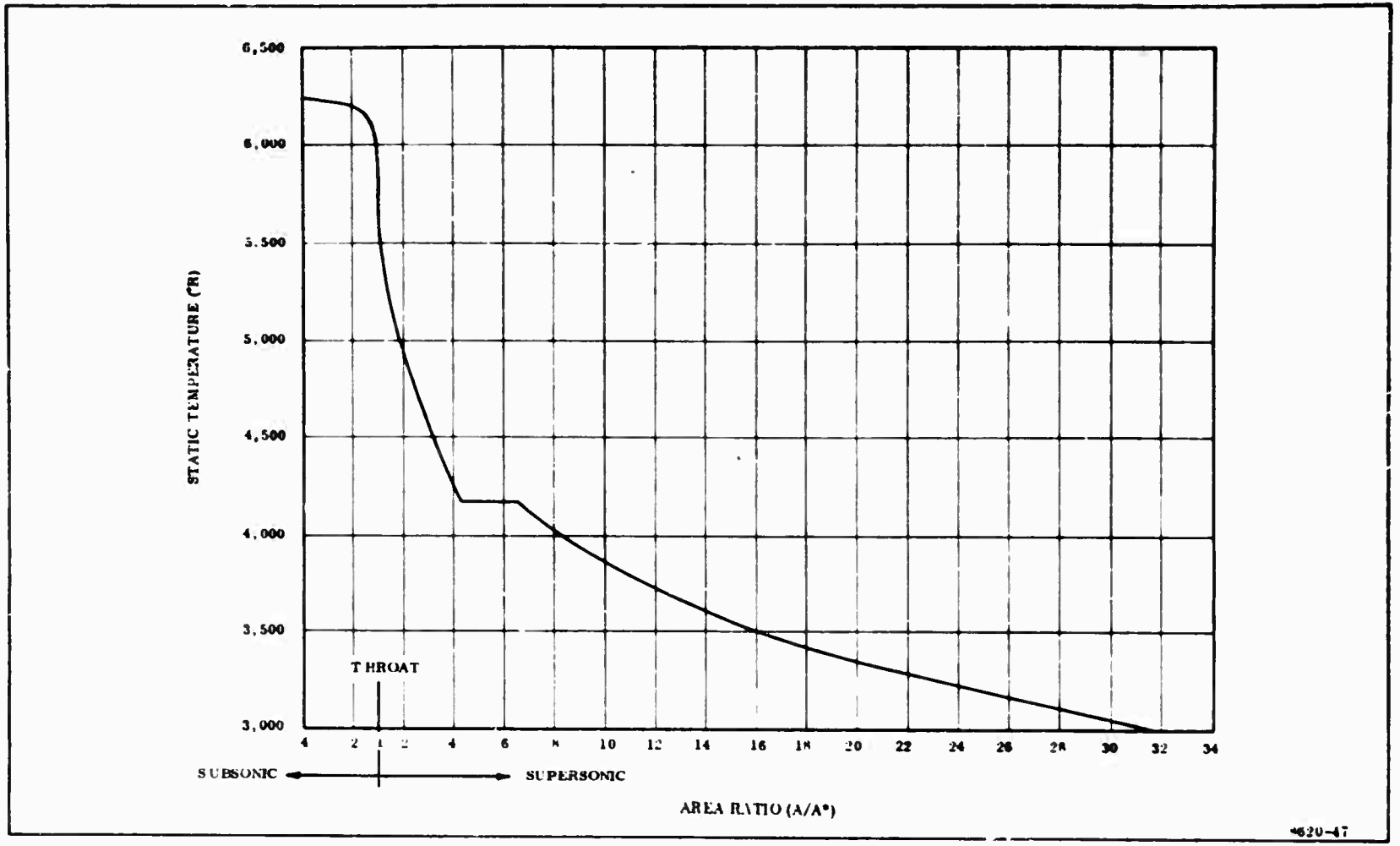

Figure 47. Static Gas Temperature vs Nozzle Area Ratio

(pyrolyzing) material. This is the heat transfer coefficient input to the computer (calculated in the absence of blowing by the Bartz correlation described earlier) and is corrected for the effects of blowing from the surface material as the solution progresses.

The equilibrium state of the surface is determined by a second computer program (surface equilibrium thermochemistry program) as a function of char rate and surface recession rate. Output from this program (which includes enthalpy of the surface gases) becomes direct input to the ablation-char computer program. Other output is shown in the sample analysis outlined in the following section.

Both of these programs are part of a set recently developed by Vidya, Inc under Air Force Contract AF 04(611)-9073 (Reference 23). The erosion depths computed by the ablation-char program are slightly higher than those estimated by scaling techniques from test data. This may be attributed to small errors in computing the convective heat transfer coefficient since erosion rate and the heat transfer coefficient are directly related. Other methods than the Bartz correlation are available for computing boundary layer conditions (e.g., the Ambrok, Rubesin, Mayer method; and Bartz, et al.; References 24 and 25) but have not yet been fully evaluated in conjunction with the programs described above.

In the subsonic nose region, where three-dimensional effects are important, a boundary layer program based on a more rigorous interpretation of the Bartz equation is used in conjunction with a flow net analysis. Heat transfer coefficients generated by this combination of programs are used in conjunction with an empirical correlation to obtain erosion data in this region (described later in more detail).

c. Nozzle Throat Sample Analysis--Calculations presented below show how temperature profiles along the throat centerline were obtained. Results of similar calculations for several other stations throughout the nozzle are also presented.

Computations were performed on the IBM 7040 computer using the ablation-char program described earlier.

Input to the computer requires the definition of boundary conditions. This procedure is outlined below.

1. Boundary Conditions

   Definition of motor parameters

   Average chamber pressure = 550 psia

   Propellant: 16-86 HB

   Throat diameter = 20.00 in.

   $A/A^* = 1.0$ (transonic)

2. Convective Heat Flux

   $P/P_c = 0.568$

   P = 400 psia

   $T_c = 6,240°R$

   T = 5,800°R (Figure 47)

   Heat transfer coefficients (Figure 46)

Temperature (°R)	C_H at 1,000 psi (lb/sq ft-sec)
3,125	1.030
4,690	0.930
6,250	0.878

Since chamber pressure is a function of time, the above coefficients are corrected (as a function of time) by the ratio $(P_c/1,000)^{0.8}$.

3. Radiant Heat Flux--The net radiant heat flux at the nozzle throat is small compared to the convective heating. It was calculated by the conventional equations described previously.

$$q_{rad} = \epsilon_{w'} \sigma (\epsilon_g T_g - \alpha_g T_w^4,$$

Temperature is the only value in the equation which varies throughout the nozzle. Gas temperature at the throat was 5,800° R.

Values for the other constants were:

$\epsilon_g = \alpha_g = 1$

$\epsilon_{w'} = 0.78$

$\sigma = 0.476 \times 10^{-12}$ Btu/sq ft-sec $(°R)^4$

q_{rad} was calculated by the computer as a function of T_w.

4. Evaluation of Throat Temperature History

The above boundary conditions were input to the computer. Results of the computer analysis are plotted in Figure 48. Runs at various other locations were made and results at representative locations are plotted in Figures 49 through 56. These illustrations are composite plots which not only show temperature gradients through the wall at various times, but also indicate the predicted erosion depths. The depth of erosion at any particular time is indicated by the point at which that particular time curve intersects the erosion curve. There is no sharp

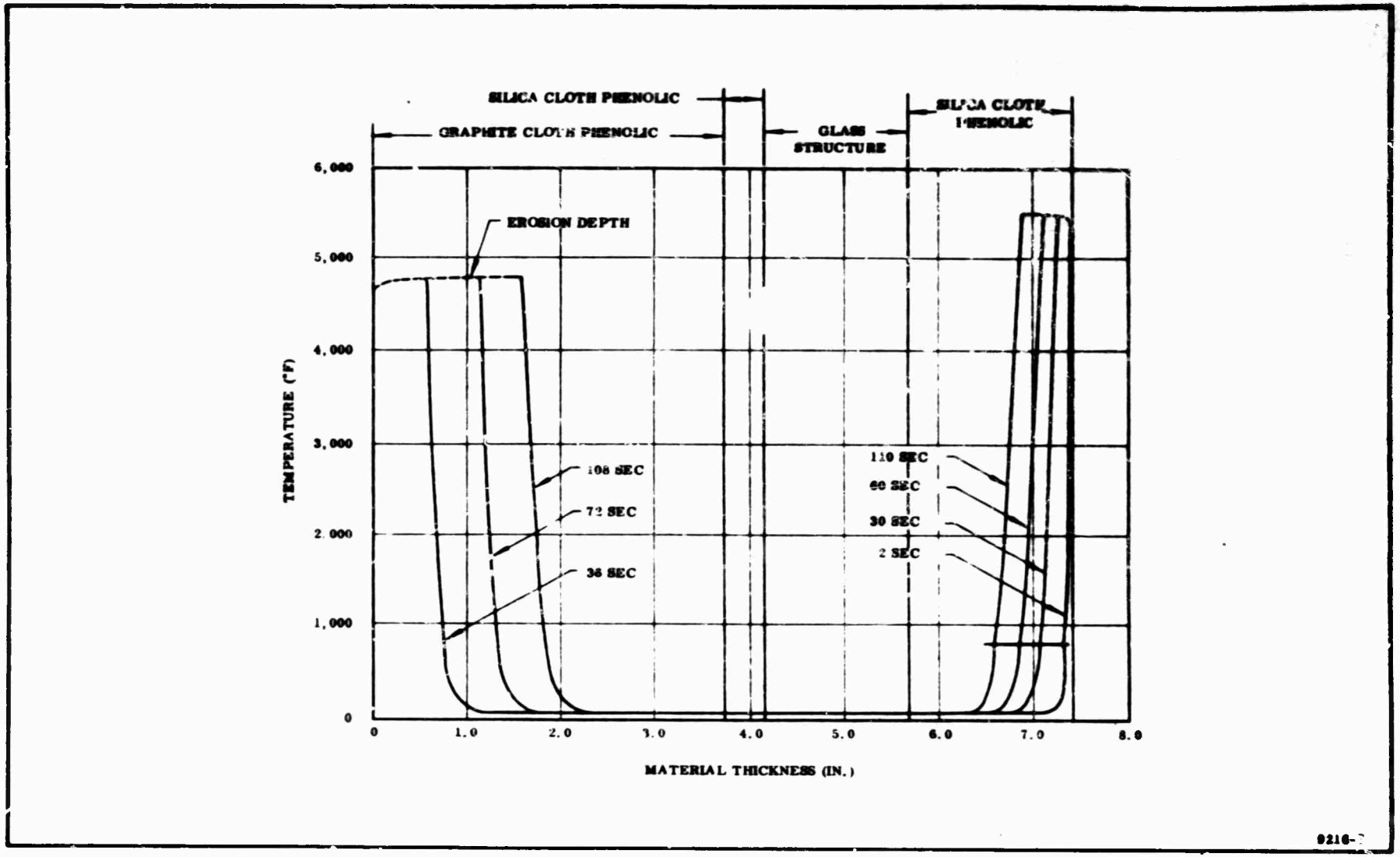

Figure 48. Predicted Temperature Profiles, 156-7 Nozzle Section Through Throat

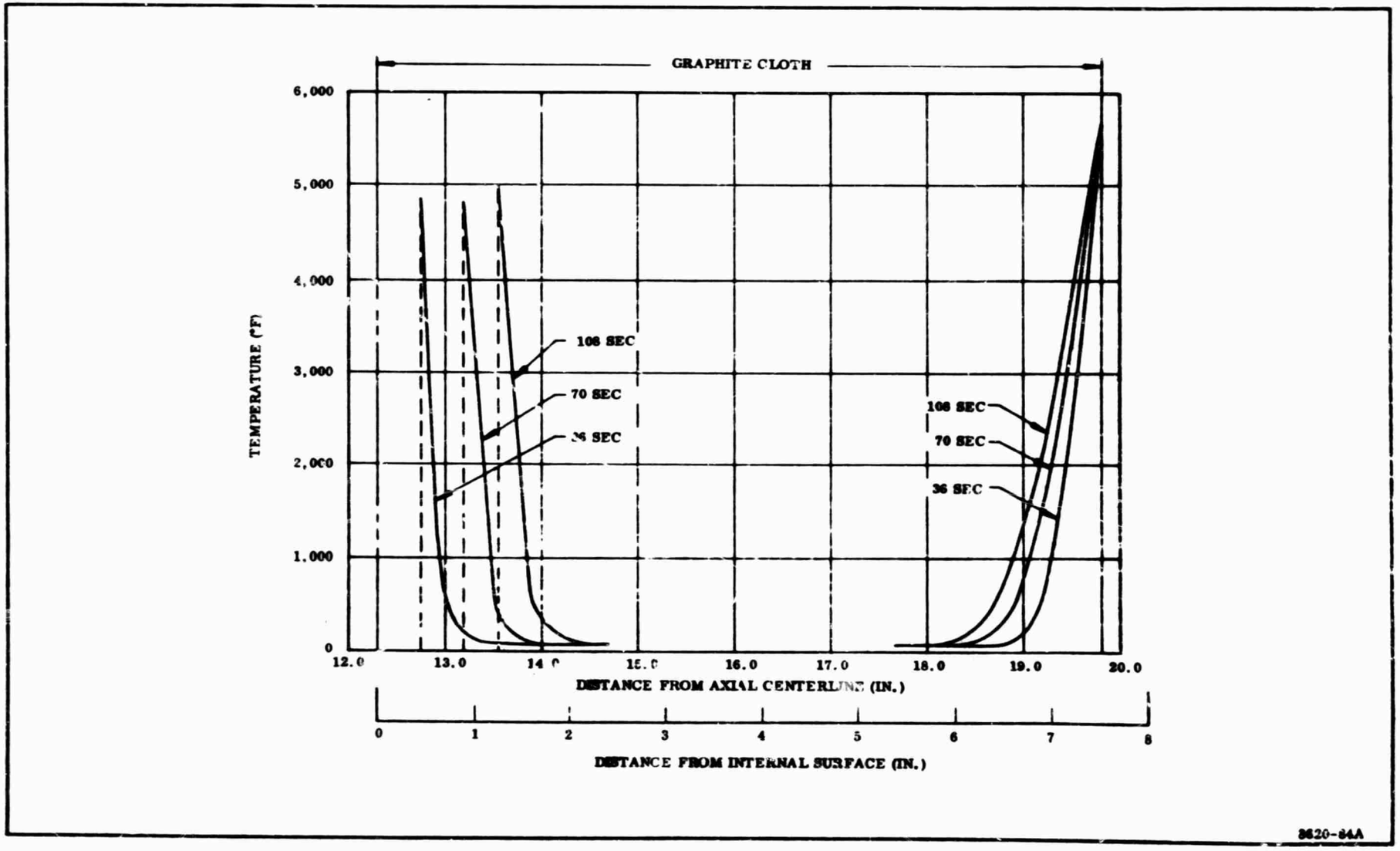

Figure 49. Temperature Distribution, 156-7 Nozzle Section 8 In. Forward of Throat ($A/A^* = 1.54$; Time = 108 Sec)

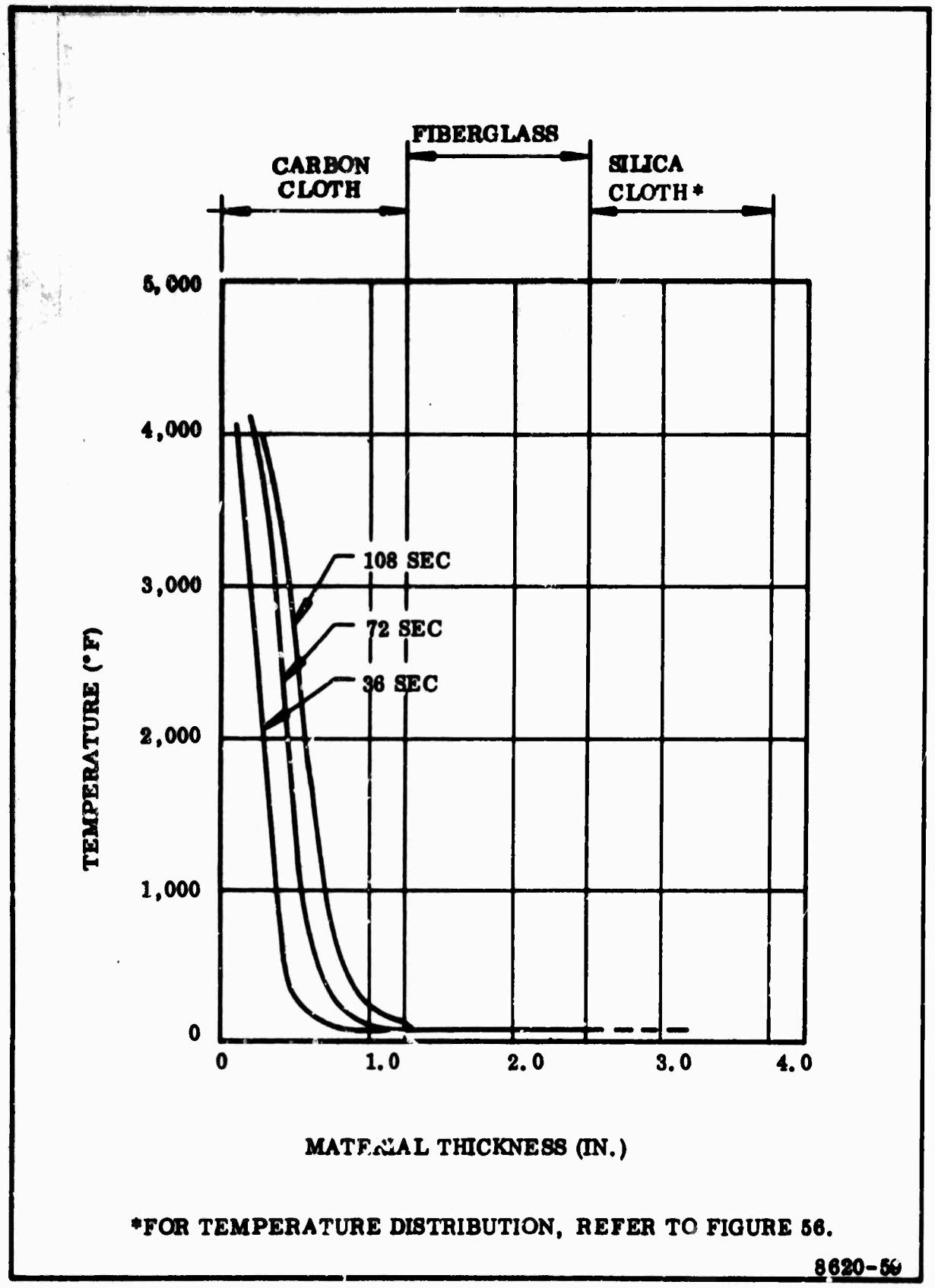

Figure 50. Predicted Temperature Profiles, 156-7 Nozzle Section at A/A* = 4.0

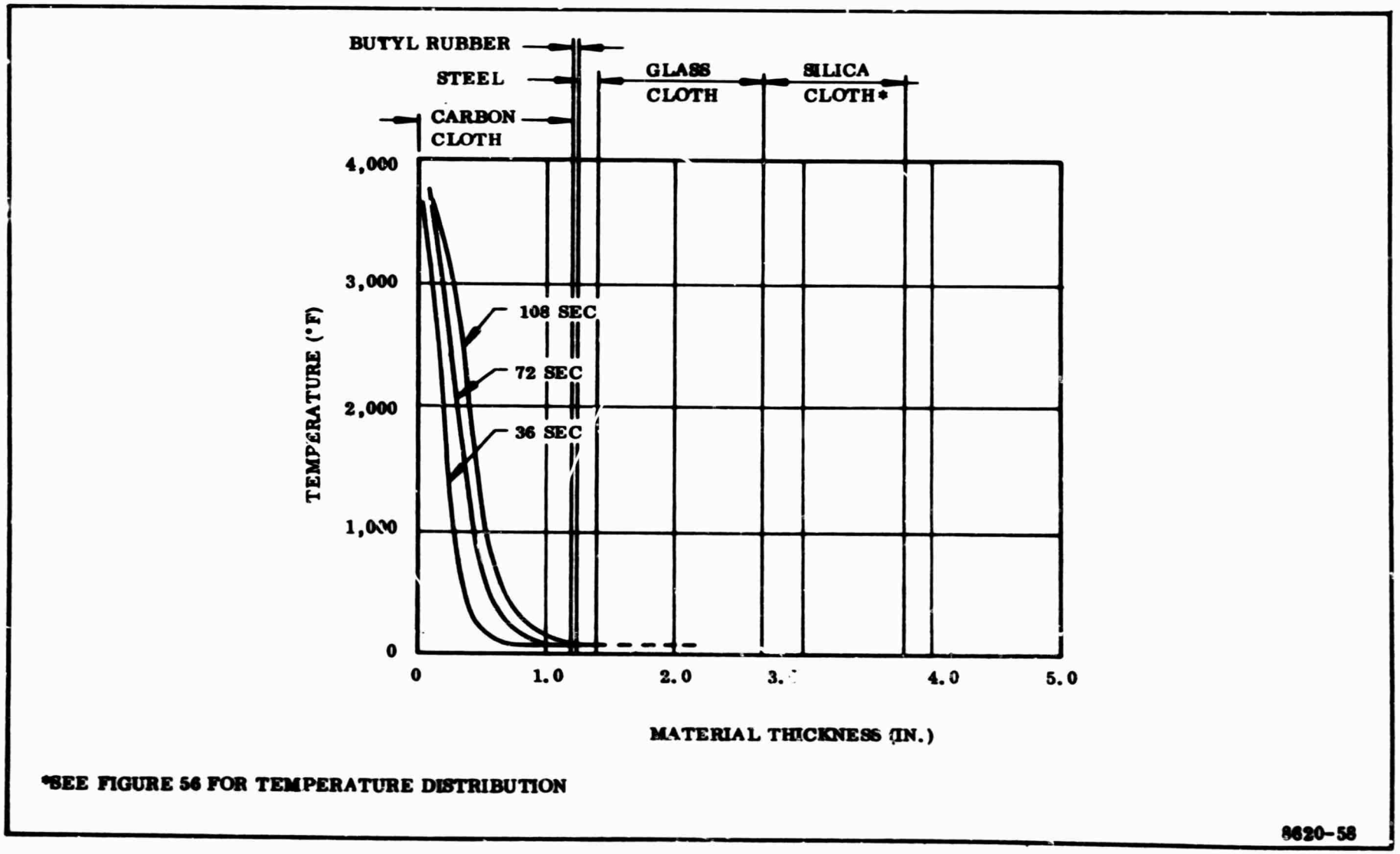

Figure 51. Predicted Temperature Profiles, 156-7 Nozzle Section at A/A* = 8.6

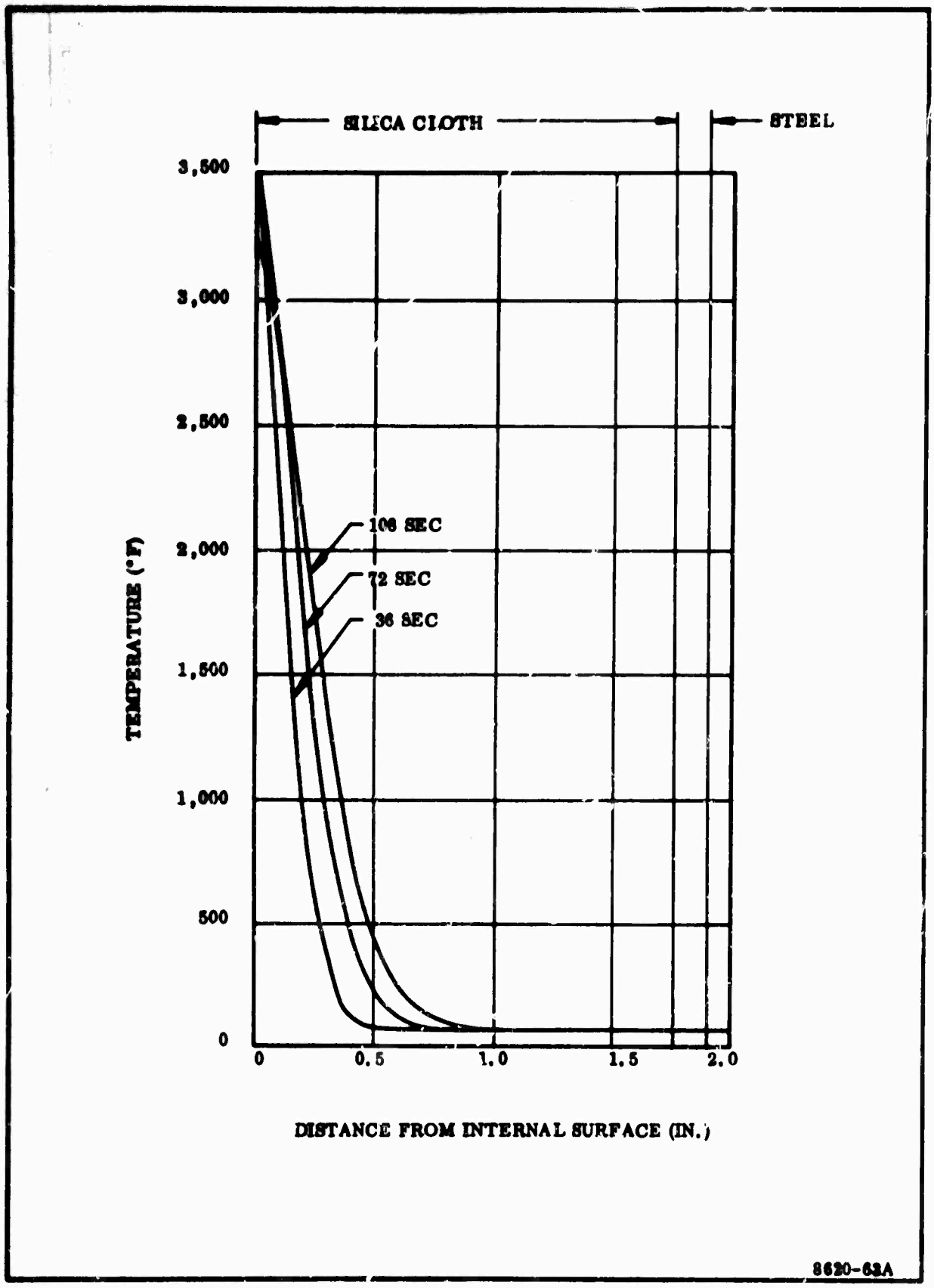

Figure 52. Predicted Temperature Profiles, 156-7 Nozzle Section at $A/A^* = 12.9$

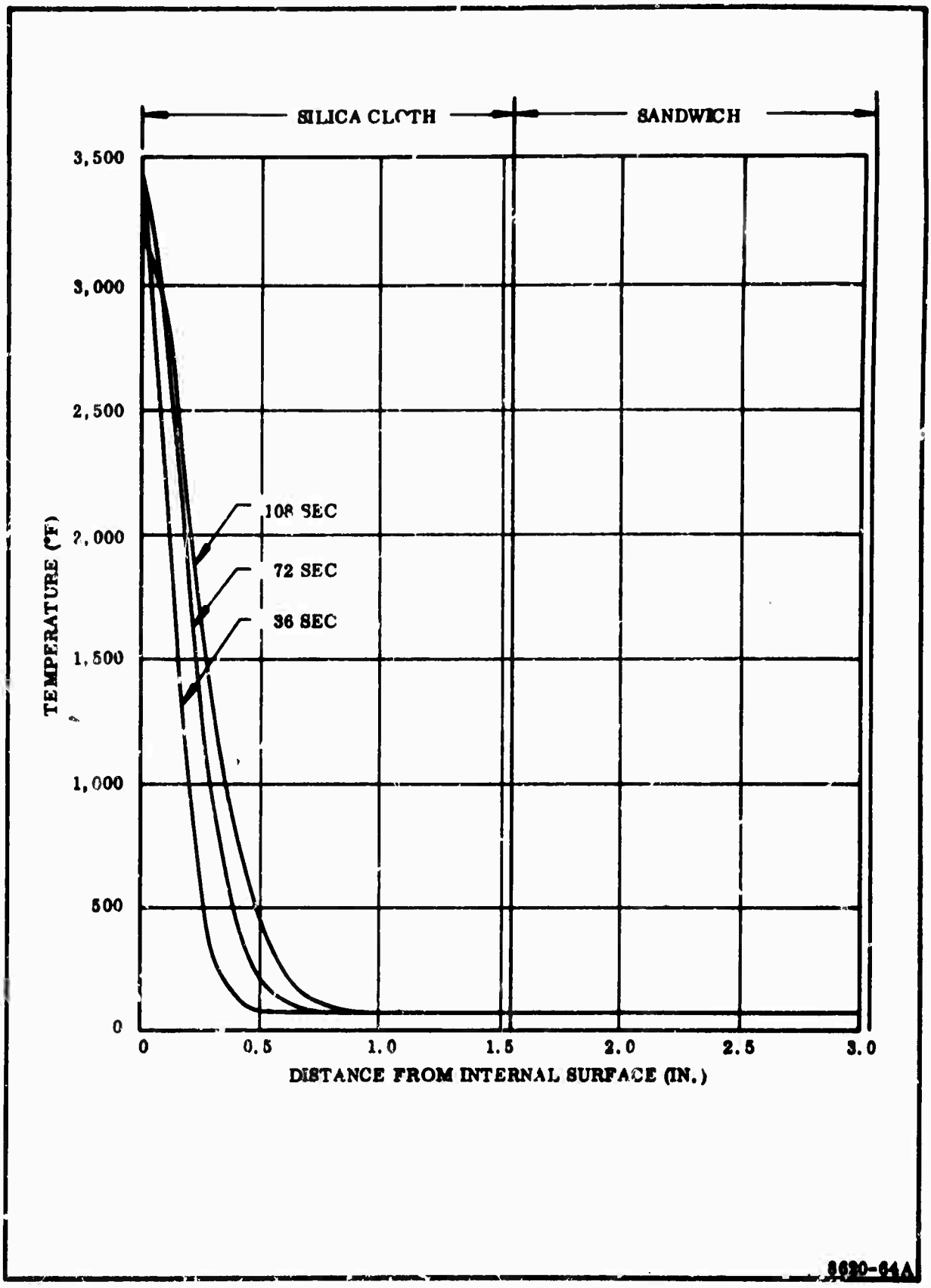

Figure 53. Predicted Temperature Profiles, 156-7 Nozzle Section at A/A* = 14.7

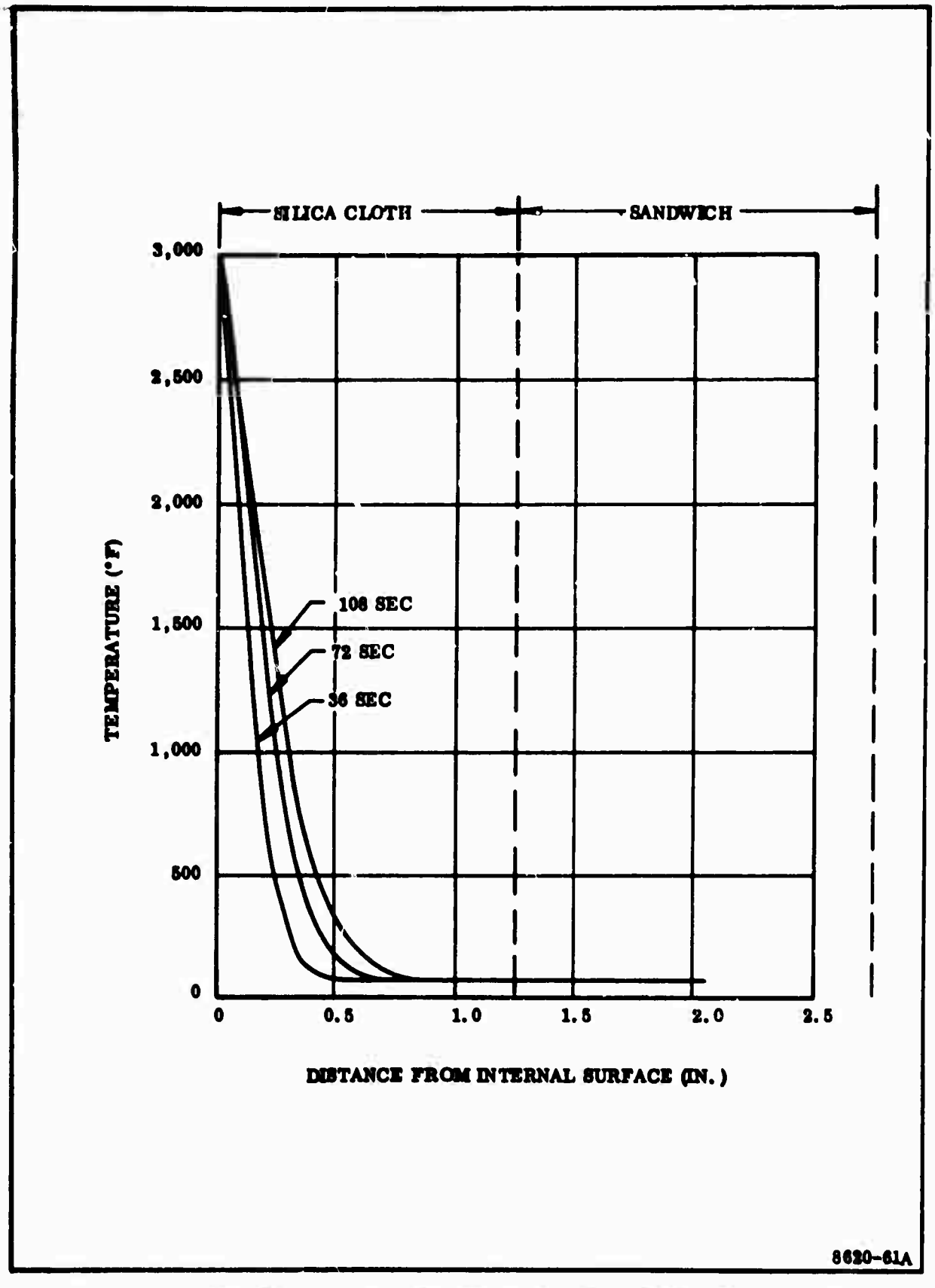

Figure 54. Predicted Temperature Profiles, 156-7 Nozzle Section at A/A* = 22.5

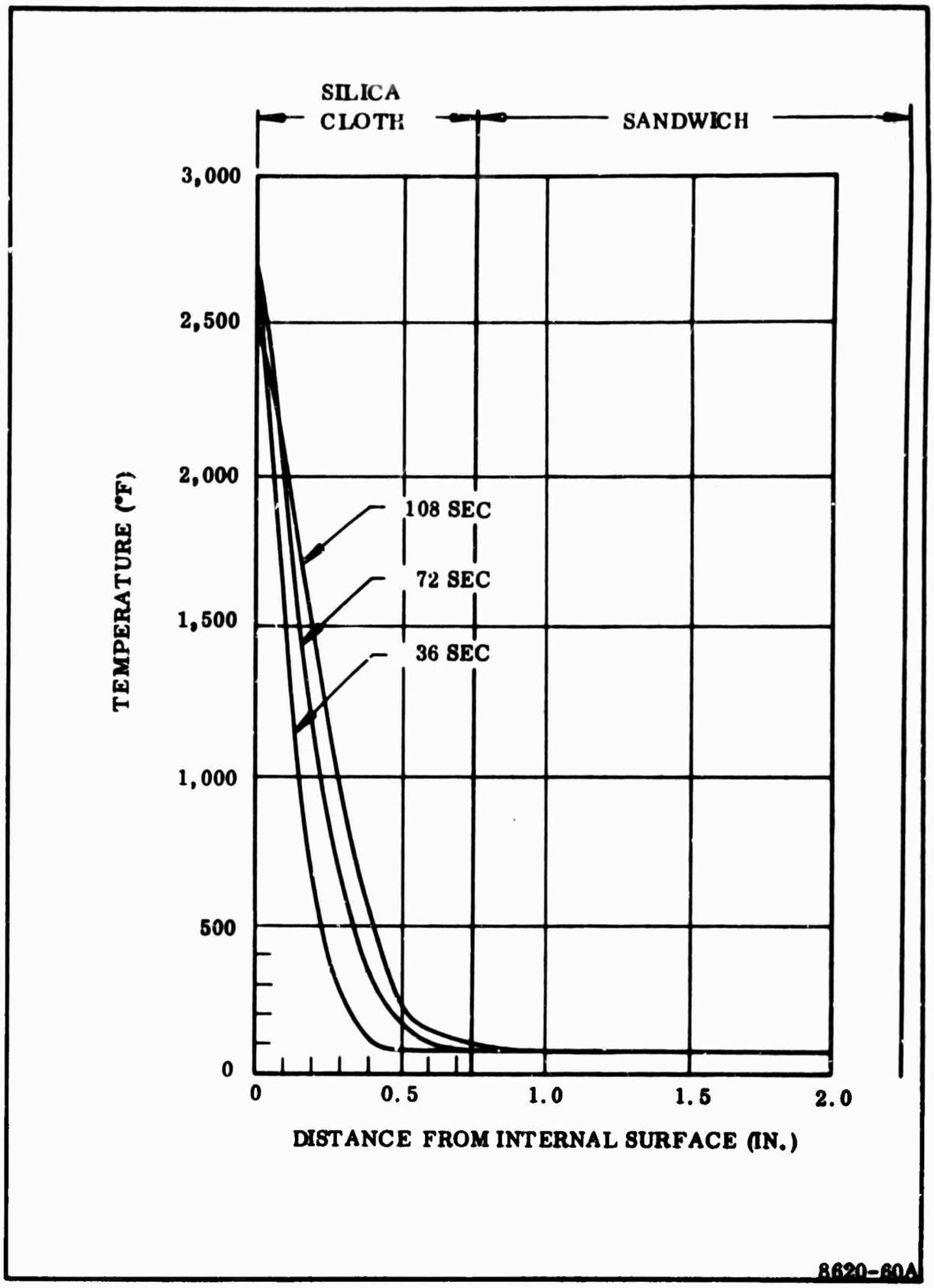

Figure 55. Predicted Temperature Profiles, 156-7 Nozzle Section at A/A* = 33.0

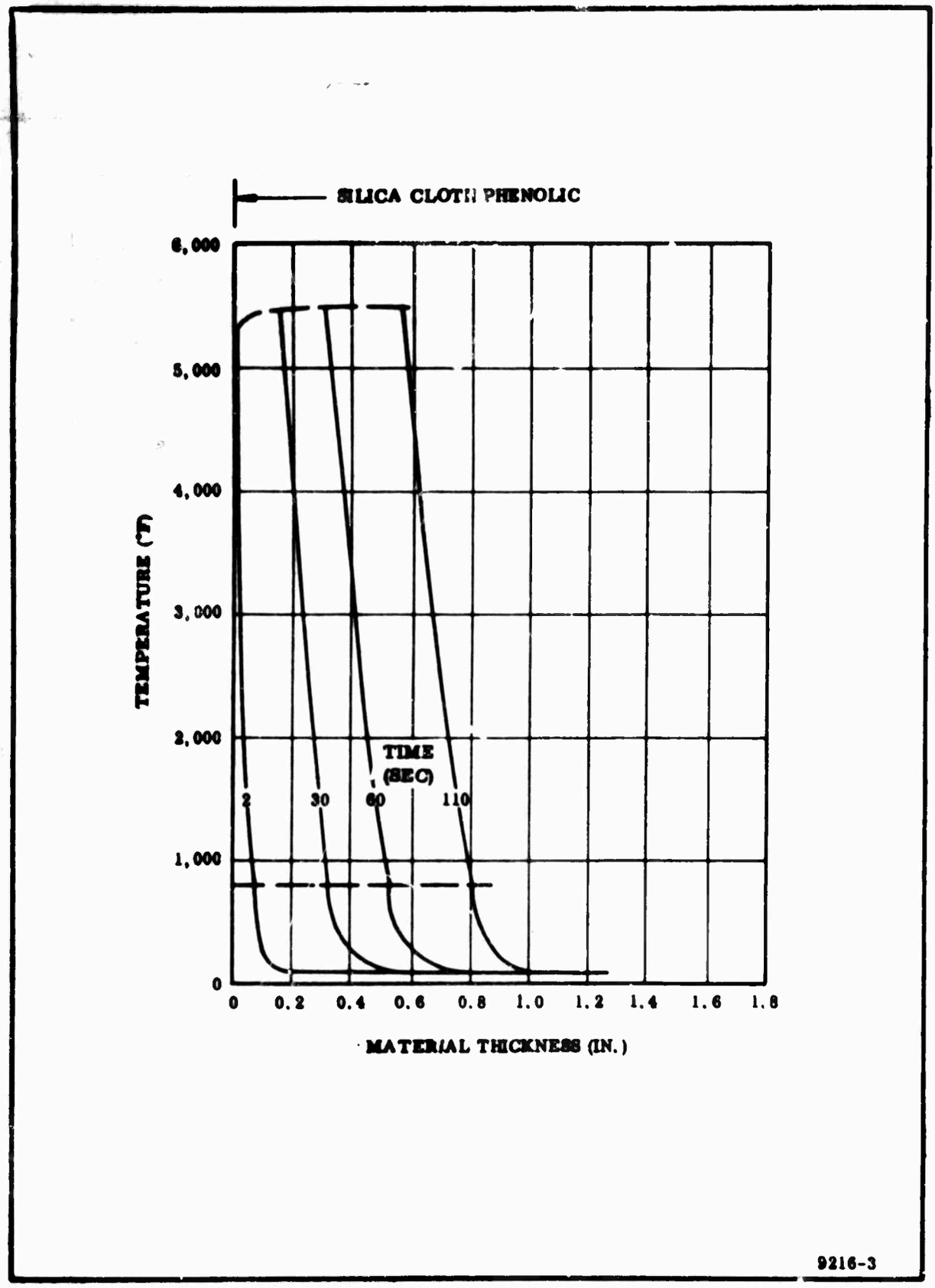

Figure 56. Temperature Profiles Through Insulation on Chamber Side of 156-7 Nozzle

line of demarcation between the virgin and charred material. In the charring region, material properties vary depending on the depth, length of exposure, and surface boundary conditions. Pyrolysis of the resin is assumed to begin at about 500° F; therefore, all material above this temperature has been charred to some extent. Surface temperatures shown in the illustrations are lower than those usually shown due to the more accurate treatment of the endothermic chemical reactions (corrosion) occurring at the surface and the resultant effect on wall enthalpy.

d. Material Loss Due to Erosion (Corrosion)--The foregoing analysis requires an estimation of erosion rates. The erosion depths calculated by the newly developed Vidya computer programs are included in Figures 48 through 56 for those locations at which erosion is expected. These depths are considered to be greater than will actually occur; therefore, scaling techniques from test data were used to obtain the final eroded nozzle configuration. Erosion data obtained in numerous firings with a propellant almost identical in formulation to that to be used in the subject nozzle test were correlated with the convective heat transfer coefficient. These correlations are shown in Figure 57 (nose region), Figure 58 (nozzle exit carbon cloth) and Figure 59 (nozzle exit silica cloth).

The assumption implicit in the use of the correlation is that erosion is primarily a reaction of certain chemical species in the combustion gases with the nozzle material. Furthermore, it is assumed that the material is at a sufficiently high temperature so that the reaction rate of the reacting species and the wall material is infinite and that the overall rate of erosion (corrosion) is determined only by boundary conditions which control the transport rate of reactants and

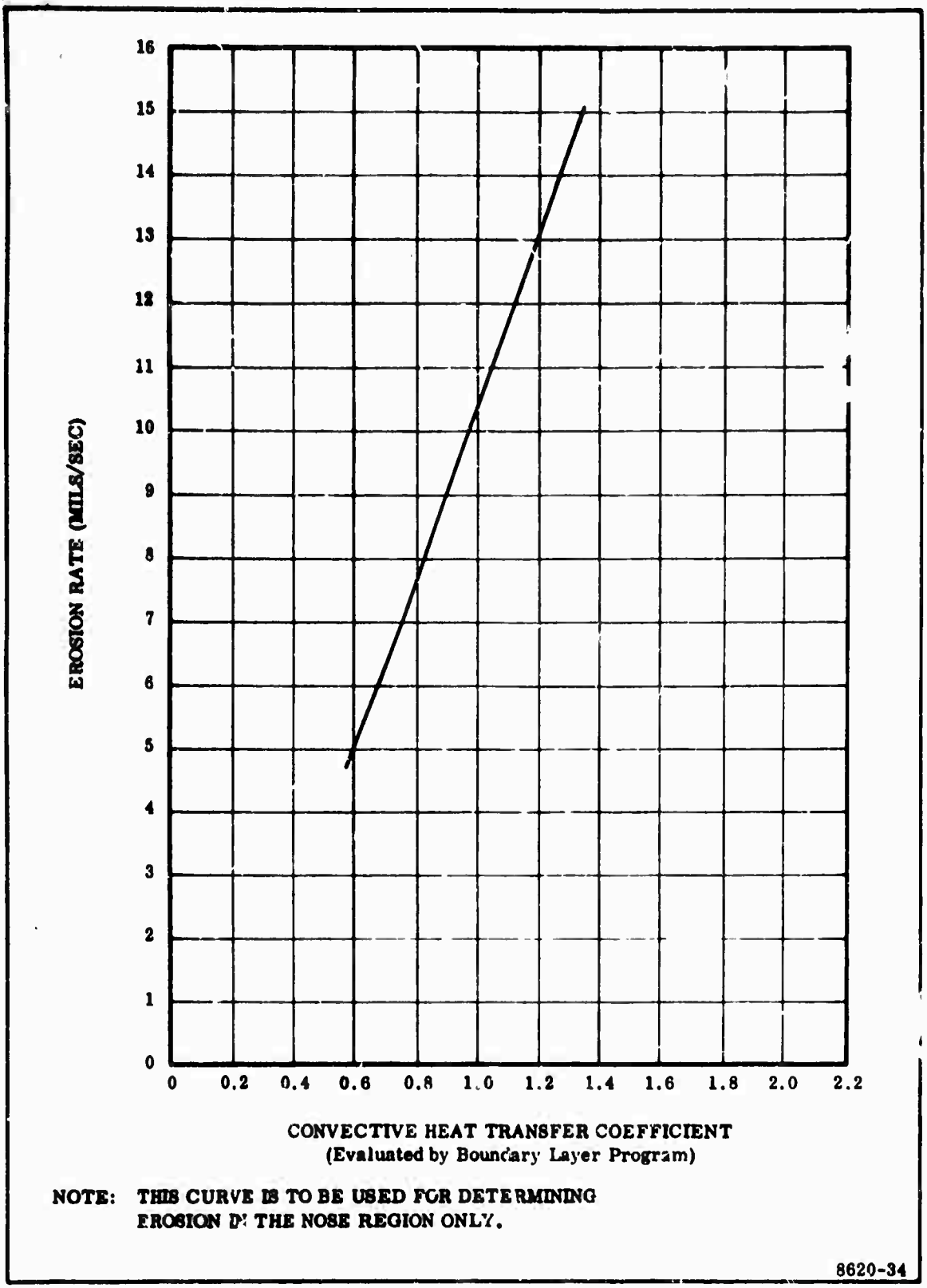

Figure 57. Graphite Cloth Phenolic Erosion Rate vs Convective Heat Transfer Coefficient

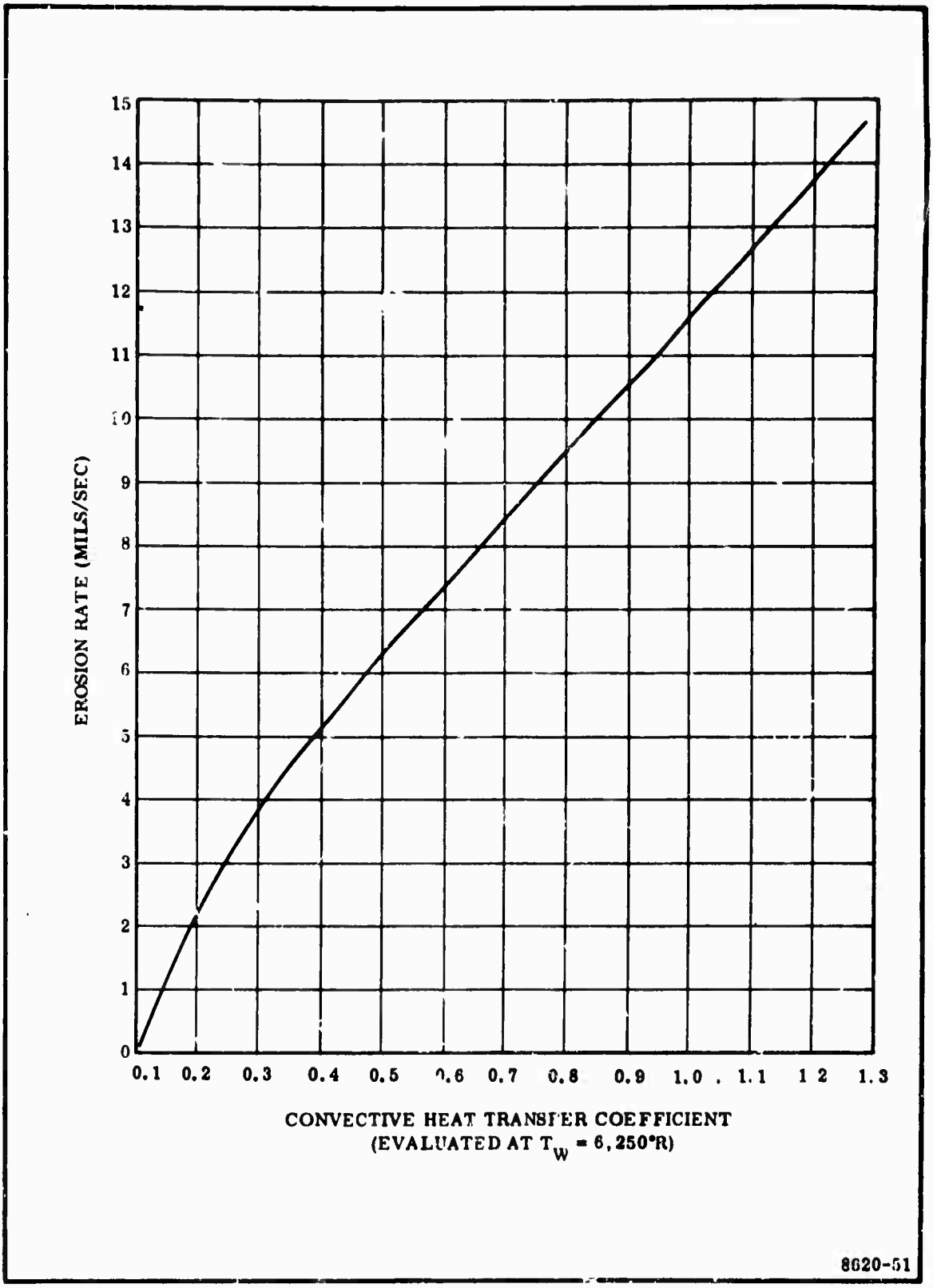

Figure 58. Graphite (Carbon) Cloth Phenolic Erosion Rate vs Convective Heat Transfer Coefficient

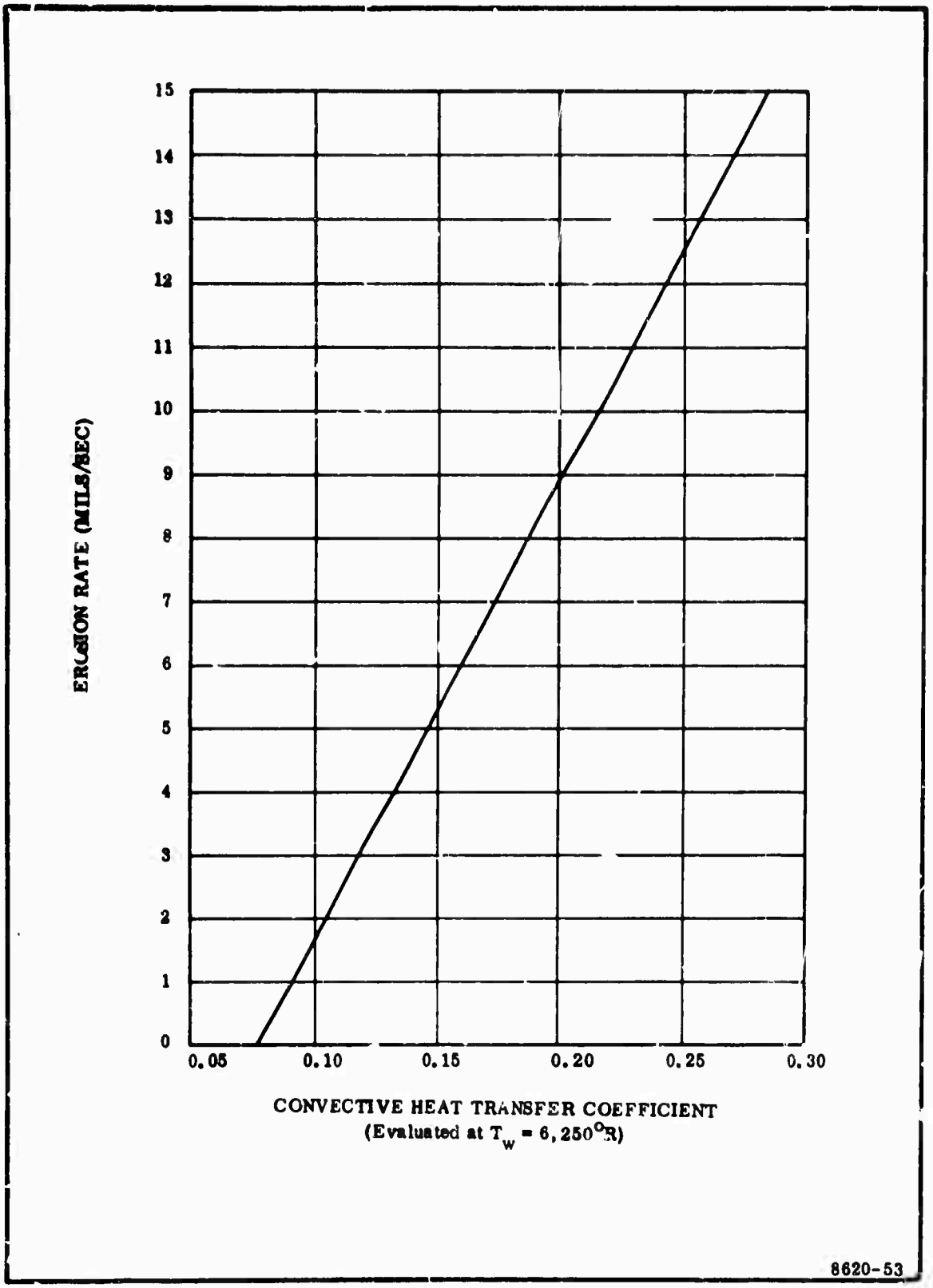

Figure 59. Silica Cloth Phenolic Erosion Rate vs Convective Heat Transfer Coefficient

reaction products. These controlling boundary conditions are satisfactorily defined by the convective heat transfer coefficient.

It is recognized that this approach is somewhat specious with silica cloth since physical changes (melting, vaporization) controlled by environmental temperature play a more prominent role here than do chemical reactions. The correlation has, however, been found to yield dependable design data in applications and conditions similar to those from which the reference test data was obtained.

This empirical technique somewhat circumvents uncertainties in the heat transfer coefficient calculation. The same method for computing this coefficient is used both to set up the correlation and to read values from it. Uncertainty in the heat transfer coefficient is thus cancelled out.

Separate correlations are used for the graphite cloth in the nose region and in the nozzle exit because the convective heat transfer coefficient is calculated by different methods in the two cases. In the nose region where flow is axisymmetric, two-dimensional, a boundary layer program is used to obtain the heat transfer coefficients (more fully discussed in Section IV, Aerodynamics). The correlation shown in Figure 57 is used in conjunction with these coefficients to determine erosion in the nose region.

For the nozzle exit, the heat transfer coefficients are calculated by the simplified Bartz correlation (plotted in Figure 46) and used in conjunction with Figure 58 and Figure 59 to obtain erosion rates in the nozzle exit. In either case, it is necessary to know only the convective heat transfer coefficient at a particular

location and the erosion rate may then be read from Figures 57, 58, or 59, whichever is applicable.

Multiplying these rates by the web time gives the final eroded configuration of the nozzle (Figure 60).

e. Erosion Due to LITVC--Erosion around the injector port during liquid injection is primarily a function of the type of injectant and the relative weight flow rate of the injectant and the main exhaust stream.

Data showing the relationship of erosion rate to the flow rate ratio of injectant to mainstream was obtained in Program 623A (TITAN III-C Booster) Reference 26. This relationship is shown in Figure 61. In the TITAN III-C Booster, injection occurs at an expansion ratio of 3.5 where the normal erosion rate without TVC varies from 4 to 7 mils/sec. In the motor from which data shown in Figure 30 was obtained, the normal rate was 7 mils/sec. In the 156-7 nozzle, no erosion is anticipated around the TVC port in the absence of injection. Therefore, the curves shown for the TITAN III-C Booster are shifted downward to indicate zero erosion when the injectant flow rate is zero.

In the subject nozzle, the worst condition (from an erosion standpoint) would be if the injection valves remained in the full open position until the supply of injectant was depleted. This corresponds to a weight flow rate ratio of 0.044, based on the following data.

$A/A^* = 13.1:1$

Motor weight flow rate 122,000/107 = 1,140 lb/sec

Maximum injectant weight flow rate = 50 lb/sec

Flow rate ratio 50/1,140 = 0.044

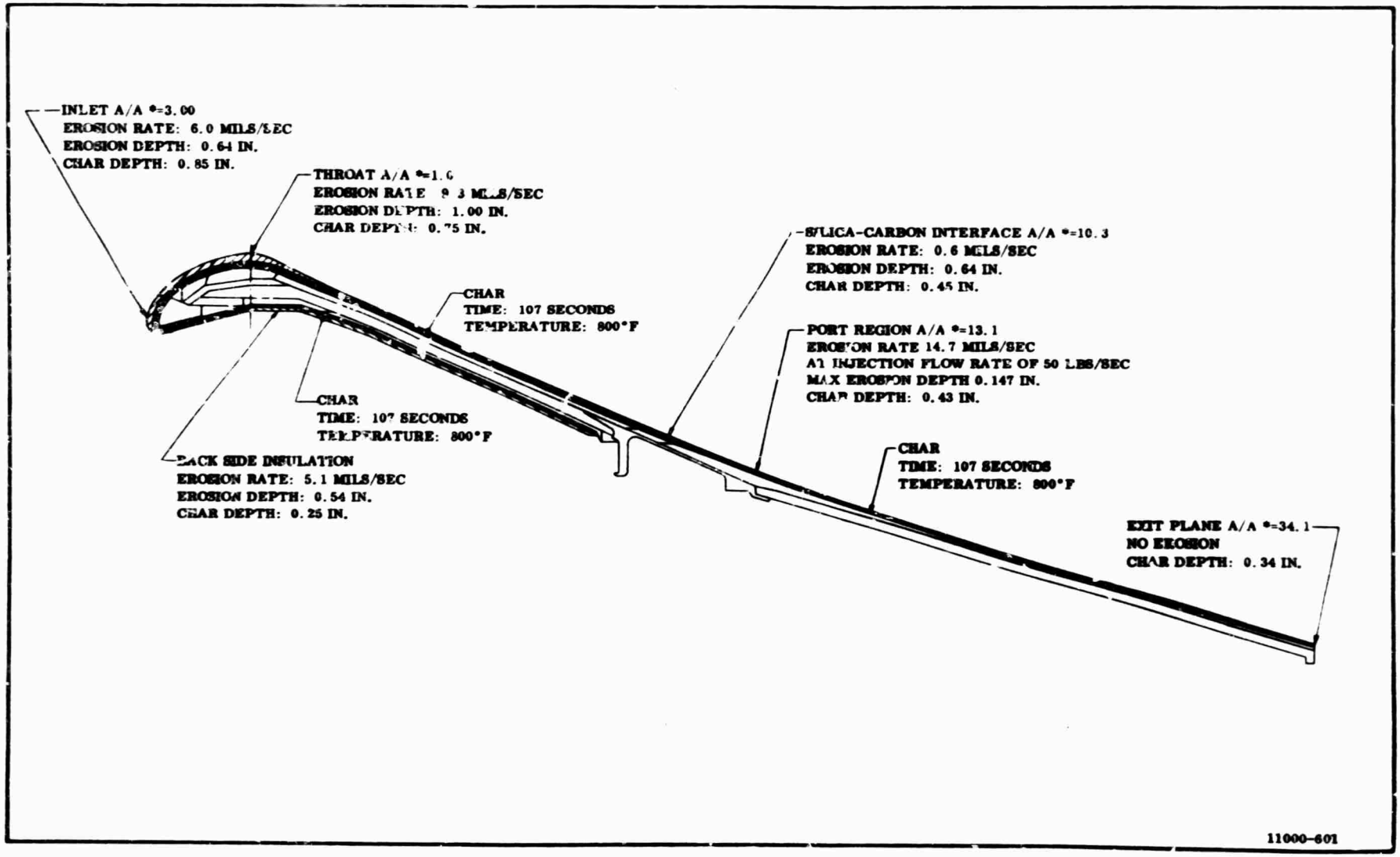

Figure 60. 156-7 Nozzle Erosion and Char Profile

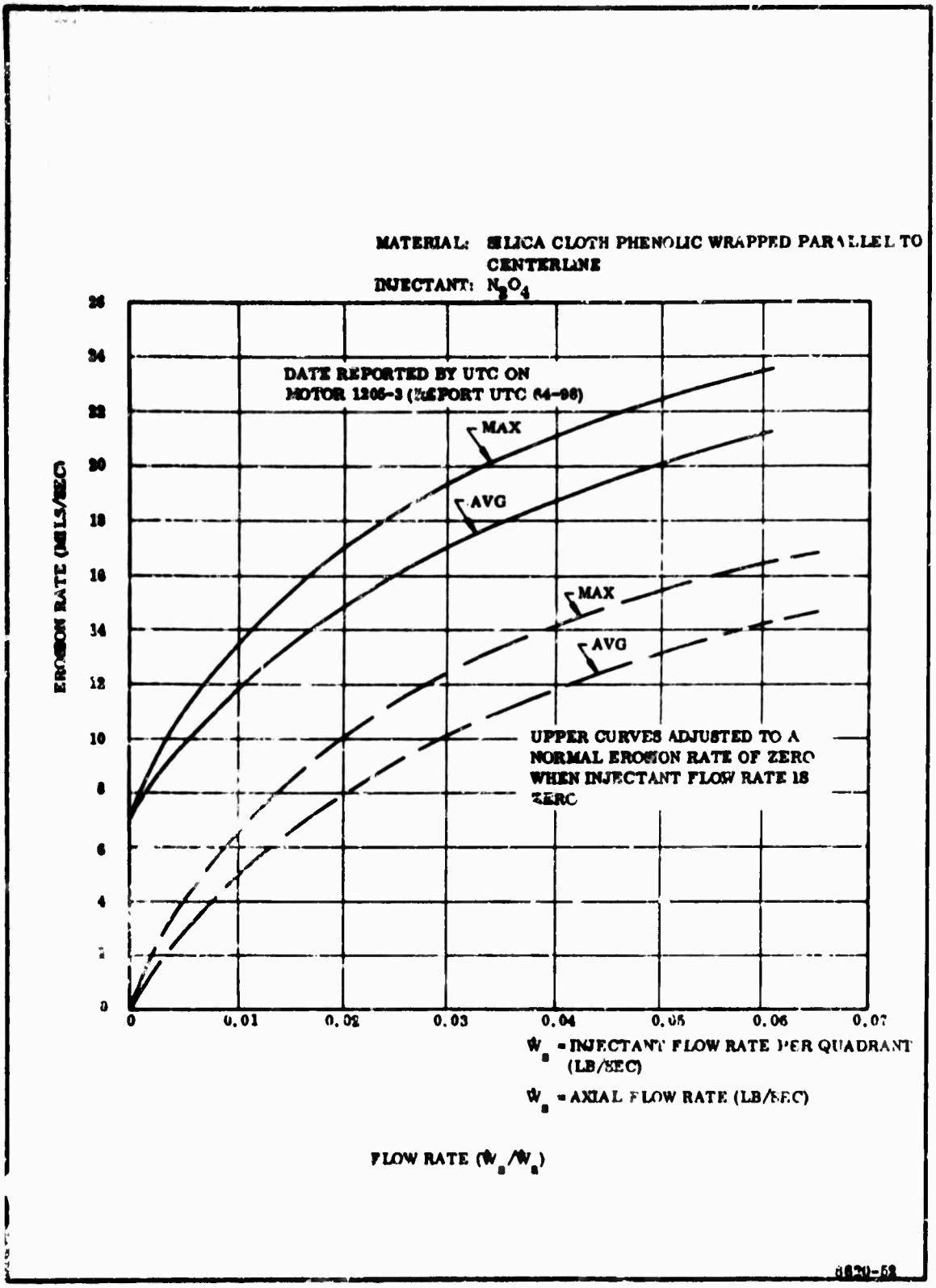

Figure 61. Ablation Rates as a Function of Flow Rate Ratio (Injectant Flow Rate/Axial Flow Rate)

Under these conditions the erosion rate would be 14.7 mils/sec. The supply of injectant would be depleted in 10 sec and therefore the maximum eroded depths would be 0.147 inch.

Measured rates are expected to be less than indicated in Figure 60. With the injectant flow evenly distributed among the four quadrants the average depth per quadrant will be less than 0.050 inch.

f. Conclusions--The thermal analysis indicates that the subject nozzle is conservatively designed and that sufficient material has been provided to allow for anticipated losses as well as to maintain the temperature of the structural parts within acceptable limits during firing.

3. STRUCTURAL ANALYSIS

The structural design philosophy in designing this nozzle was to provide a lightweight structure consistent with case and nozzle requirements of strength and rigidity.

Preliminary structural analyses were based on classical shell and frame structural calculation methods. Most of the analyses are programed on computers. The programs were developed and modified during the present 156 Inch Motor Program to handle problems peculiar to nozzle design (Reference 8; Figure 2-25). This includes discontinuity shell analysis for the nozzle/case interface and ring analysis for inplane loading of various types.

Throughout the analysis, the following design criteria were applied.

1. All loads for stress and deflection calculations are based on the maximum expected chamber pressure considering a three sigma variation for propellant burning rate.
2. All steel structural components have a minimum safety factor of 1.25 based upon minimum yield strength of the material. Glass cloth reinforced plastics have a safety factor of 1.50 based on ultimate strength of the material.

A tabulation of the critical discontinuity stresses at the nozzle/case interface and the resulting margins of safety are shown in Section III.

The materials used in this analysis and the physical and mechanical properties are listed in Section II. Nomenclature is listed in Figure 62.

The submerged conical shell was sized using accepted buckling criteria for monocoque truncated cones under combined external lateral pressure and axial compression. The critical pressure for the proposed design is 1,088 psi meeting the required 1.25 safety factor.

The steel flange shell and sandwich exit cone structures were sized on the basis of buckling criteria for combined transverse shear, axial compression, and bending loads resulting from injection loads.

Thermomechanical stresses are shown in Figures 63 through 65 at selected stations (throat, a supersonic area ratio = 4.0, and 8 in. forward of throat) to provide a margin of safety for the insulation and radial interface pressures for the shell discontinuity stresses.

The injector ring and tank support must support the majority of the LITVC system weight times acceleration factor (g's) and the maximum injection wall pressure. Standard ring analysis (Reference 15) indicates the maximum bending, shear and axial loading on the ring will provide an adequate 0.25 margin of safety.

Plane sections of the nozzle exit cone from injection port to exit plane indicate the margin of safety is satisfactory for the steel and sandwich cone.

Nozzle attachments of the exit cone and diffuser are investigated for critical loading conditions: axial load, pressure, transverse bending moments and shears. The exit cone bolts are also satisfactory.

p = pressure, psi, positive when directed outward

Q = total shear force, lb: unit shear force, lb/in.

q = uniform load, lb/in.

M = total moment, in. lb; unit moment, in. lb/in.

T = unit force, lb/in., positive when inducing tension; temperature, °F; or torsional load, in. lb

P = load, lb

E = modulus of elasticity, psi

G = shear modulus, psi

μ = Poisson's ratio

α = coefficient of thermal expansion, in./in./°F

σ_{TU} = ultimate tensile strength, psi

σ_{BU} = ultimate bearing strength, psi

σ_{TY} = yield strength, psi

σ_{SU} = ultimate shear strength, psi

σ_{CU} = ultimate compressive strength, psi

R = radius, in., perpendicular to the axis of revolution

L = length, in.

t = thickness, in.

A = area, sq in.

Figure 62. Nomenclature

I = moment of inertia, $in.^4$

c = distance from centroid of a section to fiber being evaluated, in.

D = flexural rigidity, in./lb; diameter, in.

K = torsional shape factor, $in.^4$

β = angle of twist, radians; damping function

ϕ = an angle in degrees

θ = angle of slope change, radians, positive when counterclockwise

σ = normal stress, lb per square inch, positive when tensile

ω = radial component of displacement, in., positive when directed toward axis of revolution

δ = deflection, in.

M.S. = margin of safety

λ = ratio of torsional to flexural rigidity, GK/EI

SUBSCRIPTS

The foregoing symbols used in conjunction with subscript notations listed below will have the following meanings:

p = denotes the effect of pressure load

b = denotes the effect of bearing loads

s = denotes the shear stress

m, M = denotes the effect of moment load

Figure 62. Nomenclature (Cont)

1	=	refers to meridional direction
2	=	refers to hoop or tangential direction
Q	=	denotes the effect of shear load

Figure 62. Nomenclature (Cont)

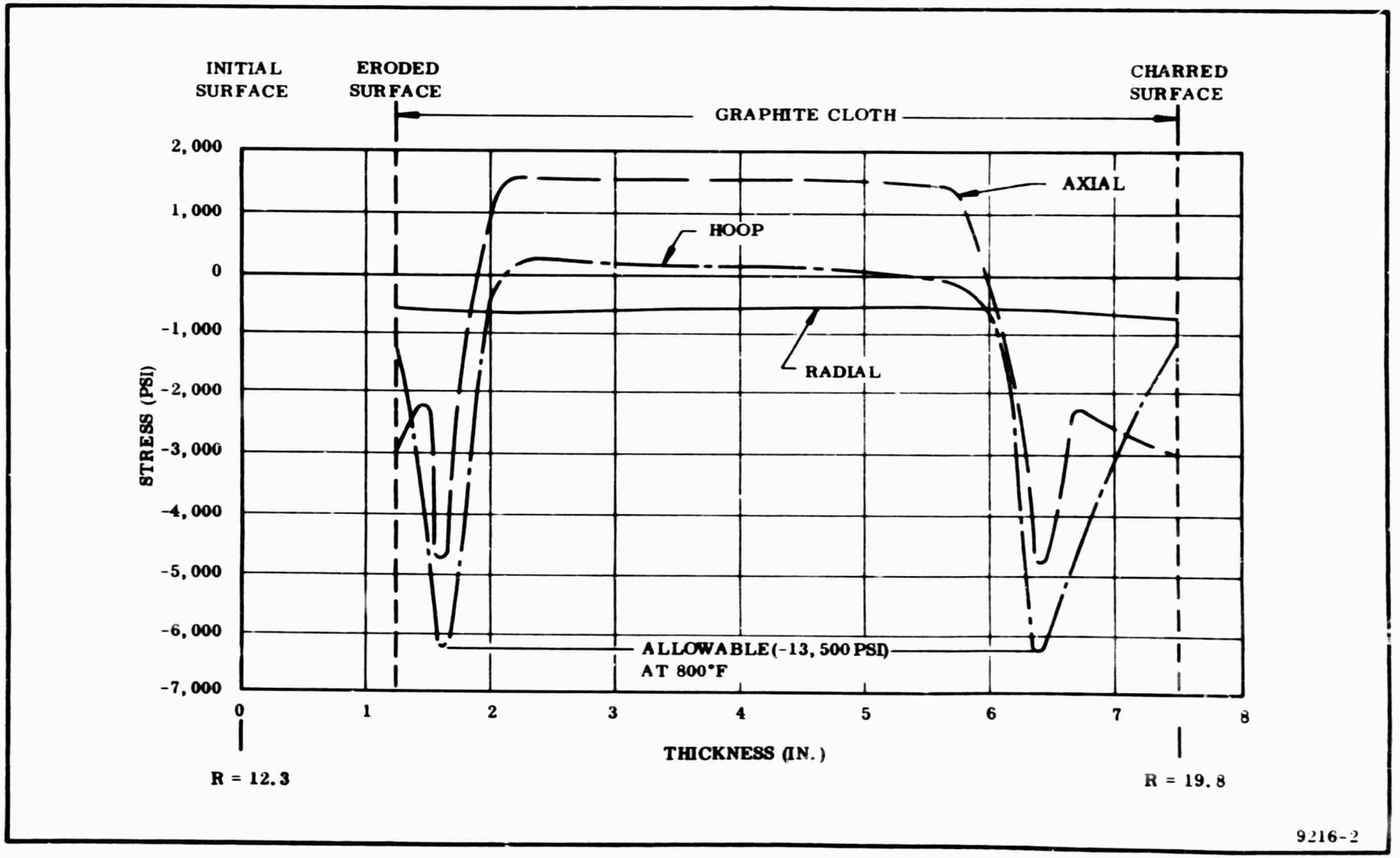

Figure 63. 156-7 Nozzle Thermal Stresses 8.0 In. Forward of Throat (Time = 108 Sec)

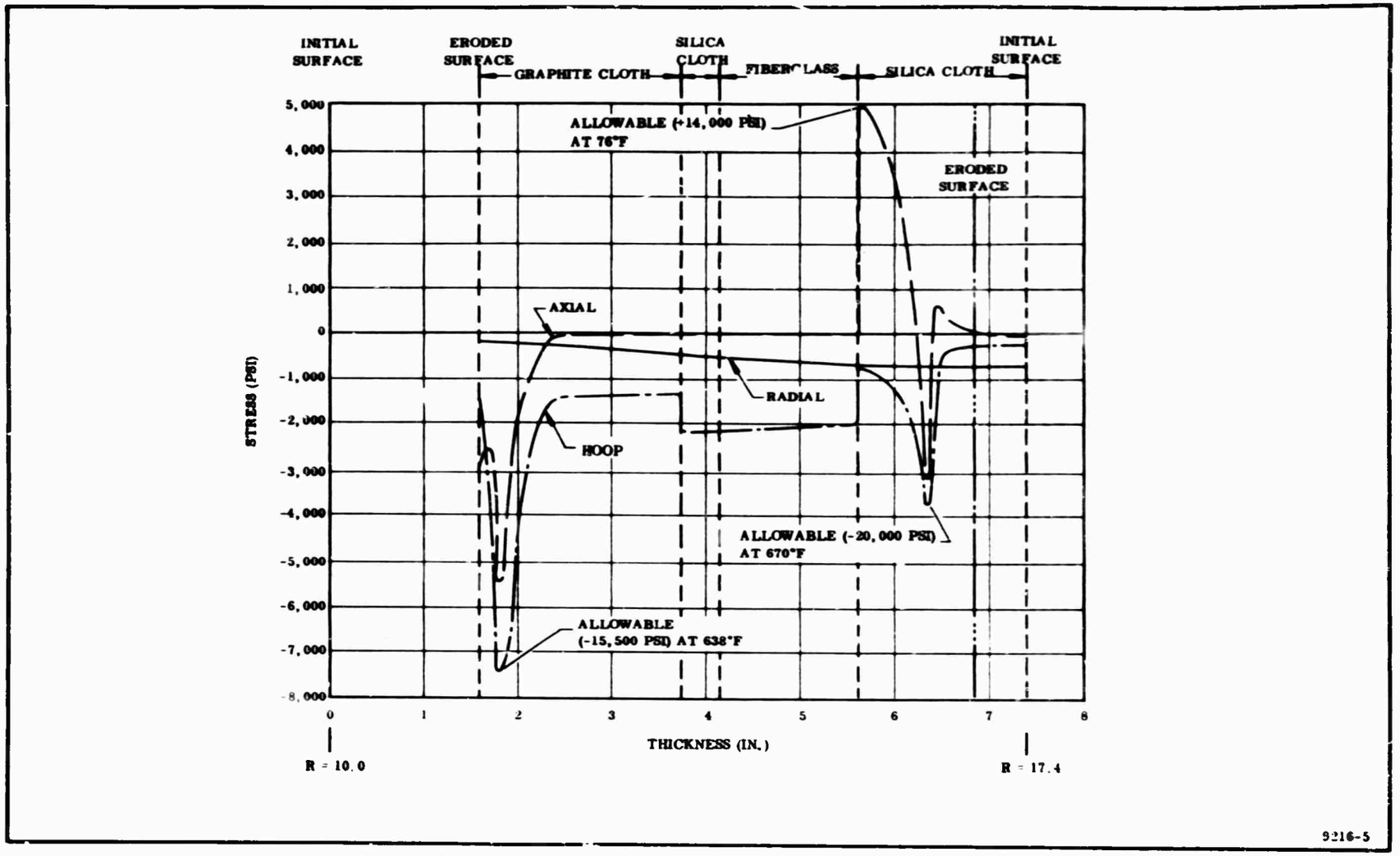

Figure 64. 156-7 Nozzle Thermal Stresses at Throat (Time = 108 Sec)

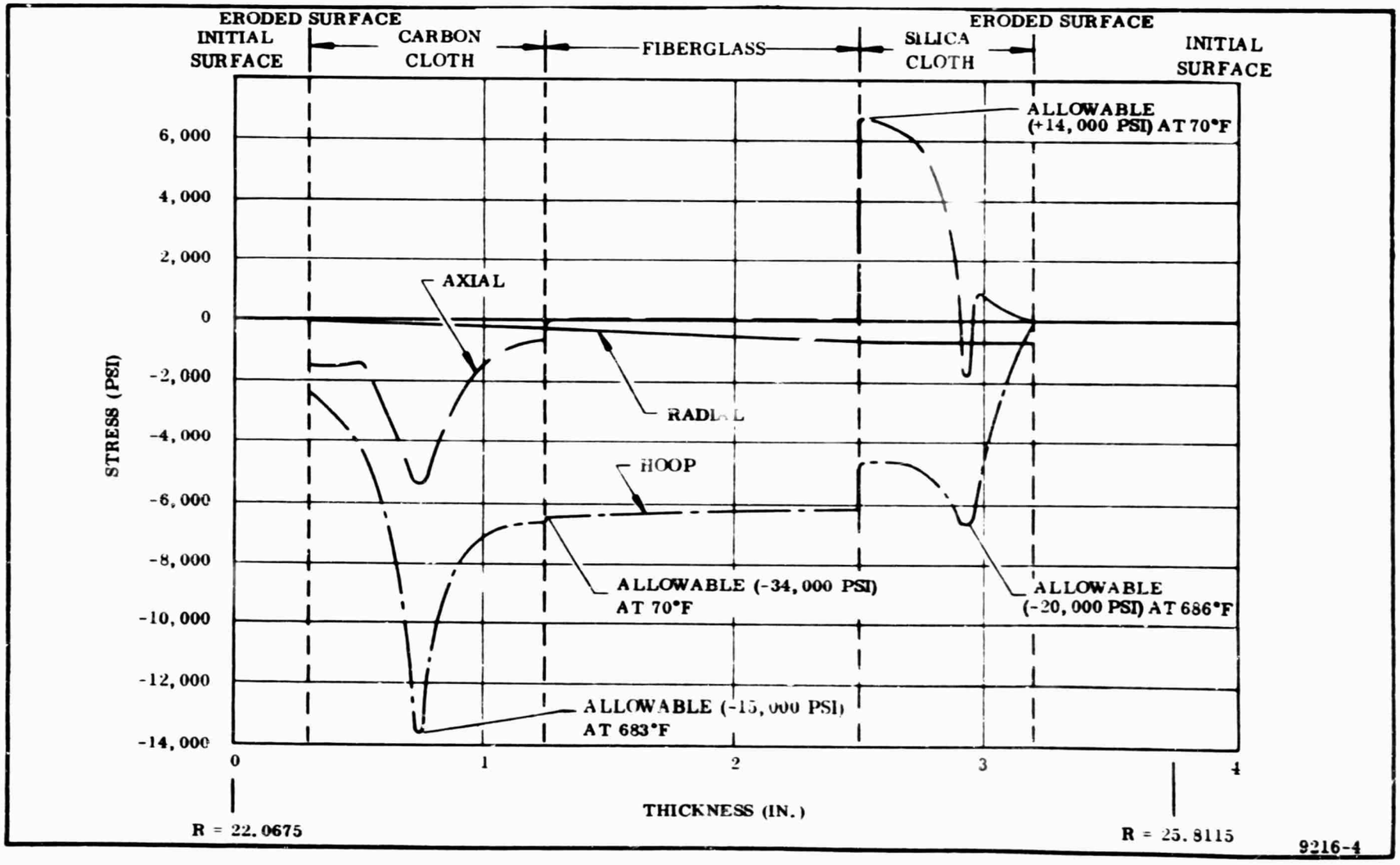

Figure 65. 156-7 Nozzle Thermal Stresses at A/A* = 4.0 (Time = 108 Sec)

a. Thermal Stress Analysis--An analysis was made of the stresses resulting from pressurization and temperature gradients in the submerged section of the nozzle. Three cross sections of the nozzle were analyzed using a computer program. Figure 7 shows the location of those sections.

At each section analyzed, the various materials are subdivided into numerous thin concentric cylinders such that the temperature in the cylinder is considered constant. The equation for radial deflection is written for the inside and outside of each cylinder based on material properties programed into the computer. These material properties have been compiled by Thiokol from vendor data, Government reports, and development tests. Each cylinder is allowed to deform internally and the deflections at the boundaries are set equal. The resulting matrix is solved for the interface contact pressures, and the values are used to calculate the tangential stresses and radial deflections. The program is set up so that various combinations of external boundary conditions can be imposed, such as known internal and external pressures or known inside and outside deflections.

The equations for this analysis were based on the solution given by Timoshenko (Reference 31). The general equation for radial stress in a cylinder subjected to thermal gradient is as follows:

$$\sigma_r = \frac{E}{(1+\mu)}\left[\frac{-(1+\mu)}{1-\mu}\frac{1}{R^2}\int_{R_1}^{R}\alpha\, TR\,dR + \frac{C_1}{1-2\mu} - \frac{C_2}{R^2} + \frac{\mu}{1-2\mu}\epsilon_z\right]$$

The longitudinal strain, ϵ_z, is:

$$\epsilon_z = \frac{\sigma 2}{E} - \frac{\mu}{E} (\sigma_r + \sigma_t) + \alpha T$$

and the boundary conditions are as follows:

at $R = R_1$ $\quad \sigma_r = \sigma_{r_i} = - P_i$ (internal pressure)

$R = R_o$ $\quad \sigma_r = \sigma_{ro} = - P_o$ (external pressure)

At the inside boundary the integral of the temperature term becomes zero:

$$\int_{R_i}^{R_i} \alpha TRdR = O$$

therefore:

$$\sigma_{r\,i} = - P_i = \frac{E}{1 + \mu}\left[\frac{C_1}{1 - 2\mu} + \frac{C_2}{R_i^2} + \frac{\mu}{1 - 2\mu} \epsilon_z\right] .$$

At the outside boundary of a cylinder, thin enough to consider the temperature constant, the integral of the temperature term reduces to:

$$\int_{R_i}^{R_o} \alpha TRdR = \frac{\alpha T}{2} (R_o^2 - R_i^2)$$

Therefore:

$$\sigma_{ro} = -P_o = \frac{E}{1 + \mu}\left[\frac{-(1 + \mu)\alpha T}{(1 - \mu) 2 R_o^2} (R_o^2 - R_i^2) + \frac{C_1}{1 - 2\mu} - \frac{C_2}{R_o^2} + \frac{\mu}{1 - 2\mu} \epsilon_z\right]$$

By taking the difference between the internal and external radial stress the constant C_2 is found:

$$C_2 = \frac{R_i^2 R_o^2}{(R_o^2 - R_i^2)}\left[\frac{(P_i - P_o)(1+\mu)}{E} + \frac{(1+\mu)}{(1-\mu)} \frac{\alpha T (R_o^2 - R_i^2)}{2 R_o^2}\right] .$$

The Constant C_1 can be found in terms of C_2 :

$$C_1 = -P_i \frac{(1+\mu)(1-2\mu)}{E} \frac{C_2 (1-2\mu)}{R_i^2} - \mu \epsilon_z .$$

The equation for the radial deflection can now be written, inward deflection being positive:

$$\Delta R = \omega = \frac{1}{R} \frac{(1+\mu)}{(1-\mu)} \int_{R_i}^{R} \alpha T R dR - C_1 R - \frac{C_2}{R} .$$

Considering the temperature to be constant, substituting for C_1 and C_2, and simplifying:

$$\omega = \frac{R_o^2 (1+\mu)}{ER (R_o^2 - R_i^2)}\left[R_o^2 + (1-2\mu)R^2\right] P_o - \frac{R_i^2 (1+\mu)}{ER (R_o^2 - R_i^2)}\left[R_o^2 + (1-2\mu)R^2\right] P$$

$$- (1+\mu) \alpha T R + \mu R \epsilon_z$$

The computer program has been setup so that the plane strain condition can be imposed by solving for an axial load, P_z, which causes ϵ_z to be constant.

This load is found through an iteration of the matrix solution using the following equation for the strain:

$$\epsilon_z = \frac{N_z + N_{zo}}{(R_o - R_i')\ E_i'} - \frac{u}{E_c}\ (\sigma_r + \sigma_t) + \alpha_i\ T$$

where:

N_{zo} is an input axial load if a known condition exists. The computer program will also select the material properties for the axial direction if a difference should exist.

Figures 63 through 65 are plots of the combined pressurization and thermal tangential stress distribution at the sections analyzed for several different times during the firing. The maximum predicted compressive stresses in the graphite cloth are at all times below the ultimate compressive strength of the material at that temperature.

b. Discontinuity Analysis of Flange-Submerged Shell and Case Polar Boss--

The flange shell as the main structural member in the nozzle distributes the blowout load, secondary injection side load and dynamic loads into the case closure with axial, shear, and bending moments through the bolted attachments. The components are broken down into small free bodies with all loads and reactions shown and then the deflections and rotations of the bodies are equated to each other and solved for the shear and moments per circumferential inch.

Figure 66 indicates the present design of flange and submerged shell and the stresses existing at critical locations in the cross sections. Inspection of the stresses and allowables indicate all exhibit a safety factor of 1.25 on yield stress.

The aft polar boss and the nozzle flange, attached together by 100 3/4 in. dia tensile type bolts (220,000 psi ultimate), are subjected to the highest discontinuity firing loads at static test.

The following loading conditions have been taken into consideration (Figure 67):

1. Internal case pressure
2. Deformation of shear ply between the fiberglass reinforced plastic and polar boss face
3. Thrust
4. External pressure

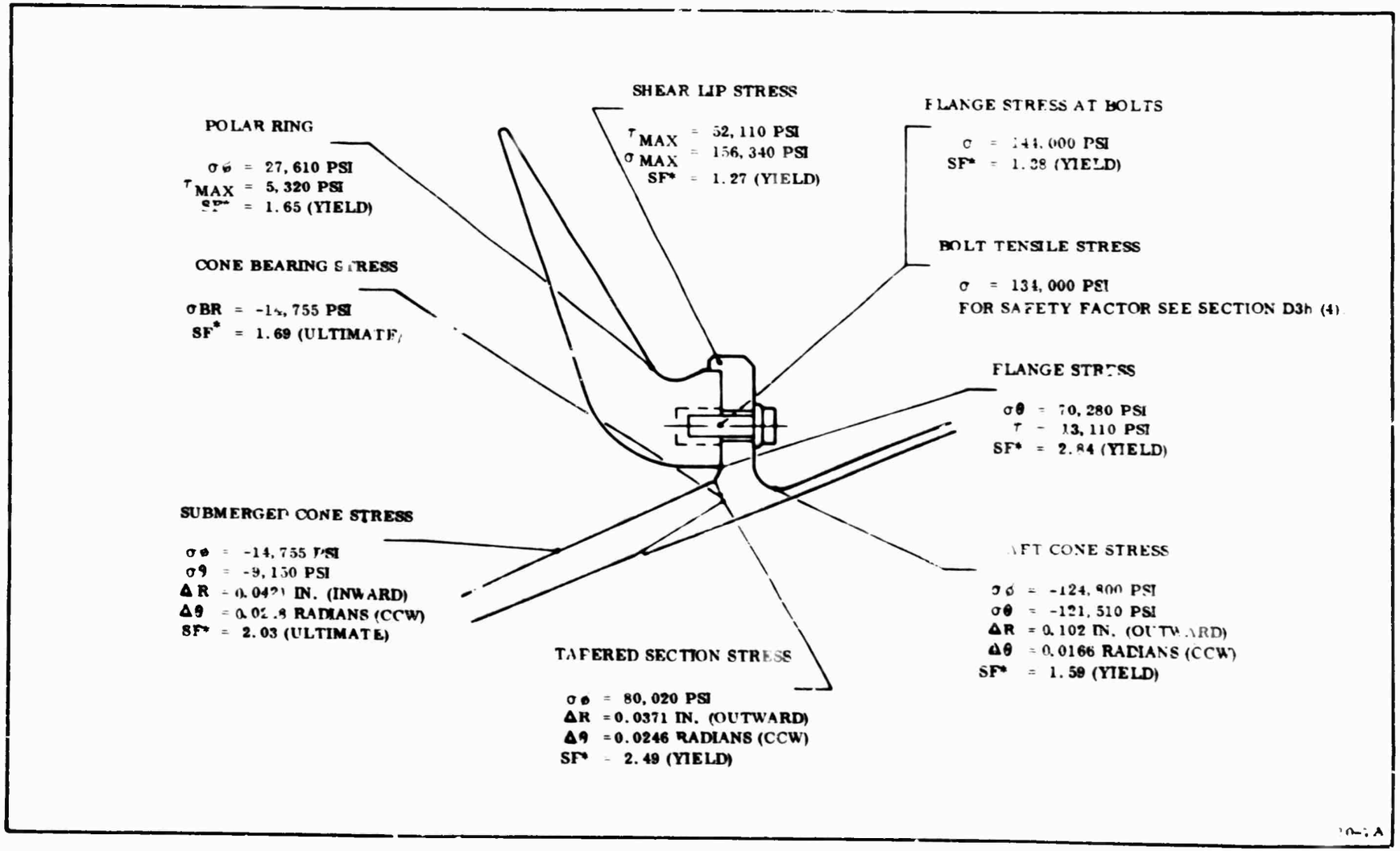

Figure 66. 156-7 Nozzle Discontinuity Stresses at Attachment Flange (Loads During Static Firing at MEOP)

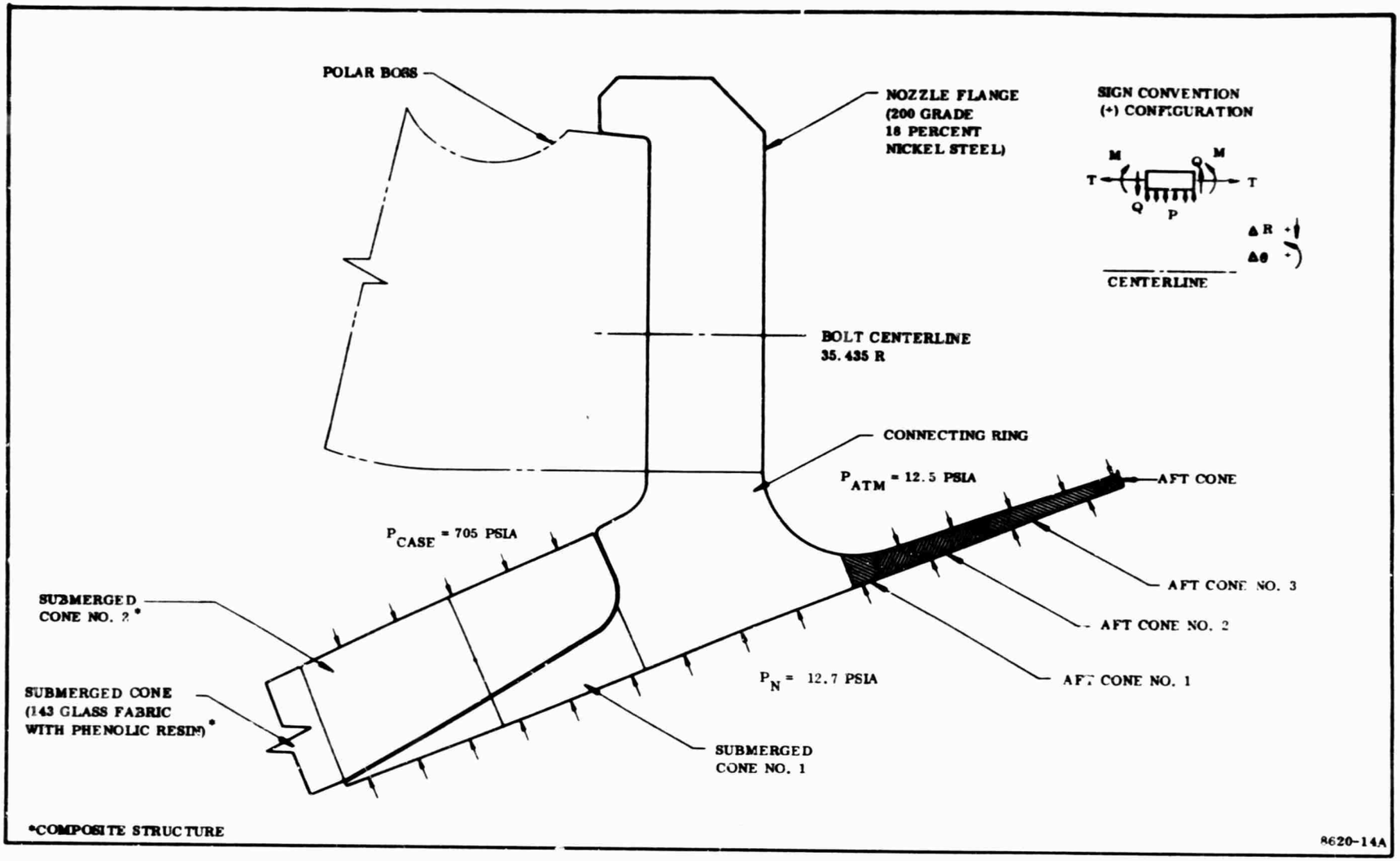

Figure 67. 156-7 Nozzle Flange Area

5. Axial loading due to:

LITVC

External pressure on nozzle cone

3g acceleration of nozzle relative to the case

Results shown on Figure 66 are based on a MEOP of 705 psia. Factors of safety shown for metal parts are based on material yield and those for non-metal parts are based on material ultimate strengths.

(1) Material Properties

Polar Boss

2014 - T652 Aluminum Alloy
(After case cure)

	F_{TU} (psi)	F_{TY} (psi)
Tangential	55,000	47,500
Radial	53,250	45,600
Axial	52,250	43,700

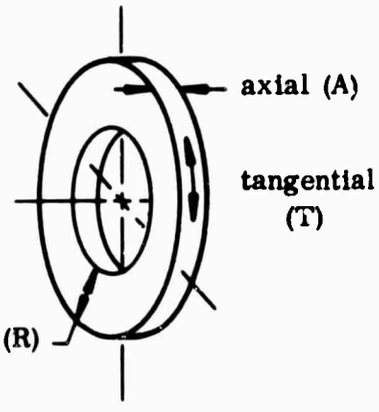

$F_S = 0.6\ F_T$

$E = 10.5 \times 10^6$ psi

$\mu = 0.33$

Nozzle Flange

18 percent Nickel Steel - 200 Grade

$F_{TU} = 210,000$ psi

$F_{TY} = 200,000$ psi

$F_S = 0.6\ F_T$

$E = 27 \times 10^6$ psi

$\mu = 0.3$

Bolt (tensile type)

3/4 - 16 UNF

F_{TY} = 180,000 psi

F_{TU} = 220,000 psi

Insert

(Cres 303)

F_{TU} = 110,000 psi

F_{TY} = 75,000 psi

Fiberglass Reinforced Plastic Cone

(58 percent horizontal, 42 percent longitudinal - 143 Glass Fabric with Phenolic Resin)

$F_{TU\phi}$ = 30,000 psi

$F_{TU\theta}$ = 33,000 psi

μ = 0.25

$E_{\phi} = E_{\theta}$ = 4×10^6 psi

(2) Boundary Load Summary

Internal case pressure	705 lb/sq in.
Load due to shear deformation of shear ply due to case strain parallel to polar boss surface	4,980 lb/in.
Thrust	400,000 lb
External pressure at Utah	12.5 lb/sq in.

Axial loading

LITVC	- 7,800 lb
External pressure	+ 84,000 lb
3g acceleration	+ 3,800 lb

(3) Discontinuity Analysis--Thiokol Program No. 3239, IBM 7040 Computer Program for Stress Analysis of a System of Free Bodies, computes and solves the discontinuity equations resulting from the input of the above boundary loads and the geometry of structural components.

(4) Maximum Stress in Polar Boss (Station 2)

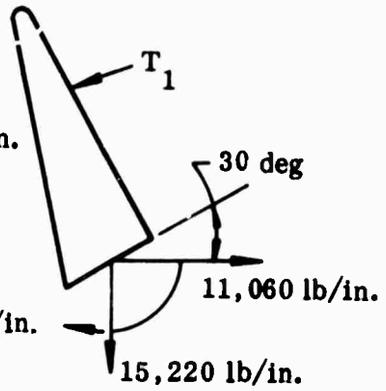

$M = -49{,}100$ in. lb/in. $\quad t = 3.6$ in.

$Q = -15{,}220$ lb/in.

$T = 11{,}060$ lb/in.

$$\sigma_{max} = \frac{6M}{t^2} + \frac{Q}{t}$$

$$\tau_{max} = \left(\frac{3}{2}\right)\left(\frac{T}{t \cos 30 \text{ deg}}\right)$$

At outboard side of junction

$$\sigma_{max} = \frac{6(49{,}100)}{(3.60)^2} + \frac{15{,}220}{(3.60) \cos 30 \text{ deg}}$$

$$= 22{,}730 + 4{,}880$$

$$= 27{,}610 \text{ psi}$$

$$\tau_{max} = \frac{(3)(11{,}060)}{2(3.60) \cos 30 \text{ deg}} = 5{,}320 \text{ psi}$$

$$F.S._{(min)} = \frac{F_{TYR}}{\sigma_{max}} = \frac{45{,}600}{27{,}610} = 1.65$$

(5) Stress in Bolt and Area Around Insert (Station 3)

$T = 10,340$ lb/in. $\quad \Delta R = -0.0444$ in.

$M = -20,850$ lb/in. $\quad \Delta\theta = +0.0246$ rad

Q is reacted by the shear lip

Bolt Stress

$\sigma_{bolt} = 134,000$ psi $\quad \sigma_{allowable} = 200,000$ psi

$$F.S. = \frac{F_{TY}}{\sigma_{bolt}} = \frac{180,000}{134,000} = 1.34$$ (See Section D3h (4))

Insert Stress

$$P_b = \sigma_{bolt} A_s$$

$$= 134,000\ (0.3734) = 50,040 \text{ lb/bolt}$$

Bolt - Insert Thread (Assume failure to be 2/3 the distance between pitch and minor dia in insert)

$$A_T = \frac{2}{3} \pi D_{so} L$$

$$= \frac{2\pi\ (0.71)\ (0.95)}{3}$$

$$= 1.413 \text{ sq in.}$$

$$\tau = \frac{P_b}{A_T}$$

$$= \frac{50,040}{1.413}$$

$$= 35,414 \text{ psi}$$

$$F.S. = \frac{F_{SY} \text{ (Insert)}}{\tau}$$

$$= \frac{0.6\ (75,000)}{35,414}$$

$$= 1.27$$

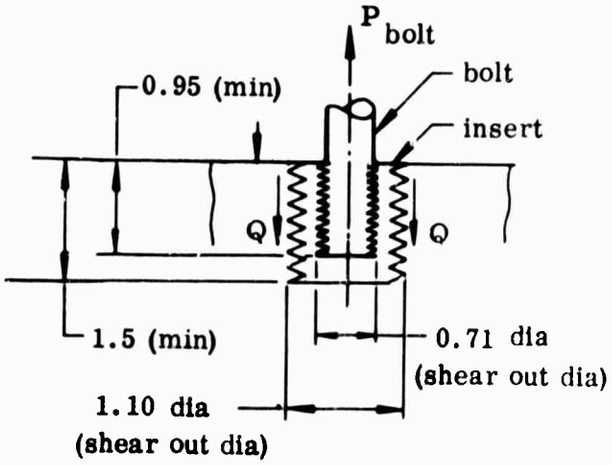

Insert - Polar Boss Thread (Assume failure to be 3/4 the distance between pitch and minor dia in polar boss)

$$A_T = \frac{3}{4} \pi D_{so} L$$

$$= \frac{3 \pi (1.10) (1.5)}{4}$$

$$= 3.887 \text{ sq in.}$$

$$\tau_{thread} = \frac{P_{bolt}}{A_T} = \frac{50,040}{3,887} = 12,870 \text{ psi}$$

$$F.S. = \frac{F_{SY} \text{ (Polar Boss)}}{\tau_{thread}}$$

$$= \frac{(0.6) (43,700)}{12,870} = 2.03$$

Stress in Shear Lip

$$Q = 20,845 \text{ lb/in.}$$

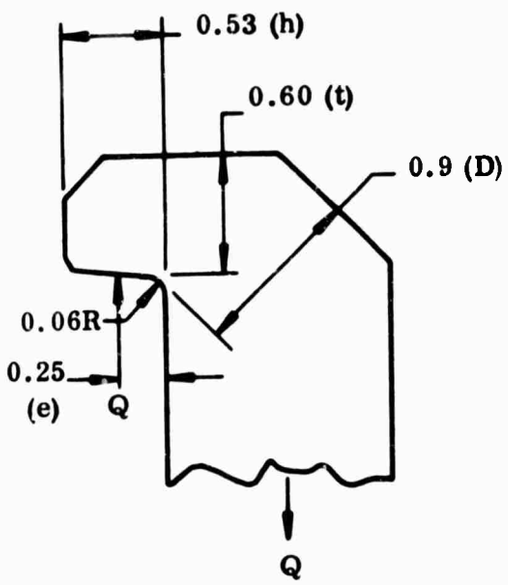

Shear

$$\tau_{max} = \left(\frac{3}{2}\right)\left(\frac{Q}{t}\right)$$

$$= \frac{(3) (20,845)}{(2) (0.60)} = 52,110 \text{ psi}$$

$$F.S. = \frac{F_{SY}}{\tau_{max}} = \frac{(200,000)\ (0.6)}{52,110} = 2.30$$

Bending

$$\sigma_{max} = K\left(\frac{6M}{t^2}\right)$$

where: K = Stress concentration factor (Reference 40 Figure 60)

$$\frac{r}{t} = \frac{0.06}{0.60} = 0.10$$

$$\frac{D}{t} = \frac{0.9}{0.60} = 1.5$$

K = 1.80 (From Figure 60 Reference 40)

$$\sigma_{max} = \frac{1.85\ (6)\ (Qe)}{(0.60)^2} = \frac{(1.80)(6)(20,845)(0.25)}{0.36}$$

$$= 156,340 \text{ psi}$$

$$F.S. = \frac{F_{TY}}{\sigma_{max}} = \frac{200,000}{156,340} = 1.27$$

Shear Stress in Polar Boss at Shear Lip

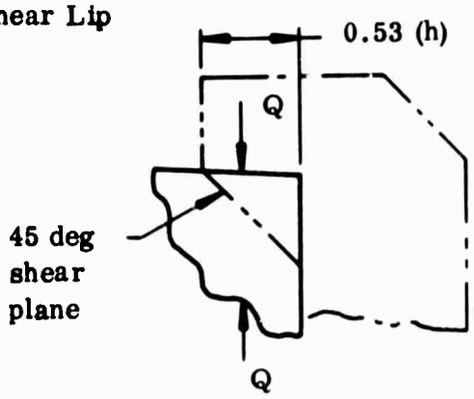

$$\tau_{45\ deg} = \frac{Q \cos^2 45\ deg}{h}$$

$$= \frac{(20,845)\ (0.707)^2}{0.53} = 19,660 \text{ psi}$$

$$F.S. = \frac{F_{SY}}{\tau_{45\ deg}} = \frac{(43,700)(0.6)}{19,660} = 1.33$$

(6) Stress in Nozzle Flange (Station 3)

$M = 17,000$ in. lb/in.

$Q = 20,845$ lb/in.

$S_B = 2.22$ in. between bolts

Typical Section Between Bolts

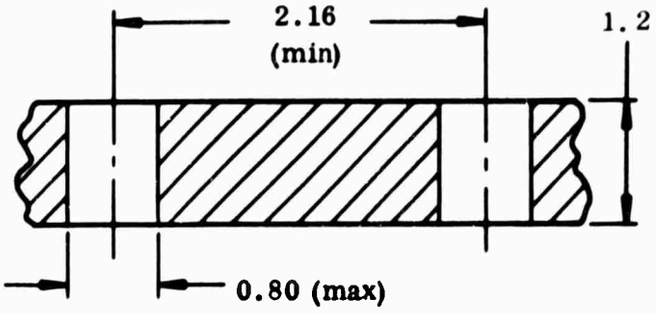

$$M_{sect} = MS_B = 17,000\ (2.22) = 37,740 \text{ in. lb}$$

$$Q_{sect} = QS_B = 20,845\ (2.22) = 46,280 \text{ lb}$$

$$I_{sect} = \frac{b\ h^3}{12} = \frac{(2.16 - 0.80)(1.2)^3}{12} = 0.1958 \text{ in.}^4$$

$$\sigma = \frac{Mc}{I} + \frac{Q}{A}$$

$$= \frac{(37,740)(0.6)}{0.1958} + \frac{46,280}{(2.16 - 0.80)(1.2)}$$

$$= 115,650 + 28,360 = 144,000 \text{ psi}$$

$$F.S. = \frac{F_{TY}}{\sigma} = \frac{200,000}{144,000} = 1.38$$

(7) Stress in Flange Connection Ring Junction (Station 4)

$M = 13,920$ in. lb/in. $\quad \Delta\theta = +0.0246$ rad

$Q = -14,740$ lb/in. $\quad \Delta R = -0.0595$ in.

$T = 10,490$ lb/in.

Shear

$$\tau_{max} = \left(\frac{3}{2}\right)\left(\frac{T}{t}\right) = \frac{(3)\ (10,490)}{(2)\ (1.2)} = 13,110 \text{ psi}$$

$$\text{F.S.} = \frac{F_{SY}}{\tau_{max}} = \frac{(200,000)\ 0.6}{13,110} = 9.15$$

Bending

$$\sigma_{max} = \frac{6M}{t^2} + \frac{Q}{t}$$

$$= \frac{(6)\ (13,920)}{(1.2)^2} + \frac{14,740}{1.2}$$

$$= 58,000 + 12,280 = 70,280 \text{ psi}$$

$$\text{F.S.} = \frac{F_{TY}}{\sigma_{max}} = \frac{200,000}{70,280} = 2.84$$

(8) Stress in Aft Cone Junction with Ring (Station 6)

$M = -1,636$ in. lb/in. $\quad \Delta\theta = +0.0166$ rad

$Q = -1,400$ lb/in. $\quad \Delta R = -0.102$ in.

$T = +417$ lb/in.

Inside Surface of Cone

$\sigma_\phi = -125,640$ psi

$\sigma_\theta = +46,380$ psi

Outside Surface of Cone

$\sigma_\phi = -124,800$ psi

$\sigma_\theta = -121,510$ psi

$$\text{F.S. (min)} = \frac{F_{TY}}{\sigma_{\phi}\ \text{(inside)}}$$

$$= \frac{200,000}{125,640} = 1.59$$

(9) Stress in Submerged Cone Junction with Ring (Station 9)

$M = -3,912$ in. lb/in. $\quad \Delta\theta = +0.0246$ rad

$Q = +3,267$ lb/in. $\quad \Delta R = -0.0371$ in.

$T = -10,320$ lb/in.

The steel section of the cone segment is assumed to react the moment and shear loading.

At Outside Surface of Steel Section

$$\sigma_{\phi o} = -\frac{6M}{t^2} + \left(\frac{Q}{t}\right)\cos\phi$$

$$= -\frac{(6)(-3,912)}{(0.55)^2} + \frac{(+3,267)(\cos 66\ \text{deg})}{0.55}$$

$$= +77,600 + 2,420 = 80,020 \text{ psi}$$

$$F.S. = \frac{F_{TY}}{\sigma_{\phi o}} = \frac{200,000}{80,020} = 2.49$$

Hoop Stress at Outside Surface of Fiberglass Reinforced Plastic Section

$$\sigma_{\theta} = -\frac{E_{\theta}}{R_o}\left[\Delta R_9\right]$$

$$= -\frac{11.7 \times 10^6}{33.3}\left[-0.03706\right]$$

$$= 13,000 \text{ psi}$$

$$F.S. = \frac{F_{TU\theta}}{\sigma_{\theta}} = \frac{33,000}{13,000} = 2.53$$

Bearing Stress Between Fiberglass Reinforced Plastic Section and Ring

$$\sigma_{br} = \frac{T}{A_b} = \frac{10,320}{0.50} = 20,640 \text{ psi}$$

$$F.S. = \frac{F_{BRU}}{\sigma_{br}} = \frac{35,000}{20,640} = 1.69$$

(10) Stress in Fiberglass Reinforced Plastic Cone at Junction with Steel Tongue (Station 11)

$M = + 1,588$ in. lb/in. $\quad \Delta\theta = + 0.0248$ rad

$Q = + 846$ lb/in. $\quad \Delta R = + 0.0421$ in.

$T = - 10,110$ lb/in.

Inside Surface of Cone

$$\sigma_{\phi} = - 1,522 \text{ psi}$$

$$\sigma_{\theta} = - 5,840 \text{ psi}$$

Outside Surface of Cone

$$\sigma_{\phi} = - 14,755 \text{ psi}$$

$$\sigma_{\theta} = - 9,150 \text{ psi}$$

$$F.S._{\phi} = \frac{F_{TU\phi}}{\sigma_{\phi}} = \frac{30,000}{14,755} = 2.03$$

$$F.S._{\theta} = \frac{F_{TU\theta}}{\sigma_{\theta}} = \frac{33,000}{9,150} = 3.60$$

Since σ_{ϕ} and σ_{θ} are both compressive at the surface bonded to the steel tongue, the pressure between the two is positive; therefore, there is no tendency to peel the adhesive between the two surfaces.

An aft polar boss and nozzle discontinuity analysis for flight test conditions was conducted (IBM 7040 computer program No. 3239). The revised aft polar boss is shown on page 130.

The preliminary analysis revealed that the static test condition was the critical condition. Therefore the flight test condition was not re-run when the nozzle flange was redesigned for grade 200 18 percent nickel steel.

The aft polar boss and nozzle discontinuity analysis was then conducted for static test conditions. The results of this analysis are presented on pages 131 through 152.

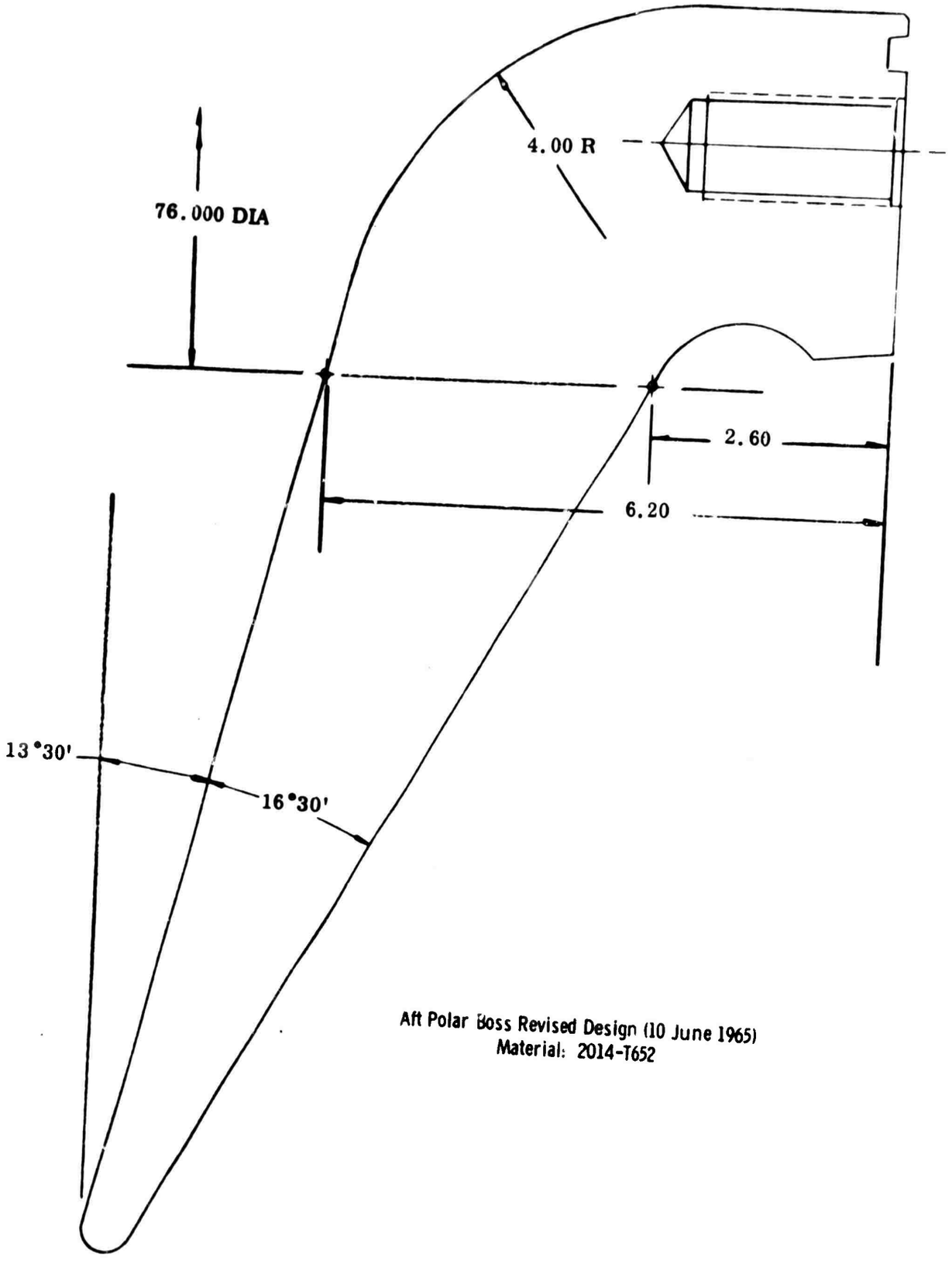

Aft Polar Boss Revised Design (10 June 1965)
Material: 2014-T652

TU-394 AFT POLAR BOSS(7U37724A) AND NOZZLE DISCONTINUITY STRESS ANALYSIS
STATIC FIRING CONDITIONS AT MEOP 23JULY 65
CASE PRESS.# 705PSIA THRUST # 400000LBS EXT. AXIAL LOAD # +80000LBS

FAKE BODY TO ORIENT REACTED LOAD ON POLAR BOSS

FREE BODY NUMBER 1 SEMI-INFINITE CONE

0.00000 --- INTERNAL PRESSURE, PSI	100.000000 --- THICKNESS FOR STRESSES AT STATION(1), IN.
43.50000 --- RADIUS TO MID-POINT OF STATION(1), IN.	0.000010 --- THICKNESS FOR DEFLECTIONS, IN.
13.44000 --- RADIUS OF THROAT, IN.	0.000010 X 10E6 - MODULUS OF ELASTICITY, PSI
-4.61090 --- PRESSURIZED RADIUS AT STATION(1), IN.	0.330000 --- POISSONS RATIO
74.20000 --- PHI, DEGREES	60.138698 --- DAMPING FUNCTION
-0.27228 --- COSINE OF PHI	0.000000 X 10E6 --- FLEXURAL RIGIDITY, IN-LBS.
0.96222 --- SINE OF PHI	0.000000 --- AXIAL LOAD AT STATION(1), LBS/IN.
45.20805 --- MEAN RADIUS OF CURVATURE NORMAL TO MERIDIAN (R2), IN.	

0.0000000 --- M(1) - MOMENT, IN-LBS/IN.	0.0246294 --- DELTA THETA (1) - ROTATION, RADIANS
-0.0000000 --- Q(1) - SHEAR FORCE, LBS/IN.	0.0976670 --- DELTA RADIUS (1) - CHANGE IN RADIUS, IN.

DELTA THETA (1) --- •••••••••••••••• M(1) •••••••••••••••• Q(1) 0.0000000
DELTA RADIUS(1) --- •••••••••••••••• M(1) •••••••••••••••• Q(1) 0.0000000

STRESSES AT STATION(1)

0.0000000 --- SIGMA(1P)	BASIC MERIDIONAL STRESS, PSI
-0.0000000 --- SIGMA(1Q)	MERIDIONAL STRESS DUE TO SHEAR, PSI
0.0000000 --- SIGMA(1M)	MERIDIONAL STRESS DUE TO MOMENT, PSI
-0.0000000 --- SIGMA(1I)	MAXIMUM COMBINED INSIDE MERIDIONAL STRESS,PSI
-0.0000000 --- SIGMA(1O)	MAXIMUM COMBINED OUTSIDE MERIDIONAL STRESS, PSI
0.0000000 --- SIGMA(2P)	BASIC TANGENTIAL STRESS, PSI
-0.0000000 --- SIGMA(2Q)	TANGENTIAL STRESS DUE TO SHEAR, PSI
0.0000000 --- SIGMA(2M)	TANGENTIAL STRESS DUE TO MOMENT, PSI
0.0000000 --- SIGMA(2,1M)	TANGENTIAL STRESS DUE TO SIGMA(1M), PSI
-0.0000000 --- SIGMA(2I)	MAXIMUM COMBINED INSIDE TANGENTIAL STRESS, PSI
-0.0000000 --- SIGMA(2O)	MAXIMUM COMBINED OUTSIDE TANGENTIAL STRESS, PSI

TAPER SECTION OF POLAR RING

FREE BODY NUMBER 2 RING

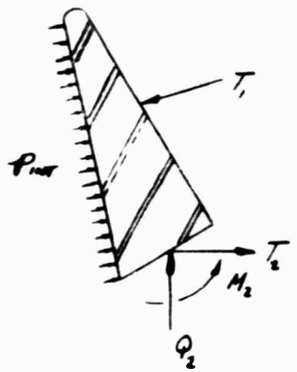

705.0000000 --- INTERNAL PRESSURE(1), PSI.
12.0000000 --- THROAT RADIUS(1), IN.
43.5000000 --- RADIUS TO MID-POINT OF STATION(1), IN.

705.0000000 --- INTERNAL PRESSURE(2), PSI.
12.0000000 --- THROAT RADIUS(2), IN.
36.9499992 --- RADIUS TO MID-POINT OF STATION(2), IN.

40.6465352 --- RADIUS TO CENTROID, IN.

105.8000000 --- PHI AT STATION(1), DEGREES
0.9622180 --- SINE PHI AT STATION(1)
-0.2722803 --- COSINE PHI AT STATION(1)

89.9999984 --- PHI AT STATION(2), DEGREES
1.0000000 --- SINE PHI AT STATION(2)
-0.0000000 --- COSINE PHI AT STATION(2)

10.500 X 10E6 - ELASTIC MODULUS, PSI.

28.9879992 --- AREA OF CROSS-SECTION OF RING, SQ. IN.

48.1619700 --- MOMENT OF INERTIA ABOUT THE Y-AXIS, IN.(4TH)

7964.9999872 --- HORIZONTAL COMPONENT OF PRESSURE, P1, LB/IN.
1874.0000000 --- VERTICAL COMPONENT OF PRESSURE, P2, LB/IN.
0.0000000 --- HORIZONTAL COMPONENT OF PRESSURE, P3, LB/IN.

-1.1034644 --- VERTICAL DISTANCE FROM CENTROID TO P1, IN.
1.0997541 --- HORIZONTAL DISTANCE FROM CENTROID TO P2, IN.
0.0000000 --- VERTICAL DISTANCE FROM CENTROID TO P3, IN.

2.8534644 --- VERTICAL DISTANCE FROM CENTROID TO AXIAL LOAD(1), IN.
-3.6965356 --- VERTICAL DISTANCE FROM CENTROID TO AXIAL LOAD(2), IN.

-0.1802458 --- HORIZONTAL DISTANCE FROM CENTROID TO AXIAL LOAD(1), IN.
1.8702458 --- HORIZONTAL DISTANCE FROM CENTROID TO AXIAL LOAD(2), IN.

-4.6108985 --- PRESSURIZED RADIUS AT STATION(1), IN.
36.0999996 --- PRESSURIZED RADIUS AT STATION(2), IN.

20449.9998720 --- AXIAL LOAD AT STATION(1), LB/IN. (T_1)
11058.7692032 --- AXIAL LOAD AT STATION(2), LB/IN. (T_2)

4.5465356 --- VERTICAL DISTANCE TO CENTROID, IN.

2.4997541 --- HORIZONTAL DISTANCE TO CENTROID, IN.

0.0000000 --- M(1) --- MOMENT, IN-LB/IN.
-49065.9790848 --- M(2) --- MOMENT, IN-LB/IN.

-0.0000000 --- Q(1) --- SHEAR, LB/IN.
-15216.9185280 --- Q(2) --- SHEAR, LB/IN.

0.0976670 --- DELTA RADIUS(1) - CHANGE IN RADIUS, IN.
0.0560432 --- DELTA RADIUS(2) - CHANGE IN RADIUS, IN.

0.0246294 --- DELTA THETA(1) - ROTATION, RADIANS
0.0246294 --- DELTA THETA(2) - ROTATION, RADIANS

Q(NET)

1.0000 Q(1) -1.0000 Q(2) 3594.1317

DELTA RADIUS (C)

5.4280 Q(1) -5.4280 Q(2) 19508.9326

M(NET)

-1.0000 M(1) -0.1802 Q(1) 1.0000 M(2) 1.8702 Q(2) 85064.1296

DELTA THETA (1)

-3.2670 M(1) -0.5889 Q(1) 3.2670 M(2) 6.1102 Q(2) 277907.3184

DELTA RADIUS(1)

0.5889 M(1) 5.5341 Q(1) -0.5889 M(2) -6.5293 Q(2) -30582.7072

DELTA THETA (2)

-3.2670 M(1) -0.5889 Q(1) 3.2670 M(2) 6.1102 Q(2) 277907.3184

DELTA RADIUS(2)

6.1102 M(1) 6.5293 Q(1) -6.1102 M(2) -16.8555 Q(2) -500246.0608

BOLTED SECTION OF POLAR RING

FREE BODY NUMBER 3 RING

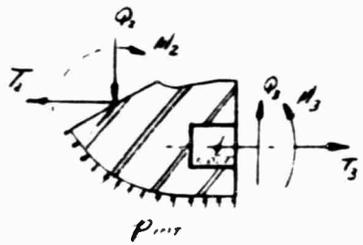

705.0000000	--- INTERNAL PRESSURE(2), PSI.	89.9999984	--- PHI AT STATION(2), DEGREES
12.0000000	--- THROAT RADIUS(2), IN.	1.0000000	--- SINE PHI AT STATION(2)
36.9599992	--- RADIUS TO MID-POINT OF STATION(2), IN.	-0.0000000	--- COSINE PHI AT STATION(2)
705.0000000	--- INTERNAL PRESSURE(3), PSI.	89.9999984	--- PHI AT STATION(3), DEGREES
12.0000000	--- THROAT RADIUS(3), IN.	1.0000000	--- SINE PHI AT STATION(3)
35.4169988	--- RADIUS TO MID-POINT OF STATION(3), IN.	-0.0000000	--- COSINE PHI AT STATION(3)
35.7792636	--- RADIUS TO CENTROID, IN.	10.500 X 10E6	- ELASTIC MODULUS, PSI.

15.7867892	--- AREA OF CROSS-SECTION OF RING, SQ. IN.	31.7246856	--- MOMENT OF INERTIA ABOUT THE Y-AXIS, IN.(4TH)
1495.0000000	--- HORIZONTAL COMPONENT OF PRESSURE, P1, LB/IN.	0.7392647	--- VERTICAL DISTANCE FROM CENTROID TO P1, IN.
3989.9999744	--- VERTICAL COMPONENT OF PRESSURE, P2, LB/IN.	0.5115887	--- HORIZONTAL DISTANCE FROM CENTROID TO P2, IN.
282.0000000	--- HORIZONTAL COMPONENT OF PRESSURE, P3, LB/IN.	-1.3992646	--- VERTICAL DISTANCE FROM CENTROID TO P3, IN.
1.1807353	--- VERTICAL DISTANCE FROM CENTROID TO AXIAL LOAD(2), IN.	1.7615887	--- HORIZONTAL DISTANCE FROM CENTROID TO AXIAL LOAD(2), IN.
-0.3622646	--- VERTICAL DISTANCE FROM CENTROID TO AXIAL LOAD(3), IN.	2.3184113	--- HORIZONTAL DISTANCE FROM CENTROID TO AXIAL LOAD(3), IN.
36.0999996	--- PRESSURIZED RADIUS AT STATION(2), IN.	11055.7770752	--- AXIAL LOAD AT STATION(2), LB/IN. (T_2)
34.3999996	--- PRESSURIZED RADIUS AT STATION(3), IN.	10344.5913600	--- AXIAL LOAD AT STATION(3), LB/IN. (T_3)
1.7992646	--- VERTICAL DISTANCE TO CENTROID, IN.	3.3415887	--- HORIZONTAL DISTANCE TO CENTROID, IN.

-49965.9790848	--- M(2) --- MOMENT, IN-LB/IN.	-15216.9185280	--- QI 2) --- SHEAR, LB/IN.
17007.0132736	--- M(3) --- MOMENT, IN-LB/IN.	-20845.7488384	--- QI 3) --- SHEAR, LB/IN.

0.0560432	--- DELTA RADIUS(2) - CHANGE IN RADIUS, IN.	0.0246294	--- DELTA THETAI 2) - ROTATION, RADIANS
-0.0444448	--- DELTA RADIUSI 3) - CHANGE IN RADIUS, IN.	0.0246294	--- DELTA THETAI 3) - ROTATION, RADIANS

Q(NET)

1.0000 Q(2) -1.0000 Q(3) -3990.0000

DELTA RADIUS (C)

7.7228 Q(2) -7.7228 Q(3) -30813.9288

M(NET)

-1.0000 M(2) 1.7616 Q(2) 1.0000 M(3) 2.3184 Q(3) 15470.7964

DELTA THETA (2)

-3.8431 M(2) 6.7699 Q(2) 3.8431 M(3) 8.9098 Q(3) 59455.0624

DELTA RADIUS(2)

-6.7699 M(2) 19.6485 Q(2) 6.7699 M(3) 7.9726 Q(3) 73921.4368

DELTA THETA (3)

-3.8431 M(2) 6.7699 Q(2) 3.8431 M(3) 8.9098 Q(3) 59455.0624

DELTA RADIUS(3)

8.9098 M(2) -7.9726 Q(2) -8.9098 M(3) -28.3793 Q(3) -168655.2144

3/4-16UNF BOLTS(100)

BOLT NO. 7 CONNECTING FREE BODIES 3 AND 4

2.2200000 --- BOLT SPACING, IN.
1.4000000 --- DISTANCE TO PIVOT POINT, IN.
0.3734000 --- STRESS AREA OF BOLT, SQ. IN.
0.0000000 --- EFFECTIVE LENGTH OF BOLT, IN.
30.0000000 X 10E6 - ELASTIC MODULUS OF BOLT, PSI
90.0000000 --- PHI, DEGREES
34.3999996 --- PRESSURIZED RADIUS, IN.

17007.0132736 --- M(3) - MOMENT, IN-LB/IN.

-20845.7488384 --- Q(3) - SHEAR, LB/IN (REACTED BY SHEAR LIP)

0.0000000 --- DELTA THETA (3) - ANGLE OF SEPARATION BETWEEN MATING SURFACES, RADIANS

DELTA THETA (3) --- 0.0000000 M(3) 0.0000000

61502.3902720 --- SIGMA (1P) BASIC BOLT STRESS, PSI

72223.5228160 --- SIGMA (1M) BOLT STRESS DUE TO BENDING, PSI

133725.9130880 --- SIGMA (T) TOTAL TENSILE STRESS, PSI

NOZZLE FLANGE (18-NI STEEL - 200 GRADE)

FREE BODY NUMBER 4 RING

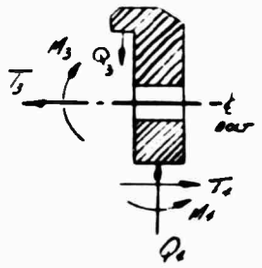

705.0000000 --- INTERNAL PRESSURE(3), PSI.
12.0000000 --- THROAT RADIUS(3), IN.
35.4349996 --- RADIUS TO MID-POINT OF STATION(3), IN.

89.9999984 --- PHI AT STATION(3), DEGREES
1.0000000 --- SINE PHI AT STATION(3)
-0.0000000 --- COSINE PHI AT STATION(3)

705.0000000 --- INTERNAL PRESSURE(4), PSI.
12.0000000 --- THROAT RADIUS(4), IN.
33.9999992 --- RADIUS TO MID-POINT OF STATION(4), IN.

89.9999984 --- PHI AT STATION(4), DEGREES
1.0000000 --- SINE PHI AT STATION(4)
-0.0000000 --- COSINE PHI AT STATION(4)

36.1430572 --- RADIUS TO CENTROID, IN.

27.000 X 10E6 - ELASTIC MODULUS, PSI.

5.1339999 --- AREA OF CROSS-SECTION OF RING, SQ. IN.

0.7654962 --- MOMENT OF INERTIA ABOUT THE Y-AXIS, IN.(4TH)

282.0000000 --- HORIZONTAL COMPONENT OF PRESSURE, P1, LB/IN.
0.0000000 --- VERTICAL COMPONENT OF PRESSURE, P2, LB/IN.
0.0000000 --- HORIZONTAL COMPONENT OF PRESSURE, P3, LB/IN.

1.9430575 --- VERTICAL DISTANCE FROM CENTROID TO P1, IN.
1.0718365 --- HORIZONTAL DISTANCE FROM CENTROID TO P2, IN.
0.0000000 --- VERTICAL DISTANCE FROM CENTROID TO P3, IN.

-0.7080575 --- VERTICAL DISTANCE FROM CENTROID TO AXIAL LOAD(3), IN.
-2.1430575 --- VERTICAL DISTANCE FROM CENTROID TO AXIAL LOAD(4), IN.

0.5318365 --- HORIZONTAL DISTANCE FROM CENTROID TO AXIAL LOAD(3), IN.
0.0781635 --- HORIZONTAL DISTANCE FROM CENTROID TO AXIAL LOAD(4), IN.

34.3999996 --- PRESSURIZED RADIUS AT STATION(3), IN.
34.0000000 --- PRESSURIZED RADIUS AT STATION(4), IN.

10339.3363968 --- AXIAL LOAD AT STATION(3), LB/IN. (T_3)
10492.0588288 --- AXIAL LOAD AT STATION(4), LB/IN. (T_4)

2.1430575 --- VERTICAL DISTANCE TO CENTROID, IN.

1.0718365 --- HORIZONTAL DISTANCE TO CENTROID, IN.

17807.0132736 --- M(3) --- MOMENT, IN-LB/IN.
13923.1428608 --- M(4) --- MOMENT, IN-LB/IN.

-20845.7488384 --- Q(3) --- SHEAR, LB/IN.
-14739.6089856 --- Q(4) --- SHEAR, LB/IN.

-0.0444448 --- DELTA RADIUS(3) - CHANGE IN RADIUS, IN.
-0.0594687 --- DELTA RADIUS(4) - CHANGE IN RADIUS, IN.

0.0246294 --- DELTA THETA(3) - ROTATION, RADIANS
0.0246294 --- DELTA THETA(4) - ROTATION, RADIANS

Q(NET)

1.0000 Q(3)	-1.0000 Q(4)	-0.0000

DELTA RADIUS (C)

9.4239 Q(3)	-9.4239 Q(4)	-0.0000

M(NET)

-1.0000 M(3)	0.5318 Q(3)	1.0000 M(4)	0.0782 Q(4)	15716.1826

DELTA THETA (3)

-63.2038 M(3)	33.6141 Q(3)	63.2038 M(4)	4.9402 Q(4)	993069.1456

DELTA RADIUS(3)

-33.6141 M(3)	27.3011 Q(3)	33.6141 M(4)	-6.7965 Q(4)	528150.3936

DELTA THETA (4)

-63.2038 M(3)	33.6141 Q(3)	63.2038 M(4)	4.9402 Q(4)	993069.1456

DELTA RADIUS(4)

4.9402 M(3)	6.7965 Q(3)	-4.9402 M(4)	-9.8100 Q(4)	-77621.7640

RING CONNECTING FLANGE WITH CONES

FREE BODY NUMBER 5 RING

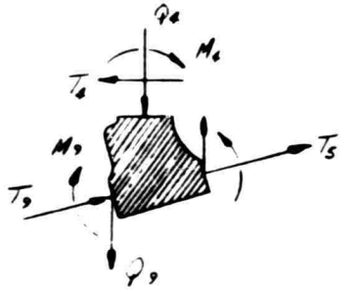

705.0000000 --- INTERNAL PRESSURE(4), PSI.
12.0000000 --- THROAT RADIUS(4), IN.
34.0000000 --- RADIUS TO MID-POINT OF STATION(4), IN.

89.9999984 --- PHI AT STATION(4), DEGREES
1.0000000 --- SINE PHI AT STATION(4)
-0.0000000 --- COSINE PHI AT STATION(4)

-6.0000000 --- INTERNAL PRESSURE(5), PSI.
0.0000000 --- THROAT RADIUS(5), IN.
32.9499992 --- RADIUS TO MID-POINT OF STATION(5), IN.

112.4999984 --- PHI AT STATION(5), DEGREES
0.9238795 --- SINE PHI AT STATION(5)
-0.3826835 --- COSINE PHI AT STATION(5)

-705.0000000 --- INTERNAL PRESSURE(9), PSI.
13.4399998 --- THROAT RADIUS(9), IN.
32.7999992 --- RADIUS TO MID-POINT OF STATION(9), IN.

114.0000000 --- PHI AT STATION(9), DEGREES
0.9135456 --- SINE PHI AT STATION(9)
-0.4067367 --- COSINE PHI AT STATION(9)

33.0098880 --- RADIUS TO CENTROID, IN.

27.000 X 10E6 - ELASTIC MODULUS, PSI.

3.4999498 --- AREA OF CROSS-SECTION OF RING, SQ. IN.

1.2659461 --- MOMENT OF INERTIA ABOUT THE Y-AXIS, IN.(4TH)

437.0000000 --- HORIZONTAL COMPONENT OF PRESSURE, P1, LB/IN.
-388.0000000 --- VERTICAL COMPONENT OF PRESSURE, P2, LB/IN.
0.0000000 --- HORIZONTAL COMPONENT OF PRESSURE, P3, LB/IN.

-0.6601115 --- VERTICAL DISTANCE FROM CENTROID TO P1, IN.
0.9333305 --- HORIZONTAL DISTANCE FROM CENTROID TO P2, IN.
0.0000000 --- VERTICAL DISTANCE FROM CENTROID TO P3, IN.

0.9901115 --- VERTICAL DISTANCE FROM CENTROID TO AXIAL LOAD(4), IN.
-0.0598885 --- VERTICAL DISTANCE FROM CENTROID TO AXIAL LOAD(5), IN.
0.2098885 --- VERTICAL DISTANCE FROM CENTROID TO AXIAL LOAD(9), IN.

0.0483305 --- HORIZONTAL DISTANCE FROM CENTROID TO AXIAL LOAD(4), IN.
1.4416695 --- HORIZONTAL DISTANCE FROM CENTROID TO AXIAL LOAD(5), IN.
-0.9583305 --- HORIZONTAL DISTANCE FROM CENTROID TO AXIAL LOAD(9), IN.

34.0000000 --- PRESSURIZED RADIUS AT STATION(4), IN.
32.7644624 --- PRESSURIZED RADIUS AT STATION(5), IN.
32.3687748 --- PRESSURIZED RADIUS AT STATION(9), IN.

10492.0586240 --- AXIAL LOAD AT STATION(4), LB/IN. (T_4)
418.0000000 --- AXIAL LOAD AT STATION(5), LB/IN. (T_5)
10659.9999488 --- AXIAL LOAD AT STATION(9), LB/IN. (T_9)

1.1598885 --- VERTICAL DISTANCE TO CENTROID, IN.

1.2083305 --- HORIZONTAL DISTANCE TO CENTROID, IN.

13923.1428608 --- M(4) --- MOMENT, IN-LB/IN.
-2986.9587968 --- M(5) --- MOMENT, IN-LB/IN.
-3912.1496576 --- M(9) --- MOMENT, IN-LB/IN.

-14739.6089856 --- Q(4) --- SHEAR, LB/IN.
-1647.6411264 --- Q(5) --- SHEAR, LB/IN.
3267.5422208 --- Q(9) --- SHEAR, LB/IN.

-0.0594687 --- DELTA RADIUS(4) - CHANGE IN RADIUS, IN.
-0.0961865 --- DELTA RADIUS(5) - CHANGE IN RADIUS, IN.
-0.0370559 --- DELTA RADIUS(9) - CHANGE IN RADIUS, IN.

0.0246294 --- DELTA THETA(4) - ROTATION, RADIANS
0.0246294 --- DELTA THETA(5) - ROTATION, RADIANS
0.0246294 --- DELTA THETA(9) - ROTATION, RADIANS

C(NET)

1.0000 Q(4) -1.0000 Q(5) 1.0000 Q(9) 4563.8517

DELTA RADIUS (C)

11.5309 C(4) -11.5309 Q(5) 11.5309 Q(9) 52625.2336

M(NET)

-1.0000 M(4) 0.0483 Q(4) 1.0000 M(5) 1.4417 Q(5) -1.0000 M(9) 0.9583 Q(9) 12026.8757

DELTA THETA (4)

-31.8793 M(4) 1.5407 G(4) 31.8793 M(5) 45.9595 Q(5) -31.8793 M(9) 30.5509 Q(9) 408912.1443

DELTA RADIUS(4)

-1.5407 M(4) 11.6053 Q(4) 1.5407 M(5) -9.3096 Q(5) -1.5407 M(9) 13.0074 Q(9) 72388.1550

DELTA THETA (5)

-31.8793 M(4) 1.5407 Q(4) 31.8793 M(5) 45.9595 Q(5) -31.8793 M(9) 30.5509 Q(9) 408912.1443

DELTA RADIUS(5)

45.9595 M(4) 9.3096 Q(4) -45.9595 M(5) -77.7892 Q(5) 45.9595 M(9) -32.5135 Q(9) -536890.9249

DELTA THETA (9)

-31.8793 M(4) 1.5407 Q(4) 31.8793 M(5) 45.9595 Q(5) -31.8793 M(9) 30.5509 Q(9) 408912.1443

DELTA RADIUS(9)

-30.5509 M(4) 13.0074 Q(4) 30.5509 M(5) 32.5135 Q(5) -30.5509 M(9) 40.8088 Q(9) 444498.2016

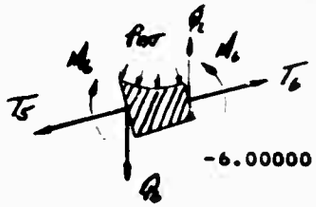

SHORT AFT CONE SEGMENT NO.1

FREE BODY NO. 6 SHORT CONE

-6.00000 --- INTERNAL PRESSURE, PSI	0.380000 --- THICKNESS FOR STRESSES AT STATION(5), IN.
0.32000 --- LENGTH OF SHORT CONE, IN.	0.280000 --- THICKNESS FOR STRESSES AT STATION(6), IN.
32.94000 --- RADIUS TO MID-POINT OF STATION(5), IN.	0.310000 --- THICKNESS FOR DEFLECTIONS, IN.
33.00000 --- RADIUS TO MID-POINT OF STATION(6), IN.	67.499999 --- PHI, DEGREES
0.00000 --- THROAT RADIUS(5), IN.	0.00000 --- THROAT RADIUS(6), IN.
32.76446 --- PRESSURIZED RADIUS OF STATION(5), IN.	0.923880 --- SINE PHI
32.87066 --- PRESSURIZED RADIUS OF STATION(6), IN.	-0.382683 --- COSINE PHI
32.97000 --- RADIUS TO CENTROID, IN.	27.000000 X 10E6 - ELASTIC MODULUS, PSI
35.68647 --- MEAN RADIUS OF CURVATURE NORMAL TO MERIDIAN (R2), IN.	0.300000 --- POISSONS RATIO
	0.073659 X 10E6 --- FLEXURAL RIGIDITY, IN-LB
35.65400 --- MEAN RADIUS OF CURVATURE NORMAL TO MERIDIAN AT STATION(5) (R2), IN.	0.386463 --- DAMPING FUNCTION
35.71894 --- MEAN RADIUS OF CURVATURE NORMAL TO MERIDIAN AT STATION(6) (R2), IN.	
418.0000000 --- AXIAL LOAD AT STATION(5), LB/IN (T_5)	417.0000000 --- AXIAL LOAD AT STATION(6), LB/IN (T_6)

INFLUENCE COEFFICIENTS

196.1575120 --- K	196.1600624 --- B	3172.4269312 --- S
3172.3032320 --- Y	16.1724096 --- L	8.0861839 --- V

-2086.9587968 --- M(5) - MOMENT, IN-LB/IN	-1647.6411264 --- Q(5) - SHEAR, LB/IN
-1636.1663488 --- M(6) - MOMENT, IN-LB/IN	-1399.4689920 --- Q(6) - SHEAR, LB/IN
0.0244300 --- DELTA THETA (5) - ROTATION, RADIANS	-0.0961665 --- DELTA RADIUS (5) - CHANGE IN RADIUS, IN.
0.0165670 --- DELTA THETA (6) - ROTATION, RADIANS	-0.1022025 --- DELTA RADIUS (6) - CHANGE IN RADIUS, IN.

DELTA THETA (5) ---	-55722.0929536 M(5)	8236.7084544 Q(5)	55719.9196160 M(6)	8236.6012416 Q(6)	-15.8944322
DELTA RADIUS (5) ---	-8236.7084544 M(5)	1623.3985408 Q(5)	8236.6012416 M(6)	811.6971648 Q(6)	1335.4040963
DELTA THETA (6) ---	-55719.9196160 M(5)	8236.6012416 Q(5)	55722.0929536 M(6)	8236.7084544 Q(6)	-15.8944322
DELTA RADIUS (6) ---	8236.6012416 M(5)	-811.6971648 Q(5)	-8236.7084544 M(6)	-1623.3985408 Q(6)	1338.1900416

STRESSES AT STATION(5)

1100.0000000 --- SIGMA (1P)		BASIC MERIDIONAL STRESS, PSI
-1659.2763392 --- SIGMA (1Q)		MERIDIONAL STRESS DUE TO SHEAR, PSI
-86715.7385216 --- SIGMA (1M)		MERIDIONAL STRESS DUE TO MOMENT, PSI
-87275.0145536 --- SIGMA (1I)		MAXIMUM COMBINED INSIDE MERIDIONAL STRESS, PSI
86156.4624896 --- SIGMA (1O)		MAXIMUM COMBINED OUTSIDE MERIDIONAL STRESS, PSI
-562.9578752 --- SIGMA (2P)		BASIC TANGENTIAL STRESS, PSI
79919.5807744 --- SIGMA (2M,Q)		TANGENTIAL STRESS DUE TO MOMENT AND SHEAR, PSI
-26014.7214336 --- SIGMA (2M1)		TANGENTIAL STRESS DUE TO SIGMA (1M),PSI
53341.9012096 --- SIGMA (2I)		MAXIMUM COMBINED INSIDE TANGENTIAL STRESS, PSI
105371.3432576 --- SIGMA (2O)		MAXIMUM COMBINED OUTSIDE TANGENTIAL STRESS, PSI

STRESSES AT STATION(6)

1489.2857088 --- SIGMA (1P)		BASIC MERIDIONAL STRESS, PSI
-1912.6915840 --- SIGMA (1Q)		MERIDIONAL STRESS DUE TO SHEAR, PSI
-125216.8138752 --- SIGMA (1M)		MERIDIONAL STRESS DUE TO MOMENT, PSI
-125640.2206720 --- SIGMA (1I)		MAXIMUM COMBINED INSIDE MERIDIONAL STRESS, PSI
124793.4070784 --- SIGMA (1O)		MAXIMUM COMBINED OUTSIDE MERIDIONAL STRESS, PSI
-765.4059200 --- SIGMA (2P)		BASIC TANGENTIAL STRESS, PSI
84715.1300608 --- SIGMA (2M,Q)		TANGENTIAL STRESS DUE TO MOMENT AND SHEAR, PSI
-37565.0439168 --- SIGMA (2M1)		TANGENTIAL STRESS DUE TO SIGMA (1M),PSI
46384.6805504 --- SIGMA (2I)		MAXIMUM COMBINED INSIDE TANGENTIAL STRESS, PSI
121514.7671552 --- SIGMA (2O)		MAXIMUM COMBINED OUTSIDE TANGENTIAL STRESS, PSI

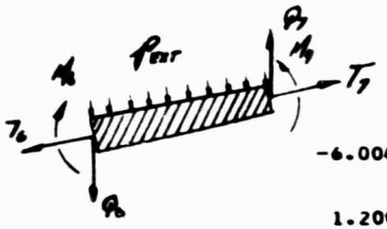

SHORT AFT CONE SEGMENT NO.2

FREE BODY NO. 7 SHORT CONE

-6.00000 --- INTERNAL PRESSURE, PSI	0.280000 --- THICKNESS FOR STRESSES AT STATION(6), IN.
1.20000 --- LENGTH OF SHORT CONE, IN.	0.210000 --- THICKNESS FOR STRESSES AT STATION(7), IN.
33.00000 --- RADIUS TO MID-POINT OF STATION(6), IN.	0.240000 --- THICKNESS FOR DEFLECTIONS, IN.
33.42000 --- RADIUS TO MID-POINT OF STATION(7), IN.	67.499999 --- PHI, DEGREES
0.00000 --- THROAT RADIUS(6), IN.	0.00000 --- THROAT RADIUS(7), IN.
32.87066 --- PRESSURIZED RADIUS OF STATION(6), IN.	0.923880 --- SINE PHI
33.32299 --- PRESSURIZED RADIUS OF STATION(7), IN.	-0.382683 --- COSINE PHI
33.21000 --- RADIUS TO CENTROID, IN.	27.000000 X .0E6 - ELASTIC MODULUS, PSI
35.94625 --- MEAN RADIUS OF CURVATURE NORMAL TO MERIDIAN (R2), IN.	0.300000 --- POISSONS RATIO
35.71894 --- MEAN RADIUS OF CURVATURE NORMAL TO MERIDIAN AT STATION(6) (R2), IN.	0.034180 X 10E. --- FLEXURAL RIGIDITY, IN-LB
36.17355 --- MEAN RADIUS OF CURVATURE NORMAL TO MERIDIAN AT STATION(7) (R2), IN.	0.437631 --- DAMPING FUNCTION
417.0000000 --- AXIAL LOAD AT STATION(6), LB/IN (T_6)	412.0000000 --- AXIAL LOAD AT STATION(7), LB/IN (T_7)

INFLUENCE COEFFICIENTS

10.8607692 --- K	10.9067093 --- B	41.8169300 --- S
41.2919940 --- Y	3.8111396 --- L	1.9021234 --- V

-1636.1663488 --- M(6) - MOMENT, IN-LB/IN	-1399.4689920 --- Q(6) - SHEAR, LB/IN
-497.6315008 --- M(7) - MOMENT, IN-LB/IN	-560.8546176 --- Q(7) - SHEAR, LB/IN
0.0165678 --- DELTA THETA (6) - ROTATION, RADIANS	-0.1022026 --- DELTA RADIUS (6) - CHANGE IN RADIUS, IN.
-0.0184787 --- DELTA THETA (7) - ROTATION, RADIANS	-0.0974474 --- DELTA RADIUS (7) - CHANGE IN RADIUS, IN.

DELTA THETA (6) ---	-1397.7806976 M(6)	769.6400896 Q(6)	1380.2340736 M(7)	766.3982912 Q(7)	-20.6797552
DELTA RADIUS (6) ---	-769.6400896 M(6)	567.7483136 Q(6)	766.3982912 M(7)	283.3607424 Q(7)	1728.4954624
DELTA THETA (7) ---	-1380.2340736 M(6)	766.3982912 Q(6)	1397.7806976 M(7)	769.6400896 Q(7)	-20.6797552
DELTA RADIUS (7) ---	766.3982912 M(6)	-283.3607424 Q(6)	-769.6400896 M(7)	-567.7483136 Q(7)	1756.9258336

STRESSES AT STATION(6)

1489.2857088 --- SIGMA (1P)	BASIC MERIDIONAL STRESS, PSI
-1912.6915840 --- SIGMA (1Q)	MERIDIONAL STRESS DUE TO SHEAR, PSI
-125216.8138752 --- SIGMA (1M)	MERIDIONAL STRESS DUE TO MOMENT, PSI
-125640.2206720 --- SIGMA (1I)	MAXIMUM COMBINED INSIDE MERIDIONAL STRESS, PSI
124793.4070784 --- SIGMA (1O)	MAXIMUM COMBINED OUTSIDE MERIDIONAL STRESS, PSI
-765.4059200 --- SIGMA (2P)	BASIC TANGENTIAL STRESS, PSI
85034.5549824 --- SIGMA (2M,Q)	TANGENTIAL STRESS DUE TO MOMENT AND SHEAR, PSI
-37565.0439168 --- SIGMA (2M1)	TANGENTIAL STRESS DUE TO SIGMA (1M),PSI
46704.1050624 --- SIGMA (2I)	MAXIMUM COMBINED INSIDE TANGENTIAL STRESS, PSI
121834.1928960 --- SIGMA (2O)	MAXIMUM COMBINED OUTSIDE TANGENTIAL STRESS, PSI

STRESSES AT STATION(7)

1961.9047680 --- SIGMA (1P)	BASIC MERIDIONAL STRESS, PSI
-1204.2768384 --- SIGMA (1Q)	MERIDIONAL STRESS DUE TO SHEAR, PSI
-67704.9663488 --- SIGMA (1M)	MERIDIONAL STRESS DUE TO MOMENT, PSI
-66[illegible]7.3374208 --- SIGMA (1I)	MAXIMUM COMBINED INSIDE MERIDIONAL STRESS, PSI
68462.5936384 --- SIGMA (1O)	MAXIMUM COMBINED OUTSIDE MERIDIONAL STRESS, PSI
-1033.5299072 --- SIGMA (2P)	BASIC TANGENTIAL STRESS, PSI
80147.0734336 --- SIGMA (2M,Q)	TANGENTIAL STRESS DUE TO MOMENT AND SHEAR, PSI
-20311.4897408 --- SIGMA (2M1)	TANGENTIAL STRESS DUE TO SIGMA (1M),PSI
58802.0539392 --- SIGMA (2I)	MAXIMUM COMBINED INSIDE TANGENTIAL STRESS, PSI
99425.0326016 --- SIGMA (2O)	MAXIMUM COMBINED OUTSIDE TANGENTIAL STRESS, PSI

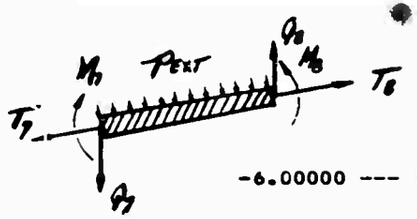

SHORT AFT CONE SEGMENT NO.3

FREE BODY NO. 8 SHORT CONE

-6.00000 --- INTERNAL PRESSURE, PSI	0.210000 --- THICKNESS FOR STRESSES AT STATION(7), IN.
1.20000 --- LENGTH OF SHORT CONE, IN.	0.150000 --- THICKNESS FOR STRESSES AT STATION(8), IN.
33.42000 --- RADIUS TO MID-POINT OF STATION(7), IN.	0.180000 --- THICKNESS FOR DEFLECTIONS, IN.
33.85000 --- RADIUS TO MID-POINT OF STATION(8), IN.	67.499999 --- PHI, DEGREES
0.00000 --- THROAT RADIUS(7), IN.	0.00000 --- THROAT RADIUS(8), IN.
33.32299 --- PRESSURIZED RADIUS OF STATION(7), IN.	0.923880 --- SINE PHI
33.78071 --- PRESSURIZED RADIUS OF STATION(8), IN.	-0.382683 --- COSINE PHI
33.63500 --- RADIUS TO CENTROID, IN.	27.000000 X 10E6 - ELASTIC MODULUS, PSI
36.40626 --- MEAN RADIUS OF CURVATURE NORMAL TO MERIDIAN (R2), IN.	0.300000 --- POISSONS RATIO
36.17355 --- MEAN RADIUS OF CURVATURE NORMAL TO MERIDIAN AT STATION(7) (R2), IN.	0.014420 X 10E6 --- FLEXURAL RIGIDITY, IN-LB
36.63898 --- MEAN RADIUS OF CURVATURE NORMAL TO MERIDIAN AT STATION(8) (R2), IN.	0.502130 --- DAMPING FUNCTION
412.0000000 --- AXIAL LOAD AT STATION(7), LB/IN (T_7)	406.0000000 --- AXIAL LOAD AT STATION(8), LB/IN (T_8)

INFLUENCE COEFFICIENTS

9.2403289 --- K	8.3007843 --- B	27.8731272 --- S
27.2710212 --- Y	3.3233556 --- L	1.6564743 --- V

-497.6315008 --- M(7) - MOMENT, IN-LB/IN	-660.8546176 --- Q(7) - SHEAR, LB/IN
-22.5299584 --- M(8) - MOMENT, IN-LB/IN	-226.2456064 --- Q(8) - SHEAR, LB/IN
-0.0184787 --- DELTA THETA (7) - ROTATION, RADIANS	-0.0974474 --- DELTA RADIUS (7) - CHANGE IN RADIUS, IN.
-0.0367682 --- DELTA THETA (8) - ROTATION, RADIANS	-0.0631895 --- DELTA RADIUS (8) - CHANGE IN RADIUS, IN.

DELTA THETA (7) ---	-1924.7782400 MI(7)	1054.6615168 QI 7)	1883.1991296 MI 8)	1046.9803136 Q(8)	-27.9258694
DELTA RADIUS I 7) ---	-1054.6615168 MI(7)	776.9082688 Q(7)	1046.9803136 MI 8)	387.2377024 Q(8)	2342.4344323
DELTA THETA I 8) ---	-1883.1991296 MI(7)	1046.9803136 QI 7)	1924.7782400 MI 8)	1054.6615168 QI 8)	-27.9258694
DELTA RADIUS I 8) ---	1046.9803136 MI(7)	-387.2377024 QI 7)	-1054.6615168 MI(8)	-776.9082688 Q(8)	2379.4867959

STRESSES AT STATION(7)

1961.9047680 --- SIGMA (1P)	BASIC MERIDIONAL STRESS, PSI
-1204.2768384 --- SIGMA (1Q)	MERIDIONAL STRESS DUE TO SHEAR, PSI
-67704.9663488 --- SIGMA (1M)	MERIDIONAL STRESS DUE TO MOMENT, PSI
-66947.3374208 --- SIGMA (1I)	MAXIMUM COMBINED INSIDE MERIDIONAL STRESS, PSI
68462.5936384 --- SIGMA (1O)	MAXIMUM COMBINED OUTSIDE MERIDIONAL STRESS, PSI
-1033.5299072 --- SIGMA (2P)	BASIC TANGENTIAL STRESS, PSI
80620.1860096 --- SIGMA (2M,Q)	TANGENTIAL STRESS DUE TO MOMENT AND SHEAR, PSI
-20311.4897408 --- SIGMA (2M1)	TANGENTIAL STRESS DUE TO SIGMA (1M),PSI
59275.1656960 --- SIGMA (2I)	MAXIMUM COMBINED INSIDE TANGENTIAL STRESS, PSI
99898.1451776 --- SIGMA (2O)	MAXIMUM COMBINED OUTSIDE TANGENTIAL STRESS, PSI

STRESSES AT STATION(8)

2706.6666752 --- SIGMA (1P)	BASIC MERIDIONAL STRESS, PSI
-577.2030208 --- SIGMA (1Q)	MERIDIONAL STRESS DUE TO SHEAR, PSI
-6007.9869920 --- SIGMA (1M)	MERIDIONAL STRESS DUE TO MOMENT, PSI
-3878.5252864 --- SIGMA (1I)	MAXIMUM COMBINED INSIDE MERIDIONAL STRESS, PSI
8137.4525440 --- SIGMA (1O)	MAXIMUM COMBINED OUTSIDE MERIDIONAL STRESS, PSI
-1465.5590400 --- SIGMA (2P)	BASIC TANGENTIAL STRESS, PSI
52300.2318848 --- SIGMA (2M,Q)	TANGENTIAL STRESS DUE TO MOMENT AND SHEAR, PSI
-1802.3966720 --- SIGMA (2M1)	TANGENTIAL STRESS DUE TO SIGMA (1M),PSI
49032.2755584 --- SIGMA (2I)	MAXIMUM COMBINED INSIDE TANGENTIAL STRESS, PSI
52637.0693120 --- SIGMA (2O)	MAXIMUM COMBINED OUTSIDE TANGENTIAL STRESS, PSI

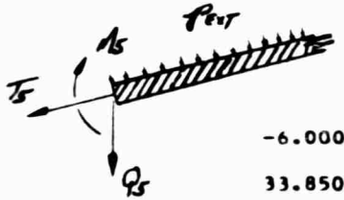

AFT CONICAL SHELL (STL)

FREE BODY NUMBER 9 SEMI-INFINITE CONE

-6.00000	--- INTERNAL PRESSURE, PSI	0.150000	--- THICKNESS FOR STRESSES AT STATION(8), IN.
33.85000	--- RADIUS TO MID-POINT OF STATION(8), IN.	0.150000	--- THICKNESS FOR DEFLECTIONS, IN.
0.00000	--- RADIUS OF THROAT, IN.	27.000000	X 10E6 - MODULUS OF ELASTICITY, PSI
33.78071	--- PRESSURIZED RADIUS AT STATION(8), IN.	0.300000	--- POISSONS RATIO
67.50000	--- PHI, DEGREES	0.548306	--- DAMPING FUNCTION
-0.38268	--- COSINE OF PHI	0.008345	X 10E6 --- FLEXURAL RIGIDITY, IN-LBS.
0.92388	--- SINE OF PHI	406.000000	--- AXIAL LOAD AT STATION(8), LBS/IN. (T_8)
36.63898	--- MEAN RADIUS OF CURVATURE NORMAL TO MERIDIAN (R2), IN.		

-22.5299584	--- M(8) - MOMENT, IN-LBS/IN.	-0.0367682	--- DELTA THETA (8) - ROTATION, RADIANS
-226.2456064	--- Q(8) - SHEAR FORCE, LBS/IN.	-0.0631895	--- DELTA RADIUS (8) - CHANGE IN RADIUS, IN.

DELTA THETA (8) ---	-218.5555040 M(8)	184.1296448 Q(8)	-33.7252500
DELTA RADIUS(9) ---	-184.1296448 M(8)	310.2527808 Q(8)	2855.3841664

STRESSES AT STATION(8)

2706.6666752 --- SIGMA(1P)	BASIC MERIDIONAL STRESS, PSI
-577.2030144 --- SIGMA(1Q)	MERIDIONAL STRESS DUE TO SHEAR, PSI
-6007.9889920 --- SIGMA(1M)	MERIDIONAL STRESS DUE TO MOMENT, PSI
-3878.5253376 --- SIGMA(1I)	MAXIMUM COMBINED INSIDE MERIDIONAL STRESS,PSI
8137.4525440 --- SIGMA(1O)	MAXIMUM COMBINED OUTSIDE MERIDIONAL STRESS, PSI
-1465.5590400 --- SIGMA(2P)	BASIC TANGENTIAL STRESS, PSI
55988.7704064 --- SIGMA(2Q)	TANGENTIAL STRESS DUE TO SHEAR, PSI
-3308.9422848 --- SIGMA(2M)	TANGENTIAL STRESS DUE TO MOMENT, PSI
-1802.3966720 --- SIGMA(2,1M)	TANGENTIAL STRESS DUE TO SIGMA(1M), PSI
49411.8719488 --- SIGMA(2I)	MAXIMUM COMBINED INSIDE TANGENTIAL STRESS, PSI
53016.6652928 --- SIGMA(2O)	MAXIMUM COMBINED OUTSIDE TANGENTIAL STRESS, PSI

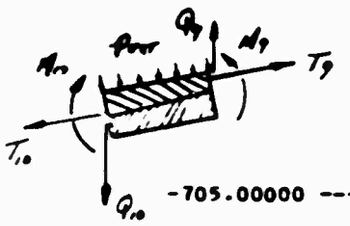

SUBMERGED CONE NO.1 (STL-FRP)

FREE BODY NO. 10 SHORT CONE

-705.00000	--- INTERNAL PRESSURE, PSI	0.550000	--- THICKNESS FOR STRESSES AT STATION(9), IN.
1.65000	--- LENGTH OF SHORT CONE, IN.	1.460000	--- THICKNESS FOR STRESSES AT STATION(10), IN.
32.62000	--- RADIUS TO MID-POINT OF STATION(9), IN.	1.500000	--- THICKNESS FOR DEFLECTIONS, IN.
31.94000	--- RADIUS TO MID-POINT OF STATION(10), IN.	65.999998	--- PHI, DEGREES
13.44000	--- THROAT RADIUS(9), IN.	13.44000	--- THROAT RADIUS(10), IN.
32.36877	--- PRESSURIZED RADIUS OF STATION(9), IN.	0.913545	--- SINE PHI
31.27311	--- PRESSURIZED RADIUS OF STATION(10), IN.	-0.406737	--- COSINE PHI
32.28000	--- RADIUS TO CENTROID, IN.	11.700000 X 10E6	- ELASTIC MODULUS, PSI
35.33486	--- MEAN RADIUS OF CURVATURE NORMAL TO MERIDIAN (R2), IN.	0.300000	--- POISSONS RATIO
		3.616071 X 10E6	--- FLEXURAL RIGIDITY, IN-LB
35.70704	--- MEAN RADIUS OF CURVATURE NORMAL TO MERIDIAN AT STATION(9) (R2), IN.	0.176560	--- DAMPING FUNCTION
34.96268	--- MEAN RADIUS OF CURVATURE NORMAL TO MERIDIAN AT STATION(10) (R2), IN.		
-10659.9999488	--- AXIAL LOAD AT STATION(9), LB/IN (T_9)	-10320.0000000	--- AXIAL LOAD AT STATION(10), LB/IN (T_{10})

INFLUENCE COEFFICIENTS

REACTED IN BEARING BY THE FRP SECTION ON BODY NO. 5

REACTED IN BEARING BY THE FRP SECTION ON BODY NO. 5

35.3428964 --- K	35.3570404 --- B	242.8882560 --- S
242.5969408 --- Y	6.8656637 --- L	3.4322439 --- V

-3912.1496576 --- M(9) - MOMENT, IN-LB/IN	3267.5422208 --- Q(9) - SHEAR, LB/IN
-345.6522112 --- M(10) - MOMENT, IN-LB/IN	1647.3655680 --- Q(10) - SHEAR, LB/IN
0.0246294 --- DELTA THETA (9) - ROTATION, RADIANS	-0.0370560 --- DELTA RADIUS (9) - CHANGE IN RADIUS, IN.
0.0255079 --- DELTA THETA (10) - ROTATION, RADIANS	0.0007423 --- DELTA RADIUS (10) - CHANGE IN RADIUS, IN.

DELTA THETA (9) ---	190.2156208 M(9)	143.2690464 Q(9)	-189.9874800 M(10)	143.2117344 Q(10)	-947.3595775
DELTA RADIUS (9) ---	-143.2690464 M(9)	-143.9447376 Q(9)	143.2117344 M(10)	-71.9600408 Q(10)	40845.5561216
DELTA THETA (10) ---	189.9874800 M(9)	143.2117344 Q(9)	-190.2156208 M(10)	143.2690464 Q(10)	-947.3595775
DELTA RADIUS (10) ---	143.2117344 M(9)	71.9600408 Q(9)	-143.2690464 M(10)	143.9447376 Q(10)	39224.5702080

STRESSES AT STATION(9)

2416.4169216 --- SIGMA (1Q)	MERIDIONAL STRESS DUE TO SHEAR, PSI
-77596.3566080 --- SIGMA (1M)	MERIDIONAL STRESS DUE TO MOMENT, PSI
-45769.9274752 --- SIGMA (2P)	BASIC TANGENTIAL STRESS, PSI
27941.3755904 --- SIGMA (2M,Q)	TANGENTIAL STRESS DUE TO MOMENT AND SHEAR, PSI
-23278.9069824 --- SIGMA (2M1)	TANGENTIAL STRESS DUE TO SIGMA (1M),PSI
-41107.4588672 --- SIGMA (2I)	MAXIMUM COMBINED INSIDE TANGENTIAL STRESS, PSI
5450.3549440 --- SIGMA (2O)	MAXIMUM COMBINED OUTSIDE TANGENTIAL STRESS, PSI

STRESSES AT STATION(10)

-7068.4931072 --- SIGMA (1P)	BASIC MERIDIONAL STRESS, PSI
458.9342592 --- SIGMA (1Q)	MERIDIONAL STRESS DUE TO SHEAR, PSI
-972.9373696 --- SIGMA (1M)	MERIDIONAL STRESS DUE TO MOMENT, PSI
-7582.4961536 --- SIGMA (1I)	MAXIMUM COMBINED INSIDE MERIDIONAL STRESS, PSI
-5636.6215168 --- SIGMA (1O)	MAXIMUM COMBINED OUTSIDE MERIDIONAL STRESS, PSI
-16882.6654720 --- SIGMA (2P)	BASIC TANGENTIAL STRESS, PSI
14096.5550080 --- SIGMA (2M,Q)	TANGENTIAL STRESS DUE TO MOMENT AND SHEAR, PSI
-291.8812064 --- SIGMA (2M1)	TANGENTIAL STRESS DUE TO SIGMA (1M),PSI
-3077.9916544 --- SIGMA (2I)	MAXIMUM COMBINED INSIDE TANGENTIAL STRESS, PSI
-2494.2292480 --- SIGMA (2O)	MAXIMUM COMBINED OUTSIDE TANGENTIAL STRESS, PSI

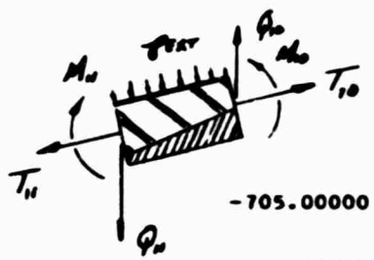

SUBMERGED CONE NO.2 (STL-FRP)

FREE BODY NO. 11 SHORT CONE

-705.00000	--- INTERNAL PRESSURE, PSI	1.500000	--- THICKNESS FOR STRESSES AT STATION(10), IN.
1.80000	--- LENGTH OF SHORT CONE, IN.	1.300000	--- THICKNESS FOR STRESSES AT STATION(11), IN.
31.94000	--- RADIUS TO MID-POINT OF STATION(10), IN.	1.400000	--- THICKNESS FOR DEFLECTIONS, IN.
31.25000	--- RADIUS TO MID-POINT OF STATION(11), IN.	65.999998	--- PHI, DEGREES
13.44000	--- THROAT RADIUS(10), IN.	13.44000	--- THROAT RADIUS(11), IN.
31.25484	--- PRESSURIZED RADIUS OF STATION(10), IN.	0.913545	--- SINE PHI
30.65620	--- PRESSURIZED RADIUS OF STATION(11), IN.	-0.406737	--- COSINE PHI
31.59500	--- RADIUS TO CENTROID, IN.	7.600000 X 10E6	- ELASTIC MODULUS, PSI
34.58503	--- MEAN RADIUS OF CURVATURE NORMAL TO MERIDIAN (R2), IN.	0.300000	--- POISSONS RATIO
		1.909744 X 10E6	--- FLEXURAL RIGIDITY, IN-LB
34.96288	--- MEAN RADIUS OF CURVATURE NORMAL TO MERIDIAN AT STATION(10) (R2), IN.	0.184728	--- DAMPING FUNCTION
34.20738	--- MEAN RADIUS OF CURVATURE NORMAL TO MERIDIAN AT STATION(11) (R2), IN.		
-10320.0000000	--- AXIAL LOAD AT STATION(10), LB/IN (T_{10})	-10109.9999232	--- AXIAL LOAD AT STATION(11), LB/IN (T_{11})

INFLUENCE COEFFICIENTS

27.1269972 --- K	27.1454232 --- B	163.4530384 --- S
163.1205488 --- Y	6.0155535 --- L	3.0069019 --- V

-345.6522112 --- M(10) - MOMENT, IN-LB/IN	1647.3655680 --- Q(10) - SHEAR, LB/IN
1587.8857984 --- M(11) - MOMENT, IN-LB/IN	945.6293504 --- Q(11) - SHEAR, LB/IN
0.0255079 --- DELTA THETA (10) - ROTATION, RADIANS	0.0007423 --- DELTA RADIUS (10) - CHANGE IN RADIUS, IN.
0.0248190 --- DELTA THETA (11) - ROTATION, RADIANS	0.0421074 --- DELTA RADIUS (11) - CHANGE IN RADIUS, IN.

DELTA THETA (10) ---	231.6623264 M(10)	190.2640048 Q(10)	-231.1910880 M(11)	190.1348560 Q(11)	-1530.4182656
DELTA RADIUS (10) ---	-190.2640048 M(10)	-208.5130384 Q(10)	190.1348560 M(11)	-104.2261960 Q(11)	64698.5867264
DELTA THETA (11) ---	231.1910880 M(10)	190.1348560 Q(10)	-231.6623264 M(11)	190.2640048 Q(11)	-1530.4182656
DELTA RADIUS (11) ---	190.1348560 M(10)	104.2261960 Q(10)	-190.2640048 M(11)	208.5130384 Q(11)	61922.0137264

STRESSES AT STATION(10)

-6880.0000000 --- SIGMA (1P)	BASIC MERIDIONAL STRESS, PSI
446.6960064 --- SIGMA (1Q)	MERIDIONAL STRESS DUE TO SHEAR, PSI
-921.7392256 --- SIGMA (1M)	MERIDIONAL STRESS DUE TO MOMENT, PSI
-7355.0431232 --- SIGMA (1I)	MAXIMUM COMBINED INSIDE MERIDIONAL STRESS, PSI
-5511.5646464 --- SIGMA (1O)	MAXIMUM COMBINED OUTSIDE MERIDIONAL STRESS, PSI
-16432.4608000 --- SIGMA (2P)	BASIC TANGENTIAL STRESS, PSI
15218.1590016 --- SIGMA (2M,Q)	TANGENTIAL STRESS DUE TO MOMENT AND SHEAR, PSI
-276.5217600 --- SIGMA (2M1)	TANGENTIAL STRESS DUE TO SIGMA (1M),PSI
-1490.8235136 --- SIGMA (2I)	MAXIMUM COMBINED INSIDE TANGENTIAL STRESS, PSI
-937.7799808 --- SIGMA (2O)	MAXIMUM COMBINED OUTSIDE TANGENTIAL STRESS, PSI

STRESSES AT STATION(11)

-7776.9230336 --- SIGMA (1P)	BASIC MERIDIONAL STRESS, PSI
264.5757536 --- SIGMA (1Q)	MERIDIONAL STRESS DUE TO SHEAR, PSI
5637.4643712 --- SIGMA (1M)	MERIDIONAL STRESS DUE TO MOMENT, PSI
-1874.8828416 --- SIGMA (1I)	MAXIMUM COMBINED INSIDE MERIDIONAL STRESS, PSI
-13149.8116096 --- SIGMA (1O)	MAXIMUM COMBINED OUTSIDE MERIDIONAL STRESS, PSI
-18550.9275648 --- SIGMA (2P)	BASIC TANGENTIAL STRESS, PSI
4818.9235200 --- SIGMA (2M,Q)	TANGENTIAL STRESS DUE TO MOMENT AND SHEAR, PSI
1691.2392960 --- SIGMA (2M1)	TANGENTIAL STRESS DUE TO SIGMA (1M),PSI
-12040.7647232 --- SIGMA (2I)	MAXIMUM COMBINED INSIDE TANGENTIAL STRESS, PSI
-15423.2432640 --- SIGMA (2O)	MAXIMUM COMBINED OUTSIDE TANGENTIAL STRESS, PSI

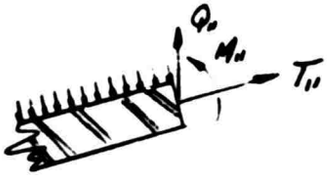

SUBMERGED CONE (FRP) 143 GLASS FABRIC AND PHENOLIC RESIN

FREE BODY NUMBER 12 SEMI-INFINITE CONE

-705.00000 --- INTERNAL PRESSURE, PSI

31.25000 --- RADIUS TO MID-POINT OF STATION(11), IN.

13.44000 --- RADIUS OF THROAT, IN.

31.79813 --- PRESSURIZED RADIUS AT STATION(11), IN.

66.00000 --- PHI, DEGREES

-0.40674 --- COSINE OF PHI

0.91355 --- SINE OF PHI

34.20738 --- MEAN RADIUS OF CURVATURE NORMAL TO MERIDIAN (R2), IN.

1.200000 --- THICKNESS FOR STRESSES AT STATION(11), IN.

1.200000 --- THICKNESS FOR DEFLECTIONS, IN.

4.000000 X 10E6 - MODULUS OF ELASTICITY, PSI

0.250000 --- POISSONS RATIO

0.202126 --- DAMPING FUNCTION

0.614400 X 10E6 --- FLEXURAL RIGIDITY, IN-LBS.

-10110.000000 --- AXIAL LOAD AT STATION(11), LBS/IN. (T_{11})

1587.8857984 --- M(11) - MOMENT, IN-LBS/IN.

845.6293504 --- Q(11) - SHEAR FORCE, LBS/IN.

0.0248190 --- DELTA THETA (11) - ROTATION, RADIANS

0.0421074 --- DELTA RADIUS (11) - CHANGE IN RADIUS, IN.

DELTA THETA (11) ---	8.0524166 M(11)	18.1971684 Q(11)	-3355.3837824
DELTA RADIUS(11) ---	-18.1971684 M(11)	-82.2453568 Q(11)	140551.4711040

STRESSES AT STATION(11)

-8424.9999360 --- SIGMA(1P) BASIC MERIDIONAL STRESS, PSI
286.6237344 --- SIGMA(1Q) MERIDIONAL STRESS DUE TO SHEAR, PSI
6816.1908736 --- SIGMA(1M) MERIDIONAL STRESS DUE TO MOMENT, PSI

-1522.1852928 --- SIGMA(11) MAXIMUM COMBINED INSIDE MERIDIONAL STRESS, PSI
-14754.5669632 --- SIGMA(10) MAXIMUM COMBINED OUTSIDE MERIDIONAL STRESS, PSI

-20096.8382464 --- SIGMA(2P) BASIC TANGENTIAL STRESS, PSI
8902.2826496 --- SIGMA(2Q) TANGENTIAL STRESS DUE TO SHEAR, PSI
3698.5629696 --- SIGMA(2M) TANGENTIAL STRESS DUE TO MOMENT, PSI
1654.0477184 --- SIGMA(2,1M) TANGENTIAL STRESS DUE TO SIGMA(1M), PSI

-5841.9449344 --- SIGMA(2I) MAXIMUM COMBINED INSIDE TANGENTIAL STRESS, PSI
-9150.0403712 --- SIGMA(2O) MAXIMUM COMBINED OUTSIDE TANGENTIAL STRESS, PSI

c. Submerged Shell Buckling--Each structural member must be checked for buckling as a column subjected to axial load, external pressure, bending moment, and radial shock loads.

To insure structural integrity, each end must be checked for local buckling including much the same loads as above and local end conditions.

Submerged Shell

The deformation in the middle of the cone due to external pressure is calculated as follows:

$$\delta = -\frac{pr^2(1-\mu/2)}{E_{c\text{-hoop}}\, t} = -\frac{684(23.50^2)(0.93)}{3.4(10^6)(1.29)} \quad \text{(Reference 14)}$$

Average R = 23.50 in.

$E_{c\text{-hoop}} = 3.40(10^6)$

t = 1.29 avg

$\mu = 0.15$

$$p = -705\,\frac{(85-14.8)}{3} + \frac{30(60\ g's)}{2\pi R} = \begin{matrix} +684\ psi \\ -660\ psi \end{matrix}$$

$\delta = -0.0803$ in. $\quad \frac{\Delta R}{R} = \frac{0.0803}{23.50} \times 100 = -0.34$ percent

(1) Column Buckling Analysis

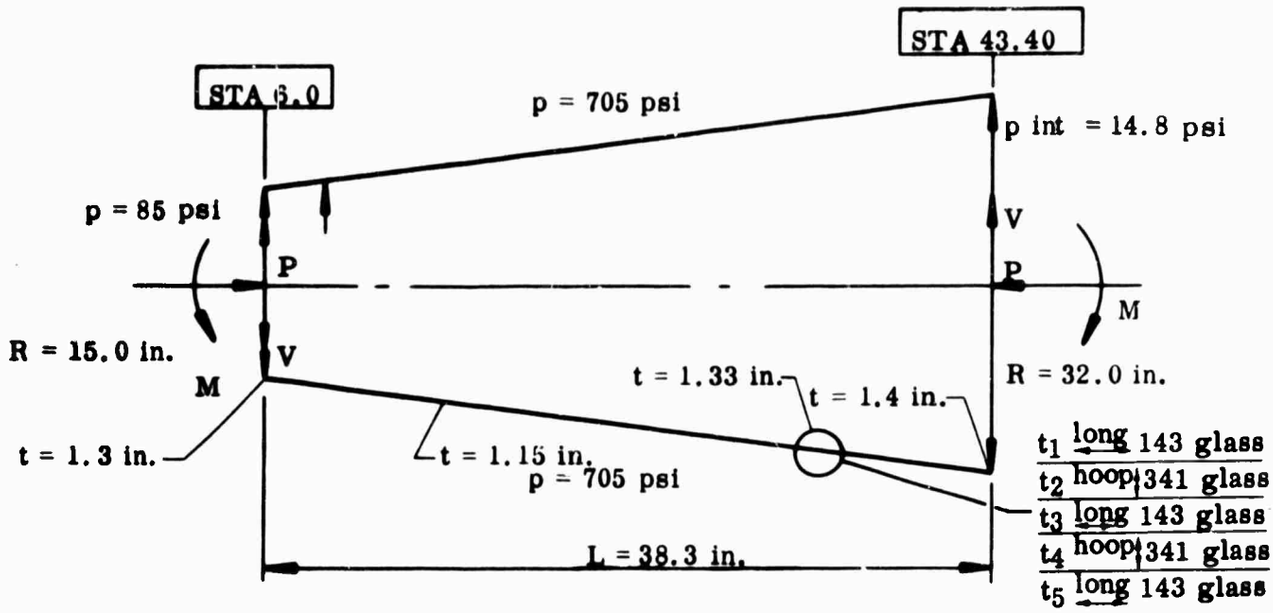

Unsupported Length Between End Rings

= 46.5 in. - 3.1 in. aft end - 5.1 in. fwd end

= 38.3 in.

Shell Loads - Flight Load Condition*

Station 6.0

P = $0.440(10^6)$ + neg acceleration load = 440,000 lb

$P_{internal}$ = 0.12(705) = 85 psi

M = 119,000 in. lb (acceleration)

V = neg acceleration load = 0

Station 43.40

P = 2.03×10^6 + neg acceleration load = 2.03×10^6

*Static test load condition not critical

$M = 373,000$ in. lb (acceleration)

$V = 12,950$ lb neg acceleration $= 0$

$p_{int} = 0.020(705) = 14.8$ psi

Axial Load Buckling (Reference 11)

$$\text{avg load} = -\frac{(2.03 + 0.440)\,10^6}{2} = 1.235(10^6)$$

$$\text{avg } t = 1.30 + 1.33 + 1.15 + 1.40 = 1.29$$

$$P_{critical} = 2C\pi E t^2 = 2(0.475)(3.14)(3.0)(10^6)(1.29)^2$$

$$P_{critical} = 14.85 \times 10^6$$

$$R/t = 23.50/1.29 = 18.20$$

$$\text{avg } R = 15.00 + 32.0 = \frac{47.0}{2} = 23.5 \text{ in.}$$

$$Z = \frac{L^2\sqrt{1-\mu^2}}{R_t} = \frac{(38.3)^2\,0.98}{23.50(1.29)} = 47.5$$

$$c_p = 0.475 \qquad R_c = \frac{1.23(10^6)}{14.85(10^6)} = 0.082$$

Glass Cloth Phenolic Shell Composite Allowables (Reference 36)

Hoop Direction $\mu = 0.15$

Compression Stress (Composite)

0.722	(45,000) =	32,500	341 glass phenolic hoop oriented
0.568	(19,000) =	10,800	143 glass phenolic longitudinally oriented
1.290		43,300	

$$\sigma_{\text{Hoop Compression}} = \frac{43,300}{1.29} = 33,800 \text{ psi}$$

Compression Modulus of Elasticity (Composite)

$$0.722\ (4.910 \times 10^6) = 3.54\ (10^6)$$
$$\underline{0.568}\ (1.51 \times 10^6) = \underline{0.85}\ (10^6)$$
$$1.290 \qquad\qquad 4.39\ (10^6)$$

$$E_{\text{Hoop Compression}} = \frac{4.39\ (10^6)}{1.29} = 3.40\ (10^6)\ \text{psi}$$

Longitudinal Direction $\mu = 0.15$

Compression Stress (Composite)

$$0.722\ (19,000) = 13,700$$
$$\underline{0.568}\ (45,000) = \underline{25,500}$$
$$1.290 \qquad\qquad 39,200$$

$$\sigma_{\text{Longitudinal Compression}} = \frac{39,200}{1.290} = 30,400\ \text{psi}$$

$$0.722\ (1.51 \times 10^6) = 1.09\ (10^6)$$
$$\underline{0.568}\ (4.91 \times 10^6) = \underline{2.79}\ (10^6)$$
$$1.290 \qquad\qquad 3.88$$

$$E_{\text{Longitudinal Compression}} = \frac{3.88\ (10^6)}{1.290} = 3.00\ (10^6)\ \text{psi}$$

External Pressure Buckling (Reference 11)

$$P_{cr} = c_p \frac{\pi^2 D}{RL^2} = \frac{7.5(3.14^2)(0.622)10^6}{23.5(38.3)^2}$$

$$Z = 47.5$$

$$D = \frac{Ect^3}{11.75} = \frac{3.40 \times 10^6 (1.29)^3}{11.75} = 0.622(10^6)$$

$$c_p = 7.5$$

$$P_{cr} = 1,335 \text{ psi}$$

$$P_{act} = +705 - \frac{(85+14.8)}{3} \pm \frac{30 \text{ lb/in.} \times 60 \text{ g's}}{2\pi R}$$

(External) + (Internal) (Shock)

$$= 705 - 33 \pm 12.2 = \begin{matrix} +684 \text{ psi} \\ -660 \text{ psi} \end{matrix} \quad R_p = \frac{684}{1,335} = 0.512$$

Bending Moment Buckling (Reference 11)

avg bending moment = 246,000 in. lb R/t = 18.20

$$C_B = 0.50$$

$$M_{cr} = C_B \pi ERt^2 = 0.50(3.14)(3.00)10^6(23.50)(1.29)^2$$

$$M_{cr} = 184(10^6) \text{ in. lb}$$

$$R_B = \frac{0.246(10^6)}{184(10^6)} = \text{neg}$$

Combined Axial Compression and Lateral External Pressure

$$F.S. = \frac{1}{\sqrt{0.083^3 + 0.512^2}} = \frac{1}{0.522} = 1.91$$

(2) Local Stress (Station 6.0)

Local Stress Loads

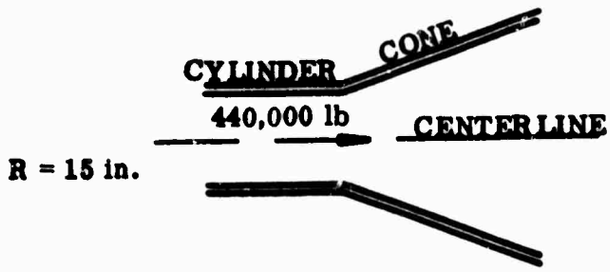

$$\text{Cylinder Load} = \frac{440,000}{2\pi R}$$

$$= \frac{440,000}{6.28(15)}$$

$$= 4,670 \text{ lb/in.}$$

Therefore cone load is an angle function of cylinder loads.

Assume no discontinuity bending and shear loads.

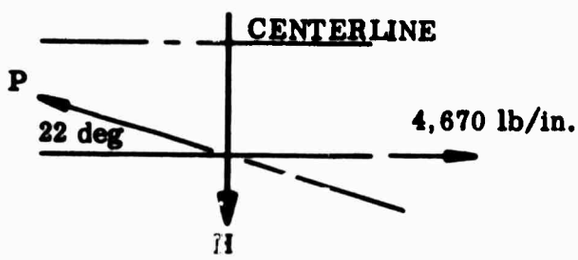

P = Membrane Load lb/in.

H = Uniform Axisymmetrical Shear Load lb/in.

$$P \cos 22 \text{ deg} = 4,670 \text{ lb/in.}$$

$$P = \frac{4,370}{0.9272} = 5,050 \text{ lb/in.}$$

$$H = \sin 22 \text{ deg } (5,050) = 0.3746(5,050) = 1,890 \text{ lb/in.}$$

Bending Moments - Due to Horizontal Shear (H) (Reference 13)

Assume a cylindrical shell with R = 15.0 in.

$$MX = \frac{0.322\,H}{\lambda} \text{ at } \frac{\pi}{4\lambda} = \frac{3.14}{4(0.296)} = 2.65 \text{ in. from edge}$$

$$\lambda = \sqrt[4]{\frac{3(1-\mu^2)}{R_2^2 t^2}} = \sqrt[4]{\frac{3(0.98)}{(15.0)^2 (1.3^2)}} = \sqrt[4]{0.0074} = 0.296$$

$$\lambda^3 = 0.026$$

$$\text{Max moment} = \frac{0.322(1,890)}{0.296} = 2,060 \text{ in. lb/in.}$$

Net Pressure

$$p_{net} = p_{ext} - p_{int} \pm p_{shock} = 705 - 85 \pm 19 = \begin{matrix} +639 \text{ psi} \\ -601 \text{ psi} \end{matrix}$$

Hoop Stress = pressure + shear load

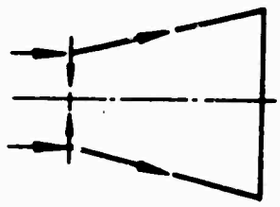

$$= -\frac{pR}{t} - \frac{2H}{t}\lambda R$$

$$= -\frac{639(15.0)}{1.30} - \frac{2(1,890)}{1.30}(0.296)(15.00)$$

$$= -7,360 - 12,900$$

$$\sigma_H = -20,260 \qquad \text{F.S.} = \frac{33,800}{20,260} = +1.66$$

Hoop Deformation (pressure and shear load)

$$\delta_H = -\frac{pR^2(1-\mu/2)}{Et} - \frac{V_o}{2D\beta^3}$$

$$D = \frac{3.4(10^6)t^3}{12(1-\mu^2)} \qquad t = 1.30$$

$$D = \frac{(3.4)(2.2)10^6}{11.75}$$

$$D = 0.635(10^6).$$

$$\delta_H = -\frac{639(15)^2(0.93)}{1.30(3.4)(10^6)} - \frac{1,890}{2(0.635)(0.026)(10^6)}$$

$$\delta_H = -0.030 - 0.057$$

$$\delta_H = -0.089 \text{ in.} \qquad \text{radial growth} = \frac{0.087}{15.00}(100) = 0.58 \text{ percent}$$

Longitudinal Stress pressure + bending moment

$$\sigma_L = -\frac{P\ \text{lb/in.}}{t} \pm \frac{6M}{bt^2} \pm \frac{Mc}{\pi R^3 t} = -\frac{5,050}{1.30}$$

$$\pm \frac{6(2,060)}{(1.30)^2} \pm \frac{119,000(15.0)}{3.14(15^3)(1.30)}$$

$$= -3,880 \pm 7,320 \pm 130$$

$$\sigma_L = \begin{matrix} +3,570\ \text{psi outside} \\ -11,330\ \text{psi inside} \end{matrix} \text{ at 2.12 in. downstream from joint}$$

$$\text{F.S.} = \frac{30,400}{11,330} = +2.68$$

Local Buckling (Reference 11) Flight Test Condition

axial load = $0.440(10^6)$

lateral pressure = $-705 + 85 \pm \frac{30\ \text{lb/in. (60 g's)}}{2\pi(15)} = -639$ psi max

axial bending moment = 119,000 in. lb

assume R = 15.0 for a cylinder of L = 38.3 in.

t = 1.30 in.

Axial Load

$$P_{\text{critical}} = 2C\pi Et^2 = 2(0.50)(3.14)(3.00)10^6(1.30^2)$$

$$P_{\text{critical}} = 12.2(10^6)$$

$$R/t = \frac{15.0}{1.30} = 11.52$$

$$\therefore C = 0.50$$

$$R_C = \frac{0.440(10^6)}{12.2(10^6)} = 0.036$$

Transverse External Pressure

$$Z = \frac{I^2(0.99)}{R_t} = \frac{38.3^2(0.99)}{15(1.30)} = 74.4 \qquad D = \frac{Et^3}{12(1-\mu^2)}$$

$$D = \frac{3.4(10^6)(1.30^3)}{11.75} = 0.639(10^6)$$

$$C_p = 9.0$$

$$P_{critical} = \frac{(3.14)^2 C_p D}{(15.0)(38.3)^2} = \frac{9.0(0.639)10^6(9.9)}{22,000} = 2,590 \text{ psi}$$

$$R_p = \frac{639}{2,590} = 0.246$$

Axial Bending $R_B \cong 0.0$ neg

Combined Axial Compression and Lateral External Pressure

$$F.S. = \frac{1}{\sqrt{R_c^2 + R_p^2}} = \frac{1}{\sqrt{0.036^2 + 0.246^2}}$$

$$= \frac{1}{0.248} = +4.03$$

(3) Local Stress (Station 43.40)

Local Stresses - Glass Cloth Structural Shell

Loads

axial load = 2,030,000 lb

$$\text{uniform axial load} = \frac{2,03(10^6)}{2\pi R \cos 22 \text{ deg}} = \frac{2,03(10^6)}{6.28(32)(0.9272)}$$

$$= 10,900 \text{ lb/in.}$$

Since the steel seat for the submerged shell is perpendicular to the shell wall, no hoop ring will be needed to hold the glass cloth cone in place.

However to insure reliability, a glass hoop ring is installed to take 5 percent of the membrane load of 10,000 lb/in.

hoop ring load = 10,900(0.05) = 545 lb/in.

Bending Moment = 373,000 in. lb (acceleration)

Net Pressure

$$p_{net} = p_{ext} - p_{int} \pm \text{shock pressure}$$

$$= -705 + 14.8 \pm \frac{35 \text{ lb/in.}(60 \text{ g's})}{2\pi R} = -687 \pm \frac{2,100}{6.28(32)}$$

$$= -687 \pm 10.45$$

$$= -697.5 \text{ psia}$$

Stress

$$\text{hoop} = -\frac{pR}{t_{cost}} = -\frac{697.5(32)}{1.40(0.927)} = -17,250 \text{ psi}$$

$$\text{F.S.} = \frac{33,800}{17,250} = +1.96$$

$$\text{long.} = \frac{P}{A} \pm \frac{MC}{I}$$

$$= -\frac{10,900}{1(1.40)} \pm \frac{373,000(16)}{\pi R^3 t}$$

$$= -7,780 \pm \frac{5.97(10^6)}{3.14(32^3)(1.40)}$$

$$= -7,780 \pm 1,325 = \begin{matrix} -9,105 \text{ psi} \\ -6,455 \text{ psi} \end{matrix}$$

$$\text{F.S.} = \frac{30,400}{9,105} = +3.34$$

Local Stresses - 181 Glass Cloth Hoop Ring (Reference 36)

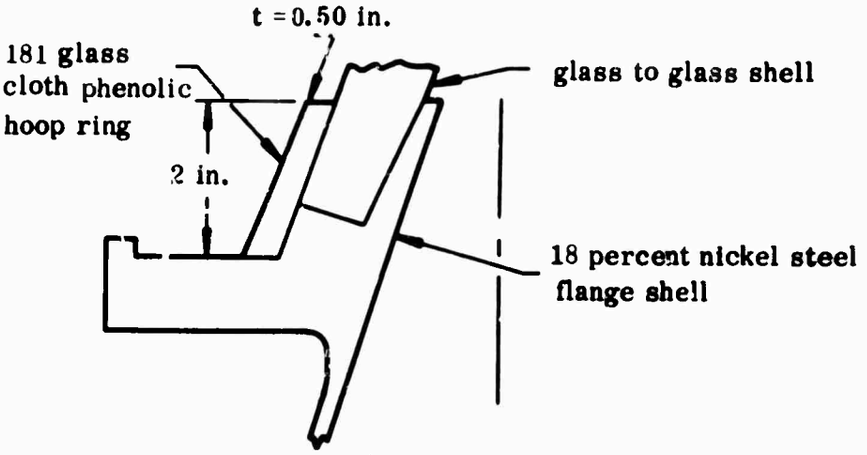

$$\text{Ring Hoop Stress } \sigma_H = \frac{FR}{A} = \frac{545 \text{ lb/in.}(33.5 \text{ in.})}{2(0.50)} = +18,250 \text{ psi tension}$$

$$\text{F.S.} = \frac{38,000}{+18,250} = +2.08$$

Local Buckling (Reference 11)

Loads - Flight Test Condition

Same as for local stresses. Assume R = 32 in. for a cylinder length (L = 38.3 in.) and thickness (t = 1.40 in.).

Axial Load Buckling

$$P_{critical} = 2C\pi Et^2 = 2(0.465)(3.14)(3.00)10^6(1.40^2)$$

$$= 17.1 \times 10^6$$

$$\therefore C = 0.465$$

$$R/t = \frac{32}{1.40} = 22.90$$

$$R_C = \frac{2.03(10^6)}{17.1(10^6)} = 0.12$$

Lateral External Pressure

$$P_{cr} = \frac{C_p \pi^2 D}{RL^2} = \frac{6.5(3.14)^2\ 0.797(10^6)}{32(38.3)^2} = 1,088 \text{ psi}$$

$$Z = \frac{L^2(0.99)}{Rt} = \frac{38.3^2(0.99)}{32(1.40)} = 32.6 \qquad \therefore C_p = 6.5$$

$$D = \frac{Et^3}{11.75} = \frac{3.40(10^6)(1.40)^3}{11.75} = 0.797(10^6)$$

$$R_p = \frac{697.5}{1,088} = 0.64$$

Axial Bending Buckling - Not considered as the allowable bending moment is many times greater than the actual bending moment.

Combined Axial Compression and Lateral Pressure

$$F.S. = \frac{1}{\sqrt{R_o^2 + R_p^2}} = \frac{1}{\sqrt{0.12^2 + 0.64^2}} = \frac{1}{0.65} = +1.54$$

Hoop Deformation

$$\delta_H = -\frac{pR^2(1-\mu/2)}{Et} \quad \text{(Reference 14)}$$

$$\delta_H = -\frac{697.5(32^2)(0.9375)}{3.40(10^6)(1.40)} = -0.140 \text{ in.}$$

$$\text{percent of radius} = \frac{0.140}{32.00} \times 100 = 0.44 \text{ percent}$$

Lateral Deflection of Nose Cap - Under flight acceleration loads.

$L = 46.5 + 13 = 59.5$ use uniform load (Reference 16)

$W = 225$ lb/in.

$$D_{max} = \frac{WL^4}{8EI} = \frac{225(59.5)^4}{8(3.0)10^6(\pi R^3 t)} = \frac{2840 \times 10^6}{2,860,000 \times 10^6} = 0.001 \text{ in.}$$

Axial Deflection of Submerged Structure

$$DL = \frac{\sigma_L L}{E} = \frac{9105(59.5)}{3 \times 10^6} = 0.180 \text{ in.}$$

d. Steel Flange Shell Stresses--The flange shell is checked for column buckling due to axial load, pressure, LITVC bending moments, shear and radial shock, and vibration loads.

Each shell end is checked for local buckling and stresses.

(1) Column Buckling Analysis--The section is analyzed for the critical bending moments, transverse shear, axial moments, and external pressure (Reference 11, Aerospace Buckling Criteria).

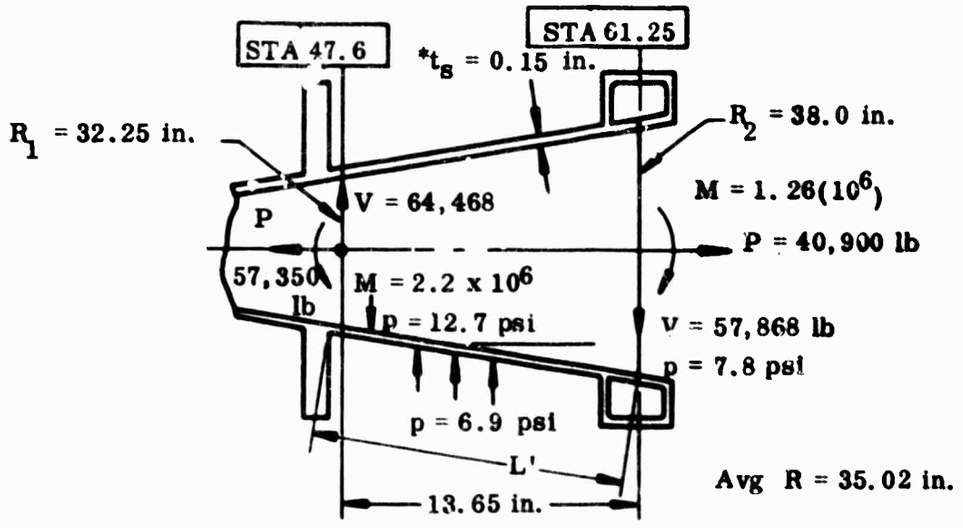

Flight Condition External Pressure (Refer Section III)

$$P_{net} = + \left(\frac{12.7 + 7.8}{2} \right) - 6.90 \pm \frac{30^2}{2\pi (32.25)} = 10.25 - 6.90 \pm 4.45 = \begin{matrix} +7.80 \\ -1.10 \end{matrix}$$

$$r_{eq} = \frac{r_2}{\cos \phi} = \frac{37.8}{\cos 23 \text{ deg}} = 41.2 \text{ in.}$$

$$L_{eq} = \frac{0.75\, r_1 + 1.45\, r_2}{2.2\, r_2} L$$

*Revision A design analysis will reflect thickness change.

$$L_{eq} = \frac{0.75\,(32.25) + 1.45\,(37.8)}{2.2\,(37.8)} \quad \frac{(13.65)}{0.92}$$

$$= 14.85 \text{ in.}$$

$$Z = \frac{L_{eq}^{\,2}}{r_{qt}} \sqrt{1-\mu^2} = \frac{(14.85)^2\ 0.955}{41.2\ (0.15)}$$

$$Z = 34.0$$

Use fixed ends for K_p coefficient

$$\therefore K_p = 5.30$$

$$P_{cr} = \frac{K_p \pi^2 E\, t^3}{12(1-\mu^2) L_{eq}^{\,2} r_{eq}} = \frac{5.30\ (9.9)\ (27)\ 10^6\ (0.0033)}{10.9\ (220)\ (41.2)}$$

$$P_{cr} = 47.4 \text{ psi} \qquad R_p = \frac{-1.10}{47.4} = 0.023 \text{ (neg)}$$

Bending Moment

$$M_{cr} = C_b \pi\, ERt^2 \qquad \text{Actual Moment} = \left(\frac{2.1 + 1.26}{2}\right)(10^6)$$

$$R/t = 35.02/0.15 = 233.0 \qquad = 1.68 \times 10^6$$

$$\text{Avg } R = \frac{37.8 + 32.25}{2} = 35.02$$

$$\therefore C_B \quad 0.332$$

$$M_{cr} = 0.332\ (3.14)\ (27)\ 10^6\ (35.02)\ (0.022) = 21.7 \times 10^6 \text{ in. lb}$$

$$R_B = \frac{1.68}{21.7} = 0.078 \text{ (neg)}$$

Axial Load

$$P_{cr} = 2C \pi\, Et^2$$

$$\therefore C = 0.267$$

$$P_{cr} = 2(0.267)(3.14)\ (27)\ 10^6 (0.022) = 1.0 \times 10^6 \text{ lb compression}$$

$$R_C = O$$

$$\text{Actual Axial Load} = \frac{57,350 + 40,900}{2}$$

$$= 49,125 \text{ lb tension} \qquad R_C = 0$$

Transverse Shear

$$V_{cr} = \frac{C_s \pi^3 DR}{L^2} \qquad D = \frac{Et^2}{12(1-\mu^2)} = \frac{Et^3}{10.9}$$

$$\therefore C_s = 17.5 \qquad Z = \frac{L^2\sqrt{1-\mu^2}}{Rt}$$

$$V_{cr} = \frac{17.5\,(31)\,Et^3\,(35.02)}{186 \quad (10.9)} \qquad = \frac{(13.65)^2\,0.955}{35.02\,(0.15)}$$

$$V_{cr} = 9.38\,(27)\,10^6\,(0.003) \qquad Z = 33.8$$

$$V_{cr} = 0.810(10^6) \qquad \text{Actual V} = \frac{57,000 + 50,400}{2} = 53,700 \text{ lb}$$

$$R_S = \frac{53,700}{810,000} = 0.066$$

Combined axial compression, bending and transverse shear

$$\text{F.S.} = \frac{2}{R_c + R_b + \sqrt{(R_c + R_b)^2 + 4\,(R_s)^2}} \qquad \text{(Reference 20)}$$

$$= \frac{2}{0 + 0.078 + \sqrt{(0.078)^2 + 0.0174}}$$

$$\text{F.S.} = \frac{2}{0.078 + 0.153} = +8.65$$

(2) Local Stress at Station 47.6--This section is designed by the bending moments, axial load, and transverse shear of pressure, the LITVC loads (N_2O_4), the acceleration, shock loads, and tank support. The section is taken far enough forward of the flange to not add to the discontinuity stresses.

Flight Condition

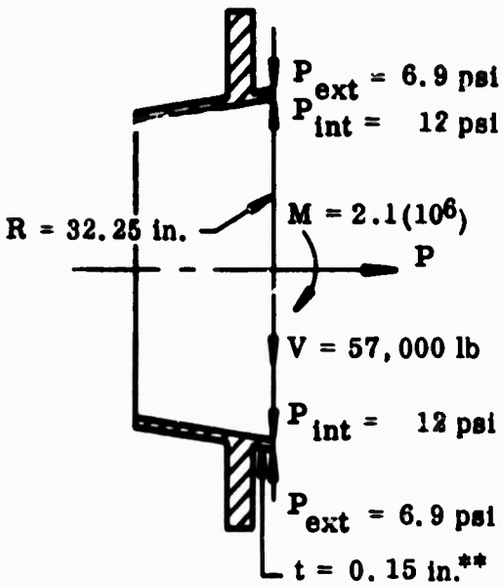

NOTE: Neglect local LITVC pressure effects at the flange.

$P_{int} = P_{ext} + P_{int} + P(shock)$

$= -6.9 + 12 \pm \frac{30\,(30)}{2\pi R} = +5.1 + 4.4$

$= +9.5$ psi

Moment = 1.23 (10^6) + 0.73 (10^6)
(LITVC) (Acceleration)

+ 0.14 (10^6)*
(Tank)

= 2.10 (10^6) in. lb

Axial Load = + 31,500 + 100,000
(Acceleration) (Pressure)

- 8,750 - π $(R_E - R)(14.7 - 6.9)$
(LITVC)

Axial Load = + 122,750 - 24.5 $(60.8^2 - 32.5^2)$

= + 122,750 - 65,400

= + 57,350 lb

yy-Transverse Shear = + 27,500 + 19,600 + 9,900 = + 57,000 lb

(LITVC) + (Acceleration) + (Tank)

*Tanks transposed from y'y' and x'x' axis to xx and yy with no change.
**Revision A design analysis will reflect thickness change.

Stresses

$$\sigma_{Hoop} = +\frac{pR}{t} = \frac{9.5\,(32.25)}{0.15} = +2,040\ \text{psi (neg)}$$

$$\sigma_{Radial} = p_{net} = +9.5\ \text{psi (neg)}$$

$$\sigma_{Axial} = +\frac{P}{A} \pm \frac{Mc}{I} = +\frac{57,350}{30.4} \pm \frac{2,100,000\,(32.25)}{\pi R^3 t\ (14,700)}$$

$$= +1,880 \pm 4,600 = \begin{matrix} +6,480\ \text{psi} \\ -2,720\ \text{psi} \end{matrix}$$

$$\sigma_{Axial\ Shear} = V/A = \frac{57,000}{2\pi R t} = \frac{57,000}{6.28\,(32.25)\,(0.15)}$$

$$= 1,880\ \text{psi (neg)}$$

$$F.S. = \frac{200,000}{+6,480} = +\text{high}$$

Local Buckling and Deformation not Considered: Negligible

(3) Local Stress at Station 54.50--This section will be subjected to axial compression - bending loads and nonsymmetrical LITVC internal pressure loads.

At the midpoint between the flange and torque box the shell will be weakest when subjected to internal pressure due to the minimum stiffening ends of the shell end restraints.

LITVC Loading--(Assume Load F is Reacted in Shear by the Adjacent Wall)

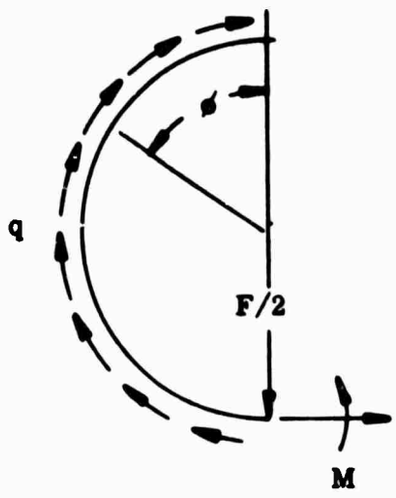

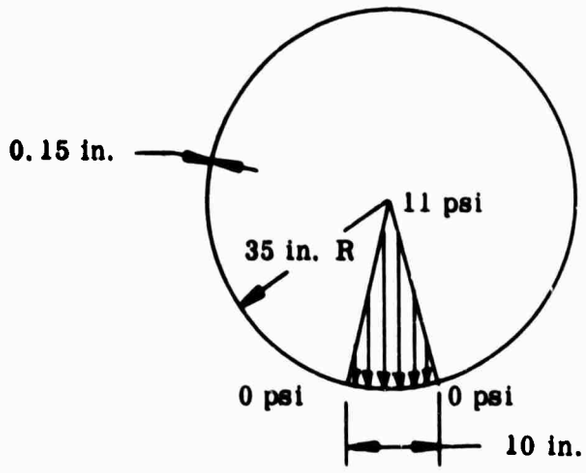

Pressure Loading on Shell at Station 54.50

Section of shell length (dx) = 1.0 in.

Maximum moment and hoop tension will be at ϕ = 180 deg
Maximum shear will be at ϕ = 90 deg

At Station 53.5 the load is $\frac{11}{2}(10)$ = 55 lb

Total load induced by LITVC pressure on inside surface of the steel cone.

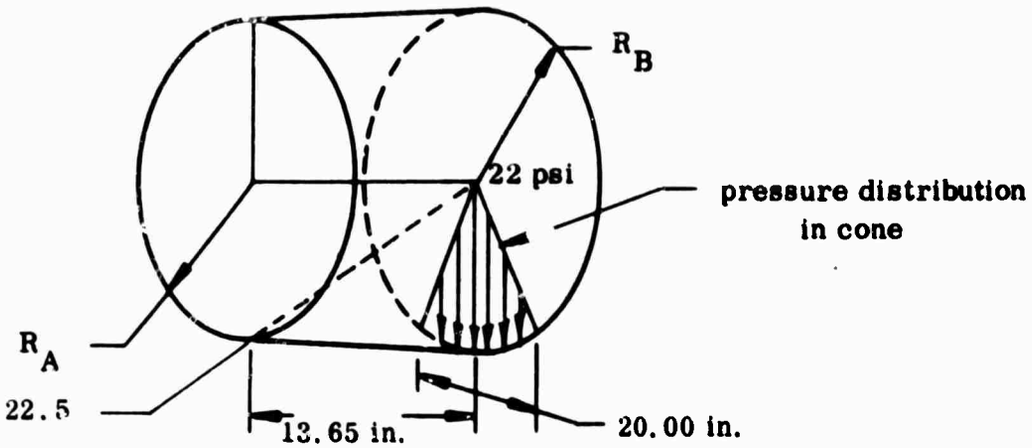

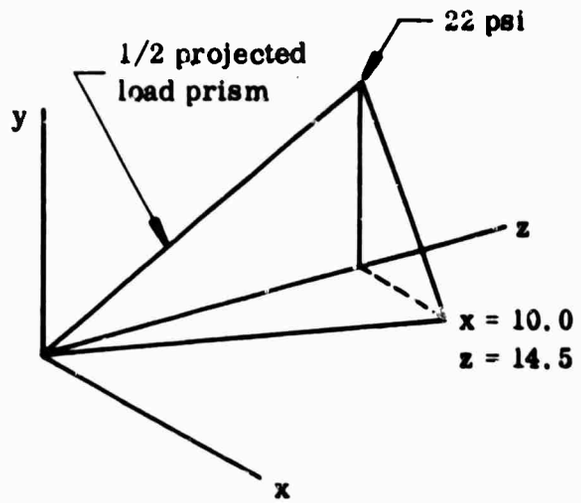

Total Internal Load (V)

$$V = 2\left(\frac{1}{4}\, p\, A_{z=10.5}\right) = 2\left[\frac{1}{4}\,(22)\frac{(13.65)\,10}{z}\right] = 752 \text{ lb}$$

Since the ends of the cone are restrained by stiff rings the radial deformations in the cone will tend to be small at the ends and gradually increase to a maximum at the center (z = 7 in.). It will be assumed that the load is equally distributed over the length of the cone and reacted in shear (Q) through the wall $v' = \frac{752}{13.65} = 55$ lb/in.

Since the local load at Station 54.50 is equal to the distribution load, use

$F = 55$ lb.

At 0 deg $\quad M = \frac{FR}{2\pi} \left(1 - \phi \sin \phi + \frac{\cos \phi}{2} \right)$

$$= \frac{(55)\ 35}{2\pi} (1 - 1.5 + 0.5) = 460 \text{ in. lb/in.}$$

$$T = -\frac{F}{2\pi} \left(\frac{3}{2} \cos \phi - \phi \sin \phi \right)$$

$$= -\frac{40}{2\pi} (-1.5 - 0) = +9.5 \text{ lb/in.}$$

$$q = \frac{F}{\pi R} \sin \phi = 0$$

At $\phi = 90$ deg

$$M = \frac{(55)\ (35)}{2\pi} \Big(1 - (1.57)\ (1.00) + 0.5\ (0) \Big) = -175 \text{ in. lb/in.}$$

$$T \quad \frac{40}{2\pi} \quad \Big((1.5)\ (0) - (1.57)\ (1) \Big) = +10 \text{ lb/in.}$$

$$q \quad \frac{(40)}{\pi\ (35)} \ (1) = 0.36 \text{ lb/in.}$$

Station 54.50 Loads

$p_{net} = +7.80$ psi
$\quad\quad\quad -1.10$ psi

M(bending moment) $= 1.68 \times 10^6$ in. lb

P(axial load) $= +49,125$ lb tension

V (transverse shear) $= +53,700$ lb

Stresses

$$\sigma_{Hoop} = + \frac{PR}{t} \pm \frac{6M}{bt^2} = + \frac{7.8\,(35)}{0.15} \pm \frac{6\,(460)}{1\,(0.15^2)}$$

$$\sigma_H = + 1,820 \pm 122,500 = \begin{matrix} + 124,320 \text{ psi} \\ - 120,680 \text{ psi} \end{matrix}$$

$$\sigma_{Axial} = + \frac{P}{A} \pm \frac{MC}{I} \pm 0.3\,(122,500) = + \frac{49,125}{2\pi\,(35)\,(0.15)} \pm \frac{1.68\,(10^6)35}{\pi\,(35^3)\,(0.15)} \pm 36,800$$

$$\sigma_{Axial} = + 1,500 \pm 2,900 \pm 36,800 = \begin{matrix} + 41,200 \text{ psi} \\ - 38,200 \text{ psi} \end{matrix}$$

$$\sigma_{Shear} = \frac{P}{A} = \frac{53,700}{2\pi\,(35)\,(0.15)} = 1,630 \text{ psi (neg)}$$

$$\text{F.S.} = \frac{200,000}{124,320} = + 1.60$$

(4) Local Stress at Station 61.25--The section at Station 61.25 is designed by the local unsymmetrical LITVC wall pressure, internal and external pressure, side load, bending moment and axial load, and acceleration g load.

Flight Condition (Refer Section III)

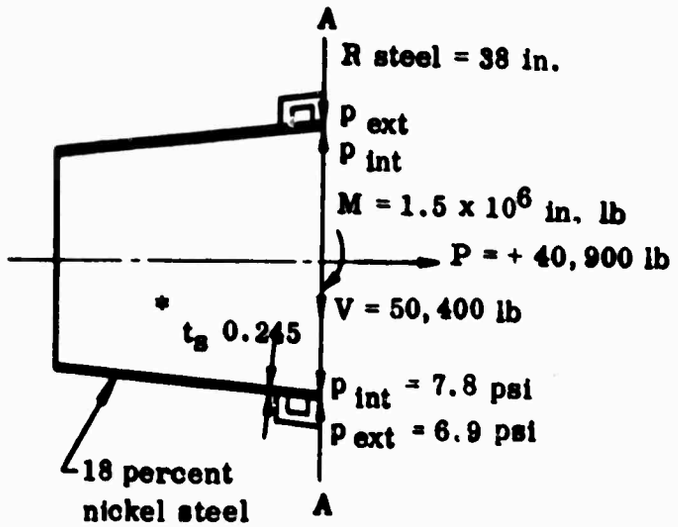

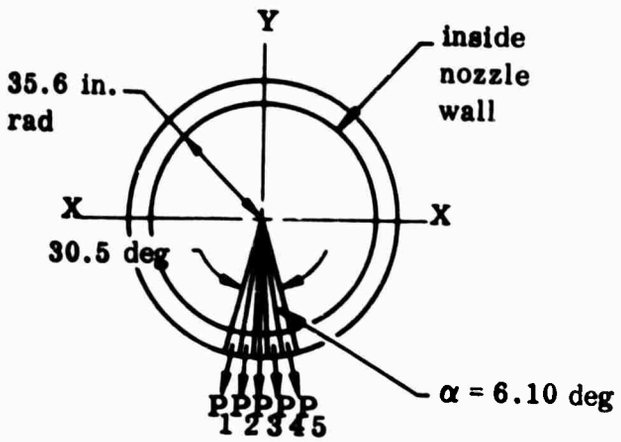

SECTION A-A

Loads

$$p\ net = p\ ext + p\ int \pm p\ (shock) = -6.94 + 7.8 \pm \frac{95\ lb/in.\ (30g's)}{2\pi\ (38)} = \begin{matrix} +12.81\ psi \\ -11.09\ psi \end{matrix}$$

$$xx\text{-Moment} = \underset{(LITVC)}{+800,000} + \underset{(Acceleration)}{459,150} + \underset{(Tanks)}{Zero} = 1.26\ (10^6)\ in.\ lb$$

*t_s - Steel thickness neglects assistance of injector pads and ring. Revision A design analysis will reflect a thickness change.

Axial Load = + 22,000 + 80,000
(Acceleration) (Internal Pressure - Atmospheric Pressure)

- 8,400 $- \pi (R_E^2 - R^2)$ (14.7 - 6.9)
(LITVC)

= + 93,600 - 3.14 $(60.8^2 - 39.3^2)$ (7.8) = + 93,600 - 52,700

= + 40,900 lb

yy-Transverse Shear = + 26,500 + 14,000 + 9,900 * = + 50,400 lb
(LITVC) (Acceleration) (Tanks)

LITVC Tangential Moment

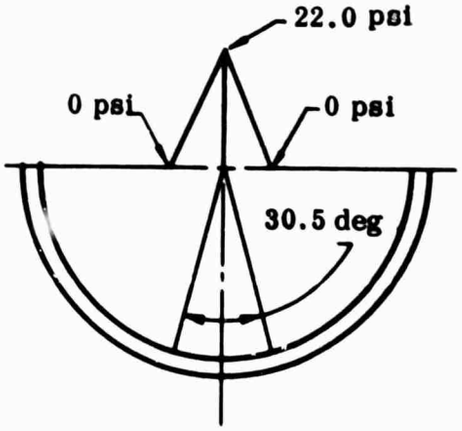

Pressure Distribution
Across Cross Section
1-In. Long Section

The analysis assumes the shell is divided into 1 in. length rings with resulting local loads and stresses (Reference 15).

Chord = 2 sin 15.25 deg (35.6 in.) = 18.7 in.

$P_1 = P_5 = \frac{0.50}{2.5}(22.0) \sin 3.05\ (35.6)^2$

= 16.5 lb at $\frac{12.20}{57.3}$ = 0.213 rad

$P_2 = P_4 = \frac{1.5}{2.5}$ (22.0) 3.78 = 50.0 lb at

$\frac{6.10}{57.3}$ = 0.106 rad

$P_3 = \frac{2.25}{2.50}$ (22) (3.78) = 75.0 lb at 0 rad

ΣP = 33 + 100 + 75 = 208 lb

*Assume tank loads transposed from x'x' to xx axis with no change.

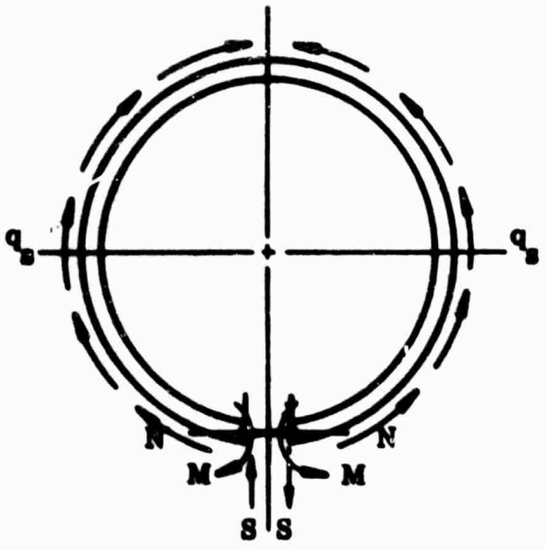

$$M = R\Sigma PW_1$$

$$= 35.6\ \left[2(16.5)0.15 + 2(50)(0.19) + 75(0.25)\right]$$

$$= 35.6\ (42.65) = 1,520 \text{ in. lb tangential}$$

$$N = \Sigma PW_2$$

$$= 16.5(0.325)2 + 2(50)(0.275) + 75(0.25)$$

$$= 56.9 \text{ lb}$$

$$S = \Sigma PW_3$$

$$= 2(16.5)(0.45) + 2(50)(0.475) + 75(0.50)$$

$$= 99.7 \text{ lb}$$

$$\sigma_{hoop} = + \frac{PR}{t} + \frac{6M}{bt^2} = \frac{+12.8\ (38.0)}{0.245} \pm \frac{6(1,520)}{(0.060)}$$

$$= + 1,980 \pm 152,000 = +153,980 \quad \text{outside}$$
$$-150,020 \quad \text{inside}$$

$$\sigma_{hoop\ shear} = \frac{S}{bt} = \frac{99.7}{(1)\ 0.245} = 406 \text{ psi (neg)}$$

$$\sigma_{radial} = p_{int} = +12.8 \text{ psi (neg)}$$

$$\sigma_{axial\ shear} = V/\text{area} = \frac{50,400}{6.28(38)(0.245)} = 864 \text{ psi (neg)}$$

$$\sigma_{axial} = + \frac{P\ axial}{area} \pm \frac{MC}{I}$$

$$= \pm \frac{40,900}{6.28\ (38)\ (0.245)} \pm \frac{1.26\ (10^6)\ 38}{\pi R^3 t} \pm 45,500 \pm 0.3\ (152,000)$$

$$= + 700 \pm \frac{47.0\ (10^6)}{42,000} \pm 45,000 = + 700 \pm 1,120 \pm 45,000 + 47,320$$

$$= +45,920$$

$$\sigma_{allowable} = 200,000 \text{ psi yield} \qquad F.S. = \frac{200,000}{153,985} = + 1.30$$

Deflections

LITVC Load (Reference 13, pg 270)

Max radial displacement under load = $+ \frac{0.135PR^2}{Et^2}$. To determine displacement of all LITVC loads use P=208 lb.

$$\delta = \frac{0.135\ (208)\ (38^2)}{27\ (10^6)\ (0.0148)} = +\ 2.65\ (0.045) = 0.101\ \text{in.}$$

Pressure (Reference 14)

$$\delta = \frac{PR^2\ (1-\mu/2)}{Et} = +\ \frac{12.31(38^2)(0.85)}{27(10^6)(0.245)} = 0.0024\ \text{in.}$$

Total Deflection

$$\delta_T = 0.101 + 0.002 = 0.103$$

$$\Delta R/R = \frac{0.103}{38.0} = 0.00321\ (100) = 0.27\ \text{percent}$$

Local Buckling

The static test condition is critical for local buckling load

$$P_{net} = -p_{ext} + p_{int} \pm p\ (\text{shock})$$

$$= 12.5 + 7.8 \pm 11.9\ \text{psi} = \begin{matrix} -16.6\ \text{psi} \\ +\ 7.2\ \text{psi} \end{matrix}$$

Neglect bending moment, shear, torsion and axial load buckling.

The allowable is very high for existing loads.

Lateral External Pressure Buckling

$$P_{cr} = \frac{Cp\pi^2 D}{RL^2} = \frac{5.5(3.14^2)(36,600)}{38(13.65)^2} = 282 \text{ psi}$$

$$Z = \frac{L^2\sqrt{1-\mu^2}}{Rt} = \frac{(13.65)^2\ 0.954}{38\ (0.245)} = 19.1$$

$$D = \frac{Et^3}{12(1-\mu^2)} = \frac{27(10^6)\ (0.0148)}{10.91} = 36.600$$

$$\therefore Cp = 5.5$$

Assume R = 38 deg for a 13.65 in. length cylinder with t = 0.23 in.

μ = 0.30

$$F.S. = \frac{282}{16.6} = +\text{high}$$

e. Exit Cone Shell--The exit cone sandwich is designed for the external and initial shock pressure and the tangential bending moments due to the LITVC wall pressure distribution. Column and local buckling in addition to deformation under loads are checked the length of the exit cone.

Special end blocks and spacers are placed into the sandwich to attach the structure to the flange shell and static test diffuser and to allow pressure transducers to be placed through the shell.

(1) Column Buckling Analysis--A check of column buckling for the sandwich panel between Station 68.0 and 133.30 for flight and static test conditions indicates the following factors of safety.

Flight Test Loads

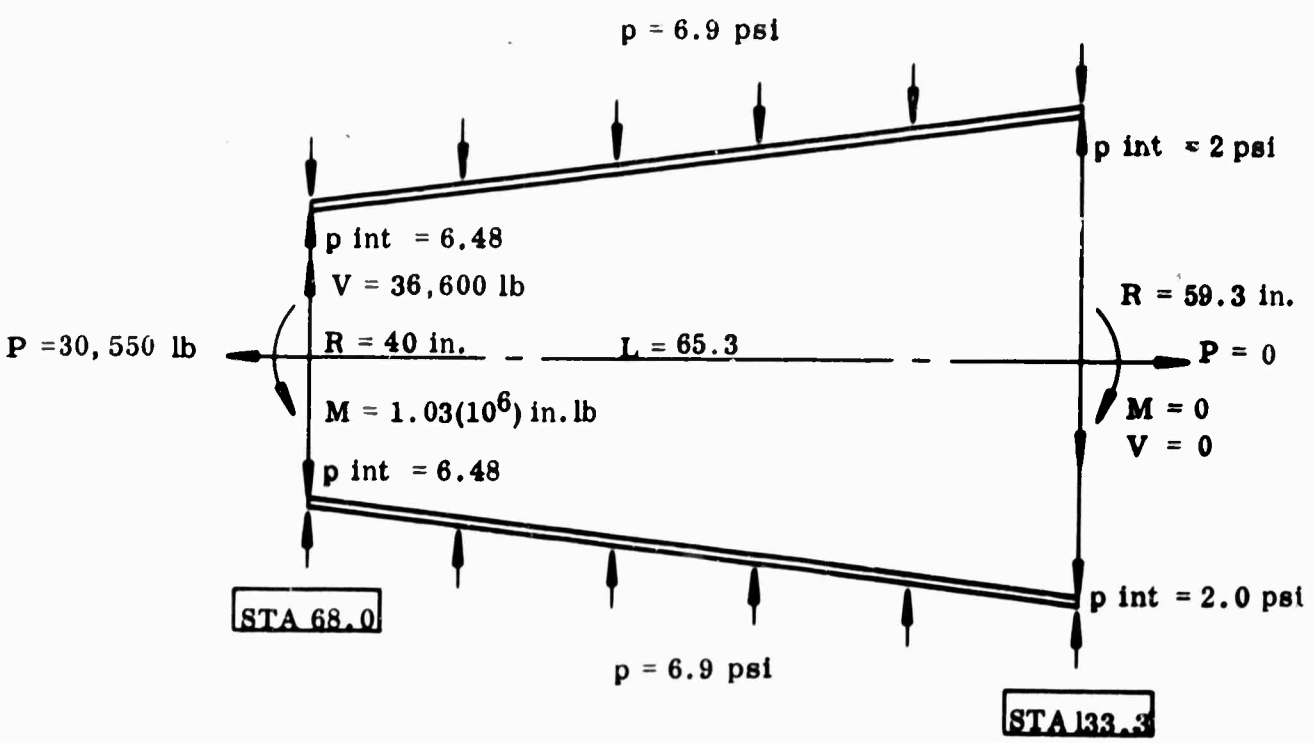

Loads

$$\text{average pressure } (p) = -6.9 + \frac{6.48 + 2.0}{2} \pm \frac{32 \text{ lb/in. x } 60 \text{ g's}}{2\pi R \text{ avg}}$$

$$= -6.9 + 4.24 \pm \frac{1,920}{6.28(49.65)} = 2.66 \pm 6.15$$

$$\therefore \text{avg R} = \frac{59.3 + 40.0}{2} = 49.65$$

$$\text{average pressure} = \begin{matrix} +3.49 \text{ psi} \\ -8.81 \text{ psi} \end{matrix}$$

Average Axial Load, P

$$P_{exit} = 0$$

$$P_{\text{station 68}} = +19,800 - 7,800 + 19,350 = +30,$$
(Pressure) - (LITVC) + (Acceleration)

$$\text{avg P} = \frac{30,550 + 0}{2} = +15,275 \text{ lb tension}$$

Average Bending Moment - Longitudinal

$$M_{exit} = 0$$

$$\text{xx moment} = +650,000 \text{ in. lb} + 379,000 = 1,029,000 \text{ in}$$
(LITVC) (Acceleration)

$$\text{avg moment} = \frac{1,029,000}{2} = 514,500 \text{ in. lb}$$

Average Shear Load

$$\text{shear exit} = 0$$

$$\text{shear at 68.0} = 24,500 \text{ lb} + 12,100 = 36,600 \text{ lb}$$
(LITVC) + (Acceleration)

$$\text{avg shear} = \frac{36,600}{2} = 18,300 \text{ lb}$$

Sandwich Properties and Equivalent Section Properties

Face Sheets - 143 glass cloth epoxy (longitudinal); 20 end S-HTS roving epoxy (hoop). (Reference 12 and Figure 9)

hoop E_c = 5.40 (10^6)

μ_{hoop} = 0.15

hoop σ_c = 55,000 psi

long. E_c = 2.28 (10^6)

$\mu_{long.}$ = 0.15

long. σ_c = 27,400 psi

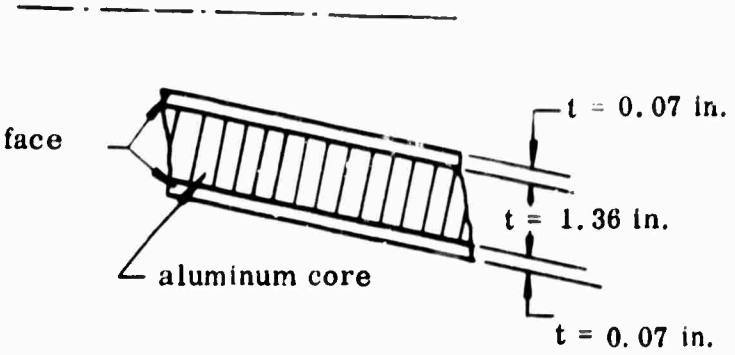

For design analysis the sandwich shell has an effective thickness (t_c) and modulus of elasticity (E_E) for use in formulas for solid isotropic plates. The values obtained for critical loads and deflections are unconservative but for large factors of safety are satisfactory.

$$I_E = 2ay^2 = 2(1)\,(0.07)\,(0.715^2) = 0.070 \text{ in.}^4$$

Sandwich Properties - Hoop

$$E_E = \frac{H}{2\sqrt{3\lambda F \frac{D}{H}}} \qquad t_e = 2\sqrt{3\lambda F \frac{D}{H}} \text{ (Reference 17)}$$

$$D = \frac{E_F}{12\lambda F}(t^3 - t_c^3) = \frac{5.40(10^6)}{12\,(0.98)}\,(1.50^3 - 1.36^3) = 390,000$$

$$\lambda F = 1-\mu^2 = 1-(0.15^2) = 0.98$$

$$H = E_F\,(t-t_c) = 5.40(10^6)\,(1.50 - 1.36) = 755,000$$

$$E_F = 3.14\,(10^6)$$

$$E_E = \frac{755,000}{2\sqrt{3(0.98)\frac{390,000}{755,000}}} = \frac{755,000}{2.46} = 307,000 \text{ psi}$$

$$t_e = 2\sqrt{3(0.98)\frac{390,000}{755,000}} = 2.46 \text{ in.}$$

Sandwich Properties-Longitudinal

$$E_E = \frac{H}{\sqrt{2 \quad 3\,\lambda_F \frac{D}{H}}} \qquad t_E = 2\sqrt{3\,\lambda_F \frac{D}{H}}$$ (Reference 17

$$D = \frac{E_F}{12\lambda_F}(t^3 - t_c^3) = \frac{2.28\,(10^6)}{12\,(0.98)}(1.50^3 - 1.36^3) = 164,500 \text{ in.}$$

$$\lambda_F = 1 - \mu^2 = 1 - (0.15^2) = 0.98$$

$$H = E_F(t - t_c) = 2.28\,(10^6)\,(1.50 - 1.36) = 319,000 \text{ lb/in.}$$

$$E_E = \frac{319,000}{2\sqrt{3\,(0.98)\frac{164,500}{319,000}}} = \frac{319,000}{2\,(1.23)} = 129,500$$

$$t_E = 2\sqrt{3\,(0.98)\quad\frac{164,500}{319,000}} = 2.46 \text{ in.}$$

External Pressure Buckling (Reference 13, p 318)

$$p_{cr} = \frac{0.807\ Et^2}{lr}\ \sqrt[4]{\frac{1}{1-\mu^2}\ 3\ \frac{t^2}{r^2}} \qquad R = 49.65$$

$$= \frac{0.807\ (307,000)\ (2.46)^2}{65.3\ (49.65)}\ \sqrt{1.07\ \frac{(2.46)^2}{(49.65)^2}}$$

$$= 460\ \frac{1.59}{7.06} = 103 \text{ psi} \qquad R_p = \frac{8.81}{103} = 0.085$$

Axial Bending Moment Buckling (Reference 11)

$$M_{cr} = C_b \pi ERt^2 = 0.495(3.14)\ 129,500\ (49.65)\ (2.46)^2$$

$$= 60.5\ (10^6) \text{ in. lb}$$

$$R/_t = \frac{49.65}{2.46} = 20.2 \qquad \therefore C_b = 0.495$$

$$R_B = \frac{1.029(10^6)}{60.5(10^6)} = 0.017$$

Transverse Shear

$$V_{cr} = \frac{C_s \pi^3 DR}{L^2} = \frac{17.5(3.14)^3\ (129,500)\ (49.65)}{(65.3)^2} = 0.81 \times 10^6$$

$$Z = \frac{L^2\ (0.99)}{Rt} = \frac{(65.3)^2\ (0.99)}{49.65\ (2.46)} = 34.6$$

$$\therefore C_s = 17.5$$

$$R_v = \frac{0.018\ (10^6)}{0.81\ (10^6)} = 0.022$$

$$F.S. = \frac{1}{\sqrt{R_c^2 + R_p^2}} = \frac{1}{\sqrt{0.085^2 + 0.017^2}}$$

$$= \frac{1}{0.0835} \leq +12.0$$

(2) Local Stress at Station 68.0 (Glass cloth-aluminum sandwich)--The start of sandwich fabrication at Station 68.0 is designed by axial, bending and shear loads in addition to the local LITVC pressure effects. Two load conditions exist: flight and static test, Utah conditions.

Local Stress

Flight Test Utah Conditions

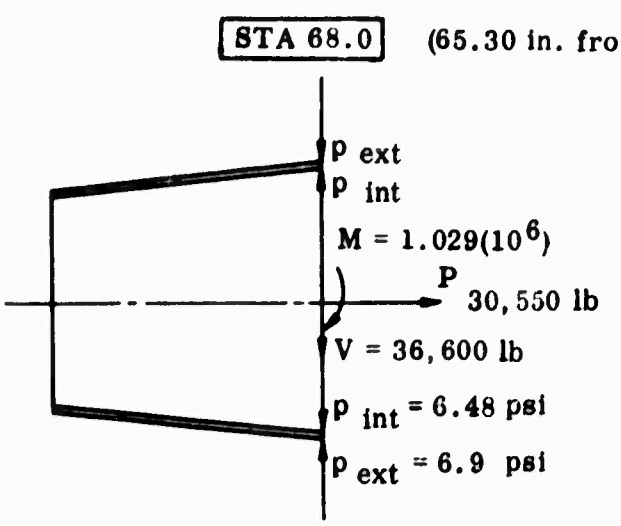

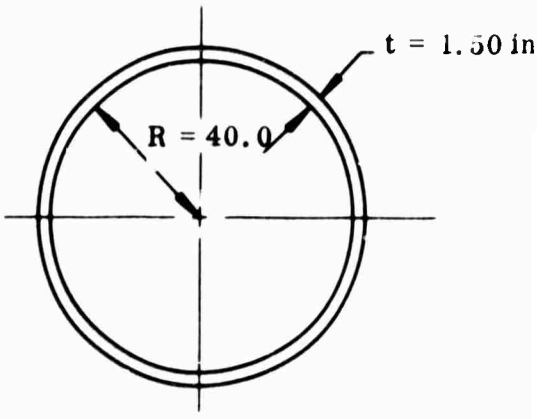

$$\text{Moment} = +650{,}000 + 379{,}000 = 1{,}029{,}000 \text{ in. lb}$$
(LITVC)+(Acceleration)

$$\text{Axial} = +19{,}000 - 7{,}800 + 19{,}350 = +30{,}550 \text{ lb}$$
(Pressure)-(LITVC)+(Acceleration)

$$\text{Shear} = +24{,}500 + 12{,}100 = +36{,}600 \text{ lb}$$
(LITVC) + (Acceleration)

$$\text{Pressure} = +6.48 - 6.9 \pm \frac{32 \text{ lb/in.} \ (60 \text{ g's})}{2\pi R_{avg}} - 0.4 \pm 6.15 = \begin{matrix} +5.75 \text{ psi} \\ -6.55 \text{ psi} \end{matrix}$$

Static Test Loads

$$\text{Axial} = +70{,}000 - 7{,}800 + 3{,}750 = +65{,}950 \text{ lb}$$
(Pressure) (LITVC) (Acceleration)

$$\text{Moment} = +650{,}000 + 114{,}000 = +764{,}000 \text{ in. lb}$$
(LITVC) (Acceleration)

$$\text{Shear} = +24{,}500 + 3{,}630 = +28{,}130 \text{ lb}$$
(LITVC) (Acceleration)

$$\text{Pressure} = \underset{\text{(External)}}{12.5 \text{ psi}} + \underset{\text{(Internal)}}{6.45 \text{ psi}} + \frac{30 \text{ lb/in. } (60 \text{ g's})}{2\pi R} \quad \begin{matrix} -13.5 \text{ psi} \\ = +\ 1.5 \text{ psi} \end{matrix}$$

Note: Use flight test load for local stresses and static test load for buckling stress.

Determination of loads $P_1 \rightarrow P_7$ is the average pressure in each arc times the chord width. The radial loads on the cone ring 1 in. wide are covered in Reference 15, p 269.

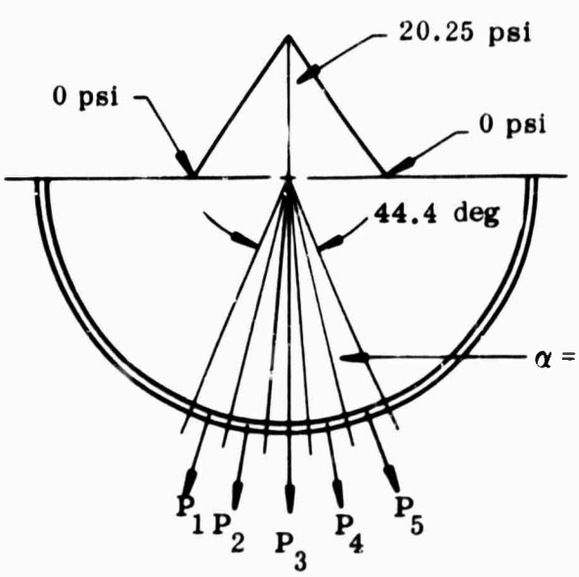

$$P_1 = P_5 = \frac{0.50}{2.50} (20.25) \sin 4.425 \text{ deg}$$

$$(40.0)\ (2)$$

$$= 25.0 \text{ lb at } \frac{17.70}{57.30} = 0.309 \text{ rad}$$

$$P_2 = P_4 = \frac{1.50}{2.50} (20.25)\ 6.17 = 75 \text{ lb}$$

at 0.1545 rad

$$P_3 = \frac{2.25}{2.50} (20.25)\ 6.17 = 112.5 \text{ lb}$$

at 0 rad

$$\Sigma P = 50 + 150 + 112 = 312 \text{ lb}$$

Solve for the moment, shear and axial load under the middle of the pressure distribution.

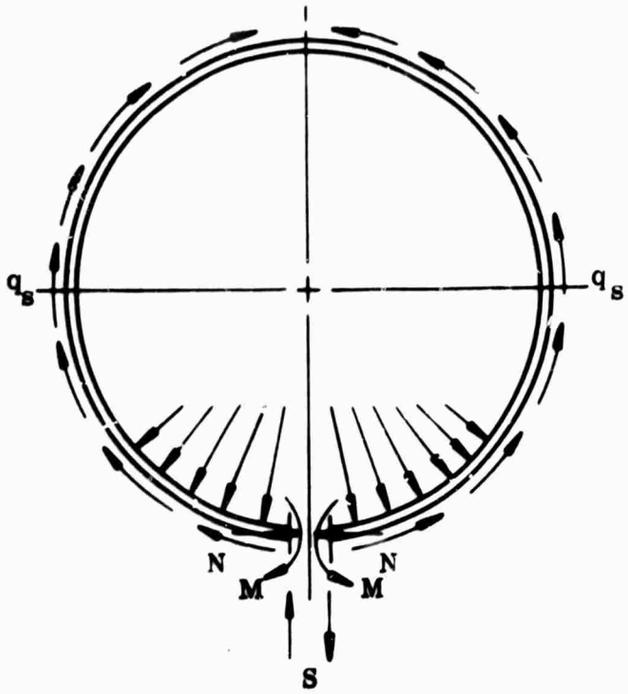

$$M = R\Sigma PW$$

$$= 40.0\left[25(0.12)2 + 75(0.17$$

$$+ 112.5(0.25)\right]$$

$$= 40(60) = 2{,}400 \text{ in. lb tan}$$

$$N = \Sigma PW_2$$

$$= 25(2)(0.36) + 75(2)(0.3$$
$$+ 112.5(0.25)$$

$$= 94.0 \text{ lb}$$

$$? = \Sigma PW_3$$

$$= 2(25)(0.42) + 2(75)(0.4$$

$$+ 112.5(0.5)$$

$$= 147.7 \text{ lb}$$

The following stresses in three directions (radial, tangential and longitudinal) combine the local and beam loads.

$$\sigma_{hoop} = N/A - \frac{pr}{t} \pm \frac{Mc}{I} = -\frac{6.55(40)}{0.14(1)} \pm \frac{2{,}400(0.725)}{0.070} + \frac{94}{1(0.14)}$$

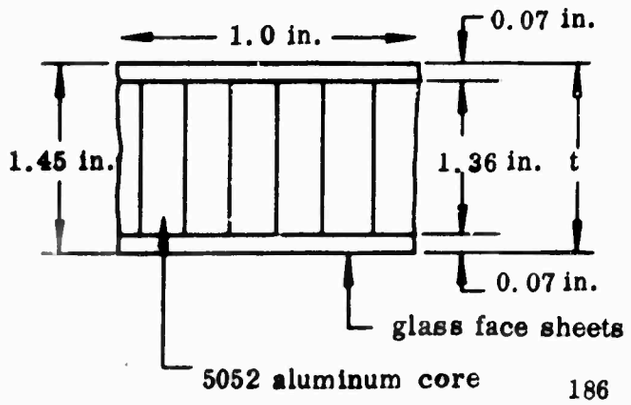

$$I = \frac{1}{12} bd^3 + ay^2$$

$$= \left[\frac{1}{12}(1)(0.10^3) + (0.07)(1)0.71\right.$$

$$= \left[\text{neg} + 0.035\right] 2$$

$$= 0.070 \text{ in.}^4$$

$$\sigma_{hoop} = -1,870 \pm 24,900 + 672 = \begin{matrix} +23,702 \text{ psi} \\ -26,098 \text{ psi} \end{matrix}$$

$$\text{F.S.} = \frac{55,000}{26,098} = +2.11$$

$$I = \pi R^3 t$$

$$\sigma_{axial} = +\frac{P}{A} \pm \frac{Mc}{I} = +\frac{30,550}{6.28\,(40)(0.14)} \pm \frac{1,029,000\,(40)}{3.14\,(40^3)\,(0.14)}$$

$$= +868 \pm 1,460 = \begin{matrix} +2,328 \text{ psi} \\ -592 \text{ psi} \end{matrix}$$

$$\text{F.S.} = \frac{27,400}{2,328} = +\text{high}$$

$$\sigma_{radial} = p = -6.55 \text{ psi} \qquad \sigma_{\substack{\text{allowable} \\ \text{compression}}} = 326 \text{ psi} \qquad \text{F.S.} = +\text{high}$$

$$\sigma_{hoop\ shear} = \frac{S}{bt} = \frac{147.7}{(1)1.50} = 99 \text{ psi}$$

$$\sigma_{\substack{\text{allowable} \\ \text{shear}}} = 210 \text{ psi}$$

$$\text{F.S.} = \frac{210}{99} = +2.12$$

$$\sigma_{axial\ shear} = V/A = \frac{36,600}{2\pi Rt} = \frac{36,600}{6.28\,(40)\,(1.50)} = 97 \text{ psi}$$

$$\sigma_{\substack{\text{allowable} \\ \text{shear}}} = 360 \text{ psi}$$

$$\text{F.S.} = \frac{360}{97} = +3.71$$

Local Buckling - Static Test Condition

$$p_{actual} = \underset{\text{(External)}}{-12.50 \text{ psi}} + \underset{\text{(Internal)}}{6.48 \text{ psi}} \pm \left(\frac{30 \text{ lb/in.}}{2\pi R}\right)_{\text{(shock)}} (60 \text{ g's})$$

$$= -6.02 \pm \frac{1,800}{6.28\,(38.0)} = \begin{matrix} -13.56 \text{ psi} \\ +1.51 \text{ psi} \end{matrix}$$

$$p_{cr} = \frac{0.807\, Et^2}{lr}\sqrt[4]{\frac{\cdot}{(1-\mu^2)}^3\left(\frac{t^2}{r^2}\right)} \qquad \text{(Refer} \cdot \text{ce 13, p 318)}$$

$$R = 40$$

$$p_{cr} = 579\ \frac{1.59}{6.33} = 145.5$$

$$\text{F.S.} = \frac{145.5}{13.56} = +\text{high}$$

Local Deformation - Flight Test Condition

Pressure (Reference 14)

$$\delta = \frac{pr^2(1-\mu/2)}{Et} = +\frac{5.75\,(40^2)\,(0.9375)}{307,000\ (2.34)} = +0.011 \text{ in.}$$

LITVC Load (Reference 13, p 270)

$$\delta = +\frac{0.135\, PR^2}{Et^3} = +\frac{0.135\ (312)\ (40^2)}{307,000\ (2.34^3)}$$

$$= +0.017$$

$$\text{Total Deflection} = +0.017 + 0.011 = 0.028 \text{ in.}$$

$$\Delta R/R = \frac{0.028}{40.0}\ (100) = 0.07 \text{ percent}$$

(3) Local Stress at Station 100.60 (Glass Cloth-Aluminum Sandwich)--Section at half the length of sandwich cone is subjected to the same type of loads as at station 61.25.

Local Stress

Flight Test - Utah Conditions

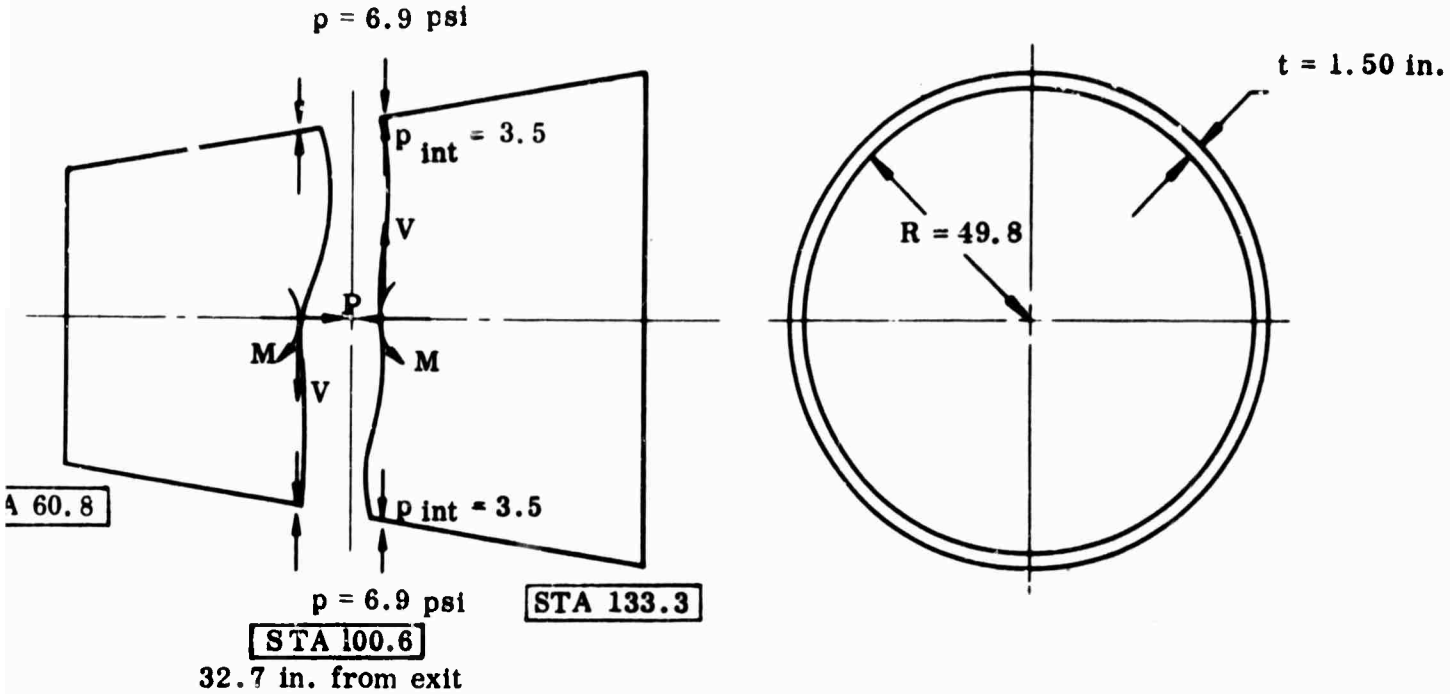

$$\text{Pressure, } p = +0.0049(705) - 6.9 = +3.5 - 6.9 = 3.4 \text{ psi} \pm \frac{35 \text{ lb/in.}(60 \text{ g's})}{2\pi\,(49.8)}$$

$$= +3.3 \text{ psi}$$

$$= -10.1 \text{ psi}$$

$$\text{Axial Load} = +15,600 \quad -3,100 \quad +8,800 = +21,300 \text{ lb}$$

(Pressure) -(LITVC) +(Acceleration)

$$\text{Moment} = +170,000 \quad +190,000 = 360,000 \text{ in. lb}$$

(LITVC) + (Acceleration)

$$\text{Transverse Shear} = +9,500 \quad +5,500 = +15,000 \text{ lb}$$

(LITVC) + (Acceleration)

With the determination of loads $P_1 \rightarrow P_7$ the bending moments shear and axial ring load may be determined (Reference 15)

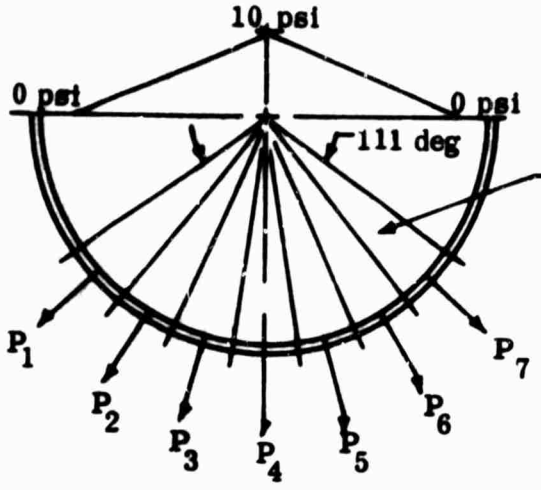

$$P_1 = P_7 = \frac{0.5}{3.5}(10) \sin 7.92 \text{ deg } (49.8)2$$

$$= 1.42\ (13.7) = 19.5 \text{ lb at}$$

$$\frac{47.5}{57.3} = 0.83 \text{ rad}$$

$$P_2 = P_6 = \frac{1.5}{3.5}(10)\ (13.7) = 58.6 \text{ lb}$$

at 0.55 rad

$$P_3 = P_5 = \frac{2.5}{3.5}(10)\ (13.7) = 97.8 \text{ lb}$$

at 0.28 rad

$$P_4 = \frac{3.25}{3.50}(10)\ (13.7) = 127 \text{ lb}$$

at 0.0 rad

$$\Sigma P = 39 + 117 + 195 + 127 = 481 \text{ lb}$$

Solve for the moment, shear and axial load under the middle of the pressure distribution.

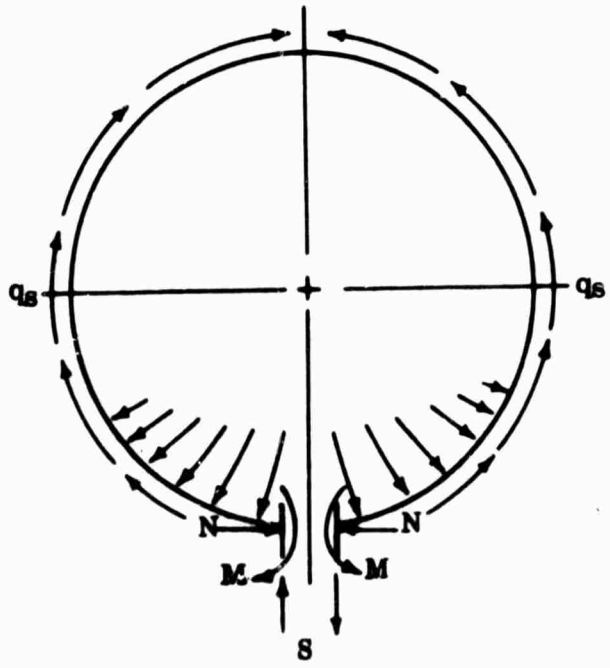

$$M = R\Sigma PW_1$$

$$= 49.8\left[2(19.5)(-0.05) + 2(58.6)\ (0.03 + 2(97.8)\ (0.12) + 127\ (0.25)\right]$$

$$= 49.8\ (56.66) = 2{,}820 \text{ in. lb tangenti}$$

$$N = \Sigma PW_2$$

$$= 19.5\ (0.44)2 + 58.6(0.42) + 97.8\ (0. + 127\ (0.25)$$

$$= 168 \text{ lb}$$

$$S = \Sigma PW_3$$

$$= 19.5(2)\ (0.18) + 58.6(2)\ (0.32) + 97.8(2)\ (0.42) + 127\ (0.5)$$

$$= 191 \text{ lb}$$

$$\sigma_{hoop} = -\frac{PR}{t} \pm \frac{MC}{I} + \frac{N}{A} = -\frac{10.1\,(49.8)}{0.14} \pm \frac{2,820\,(0.725)}{0.070} + \frac{168}{1(0.14)}$$

$$= -3,590 \pm 30,350 + 1,200 = \begin{matrix} +19,720 \text{ psi} \\ -24,080 \text{ psi} \end{matrix}$$

$$= \begin{matrix} +27,960 \text{ psi} \\ -32,740 \text{ psi} \end{matrix} \qquad F.S. = \frac{55,000}{32,740} = +1.68$$

$$\sigma_{axial} = +\frac{P}{A} \pm \frac{MC}{I} = +\frac{21,300}{6.28\,(49.8)\,(0.14)} \pm \frac{360,000\,(49.8)}{3.14\,(49.8^3)\,(0.14)}$$

$$= +487 \pm 330 = \begin{matrix} +817 \text{ psi} \\ -157 \text{ psi} \end{matrix}$$

$$F.S. = \frac{27,400}{817} = +\text{high}$$

$$\sigma_{radial} = p = -10.1 \text{ psi} \qquad \sigma_{\substack{\text{allowable} \\ \text{compression}}} = 326 \text{ psi}$$

$$F.S. = \frac{326}{10.1} = +\text{high}$$

$$\sigma_{hoop\ shear} = \frac{S}{bt} = \frac{191}{1(1.50)} = 127 \text{ psi}$$

$$\sigma_{\substack{\text{allowable} \\ \text{shear}}} = 210 \text{ psi}$$

$$F.S. = \frac{210}{127} = +1.65$$

$$\sigma_{axial\ shear} = \frac{V}{A} = \frac{15,000}{2\pi Rt} = \frac{15,000}{6.28\,(49.8)\,(1.50)} = 32 \text{ psi}$$

$$\sigma_{\substack{\text{allowable} \\ \text{shear}}} = 269 \text{ psi}$$

$$F.S. = \frac{360}{32} = +\text{high}$$

Local Buckling - Static Test Condition

$$P_{actual} = \underset{\text{(External)}}{-12.5 \text{ psi}} + \underset{\text{(Internal)}}{3.5} + \frac{27 \text{ lb/in. (60 g's)}}{2\pi R}$$

$$= -9.0 \pm 5.17 = \begin{matrix} -14.17 \text{ psi} \\ -3.8 \text{ psi} \end{matrix}$$

$$p_{cr} = 0.807 \frac{Et^2}{lr} \sqrt{\left(\frac{1}{1-\mu^2}\right)^3 \left(\frac{t^2}{r^2}\right)} \qquad R = 49.8 \text{ (Reference 13, p}$$

$$= 104 \text{ psi}$$

$$F.S. = \frac{104}{14.2} = +7.33$$

Local Deformation - Flight Test Condition

Pressure (Reference 14)

$$\delta = \frac{pr^2 (1-\mu/2)}{Et} = + \frac{3.3(49.8)^2 (0.9375)}{307,000 \ (2.46)} = +0.010 \text{ in.}$$

LITVC Load

$$\delta = + \frac{0.135 \ PR^2}{Et^3} = \frac{0.135 \ (481) \ (49.8^2)}{307,000 \ (2.46^3)}$$

$$= +0.035$$

Total Deflection

$$\delta_{tot} = +0.035 + 0.004 = 0.039 \text{ in.}$$

$$\frac{\Delta R}{R} = \frac{0.039}{49.8} (100) = +0.078 \text{ percent}$$

(4) Local Stress at Station 130.30

Exit Cone Buckling

The Utah ground test load condition is critical for the exit cone.

The only load is the external pressure and the radial shock load at ignition - moment and shear = zero at exit

$$p = \underset{\text{(External Ambient Pressure)}}{-12.5} + \underset{\text{(Internal Pressure)}}{2.0 \pm \frac{35.0 \text{ lb/sq in.}}{6.28\ (59.3)}} \quad \underset{\text{(radial g's)}}{(60.0)}$$

$$p = -10.5 \text{ psi} \pm 5.65 \text{ psi} = \begin{matrix} -4.35 \text{ psi} \\ -16.15 \text{ psi} \end{matrix}$$

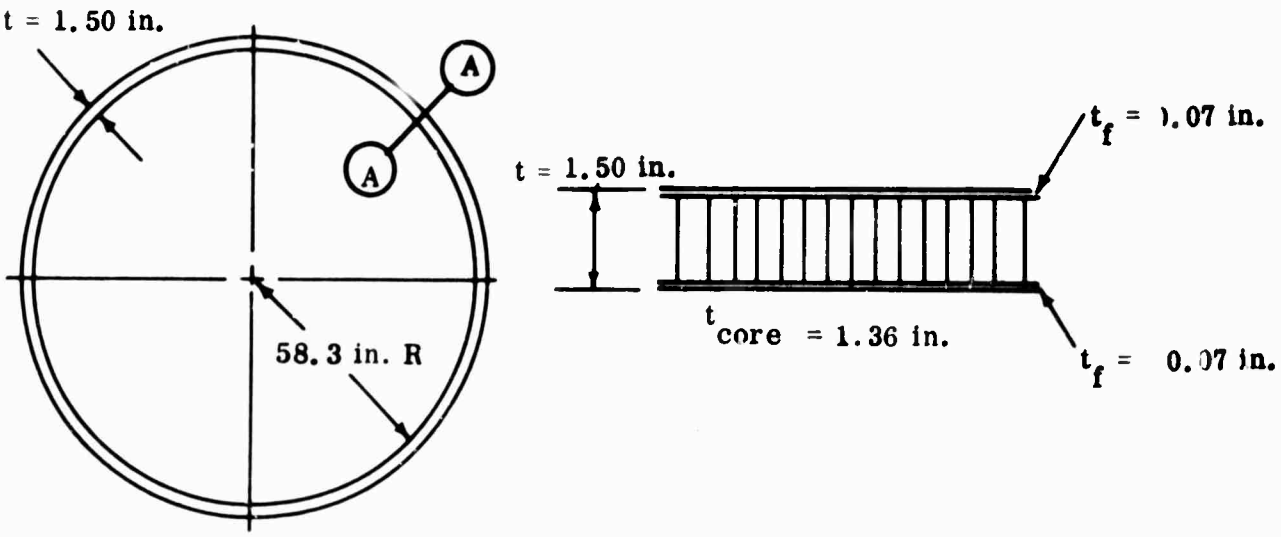

For typical sections close to the exit plane and at the exit, the end ring block is not considered in the crippling analysis.

Local Deformation

$$\delta = \frac{pr^2(1-\mu/2)}{Et} = \frac{-16.15\ (58.3)^2\ (0.9375)}{307{,}000\ (2.46)} = 0.068 \text{ in.}$$

$$\frac{\Delta R}{R} = \frac{0.068}{58.3}\ (100) = -0.12 \text{ percent}$$

An analysis is supplied in Reference 18.

1. Determine minimum face thickness from allowable compression strengt

f_{cy} = 20,000 psi p = -16.20 psi

$$t = \frac{pr}{2F_f}\ (1.25)\ \overset{F.S.}{=} \left(\frac{16.2\ (60.5)}{2\ (20,000)}\right) 1.25 = 0.030$$

use 0.070 in. face sheets

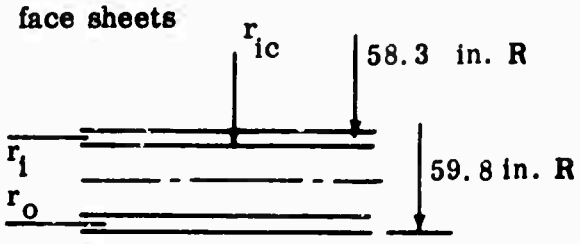

2. Select a core material frombare flat compressive strength (F_c)

$$F_c \geqq \frac{p}{1.5} = \frac{16.2}{1.5} = 10.8 \leqq F_c\ (360)$$

use 1/4 -5,052 - 0.0025 F_c = 360 G_c = 30,500

ω_c = 5.2 lb/cu ft = 0.00301 lb/cu in.

Assume t_c = 1.36

d = 1.50 in.

then r_o = 59.765 in. r_i = 58.335 in.

r_{ic} = 58.37 in. r_c = 59.05 in.

3. Determine actual radial compressive stresses in the core using:

$$f_c = K\left(p\ \frac{r_o}{r_{ic}}\right)$$

$$K = \frac{1}{\left(1 + \frac{r_i}{r_o}\right) - \left[\frac{E_{ft} \ln\left(\frac{r_i}{r_o}\right)}{E_c r_o}\right]} = \frac{1}{1 + \left(\frac{58.335}{59.765}\right) - \left[\frac{-5.4(10^6)(0.07) \ln\left(\frac{59.1}{60.4}\right.}{253,000 \quad 60.45}\right.}$$

∴ use perforated core:

$$E_c = \frac{\omega_c E_m k}{\omega_{\text{core for aluminum}}} = \frac{0.00301\,(10.2)\,(0.8)\,10^6}{0.097} = 253{,}000$$

$$K = \frac{1}{1.977 + \left[\frac{0.0087\,(10^6)}{15.3\,(10^6)}\right]} = 0.505$$

$$f_c = K\left(p\frac{r_o}{r_{ic}}\right) = 0.505\,(16.2)\left(\frac{59.765}{58.37}\right) = 8.35 \text{ psi}$$

$$\text{F.S.} = \frac{326}{8.35} - 1 = +\text{ high}$$

4. Determine hoop compressive stress in outer facing:

$$f_o = \frac{pr_o\,(1-K)}{t} = \frac{16.2\,(59.765)\,(1-0.505)}{0.070} = 6{,}850 \text{ psi}$$

$$\text{F.S.} = \frac{20{,}000}{6{,}850} = +2.90$$

5. Determine hoop compressive stress in inner facing by:

$$f_i = \frac{pr_o\,K}{t} = \frac{16.2\,(59{,}765)(0.505)}{0.070} = 7{,}000 \text{ psi}$$

$$\text{F.S.} = \frac{20{,}000}{7{,}000} = +2.86$$

6. Critical pressure at which compressive buckling of the cylinder wall will occur is:

$$p_{cr} = K^1\left(\frac{Eft}{\lambda d}\right)$$

$$V = \frac{Eft}{\lambda G_{cl} d} = \frac{5.4\,(10^6)\,0.07}{(0.98)\,30{,}500\,(1.50)} = 8.45$$

$$L/rc = \frac{65.3}{59.05} = 1.105$$

$$\frac{rc}{d} = \frac{59.05}{1.50} = 39.30$$

$$\lambda = 1 - \mu^2 = 1 - 0.15^2 = 0.98$$

K^1 is determined from charts X-1 thru X-3. Use chart X-2.

$$K^1 = 0.00028$$

$$p_{cr} = \frac{K^1 E f t}{\lambda d} = \frac{0.00028\,(5.4)\,10^6\,(0.07)}{0.98\,(1.50)}$$

$$p_{cr} = 72.0 \text{ psi} \qquad F.S. = \frac{72.0}{16.2} = +4.45$$

7. Check interface buckling

$$\frac{F_{cr}}{Ef} = 0.125$$

$$F_{cr} = 0.125\,(5.4)\,(10^6) = 660{,}000 \text{ psi allowable}$$

$$F.S = \frac{660{,}000}{7{,}000} = + \text{high}$$

Exit Cone Deformation

Neglect assistance of end ring - consider sandwich resisting -16.15 psi

$$\delta = \frac{pr^2\,(1-\mu/2)}{E_{c\ loop_c}\ t_c} = \frac{-16.15\,(58.3^2)\,(0.9375)}{307{,}000\,(2.46)}$$

$$\delta = 0.068 \text{ in.}$$

$$\frac{\Delta R}{R} = \frac{0.068}{58.3}\,(100) = 0.12 \text{ percent}$$

(5) Local Stress at Station 133.30 Nozzle Exit Plane Ring (Reference 11)--

The exit plane ring is analyzed to insure an adequate moment of inertia and polar moment of inertia to provide a nodal point at the exit plane.

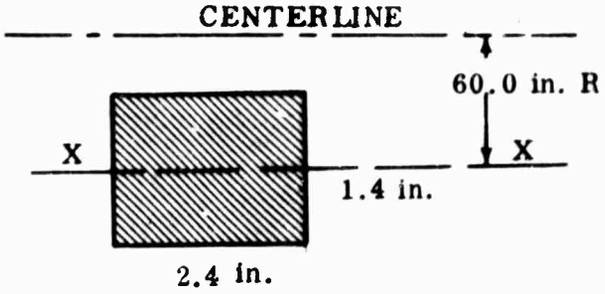

20 end S-HTS glass epoxy hoop filament winding

$$I_{xx} = \frac{1}{12} bd^3 = \frac{1}{12} (2.4)(1.4^3) = 0.55 \text{ in.}^4$$

$$I_{yy} = \frac{1}{12} (1.4)(2.4)^3 = 1.61 \text{ in.}^4$$

$$EI_{xx} = 8.1\,(10.6)(0.55) = 4.45\,(10^6)$$

$$J = I_x + I_y = 0.55 + 1.61 = 2.16 \text{ in.}^4$$

Flight Loads

Avg P = + 15,275 lb P in formula equals 0 when load is tension.

Avg M = ±514,500 in. lb avg

Avg Pressure = -8.81 psi

Required EI_{xx}, J

$$EI = 2\left[\frac{2.4(10^{-4})\,PR^3}{L} + \frac{2.4(10^{-4})\,2MR^2}{L}\right] + \frac{2.4\,(10^{-4})\,2MR^2}{L}$$

$$= (2)(0) + \frac{48\,(10^{-4})(515,000)\,(3,600)}{65.3}$$

$$EI = 0 + 27,200 = 27,200$$

$$= 0.027(10^6)$$

$$J = 2\,(3I)$$

$$J = \frac{6\,(27,200)}{8.1\,(10^6)}$$

$J = 0.022 \text{ in.}^4$ Section is satisfactory.

NOTE: No requirement for transverse shear or axial tension loads.

f. Flange Shell - Exit Cone Shell Discontinuity Analysis--As the main structure in the nozzle, the steel shell distributes the blowout, acceleration, and LITVC loads into the case-nozzle flange from the exit cone. Components are broken down into small free bodies with all loads and reactions shown and then the deflections and rotations of the bodies are equated equal to each other to solve for the shear and moments per circumferential inch.

Figure 68 indicates the present design of flange and submerged shell and the stresses at critical locations in the cross section. Inspection of the stresses and allowables indicates all exhibited a factor of safety of at least 1.25.

The exit cone discontinuity analysis was made under flight conditions.

Torque Box Area (Figure 69).

Deflection and Rotation Equations at Flight Conditions.

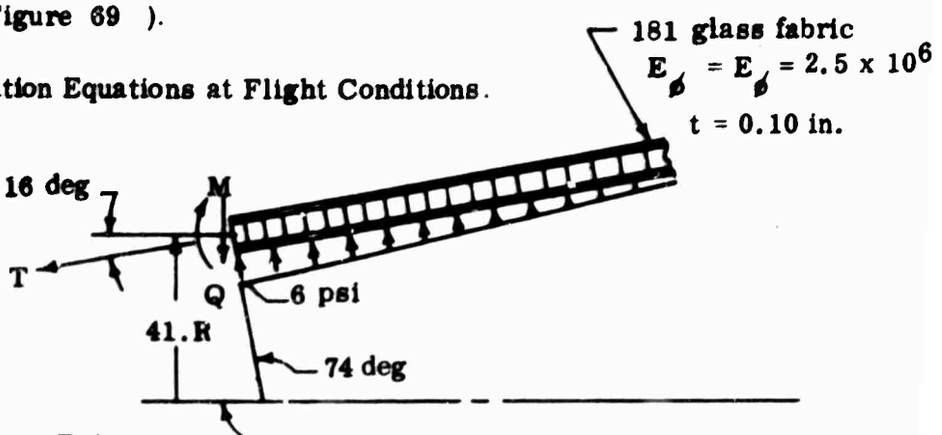

Input to program

Axial stiffness (Dy)

$$Dy = 229 \times 10^{+3} \text{ lb/sq in.}$$

Damping function (β)

$$\beta = \sqrt[4]{\frac{E\theta\, t\theta \sin^2\phi}{4 R^2 Dy}} \qquad \sqrt[4]{\frac{(2.5 \times 10^{+6})\,(0.2)\,(\sin^2 74 \text{ deg})}{4\,(41)^2\,(229 \times 10^{+3})}}$$

$$\beta = \sqrt[4]{3 \times 10^{-4}}$$

$$\left.\begin{aligned} \beta^2 &= 1.73 \times 10^{-2} \\ \beta &= 1.315 \times 10^{-1} \end{aligned}\right\} \qquad \beta^3 = 2.275 \times 10^{-3}$$

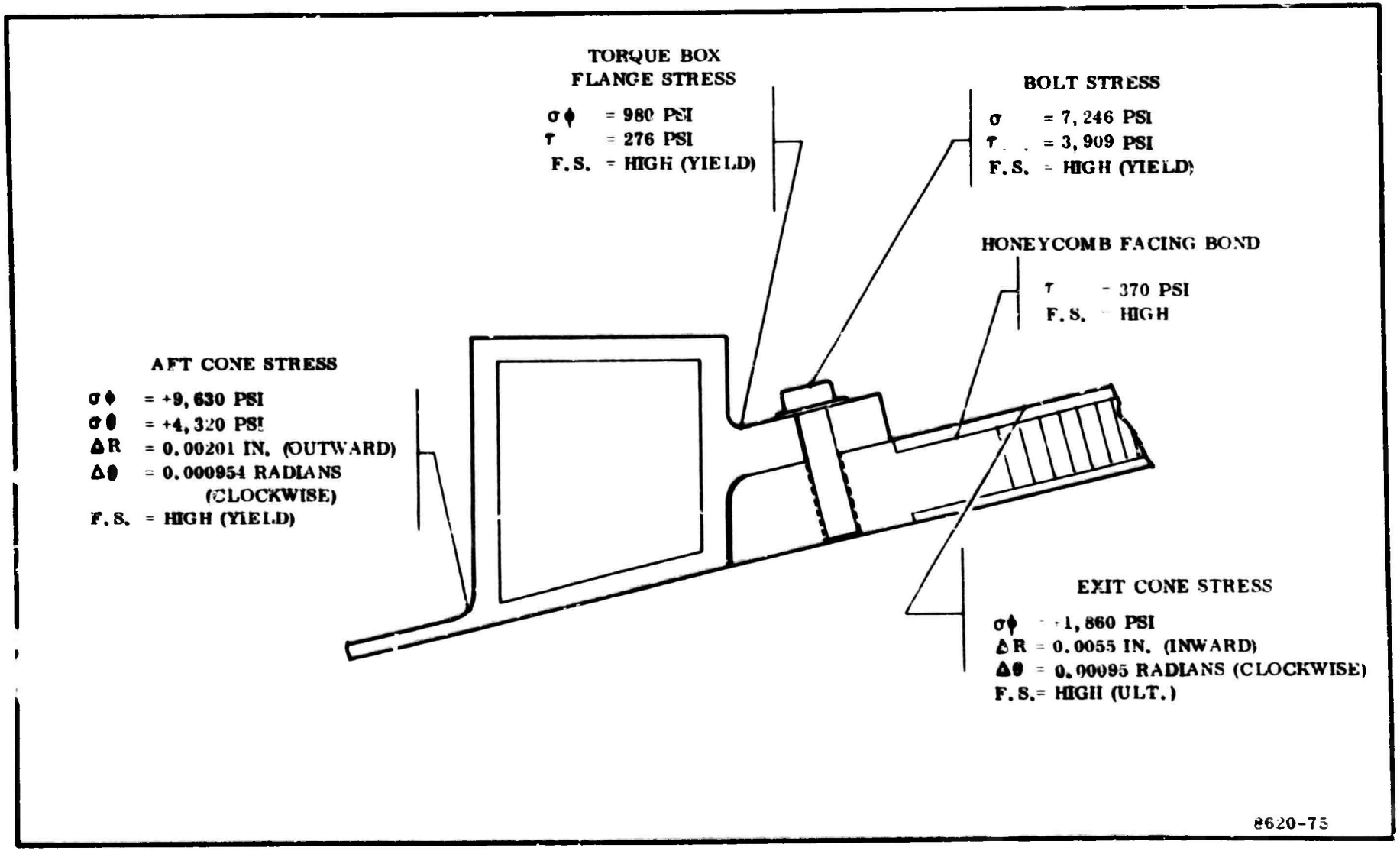

Figure 68. Submerged Nozzle Discontinuity at the Torque Box (Loads During Static Firing at MEOP)

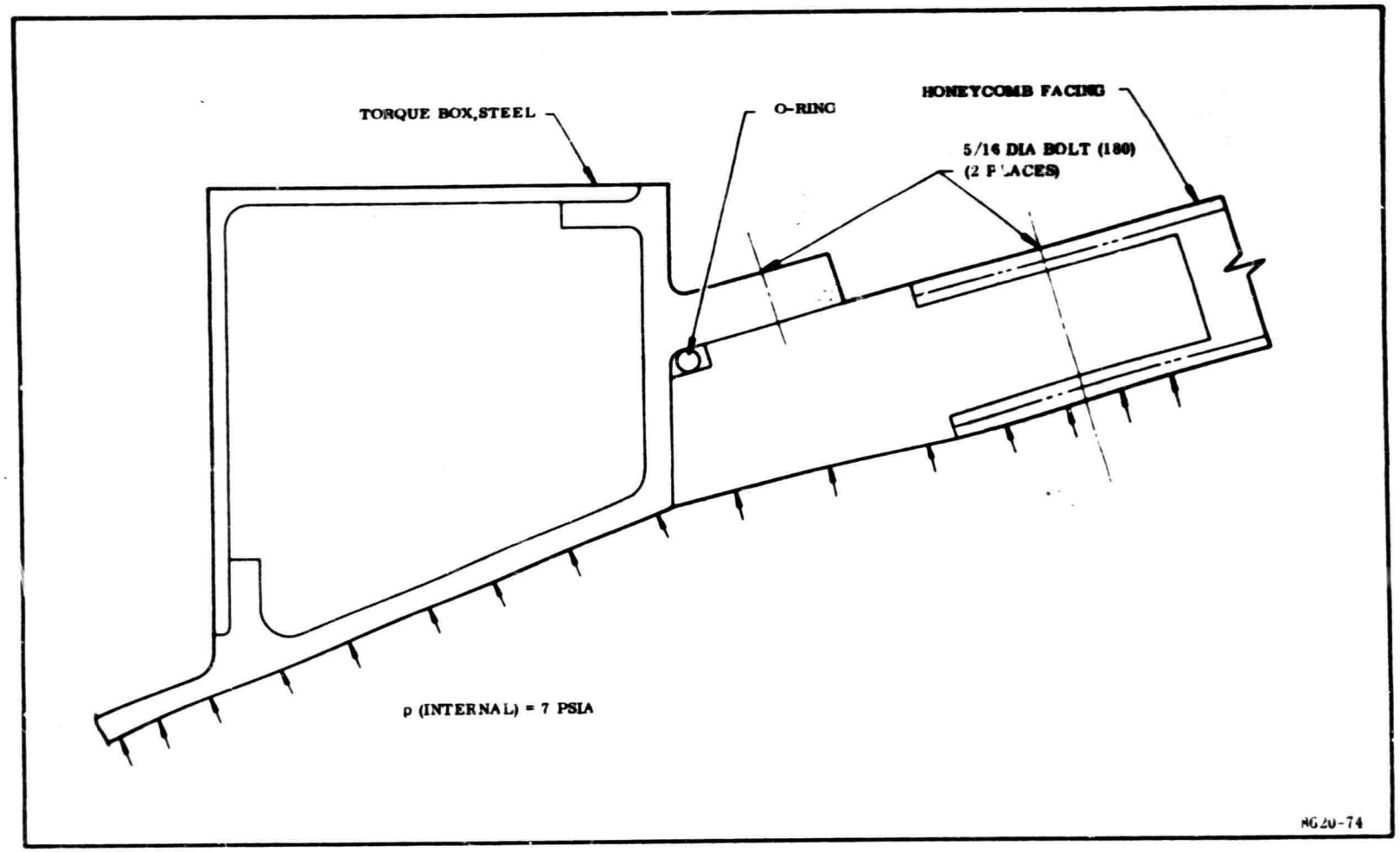

Figure 69. 156-7 Nozzle Internal Pressure During Flight

$$\Delta\theta = +\left(\frac{\sin\phi}{2\beta^2 D}\right) Q - \left(\frac{1}{\beta D}\right) M$$

$$\Delta\theta = +\frac{0.9613\ Q}{2(1.73 \times 10^{-2})\ (229 \times 10^{+3})} - \frac{M}{(1.315 \times 10^{-1})\ (229 \times 10^{+3})}$$

$$\Delta\theta = 10^{-6}\ (121.3\ Q - 33.21\ M)$$

$$\Delta R = +\frac{pR^2}{\sin\phi\ t}\left(\frac{1}{E_\theta} - \frac{\mu}{2E_\phi}\right) + \left(\frac{\sin^2\phi}{2\beta^3 D}\right) Q - \left(\frac{\sin\phi}{2\beta^2 D}\right) M$$

$$\Delta R = +\frac{(6)\ (41)^2}{(0.9613)\ (0.2)}\left(\frac{1}{2.5} - \frac{21}{2(2.5)}\right) 10^{-6} + \frac{(0.9613)^2\ Q}{2(2.275 \times 10^{-3})\ (229 \times 10^{+3})}$$

$$- \frac{(0.9613)\ M}{2(1.73 \times 10^{-2})\ (229 \times 10^{+3})}$$

$$\Delta R = 10^{-6}\ (+\ 19,931 + 886.8\ Q - 121.3\ M)$$

Axial Load (T)

T = -440 lb/in. (Summation of Back Pressure and LITVC Loads)

Results of Discontinuity Analysis (loads, stresses, radial deflections and rotations).

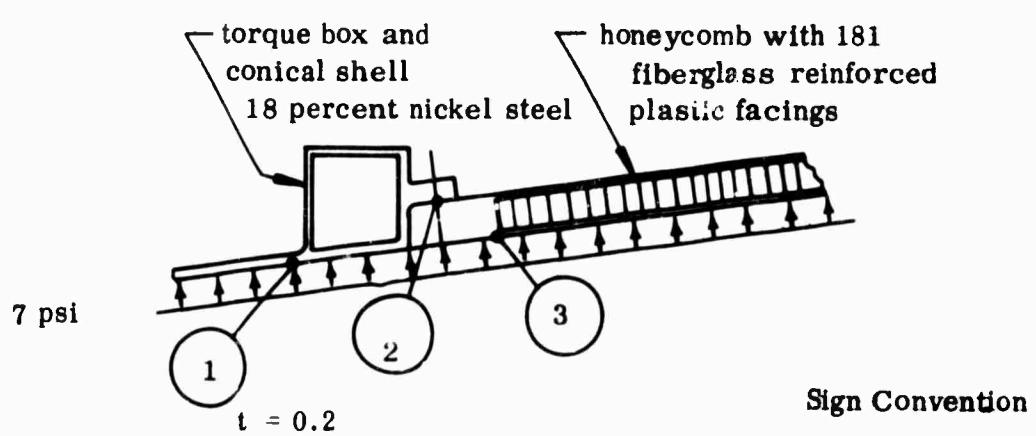

Sign Convention

M, Δθ + ↻

Q AR + ↓

◯ = Station on Computer Output

Station No. 1

$M = +37.4$ in.lb/in. $\quad \Delta\vartheta = +0.000729$ rad

$Q = -30.6$ lb/in. $\quad \Delta R = -0.000152$ in.

$N_\phi = -502$ lb/in.

ID of Cone

$\sigma_\phi = +3,040$ psi

$\sigma_\theta = +1,040$ psi

OD of Cone

$\sigma_\phi = -8,180$ psi

$\sigma_\theta = -2,330$ psi

F.S. = High (including additional stress due to bending induced by LITVC and 5g loading).

Station No. 2

5/16 dia bolt (200)

$M = -50$ in.lb/in. $\quad$ Bolt Space $= \frac{2\pi\,(41)}{200} = 1.29$ in.

$Q = -109$ lb/in. $\quad A_s = 0.058$ sq in.

$N_\phi = -452$ lb/in.

$$T_b = \left|\frac{M\ (\text{bolt space})}{d}\right| - Q\ (\text{bolt space})$$

$$T_b = \frac{(50)\ 1.29}{1.0} + 109\ (1.29)$$

$T_b = 205$ lb (loading due to discontinuity)

Station No. 3

$M = -256$ in.-lb/in. $\qquad \Delta\beta = +0.000729$ rad

$Q = -64.2$ lb/in. $\qquad \Delta R = -0.00589$ in.

$N_\phi = -440$ lb/in.

$I_{(wall)} = 0.0916$ in.^{4}

$$\sigma_{\phi(C)} = \frac{N_\phi}{A} = \frac{-440}{2(0.1)} = -2,200 \text{ psi}$$

$$\sigma_{\phi(D)} = \frac{Mc}{I} = -\frac{(256)\,0.725}{0.0916}$$

$= \pm 2,030$ (due to discontinuity moment)

The results of the nozzle discontinuity analyses (IBM 7040 computer program No. 3239) in the torque box area at flight test conditions are shown on pages 205 through 211.

TC-393 NOZZLE STRUCTURAL ANALYSIS
TORQUE BOX AREA
CASE 1 29 JUNE 65

SIL CONE SECTION (1H% NI STEEL)

FREE BODY NUMBER 1 SEMI-INFINITE CONE

7.00000	--- INTERNAL PRESSURE, PSI	0.200000	--- THICKNESS FOR STRESSES AT STATION(1), IN.
37.35000	--- RADIUS TO MID-POINT OF STATION(1), IN.	0.200000	--- THICKNESS FOR DEFLECTIONS, IN.
0.00000	--- RADIUS OF THROAT, IN.	27.000000	10E6 - MODULUS OF ELASTICITY, PSI
37.25795	--- PRESSURIZED RADIUS AT STATION(1), IN.	0.300000	--- POISSONS RATIO
67.00000	--- PHI, DEGREES	0.451225	--- DAMPING FUNCTION
-0.39073	--- COSINE OF PHI	0.019780 X 10E6	--- FLEXURAL RIGIDITY, IN-LBS.
0.92050	--- SINE OF PHI	-502.000000	--- AXIAL LOAD AT STATION(1), LBS/IN.
40.57556	--- MEAN RADIUS OF CURVATURE NORMAL TO MERIDIAN (R2), IN.		

37.3804132	--- M(1) - MOMENT, IN-LBS/IN.	0.0007285	--- DELTA THETA (1) - ROTATION, RADIANS
-30.5655164	--- Q(1) - SHEAR FORCE, LBS/IN.	-0.0001521	--- DELTA RADIUS (1) - CHANGE IN RADIUS, IN.

DELTA THETA (1) ---	112.0406176 M(1)	114.2820880 Q(1)	33.4897600
DELTA RADIUS(1) ---	-114.2820880 M(1)	-233.1368000 Q(1)	-3006.1832960

STRESSES AT STATION(1)

-2510.0000000 --- SIGMA(1P)	BASIC MERIDIONAL STRESS, PSI
-59.7145000 --- SIGMA(1Q)	MERIDIONAL STRESS DUE TO SHEAR, PSI
5607.0619648 --- SIGMA(1M)	MERIDIONAL STRESS DUE TO MOMENT, PSI
3037.3475328 --- SIGMA(1I)	MAXIMUM COMBINED INSIDE MERIDIONAL STRESS,PSI
-8176.7763968 --- SIGMA(1O)	MAXIMUM COMBINED OUTSIDE MERIDIONAL STRESS, PSI
1420.1446016 --- SIGMA(2P)	BASIC TANGENTIAL STRESS, PSI
-5151.2868864 --- SIGMA(2Q)	TANGENTIAL STRESS DUE TO SHEAR, PSI
3088.1289472 --- SIGMA(2M)	TANGENTIAL STRESS DUE TO MOMENT, PSI
1682.1185664 --- SIGMA(2,1M)	TANGENTIAL STRESS DUE TO SIGMA(1M), PSI
1039.1052288 --- SIGMA(2I)	MAXIMUM COMBINED INSIDE TANGENTIAL STRESS, PSI
-2325.1318784 --- SIGMA(2O)	MAXIMUM COMBINED OUTSIDE TANGENTIAL STRESS, PSI

TORQUE BOX AND FLANGE (18 PERCENT STEEL)

FREE BODY NUMBER 2 RING

7.0000000 --- INTERNAL PRESSURE(1), PSI.	113.0000000 --- PHI AT STATION(1), DEGREES
0.0000000 --- THROAT RADIUS(1), IN.	0.9205048 --- SINE PHI AT STATION(1)
37.3499996 --- RADIUS TO MID-POINT OF STATION(1), IN.	-0.3907312 --- COSINE PHI AT STATION(1)
7.0000000 --- INTERNAL PRESSURE(2), PSI.	89.9999984 --- PHI AT STATION(2), DEGREES
0.0000000 --- THROAT RADIUS(2), IN.	1.0000000 --- SINE PHI AT STATION(2)
39.6999992 --- RADIUS TO MID-POINT OF STATION(2), IN.	-0.0000000 --- COSINE PHI AT STATION(2)
40.0533980 --- RADIUS TO CENTROID, IN.	27.000 X 10E6 - ELASTIC MODULUS, PSI.

4.2356004 --- AREA OF CROSS-SECTION OF RING, SQ. IN.	15.2671058 --- MOMENT OF INERTIA ABOUT THE Y-AXIS, IN.(4TH)
0.0000000 --- HORIZONTAL COMPONENT OF PRESSURE, P1, LB/IN.	2.8533984 --- VERTICAL DISTANCE FROM CENTROID TO P1, IN.
30.0000000 --- VERTICAL COMPONENT OF PRESSURE, P2, LB/IN.	0.5067329 --- HORIZONTAL DISTANCE FROM CENTROID TO P2, IN.
12.5999999 --- HORIZONTAL COMPONENT OF PRESSURE, P3, LB/IN.	-2.0533984 --- VERTICAL DISTANCE FROM CENTROID TO P3, IN.
-2.7033984 --- VERTICAL DISTANCE FROM CENTROID TO AXIAL LOAD(1), IN.	2.6317329 --- HORIZONTAL DISTANCE FROM CENTROID TO AXIAL LOAD(1), IN.
-0.3533984 --- VERTICAL DISTANCE FROM CENTROID TO AXIAL LOAD(2), IN.	1.6182671 --- HORIZONTAL DISTANCE FROM CENTROID TO AXIAL LOAD(2), IN.
37.2579492 --- PRESSURIZED RADIUS AT STATION(1), IN.	-502.0000000 --- AXIAL LOAD AT STATION(1), LB/IN.
40.6999996 --- PRESSURIZED RADIUS AT STATION(2), IN.	-452.0000000 --- AXIAL LOAD AT STATION(2), LB/IN.
2.8533984 --- VERTICAL DISTANCE TO CENTROID, IN.	2.6317329 --- HORIZONTAL DISTANCE TO CENTROID, IN.

37.3804132 --- MI 1) --- MOMENT, IN-LB/IN.	-30.5655164 --- Q(1) --- SHEAR, LB/IN.
-50.4901216 --- MI 2) --- MOMENT, IN-LB/IN.	-109.1928032 --- Q(2) --- SHEAR, LB/IN.

-0.0001521 --- DELTA RADIUS(1) - CHANGE IN RADIUS, IN.	0.0007285 --- DELTA THETA(1) - ROTATION, RADIANS
-0.0032484 --- DELTA RADIUS(2) - CHANGE IN RADIUS, IN.	0.0007285 --- DELTA THETA(2) - ROTATION, RADIANS

C(NET)

1.0000 C(1) -1.0000 Q(2) -226.1470

DELTA RADIUS (C)

14.0281 C(1) -14.0281 Q(2) -3172.4215

M(NET)

-1.0000 M(1) 2.6317 Q(1) 1.0000 M(2) 1.6183 Q(2) 532.2050

DELTA THETA (1)

-3.8919 M(1) 10.2424 Q(1) 3.8919 M(2) 6.2981 Q(2) 2071.2725

DELTA RADIUS(1)

-10.2424 M(1) 40.9833 Q(1) 10.2424 M(2) 2.5467 Q(2) 2278.6145

DELTA THETA (2)

-3.8919 M(1) 10.2424 Q(1) 3.8919 M(2) 6.2981 Q(2) 2071.2725

DELTA RADIUS(2)

6.2981 M(1) -2.5467 Q(1) -6.2981 M(2) -24.2201 Q(2) -6524.2935

5/16 BOLT CONNECTING TORQUE BOX AND EXITCONE FLANGE

BOLT NO. 1 CONNECTING FREE BODIES 2 AND 3

2.3700000 --- BOLT SPACING, IN.
1.0000000 --- DISTANCE TO PIVOT POINT, IN.
0.0580000 --- STRESS AREA OF BOLT, SQ. IN.
0.0000000 --- EFFECTIVE LENGTH OF BOLT, IN.
30.0000000 X 10E6 - ELASTIC MODULUS OF BOLT, PSI
90.0000000 --- PHI, DEGREES
40.6999996 --- PRESSURIZED RADIUS, IN.

-50.4901210 --- M(2) - MOMENT, IN-LB/IN.

-109.1928052 --- Q(2) - SHEAR, LB/IN.

-0.0000000 --- DELTA THETA (2) - ANGLE OF SEPARATION BETWEEN MATING SURFACES, RADIANS

DELTA THETA (2) --- 0.0000000 M(2) -0.0000000

-18469.6547328 --- SIGMA (1P) BASIC BOLT STRESS, PSI

-2063.1307776 --- SIGMA (1M) BOLT STRESS DUE TO BENDING, PSI

-16406.5239040 --- SIGMA (T) TOTAL TENSILE STRESS, PSI

-4461.8437632 --- SIGMA (1Q) BOLT STRESS DUE TO SHEAR, PSI

1134.9154048 --- SIGMA (M) MAXIMUM PRINCIPAL TENSILE STRESS, PSI.

9238.1773312 --- SIGMA (PQ) MAXIMUM PRINCIPAL SHEAR STRESS, PSI.

EXIT CONE FLANGE (CALCULY)

FREE BODY NUMBER 3 RING

7.0000000 --- INTERNAL PRESSURE(2), PSI.	89.9999984 --- PHI AT STATION(2), DEGREES
0.0000000 --- THROAT RADIUS(2), IN.	1.0000000 --- SINE PHI AT STATION(2)
39.6999996 --- RADIUS TO MID-POINT OF STATION(2), IN.	-0.0000000 --- COSINE PHI AT STATION(2)
7.0000000 --- INTERNAL PRESSURE(3), PSI.	73.9999984 --- PHI AT STATION(3), DEGREES
0.0000000 --- THROAT RADIUS(3), IN.	0.9612617 --- SINE PHI AT STATION(3)
40.6999992 --- RADIUS TO MID-POINT OF STATION(3), IN.	0.2756373 --- COSINE PHI AT STATION(3)
40.3133168 --- RADIUS TO CENTROID, IN.	10.500 X 10E6 - ELASTIC MODULUS, PSI.

6.1257997 --- AREA OF CROSS-SECTION OF RING, SQ. IN.	11.7200846 --- MOMENT OF INERTIA ABOUT THE Y-AXIS, IN.(4TH)
0.0000000 --- HORIZONTAL COMPONENT OF PRESSURE, P1, LB/IN.	1.3133174 --- VERTICAL DISTANCE FROM CENTROID TO P1, IN.
28.8999996 --- VERTICAL COMPONENT OF PRESSURE, P2, LB/IN.	0.3210535 --- HORIZONTAL DISTANCE FROM CENTROID TO P2, IN.
6.8599999 --- HORIZONTAL COMPONENT OF PRESSURE, P3, LB/IN.	-0.8233174 --- VERTICAL DISTANCE FROM CENTROID TO P3, IN.
-0.6133174 --- VERTICAL DISTANCE FROM CENTROID TO AXIAL LOAD(2), IN.	2.2410535 --- HORIZONTAL DISTANCE FROM CENTROID TO AXIAL LOAD(2), IN.
0.3866826 --- VERTICAL DISTANCE FROM CENTROID TO AXIAL LOAD(3), IN.	1.3889465 --- HORIZONTAL DISTANCE FROM CENTROID TO AXIAL LOAD(3), IN.
40.6999996 --- PRESSURIZED RADIUS AT STATION(2), IN.	-452.0000000 --- AXIAL LOAD AT STATION(2), LB/IN.
40.0000000 --- PRESSURIZED RADIUS AT STATION(3), IN.	-440.0000000 --- AXIAL LOAD AT STATION(3), LB/IN.
1.3133174 --- VERTICAL DISTANCE TO CENTROID, IN.	2.2410535 --- HORIZONTAL DISTANCE TO CENTROID, IN.

-50.4901216 --- M(2) --- MOMENT, IN-LB/IN.	-109.1928032 --- Q(2) --- SHEAR, LB/IN.
-256.3962144 --- M(3) --- MOMENT, IN-LB/IN.	-64.1912192 --- Q(3) --- SHEAR, LB/IN.

-0.0032484 --- DELTA RADIUS(2) - CHANGE IN RADIUS, IN.	0.0007285 --- DELTA THETA(2) - ROTATION, RADIANS
-0.0058929 --- DELTA RADIUS(3) - CHANGE IN RADIUS, IN.	0.0007285 --- DELTA THETA(3) - ROTATION, RADIANS

G(NET)

	1.0000 G(2)	-1.0000 G(3)	-148.1804	

DELTA RADIUS (G)

	25.2665 G(2)	-25.2665 G(3)	-1744.6002	

M(NET)

-1.0000 M(2)	2.2411 G(2)	1.0000 M(3)	1.3889 Q(3)	594.9365

DELTA THETA (2)

-13.2062 M(2)	29.5957 G(2)	13.2062 M(3)	18.3427 Q(3)	7856.8355

DELTA RADIUS(2)

-29.5957 M(2)	91.5921 G(2)	29.5957 M(3)	15.8404 Q(3)	13863.5880

DELTA THETA (3)

-13.2062 M(2)	29.5957 G(2)	13.2062 M(3)	18.3427 Q(3)	7856.8355

DELTA RADIUS(3)

18.3427 M(2)	-15.8404 G(2)	-18.3427 M(3)	-50.7435 Q(3)	-14656.7244

EXIT CONE D=229000 LBS-IN2 BETA=.1315 I/IS4

FREE BODY NUMBER 4

-256.3962148 --- M(3) - MOMENT, IN-LBS/IN. 0.0007265 --- DELTA THETA (3) - ROTATION, RADIANS

-64.1912192 --- G(3) - SHEAR FORCE, LBS/IN. -0.0058929 --- DELTA RADIUS (3) - CHANGE IN RADIUS, IN.

DELTA THETA (3) ---	-33.2059952 M(3)	121.2999984 G(3)	0.0000000
DELTA RADIUS(3) ---	-121.2959964 M(3)	886.7999872 G(3)	19930.9998080

The results of the nozzle discontinuity analysis in the torque box area at static test conditions are provided on pages 213 through 221.

TU-393 NOZZLE STRUCTURAL ANALYSIS
TORQUE BOX AREA (6597QL8 AXIAL LOAD OURING STATIC FIRING)
C.VCGT 29 JUNE 65

STL CONE SECTION (18% NI STEEL)

FREE BODY NUMBER 1 SEMI-INFINITE CONE

-6.00000 --- INTERNAL PRESSURE, PSI	0.200000 --- THICKNESS FOR STRESSES AT STATION(1), IN.
37.35000 --- RADIUS TO MID-POINT OF STATION(1), IN.	0.200000 --- THICKNESS FOR DEFLECTIONS, IN.
0.00000 --- RADIUS OF THROAT, IN.	27.000000 X 10E6 - MODULUS OF ELASTICITY, PSI
37.25795 --- PRESSURIZED RADIUS AT STATION(1), IN.	0.300000 --- POISSONS RATIO
67.00000 --- PHI, DEGREES	0.451225 --- DAMPING FUNCTION
-0.39073 --- COSINE OF PHI	0.019780 X 10E6 --- FLEXURAL RIGIDITY, IN-LBS.
0.92050 --- SINE OF PHI	287.000000 --- AXIAL LOAD AT STATION(1), LBS/IN.
40.57556 --- MEAN RADIUS OF CURVATURE NORMAL TO MERIDIAN (R2), IN.	

-54.0445352 --- M(1) - MOMENT, IN-LBS/IN.	-0.0009535 --- DELTA THETA (1) - ROTATION, RADIANS
44.8926700 --- Q(1) - SHEAR FORCE, LBS/IN.	-0.0020104 --- DELTA RADIUS (1) - CHANGE IN RADIUS, IN.

DELTA THETA (1) ---	112.0406176 M(1)	114.2820880 Q(1)	-28.7055088
DELTA RADIUS(1) ---	-114.2820880 M(1)	-233.1368000 Q(1)	2279.4106880

STRESSES AT STATION(1)

1435.0000000 --- SIGMA(1P)	BASIC MERIDIONAL STRESS, PSI
87.7048272 --- SIGMA(1Q)	MERIDIONAL STRESS DUE TO SHEAR, PSI
-8106.6802176 --- SIGMA(1M)	MERIDIONAL STRESS DUE TO MOMENT, PSI
-6583.9753240 --- SIGMA(1I)	MAXIMUM COMBINED INSIDE MERIDIONAL STRESS,PSI
9629.3849088 --- SIGMA(1O)	MAXIMUM COMBINED OUTSIDE MERIDIONAL STRESS, PSI
-1217.2668032 --- SIGMA(2P)	BASIC TANGENTIAL STRESS, PSI
7565.8798080 --- SIGMA(2Q)	TANGENTIAL STRESS DUE TO SHEAR, PSI
-4464.8113152 --- SIGMA(2M)	TANGENTIAL STRESS DUE TO MOMENT, PSI
-2432.0040448 --- SIGMA(2,1M)	TANGENTIAL STRESS DUE TO SIGMA(1M), PSI
-548.2023616 --- SIGMA(2I)	MAXIMUM COMBINED INSIDE TANGENTIAL STRESS, PSI
4315.8056960 --- SIGMA(2O)	MAXIMUM COMBINED OUTSIDE TANGENTIAL STRESS, PSI

TORQUE BOX AND FLANGE (18 PERCENT STEEL)

FREE BODY NUMBER 2 RING

-6.0000000	--- INTERNAL PRESSURE(1), PSI.	113.0000000	--- PHI AT STATION(1), DEGREES
0.0000000	--- THROAT RADIUS(1), IN.	0.9205048	--- SINE PHI AT STATION(1)
37.3499996	--- RADIUS TO MID-POINT OF STATION(1), IN.	-0.3907312	--- COSINE PHI AT STATION(1)
7.0000000	--- INTERNAL PRESSURE(2), PSI.	89.9999984	--- PHI AT STATION(2), DEGREES
0.0000000	--- THROAT RADIUS(2), IN.	1.0000000	--- SINE PHI AT STATION(2)
40.6999992	--- RADIUS TO MID-POINT OF STATION(2), IN.	-0.0000000	--- COSINE PHI AT STATION(2)
40.0533980	--- RADIUS TO CENTROID, IN.	27.000 X 10E6	- ELASTIC MODULUS, PSI.

4.2356004	--- AREA OF CROSS-SECTION OF RING, SQ. IN.	15.2671058	--- MOMENT OF INERTIA ABOUT THE Y-AXIS, IN.(4TH)
0.0000000	--- HORIZONTAL COMPONENT OF PRESSURE, P1, LB/IN.	2.8533984	--- VERTICAL DISTANCE FROM CENTROID TO P1, IN.
30.0000000	--- VERTICAL COMPONENT OF PRESSURE, P2, LB/IN.	0.5067329	--- HORIZONTAL DISTANCE FROM CENTROID TO P2, IN.
12.5999999	--- HORIZONTAL COMPONENT OF PRESSURE, P3, LB/IN.	-2.0533984	--- VERTICAL DISTANCE FROM CENTROID TO P3, IN.
-2.7033984	--- VERTICAL DISTANCE FROM CENTROID TO AXIAL LOAD(1), IN.	2.6317329	--- HORIZONTAL DISTANCE FROM CENTROID TO AXIAL LOAD(1), IN.
0.6466016	--- VERTICAL DISTANCE FROM CENTROID TO AXIAL LOAD(2), IN.	2.6182671	--- HORIZONTAL DISTANCE FROM CENTROID TO AXIAL LOAD(2), IN.
37.2579492	--- PRESSURIZED RADIUS AT STATION(1), IN.	289.0000000	--- AXIAL LOAD AT STATION(1), LB/IN.
40.6999996	--- PRESSURIZED RADIUS AT STATION(2), IN.	274.0000000	--- AXIAL LOAD AT STATION(2), LB/IN.
2.8533984	--- VERTICAL DISTANCE TO CENTROID, IN.	2.6317329	--- HORIZONTAL DISTANCE TO CENTROID, IN.

-54.0445352	--- M(1) --- MOMENT, IN-LB/IN.	44.8926700	--- Q(1) --- SHEAR, LB/IN.
-18.4821798	--- M(2) --- MOMENT, IN-LB/IN.	92.2530616	--- Q(2) --- SHEAR, LB/IN.

-0.0020104	--- DELTA RADIUS(1) - CHANGE IN RADIUS, IN.	-0.0009535	--- DELTA THETA(1) - ROTATION, RADIANS
0.0029953	--- DELTA RADIUS(2) - CHANGE IN RADIUS, IN.	-0.0009535	--- DELTA THETA(2) - ROTATION, RADIANS

Q(NET)

1.0000 Q(1) -1.0000 Q(2) 62.9213

DELTA RADIUS (C)

14.0281 Q(1) -14.0281 Q(2) 1163.2313

M(NET)

-1.0000 M(1) 2.6317 Q(1) 1.0000 M(2) 2.6183 Q(2) -640.2389

DELTA THETA (1)

-3.8919 M(1) 10.2424 Q(1) 3.8919 M(2) 10.1900 Q(2) -2491.7260

DELTA RADIUS(1)

-10.2424 M(1) 40.9833 Q(1) 10.2424 M(2) 12.7891 Q(2) -5394.3260

DELTA THETA (2)

-3.8919 M(1) 10.2424 Q(1) 3.8919 M(2) 10.1900 Q(2) -2491.7260

DELTA RADIUS(2)

10.1900 M(1) -12.7891 Q(1) -10.1900 M(2) -40.7682 Q(2) 7687.2352

5/16 BOLT CONNECTING TORQUE BOX AND EXITCONE FLANGE

BOLT NO. 1 CONNECTING FREE BODIES 2 AND 3

1.2800000 --- BOLT SPACING, IN.
0.6500000 --- DISTANCE TO PIVOT POINT, IN.
0.0580000 --- STRESS AREA OF BOLT, SQ. IN.
0.0000000 --- EFFECTIVE LENGTH OF BOLT, IN.
30.0000000 X 10E6 - ELASTIC MODULUS OF BOLT, PSI
90.0000000 --- PHI, DEGREES
40.69?9996 --- PRESSURIZED RADIUS, IN.

-18.4821798 --- M(2) - MOMENT, IN-LB/IN.

92.2530616 --- Q(2) - SHEAR, LB/IN.

-0.0000000 --- DELTA THETA (2) - ANGLE OF SEPARATION BETWEEN MATING SURFACES, RADIANS

DELTA THETA (2) --- 0.0000000 M(2) 0.0000000

6046.8964352 --- SIGMA (1P) BASIC BOLT STRESS, PSI

-627.5116608 --- SIGMA (1M) BOLT STRESS DUE TO BENDING, PSI

6674.4081408 --- SIGMA (T) TOTAL TENSILE STRESS, PSI

2035.9296000 --- SIGMA (1Q) BOLT STRESS DUE TO SHEAR, PSI

7246.4162816 --- SIGMA (M) MAXIMUM PRINCIPAL TENSILE STRESS, PSI.

3909.2122112 --- SIGMA (MQ) MAXIMUM PRINCIPAL SHEAR STRESS, PSI.

EXIT CONE FLANGE (AL.ALY)

FREE BODY NUMBER 3 RING

-6.0000000 --- INTERNAL PRESSURE(2), PSI.	89.9999984 --- PHI AT STATION(2), DEGREES
0.0000000 --- THROAT RADIUS(2), IN.	1.0000000 --- SINE PHI AT STATION(2)
40.6999996 --- RADIUS TO MID-POINT OF STATION(2), IN.	-0.0000000 --- COSINE PHI AT STATION(2)
-6.0000000 --- INTERNAL PRESSURE(3), PSI.	73.9999984 --- PHI AT STATION(3), DEGREES
0.0000000 --- THROAT RADIUS(3), IN.	0.9612617 --- SINE PHI AT STATION(3)
40.6799992 --- RADIUS TO MID-POINT OF STATION(3), IN.	0.2756373 --- COSINE PHI AT STATION(3)
40.2933168 --- RADIUS TO CENTROID, IN.	10.500 X 10E6 - ELASTIC MODULUS, PSI.

6.1257997 --- AREA OF CROSS-SECTION OF RING, SQ. IN.	11.7200846 --- MOMENT OF INERTIA ABOUT THE Y-AXIS, IN.(4TH)
0.0000000 --- HORIZONTAL COMPONENT OF PRESSURE, P1, LB/IN.	1.3133174 --- VERTICAL DISTANCE FROM CENTROID TO P1, IN.
26.8999996 --- VERTICAL COMPONENT OF PRESSURE, P2, LB/IN.	0.3410535 --- HORIZONTAL DISTANCE FROM CENTROID TO P2, IN.
6.8599999 --- HORIZONTAL COMPONENT OF PRESSURE, P3, LB/IN.	-0.8233174 --- VERTICAL DISTANCE FROM CENTROID TO P3, IN.
0.4066826 --- VERTICAL DISTANCE FROM CENTROID TO AXIAL LOAD(2), IN.	1.2410535 --- HORIZONTAL DISTANCE FROM CENTROID TO AXIAL LOAD(2), IN.
0.3866826 --- VERTICAL DISTANCE FROM CENTROID TO AXIAL LOAD(3), IN.	1.3889465 --- HORIZONTAL DISTANCE FROM CENTROID TO AXIAL LOAD(3), IN.
40.6999996 --- PRESSURIZED RADIUS AT STATION(2), IN.	274.0000000 --- AXIAL LOAD AT STATION(2), LB/IN.
40.0000000 --- PRESSURIZED RADIUS AT STATION(3), IN.	274.0000000 --- AXIAL LOAD AT STATION(3), LB/IN.
1.3133174 --- VERTICAL DISTANCE TO CENTROID, IN.	2.2410535 --- HORIZONTAL DISTANCE TO CENTROID, IN.

-18.4821798 --- M(2) --- MOMENT, IN-LB/IN.	92.2530616 --- Q(2) --- SHEAR, LB/IN.
-61.3834008 --- M(3) --- MOMENT, IN-LB/IN.	-24.6661448 --- Q(3) --- SHEAR, LB/IN.

0.0029953 --- DELTA RADIUS(2) - CHANGE IN RADIUS, IN.	-0.0009535 --- DELTA THETA(2) - ROTATION, RADIANS
0.0055029 --- DELTA RADIUS(3) - CHANGE IN RADIUS, IN.	-0.0009535 --- DELTA THETA(3) - ROTATION, RADIANS

Q(NET)

1.0000 Q(2) -1.0000 Q(3) 48.6246

DELTA RADIUS (C)

25.2414 Q(2) -25.2414 Q(3) 1227.3554

M(NET)

-1.0000 M(2) 1.2411 Q(2) 1.0000 M(3) 1.3889 Q(3) -109.5996

DELTA THETA (2)

-13.1931 M(2) 16.3733 Q(2) 13.1931 M(3) 18.3245 Q(3) -1445.9555

DELTA RADIUS(2)

-16.3733 M(2) 45.5616 Q(2) 16.3733 M(3) -2.4998 Q(3) -567.1527

DELTA THETA (3)

-13.1931 M(2) 16.3733 Q(2) 13.1931 M(3) 18.32 Q(3) -1445.9555

DELTA RADIUS(3)

18.3245 M(2) 2.4998 Q(2) -18.3245 M(3) -50.6931 Q(3) 3235.7102

EXIT CONE D#229000 LBS-IN2 BETA#.1315 1/IN4

FREE BODY NUMBER 4

-61.3834008 --- M(3) - MOMENT, IN-LBS/IN. -0.0009535 --- DELTA THETA (3) - ROTATION, RADIANS

-24.6661448 --- Q(3) - SHEAR FORCE, LBS/IN. 0.0055029 --- DELTA RADIUS (3) - CHANGE IN RADIUS, IN.

DELTA THETA (3) ---	-33.2099992 M(3)	121.2999984 Q(3)	0.0000000
DELTA RADIUS(3) ---	-121.2999984 M(3)	886.7999872 Q(3)	19930.9998080

SECTION PROPERTY DATA FOR FREE BODY NO. 2

0.0000000 --- D(P1)	2.1250000 --- D(P2)	0.8000000 --- D(P3)
0.0000000 --- X(N1)	5.2500000 --- X(N2)	0.0000000 --- X(N3)
0.1500000 --- Y(N1)	3.5000000 --- Y(N2)	0.0000000 --- Y(N3)

UPPER CURVE		LOWER CURVE	
X	Y	X	Y
0.0000000	4.8500000	0.0000000	0.0000000
4.0000000	4.8500000	0.1500000	0.0800000
0.1500000	1.3200000	0.1500000	4.7000000
0.4400000	1.3200000	3.2600000	4.7000000
0.4200000	0.4200000	3.2600000	4.4500000
4.0000000	1.9200000	4.0000000	4.4500000
4.0000000	4.8500000	0.1500000	0.0800000
4.2500000	4.8500000	4.2500000	1.8000000
4.2500000	3.7500000	4.2500000	3.2000000
5.7200000	4.1799999	5.8600000	3.7000000
5.8600000	3.7000000	0.0000000	0.0000000
0.0000000	0.0000000	0.0000000	0.0000000
0.0000000	0.0000000	0.0000000	0.0000000
0.0000000	0.0000000	0.0000000	0.0000000
0.0000000	0.0000000	0.0000000	0.0000000
0.0000000	0.0000000	0.0000000	0.0000000
0.0000000	0.0000000	0.0000000	0.0000000
0.0000000	0.0000000	0.0000000	0.0000000
0.0000000	0.0000000	0.0000000	0.0000000
0.0000000	0.0000000	0.0000000	0.0000000
0.0000000	0.0000000	0.0000000	0.0000000
0.0000000	0.0000000	0.0000000	0.0000000
0.0000000	0.0000000	0.0000000	0.0000000
0.0000000	0.0000000	0.0000000	0.0000000
0.0000000	0.0000000	0.0000000	0.0000000
0.0000000	0.0000000	0.0000000	0.0000000
0.0000000	0.0000000	0.0000000	0.0000000
0.0000000	0.0000000	0.0000000	0.0000000
0.0000000	0.0000000	0.0000000	0.0000000
0.0000000	0.0000000	0.0000000	0.0000000
0.0000000	0.0000000	0.0000000	0.0000000
0.0000000	0.0000000	0.0000000	0.0000000

SECTION PROPERTY DATA FOR FREE BODY NO. 3

0.0000000 --- D(P1)	1.9200000 --- D(P2)	0.4900000 --- D(P3)
1.0000000 --- X(N1)	3.6300000 --- X(N2)	0.0000000 --- X(N3)
1.7200000 --- Y(N1)	1.7000000 --- Y(N2)	0.0000000 --- Y(N3)

UPPER CURVE		LOWER CURVE	
X	Y	X	Y
0.0000000	1.4200000	0.0000000	0.0000000
2.2400000	2.0800000	2.5000000	0.6400000
2.3000000	1.8600000	2.5000000	0.8500000
4.7000000	2.5400000	4.9900000	1.5400000
4.9800000	1.5400000	0.0000000	0.0000000
0.0000000	0.0000000	0.0000000	0.0000000
0.0000000	0.0000000	0.0000000	0.0000000
0.0000000	0.0000000	0.0000000	0.0000000
0.0000000	0.0000000	0.0000000	0.0000000
0.0000000	0.0000000	0.0000000	0.0000000
0.0000000	0.0000000	0.0000000	0.0000000
0.0000000	0.0000000	0.0000000	0.0000000
0.0000000	0.0000000	0.0000000	0.0000000
0.0000000	0.0000000	0.0000000	0.0000000
0.0000000	0.0000000	0.0000000	0.0000000
0.0000000	0.0000000	0.0000000	0.0000000
0.0000000	0.0000000	0.0000000	0.0000000
0.0000000	0.0000000	0.0000000	0.0000000
0.0000000	0.0000000	0.0000000	0.0000000
0.0000000	0.0000000	0.0000000	0.0000000
0.0000000	0.0000000	0.0000000	0.0000000
0.0000000	0.0000000	0.0000000	0.0000000
0.0000000	0.0000000	0.0000000	0.0000000
0.0000000	0.0000000	0.0000000	0.0000000
0.0000000	0.0000000	0.0000000	0.0000000
0.0000000	0.0000000	0.0000000	0.0000000
0.0000000	0.0000000	0.0000000	0.0000000
0.0000000	0.0000000	0.0000000	0.0000000
0.0000000	0.0000000	0.0000000	0.0000000
0.0000000	0.0000000	0.0000000	0.0000000
0.0000000	0.0000000	0.0000000	0.0000000
0.0000000	0.0000000	0.0000000	0.0000000

g. Injector Ring Analysis--The analysis checks the torque box and injector pad for stress and deflection under tank load with flight test g loads.

Maximum Loading of Injector Ring

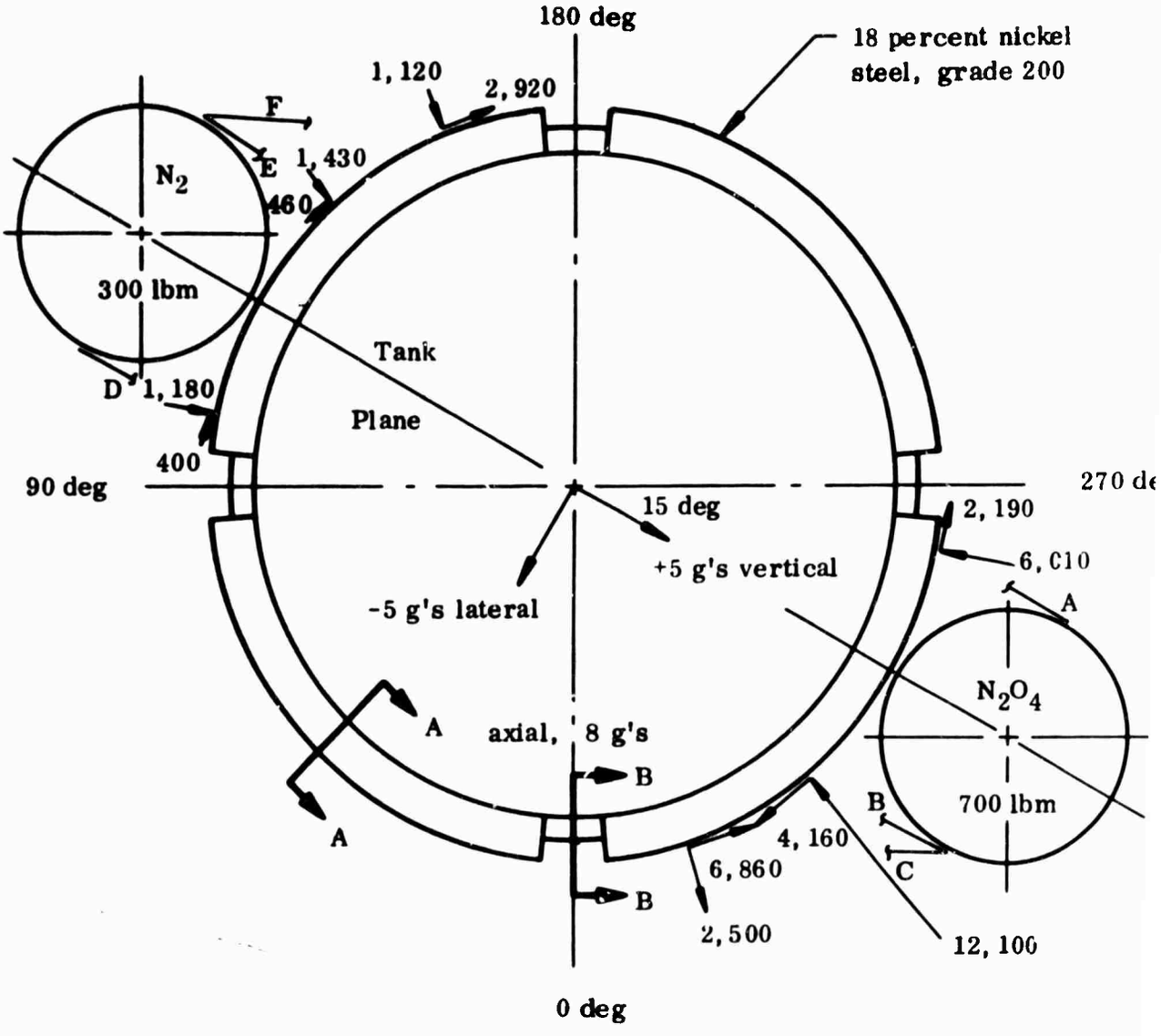

Figure 70. Torque Box Tank Loads, View Looking Forward

Assume lateral g ioads act perpendicular and parallel to tank plane.

Section A-A Properties

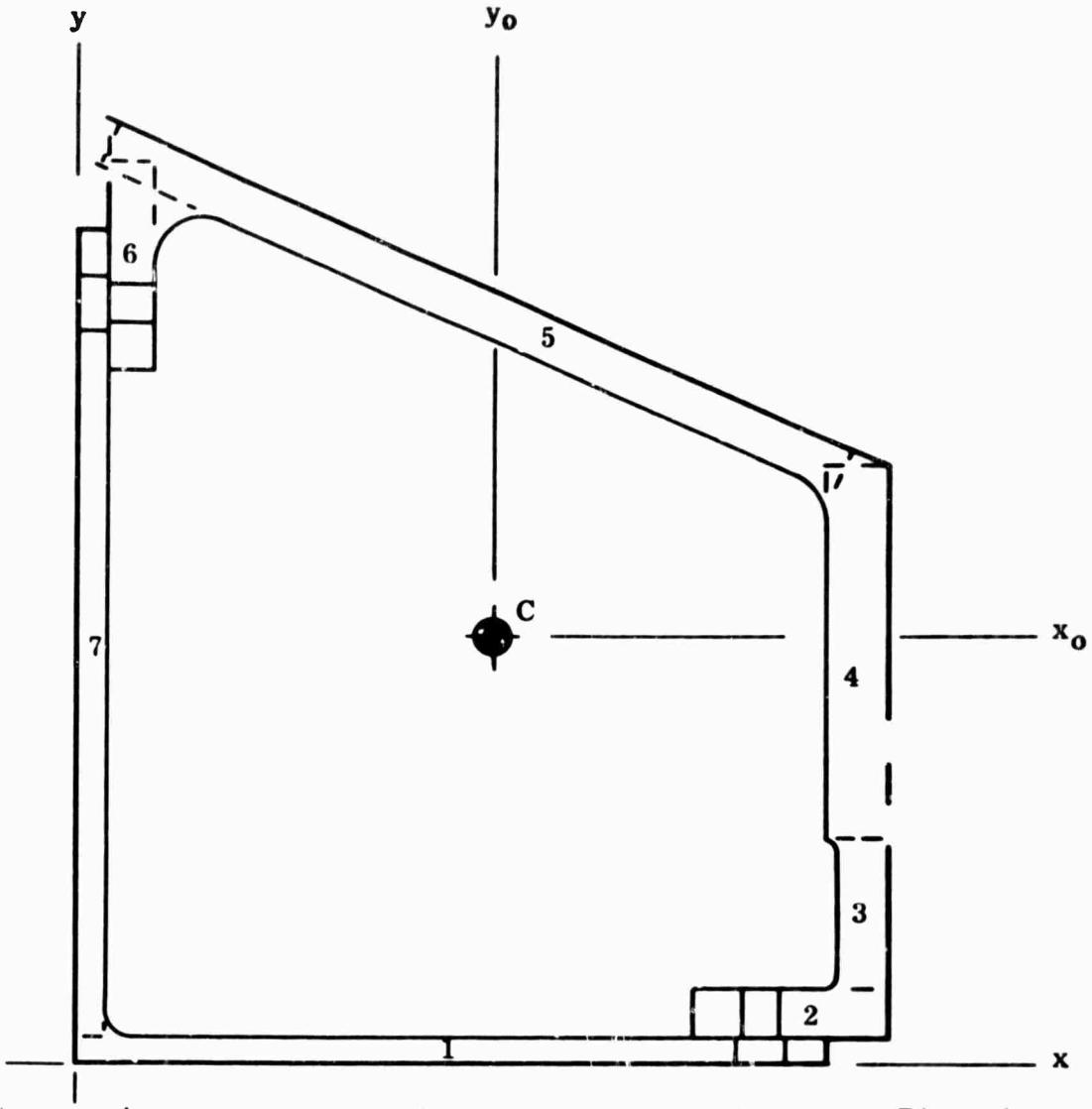

Item	Area	x	Ax	y	Ay	Dimensions
1	0.59	1.95	1.15	0.075	0.04	3.90 x 0.15
2	0.25	3.75	0.94	0.275	0.07	1.00 x 0.25
3	0.25	4.15	1.04	0.75	0.19	0.25 x 1.00
4	0.57	4.10	2.35	2.09	1.20	0.30 x 1.91
5	1.02	2.20	2.22	3.81	3.89	0.24 x 4.20
6	0.26	0.275	0.07	4.04	1.05	0.25 x 1.05
7	0.63	0.075	0.05	2.11	1.33	0.15 x 4.21
Totals	3.57		7.82		7.77	

Centroid: $\bar{x} = \frac{7.82}{3.57} = 2.19$

$\bar{y} = \frac{7.77}{3.57} = 2.18$

Item	I_o		Area	yo	yo^2	Ay_o^2
1	$bd\frac{3}{12}$	0.001	0.59	-2.11	4.45	2.62
2	$bd\frac{3}{12}$	0.001	0.25	-1.90	3.61	0.90
3	$bd\frac{3}{12}$	0.021	0.25	-1.43	2.04	0.51
4	$bd\frac{3}{12}$	0.174	0.57	-0.09	0.01	0.01
5	$bd\frac{3}{12}$	0.218	1.02	1.63	2.66	2.71
6	$bd\frac{3}{12}$	0.024	0.26	1.86	3.46	0.90
7	$bd\frac{3}{12}$	0.033	0.63	-0.07	0.005	---
Totals		1.372				7.65

$Ix_o \quad \Sigma I_o + \Sigma Ay^2 = 1.372 + 7.65 = 9.02 \text{ in.}^4$

Section Properties

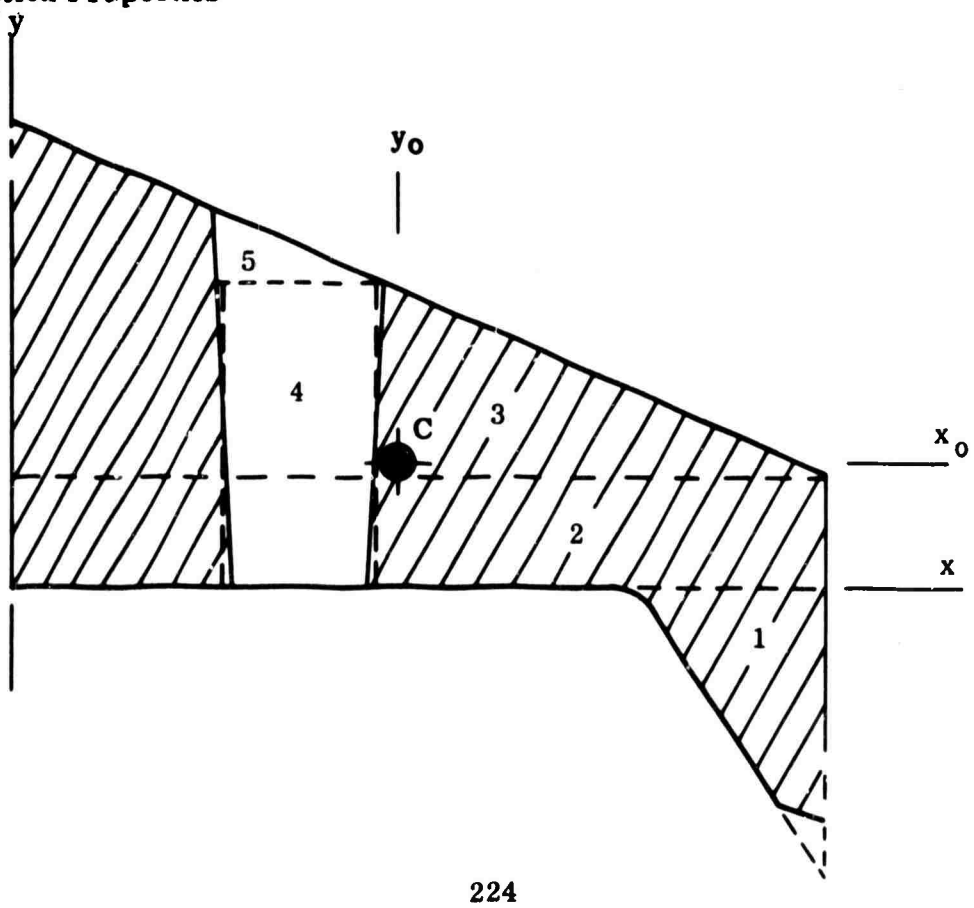

Item	Area	x	Ax	y	Ay	Dimensions
1	0.70	3.93	2.75	-0.47	-0.33	1.00 x 1.40
2	2.34	2.13	4.98	0.28	0.66	4.26 x 0.55
3	3.84	1.42	5.45	1.15	4.42	4.26 x 1.80
4	-1.23	1.50	-1.85	0.77	-0.95	0.80 x 1.54
5	-0.18	1.36	-0.25	1.65	-0.30	0.90 x 0.40
Totals	5.47		11.08		3.50	

Centroid: $\bar{x} = \frac{11.08}{5.47} = 2.02$

$\bar{y} = \frac{3.50}{5.47} = 0.64$

Moment of inertia about X_o axis through centroid:

Item	I_o		Area	y_o	y_o^2	Ay_o^2
1	$bh\frac{3}{36}$	0.076	0.70	-1.11	1.23	0.86
2	$bd\frac{3}{12}$	0.059	2.34	-0.36	0.13	0.30
3	$bh\frac{3}{36}$	0.69	3.84	0.51	0.26	1.00
4	$bd\frac{3}{12}$	-0.24	-1.23	0.13	0.02	-0.02
5	$bh\frac{3}{36}$	-0.002	-0.18	1.01	1.02	-0.18
Totals		0.58				1.96

$Ix_o = \Sigma I_o + \Sigma Ay^2 = 0.58 + 1.96 = 2.54$ in. lb

The injector ring stresses (at the minimum diameter) resulting from the strut loa. were determined as follows.

1. Maximum strut loads were determined and resolved into radial and tangential loads.
2. Using the coefficient curves [stress coefficient vs angle from applied load for a wide range of stiffness parameters (d)] in NACA Technical Note No. 929, the following components were considered around the ring.
   a. Bending moment stress for each radial load.
   b. Bending moment stress for each tangential load.
   c. Axial stress for each radial load.
   d. Axial stress for each tangential load.
   e. Shear stress for each radial load.
   f. Shear stress for each tangential load.

The relative stiffness parameter (d) was determined as follows:

$$d = \frac{KR^3}{EI} = \frac{(8.8 \times 10^6)\ (40.2)^3}{(30 \times 10^6)\ (9.0)} = 2,100$$

where R = radius of centroid (40.2 in.)

I = moment of inertia of ring cross section (9.0 in.^{4})

E = modulus of elasticity (30×10^6)

and $$K = \frac{RtG}{L} = \frac{(40.2)\ (0.15)\ (10.2 \times 10^6)}{7} = 8.8 \times 10^6$$

where R = radius of centroid (40.2 in.)

t = thickness of shell (0.15 in.)

G = shear modulus (10.2×10^6)

L = distance along shell to a section which is not distorted from a circle (7 in.)

The loads and their locations are as follows (see Figure 70).

Radial Load (lbf)	Tangential Load (lbf)	Location (deg)
+ 1,180	- 400	100
- 1,430	- 460	140
+ 1,120	+ 2,920	160
+ [illegible]010	- 2,190	280
+ 12,100	+ 4,160	320
- 2,500	- 6,860	340

+ radial load indicates direction towards ring center

- radial load indicates direction away from ring center

+ tangential load indicates clockwise direction in Figure 70

- tangential load indicates counterclockwise direction in Figure 70

The greatest stress occurs at the location of the greatest radial load (approximately 320 deg). The determination of the stress at this point will be used here as a sample calculation.

The bending moment stress, resulting from radial loads, at 320 deg was determined by adding the contribution of each radial load at this point. The contribution of each load was determined as follows:

$$\sigma_{mr} = \frac{C_{mr} P_r R C}{I} = \frac{C_{mr} P_r (40.2)(2.6)}{9.0} = 11.6\, C_{mr} P_r$$

where mr = bending moment stress resulting from radial load

P_r = radial load

R = radius of ring

C = distance from ring cross section centroid to minimum radius

I = moment of inertia of ring cross section

C_{mr} = bending moment coefficient

Bending moment stress σ_{mr} at 320 deg location resulting from radial loads:

Location of load (deg)	Angle to 320 deg location (deg)	C_{mr}	P_r	σ_{mr} (psi)
100	- 140	0	+ 1,180	0
140	+ 180	0	- 1,430	0
160	+ 160	0	+ 1,120	0
280	+ 40	- 0.023	+ 6,010	- 1,600
320	+ 0	+ 0.09[illegible]	+ 12,100	+13,200
340	- 20	- 0.013	- 2,500	+ 380
			Total =	+11,980

In a similar manner the other components of stress were determined.

Axial stress σ_{ar} at 320 deg resulting from radial loads:

$$\sigma_{ar} = \frac{C_{ar} P_r}{\text{Area}} = 0.28\, C_{ar} P_r$$

Total = -3,610 psi
(comp

Bending moment stress σ_{mt} at 320 deg resulting from tangential loads:

$$\sigma_{mt} = \frac{C_{mt} P_t R C}{I} = 11.6\, C_{mt} P_t$$

Total = -750 psi
(compre

Axial stress σ_{at} at 320 deg resulting from tangential loads:

$$\sigma_{at} = \frac{C_{at} P_t}{\text{Area}} = 0.28\, C_{at} P_t$$

Total = + 800 psi (tension)
- 360 psi (compression)

Summation of stresses from radial loads = + 11,980 - 3,610 = + 8,370 psi (at 320 deg). Stresses resulting from tangential loads are small.

Shear stress σ_{sr} at 320 deg resulting from radial loads:

$$\sigma_{sr} = \frac{C_{sr} P_r}{\text{Area}} = 0.28\, C_{sr} P_r$$

Total = + 1,680 psi
- 1,720 psi

Shear stress σ_{st} at 320 deg resulting from tangential loads:

$$\sigma_{st} = \frac{C_{st} P_t}{\text{Area}} = 0.28\, C_{st} P_t$$

Total = - 80 psi

Summation of shear stresses at 320 deg = +1,600 psi
-1,800 psi

Discontinuities in the ring occur near the 90 deg, 180 deg, 270 deg, and 360 deg locations. See Figure 70 . It is assumed that little error is introduced by using a constant ring stiffness parameter (d) around the ring. All the indicated loads are applied on the cross section used in determining this stiffness parameter (d). The stresses in these four short 10 deg sections were determined by first assuming the ring to be of uniform cross section and then applying an appropriate correction factor to compensate for changes in R, C, I and A.

Figure 71 is a plot of the tension and compression at the ring minimum diameter resulting from the bending moments and axial loads induced in the ring by the six radial loads. The maximum tension is 8,370 psi at 320 deg and the maximum compression is 8,000 psi at 355 deg.

The other components are small; when they are all added to the values indicated in Figure 71 the maximum tension is still at 320 deg but increased slightly to 8,420 psi. The maximum compression is still at 355 deg but reduced to 7,000 psi. Shear stresses are small at all points.

Factor of Safety

Material - Injector Torque Box

F_{TU} = 20,000 psi

T_{TY} = 200,000 psi

F_{SU} = 125,000 psi

σ_{Hoop} = 8,370 psi at 320 deg in Section A-A (Figure 70).

$$F.S. = \frac{200,000}{8,370} = + \text{high}$$

σ_{Shear} = -1,720 - 80 = - 1,800 psi at 320 deg in Section A-A (Figure

$$F.S. = \frac{125,000}{1,800} = + \text{high}$$

Deflection

Assume ring supported by conical shell with the deflection on one side of ring not affecting the other side (Reference 19).

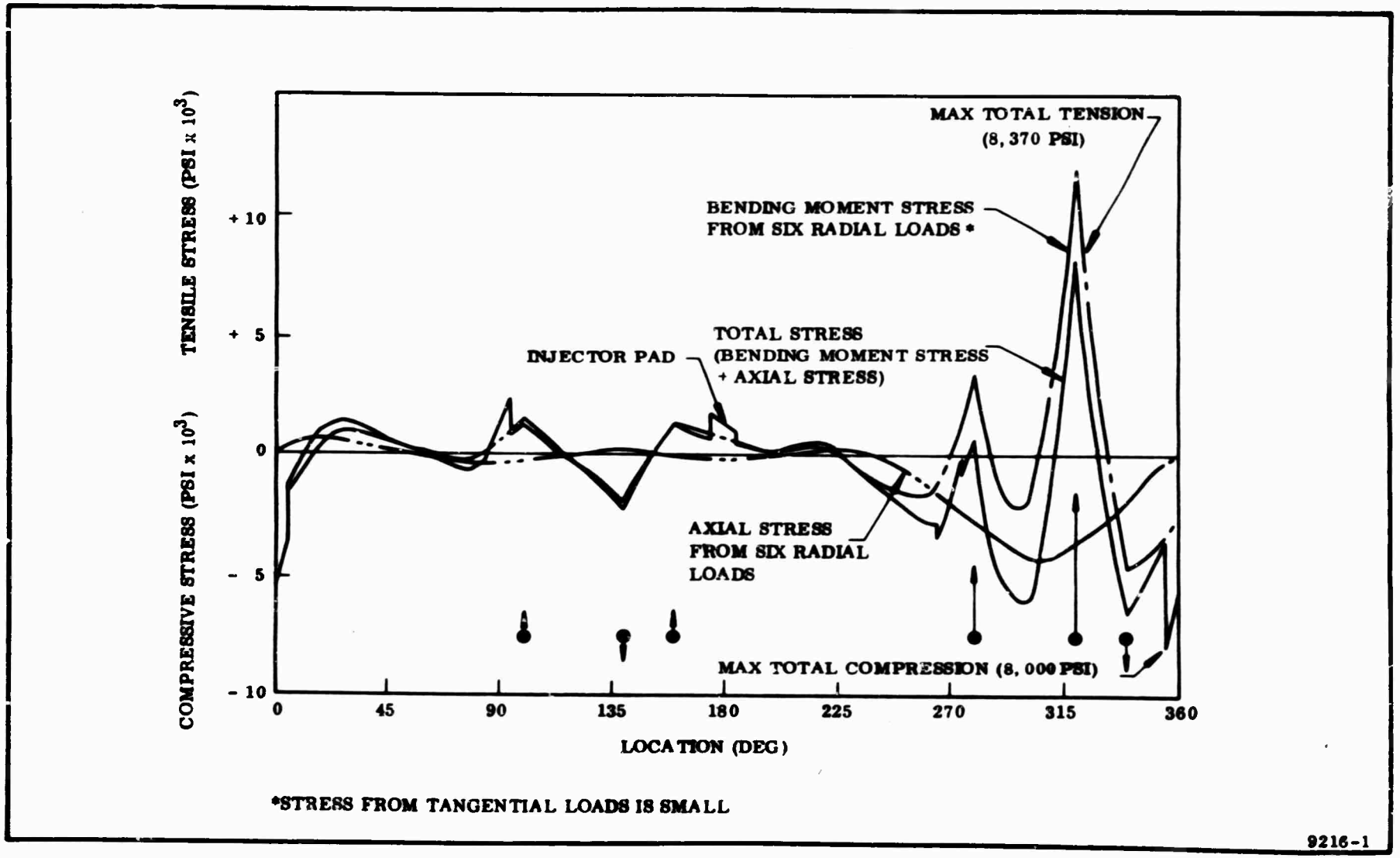

Figure 71. Total Stress in Injector Ring from Strut Radial Loads vs Location

Radial Load

$$K = \frac{R\,t\,L}{L} = 8.8 \times 10^6$$

$$d = \frac{KR^3}{EI} = 2,100$$

$$\Delta R = C_{\Delta R} \frac{Pr}{K} = \frac{12,100}{8.80\ (10^6)}\ (8) = 0.011 \text{ in.}$$

Tangential Load Negligible Deflection

Moment

$$\text{At 0 deg at } \Delta R = C \frac{M}{KR} = 0 \quad \frac{53,700}{8.8\ (10^6)\ (40.20)} = 0$$

Total Deflection

$$\delta \text{ Total} = 0.011 +$$

$$\frac{\Delta R}{R} = \frac{0.016}{40.2\ (100)} = 0.027 \text{ percent}$$

Maximum Shear Stress in Shell Adjacent to Ring

Radial Load = 12,000 lb

d = 20,300 (Reference 19, Figure 14)

$$q = Cqr \frac{Pr}{R} = \frac{4.35\ (12,100)}{40.62} = 1,295 \text{ lb/in.}$$

Maximum at 18 deg from load application

$$\sigma_s = \frac{1,295}{0.15} = 8,620 \text{ psi}$$

Material grade 200, 18 percent nickel ste

σ_s allowable = 120,000

$$\text{F.S.} = \frac{120,000}{8,620} = + \text{ high}$$

h. Exit Cone Attachment Analysis--The major attachments are analyzed for tension shear loads in the connector and tension bearing and shear in the structure.

The case-nozzle flange-exit cone shell, injector torque box, diffuser and motor LITVC attachments are examined.

(1) Torque Box Shear Screws--

Maximum Shear in Bolts (Torque Box)

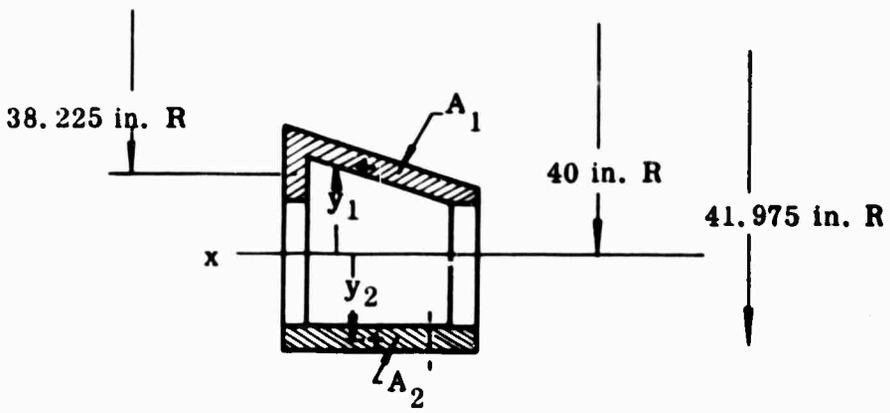

$I_x = 9.02 \text{ in.}^4$

Area 1 $= 1.46 \text{ in.}^2$

$\bar{y}_1 = 1.80 \text{ in.}$

$Q = A_1 \bar{y}_1 = 263 \text{ in.}^3$

Area 2 $= 0.5625 \text{ in.}^2$

$\bar{y}_2 = 1.97 \text{ in.}$

$Q = A_2 \bar{y}_2 = 1.11 \text{ in.}^3$

Maximum Shear Stress at Area 1

$$q = \frac{VQ}{I} = \frac{\frac{P}{2}(2.63)}{9.02} = 0.146\ P$$

$p = 12,100$ lb

$q = 1,770$ lb/in.

Bolts: 3/16 dia, 1.0 in. bolt spacing, $A_b = 0.024$ in.^{2}

$$\tau_{bolt} = \frac{q \times \text{bolt spacing}}{2\ A_b} = \frac{(1,770)\ (1.0)}{2\ (0.024)} = 36,900 \text{ psi}$$

$$\text{F.S.} = \frac{120,000\ (0.6)}{36,900} = + \frac{72,000}{36,900} = + 1.95$$

(2) Exit Cone Attachment--180 bolts, 5/16 in. 24 UNF 3A.

Loads	Flight	Static
Axial Load	= +30,550 lb	+65,950 lb
Transverse Shear Load	= +36,600 lb	28,130 lb
Bending Moment	= +1,030,000 in. lb	764,000 in. lb

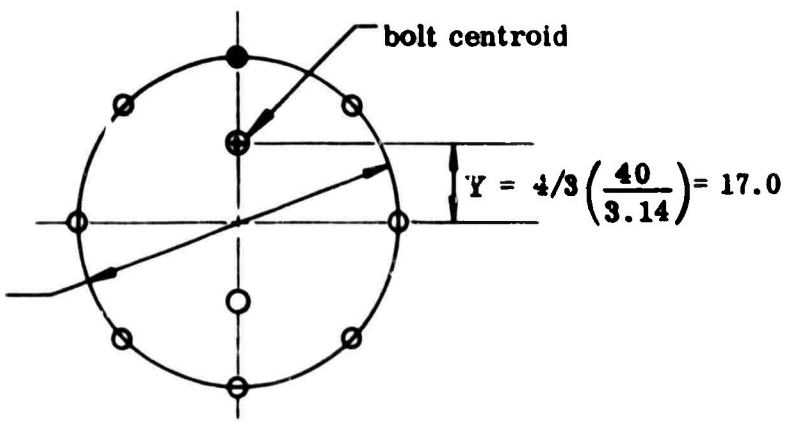

Section Properties of Bolts

$$I_{Bolts} = AD^2 = 0.07\,(180)\,(17^2)$$

$$= 290\,(12.6)$$

$$= 3,660$$

Static Test Condition

Avg Load/Bolt

Bending Load

$$\text{Bolt Load} = \frac{764,000\,(17)}{3,660}\,(0.07) = \frac{MC}{I}\,(A) = 249 \text{ lb shear}$$

Transverse
Shear Load

$$\text{Bolt Load} = \frac{28,130 \text{ lb}}{90 \text{ Bolts}} = 313 \text{ lb tension - one side}$$

Axial Load

$$\text{Bolt Load} = \frac{69,950}{180} = 388 \text{ lb shear}$$

Pressure Leak Load at Middle Exit Cone Joint

$$\text{Bolt Load} = \pi\,(R_o^2 - R_i^2)8.5 = (0.148)\,(58^2 - 32^2) = 346 \text{ lb shear}$$

Bolt Load

$$\text{Bolt Load}_{Shear} = 249 + 388 + 346 = 983 \text{ lb}$$

Bolt Spacing

$$S = \frac{2\pi R}{\text{no. of bolts}} = \frac{6.28\,(40)}{180} = 1.39 \text{ in. spacing}$$

Satisfactory

$$\frac{S}{\text{Bolt Dia}} = \frac{1.39}{0.3129} = 4.45 \text{ dia spacing}$$

(3) Sandwich Joint

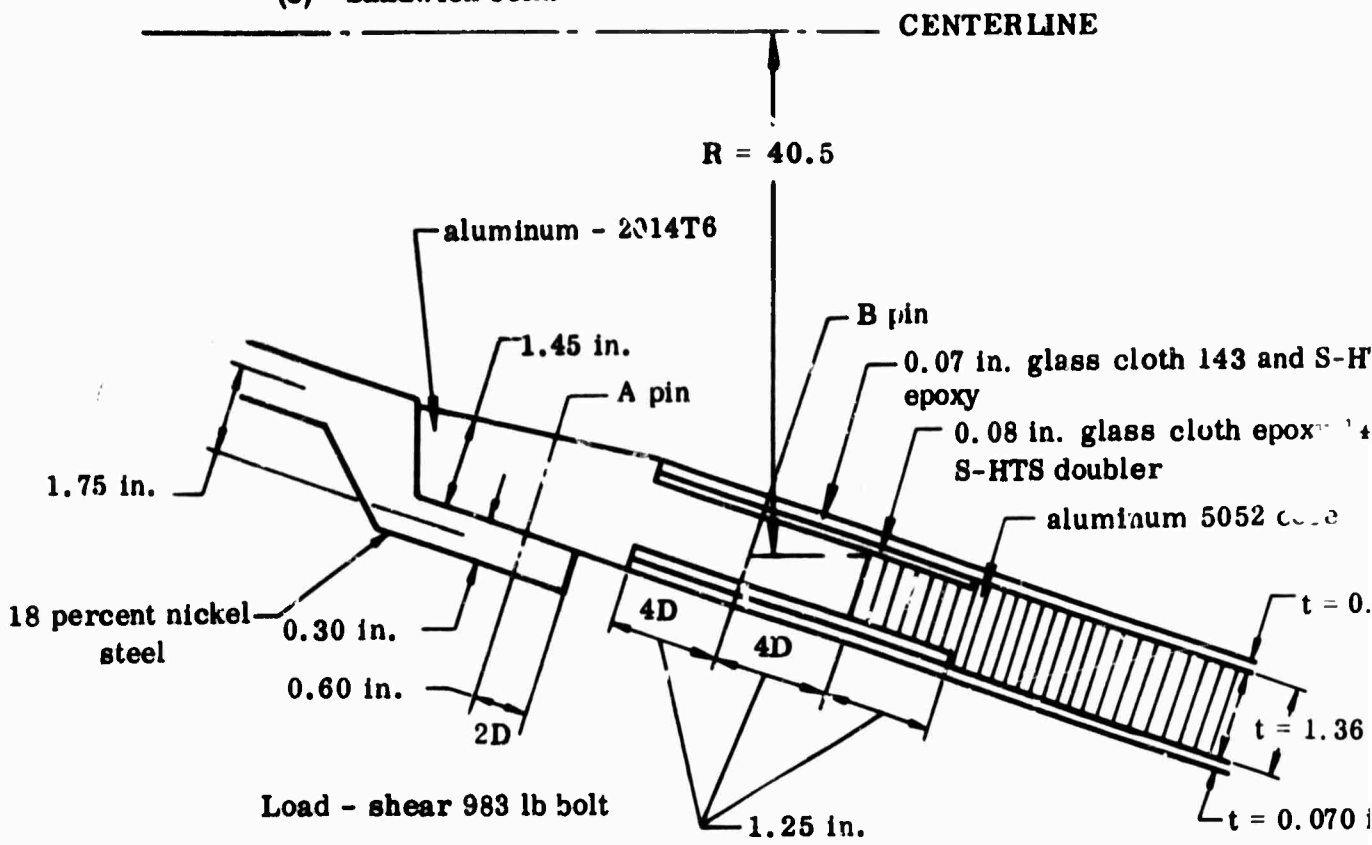

Adhesive bond = 2,000 lb/in.

143 glass cloth epoxy double and face sheet

Properties (Reference 12)

Shear = 11,600 psi
Bearing = 33,000 psi
Tension = 33,000 psi

Sandwich Face Sheets

Doubler Effective

Load Carry into Doubler by 1.25 in. of bond

$$p = 1.25\ (2,000)\ 25\ \text{deg} = 5,000\ \text{lb}$$

$$\text{F.S.} = \frac{5,000}{983} = +5.09$$

Glass Cloth Doubler and Face Sheet Stress

Edge Distance = 1.20 in. use 0.90 in.

$$\text{Shear Stress} = \frac{P}{A} = \frac{983}{2(0.40)\ (0.90)} = 1,365\ \text{psi}$$

$$\text{F.S.} = \frac{11,600}{1,365} = \text{high}$$

$$\text{Bearing Stress} = \frac{P}{A} = \frac{983}{0.40\ (0.3125)} = 7,880 \text{ psi} \quad \text{F.S.} = \frac{33,000}{7,880} = +5.7$$

$$\text{Tension Stress} = \frac{P}{A} = \frac{983(180)}{2\pi Rt\left(\frac{198}{254.0}\right)} = \frac{177,000}{6.28\ (40.5)\ (0.40)\ (0.78)}$$

$$= 2,240 \text{ psi} \qquad \text{F.S.} = \frac{33,000}{2,240} = +\text{high}$$

(a) 181 Glass Cloth Epoxy End Block to Glass Cloth Doubler and Face Sheet Attachment

$$t_1 = 1.50 - 0.30 - 0.03 = 1.14$$
(Glass) (Bond)

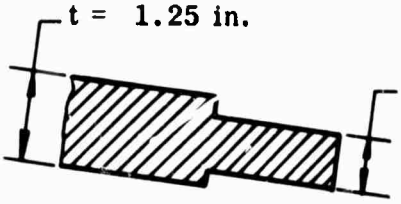

181 Glass Cloth Epoxy Properties (Reference 12)

Shear	13,800 psi
Bearing	33,000 psi
Tensile	33,000 psi

$$\text{Shear Stress} = \frac{P}{A} = \frac{983}{2(1.14)\ (1.10)} = 195 \text{ psi} \qquad \text{F.S.} = \frac{13,800}{195} = +\text{high}$$

$$\text{Bearing Stress} = \frac{P}{A} = \frac{983}{Dt} = \frac{983}{0.312\ (1.14)} = 1,436 \text{ psi} \qquad \text{F.S.} = \frac{33,000}{1,436} = +\text{high}$$

$$\text{Tension Stress} = \frac{P}{A} = \frac{983\ (180)}{2\pi Rt\left(\frac{198.0}{254.0}\right)} = \frac{198,000}{6.28\ (40.5)\left(\frac{198}{254}\right)\ (1.14)}$$

$$= 783 \text{ psi} \qquad \text{F.S.} = \frac{33,000}{783} = +\text{ high}$$

(b) Glass Cloth to Steel Connection--Ok by inspection

Steel Support for Exit Cone 18 percent Nickel Steel

Load = 983 lb/bolt R = 39.75 in.

$$\text{Shear Stress} = \frac{P}{A} = \frac{983}{2(0.45)\ 0.30} = 3,650 \text{ psi} \qquad \text{F.S.} = \frac{120,000}{3,650} = +\text{high}$$

$$\text{Bearing Stress} = \frac{P}{A} = \frac{983}{Dt} = \frac{983}{0.312\ (0.30)} = 10,500 \text{ psi}$$

$$\text{F.S.} = \frac{200,000}{10,500} =$$

$$\text{Tension Stress} = \frac{P}{A} = \frac{983\ (180)}{2\pi Rt\left(\frac{198}{254}\right)} = \frac{983\ (180)}{6.28\ (39.75)\ (0.3)\ 0.78} = 3,030$$

$$\text{F.S.} = \frac{200,000}{3,030} =$$

18 Percent Nickel Steel Properties

Tensile = 200,000 psi

Shear = 120,000 psi

Bearing = 200.000 psi

Steel Discontinuity Stress at Exit Cone Joint

Load = 983 lb/bolt Assume 983 lb/in.

Local Bending Moment = 983 (1.75) = 1,720 in. lb

$$\sigma_{long.} = \frac{P}{A} \pm \frac{6M}{bt^2} = \frac{983}{1\ (0.30)} \pm \frac{1,720(6)}{1\ (0.30)^2}$$

$$= +3,280 \text{ psi} \pm 115,000$$

$$\sigma_{long.} = \begin{matrix} +118,250 \\ -111,720 \end{matrix}$$

$$\text{F.S.} = \frac{200,000}{118,280} = +$$

5/16 In. Pin B Attachment-Sandwich to Glass Cloth End Ring

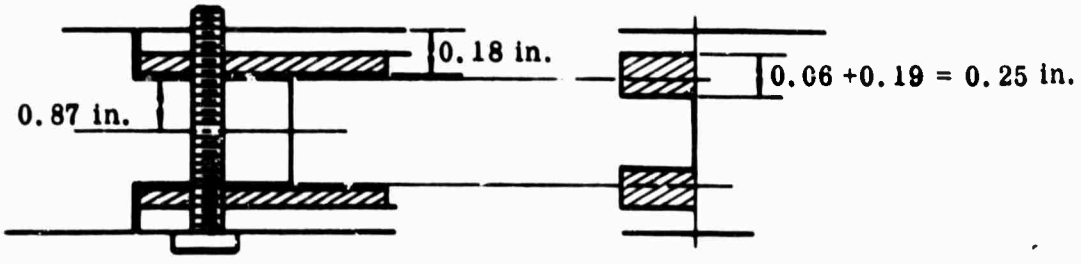

Material: Steel Pin-125,000 psi ultimate tensile strength

Shear = 491 lb per face sheet

Moment = 491 (0.25) = 123 in. lb/in.

$$\sigma_{Bending} = \frac{MC}{I} = \frac{123\ (0.156)}{0.000468} = 41,000 \text{ psi}$$

$$F.S. = \frac{100,000}{41,000} = +2.44$$

$$\sigma_{Shear} = \frac{P}{A} = \frac{491}{0.076} = 647 \text{ psi} \qquad F.S. = \frac{75,000}{647} = + \text{high}$$

5/16 In. Pin A Attachment-181 Glass Cloth Epoxy End Block to Steel Shell

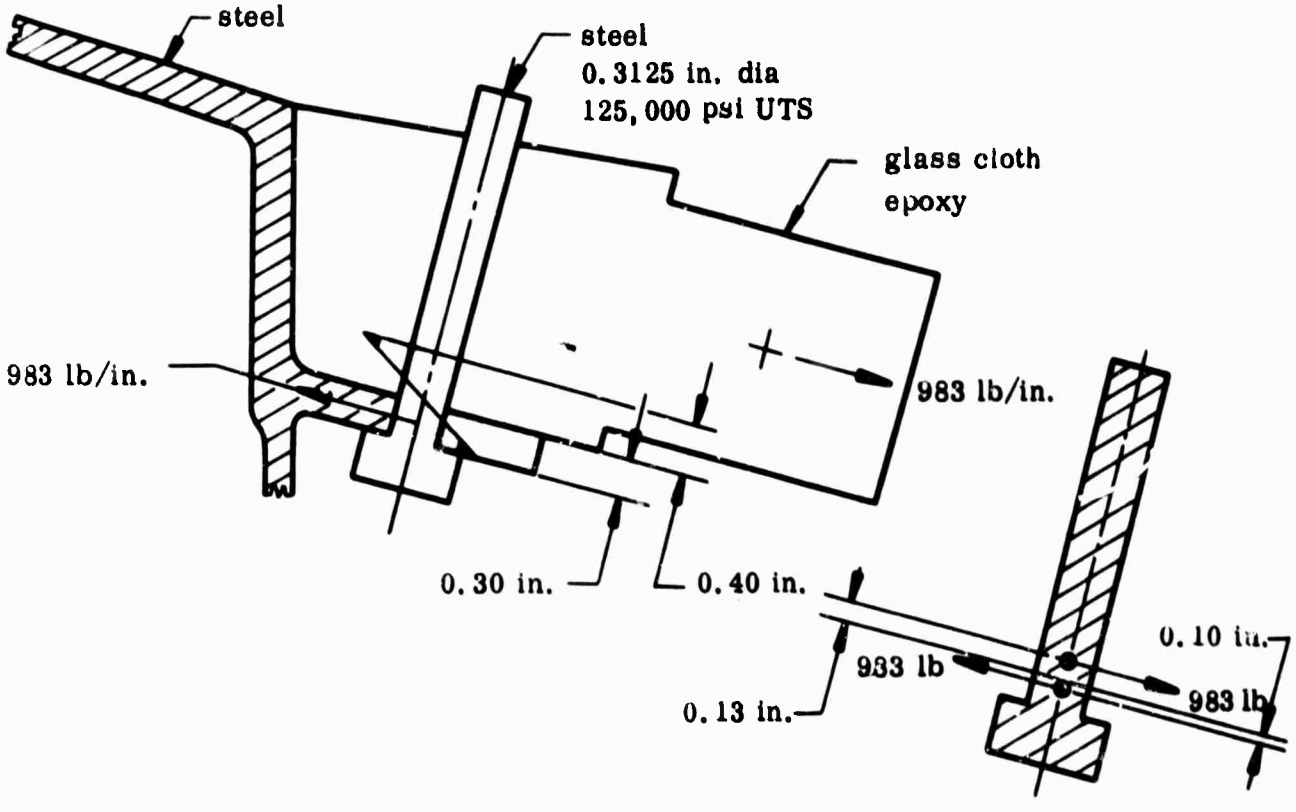

The transfer of the load/in. from the sandwich through the glass end block is accompanied by a small bending moment at the glass to steel interface.

Pin Stress

$$\sigma_{Bending} = \frac{MC}{I} = \frac{983\ (0.23)\ (0.156)}{0.00046} = 76,500 \text{ psi}$$

$$F.S. = \frac{100,000}{76,500} = +1.31$$

$$\sigma_{Shear} = \frac{P}{A} = \frac{983}{0.076} = 12,950 \text{ psi}$$

$$F.S. = \frac{75,000}{12,950} = +5.78$$

Glass Cloth Stress

$$\sigma_{Bearing} = \frac{P}{A} = \frac{983}{(0.312)\ (0.40)} = 7,880 \text{ psi}$$

$$F.S. = \frac{33,000}{7,880} = +4.18$$

(c) Exit Cone Liner Attachment

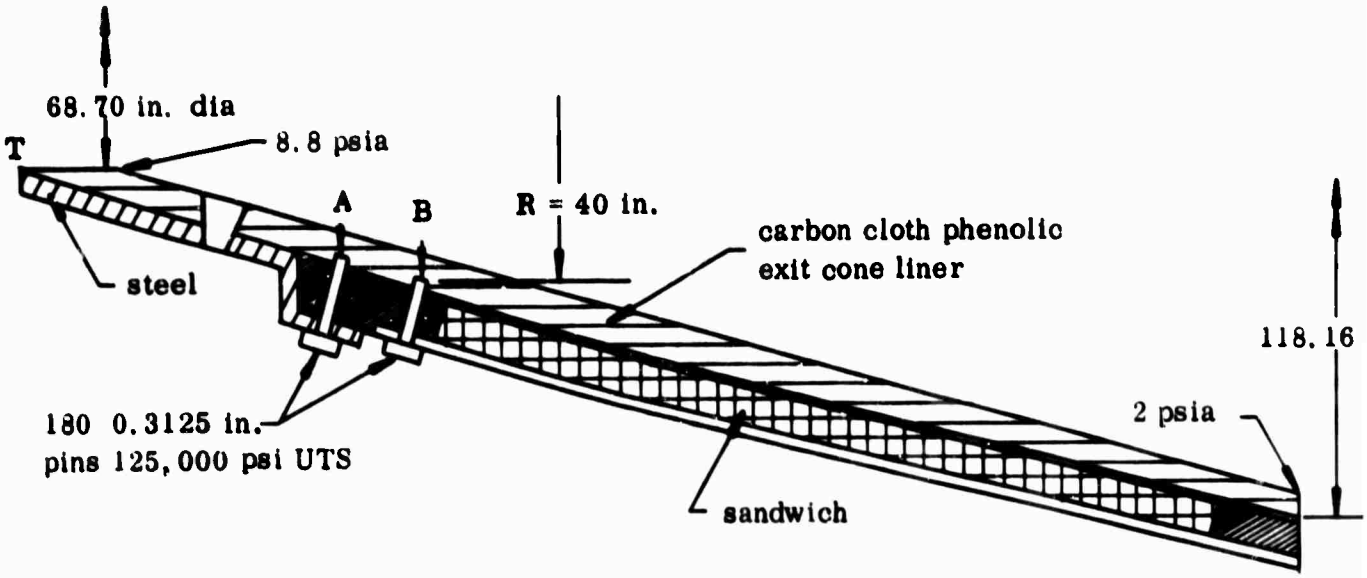

To insure retention of the exit cone liner, three lines of pins penetrate 0.250 in. into the carbon cloth to hold the T-U surface against gas leakage pressure of 8.8 psia.

Blow Out Load

$$\text{Axial Load} = \pi \left(R_o^2 - R_i^2\right) p = 3.14 \left(58.3^2 - 35.435^2\right) 8.8$$

$$= 27.6 \,(3,400 - 1,260) = 59,000 \text{ lb}$$

Neglect blow in load from internal wall pressure.

Pin Loads

The distribution of the blow out load is based on pin diameters.

$$59,000 = p\,(360) \quad \text{(forward end pins)}$$

$$360p = 59,000$$

$$P = 164 \text{ lb}$$

Pin Stress - Row B

Material: Steel, 125,000 ultimate tensile strength

$$\sigma_{\text{Bending}} = \pm \frac{MC}{I} = \pm \frac{78.6\,(0.156)}{0.000468}$$

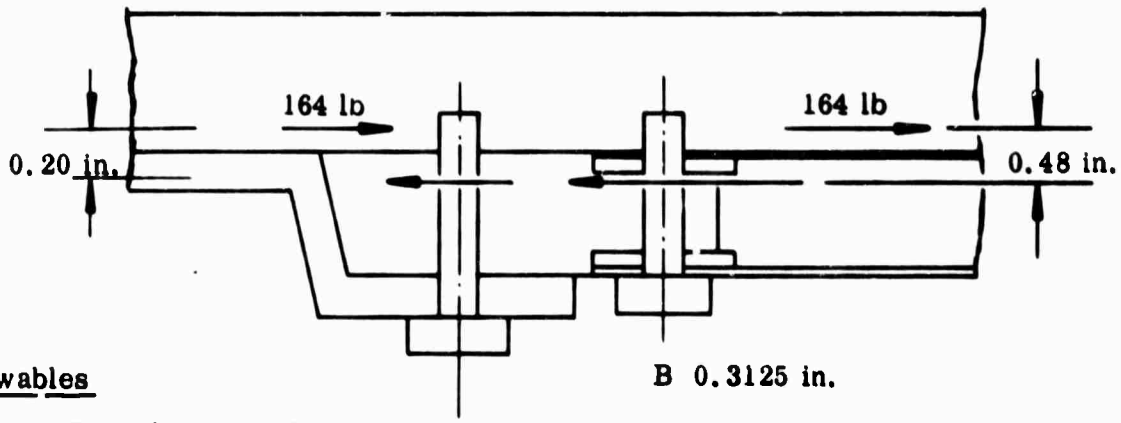

Allowables

Ultimate Tensile	=	125,000 psi
Yield	=	100,000 psi
Shear	=	75,000 psi

$$M = 164\ (0.48) = 78.6$$

$$I = 0.785\ R^4 = 0.785\ (0.156^4) = 0.785\ (0.00059)$$

$$= 0.000468$$

$$\sigma_{Bending} = 26,200 \text{ psi} \qquad F.S. = \frac{100,000}{26,200} = +3.82$$

$$\sigma_{Shear} = \frac{P}{A} = \frac{164}{\pi R^2} = \frac{164}{3.14\ (0.152^2)} = 2,260 \text{ psi}$$

$$F.S. = \frac{75,000}{2,260} = + \text{high}$$

Liner Stress - Row B

Material: Carbon Cloth Phenolic
Material Properties at
Room Temperature
Bearing Stress = 10,000 psi
Shear Stress = 10,000 psi
Tension Stress = 10,000 psi

$$\sigma_{Bearing} = \frac{P}{A} = \frac{164}{\underset{(D)}{(0.312)}\ \underset{(L)}{(0.300)}} = 1,750 \text{ psi}$$

$$F.S._{crit} = \frac{10,000}{1,750} = + 5.72$$

$$\sigma_{Shear} = \frac{P}{A} = \frac{164}{2\ \underset{(L)}{(0.150)}\ \underset{(e)}{(0.310)}} = 1,750 \text{ psi}$$

$$\sigma_{Tension} = \frac{P}{A} = \frac{180\ (164)}{[2\pi R - 180\ (0.312)]t} = \frac{29,500}{(250 - 0.56)\ (1)} = 152 \text{ psi}$$

(4) Case to Nozzle Attachment--3/4 in. 16 UNF Bolt. Ultimate tensile strength = 220,000 psi, yield = 200,000 psi, shear = 132,000 psi.

The discontinuity stress at the bolt is 134,000 psi. With tank struts RX, RX', AF, A'F' attached to the flange, an additional load is applied locally to the bolts (Reference Section IV-3h(7).

$$\text{Tension} = 8,720 \text{ lb}$$

$$\text{Shear} = 3,880 \text{ lb}$$

$$\sigma_{\text{Tension}} = 134,000 + \frac{8,720}{0.4418} = 153,700 \text{ psi} \quad R_t = \frac{153,700}{200,000} = 0.767$$

$$\sigma_{\text{Shear}} = \frac{3,880}{0.4418} = 8,780 \text{ psi} \quad R_s = \frac{8,780}{132,000} = 0.066$$

$$U = \frac{0.767}{0.990} = 0.775 \qquad \text{F.S.} = \frac{1}{U} = +1.29$$

(Reference 20 Figure 1535)

(5) Diffuser Attachment--Not Available.

(6) Nitrogen Tetroxide Tank Attachments--The nitrogen tetroxide tank is supported by four brackets on the injector ring and two brackets on the nozzle flange. The four basic brackets are analyzed for bending and axial loads in the plates with bearing shear and axial load in the fittings.

The bracket bolts sustain axial and shear loads and resist bending moments in addition to the standard loads at the injector ring and flange.

(a) Strut AF, A'F' Attachment at Nozzle Flange

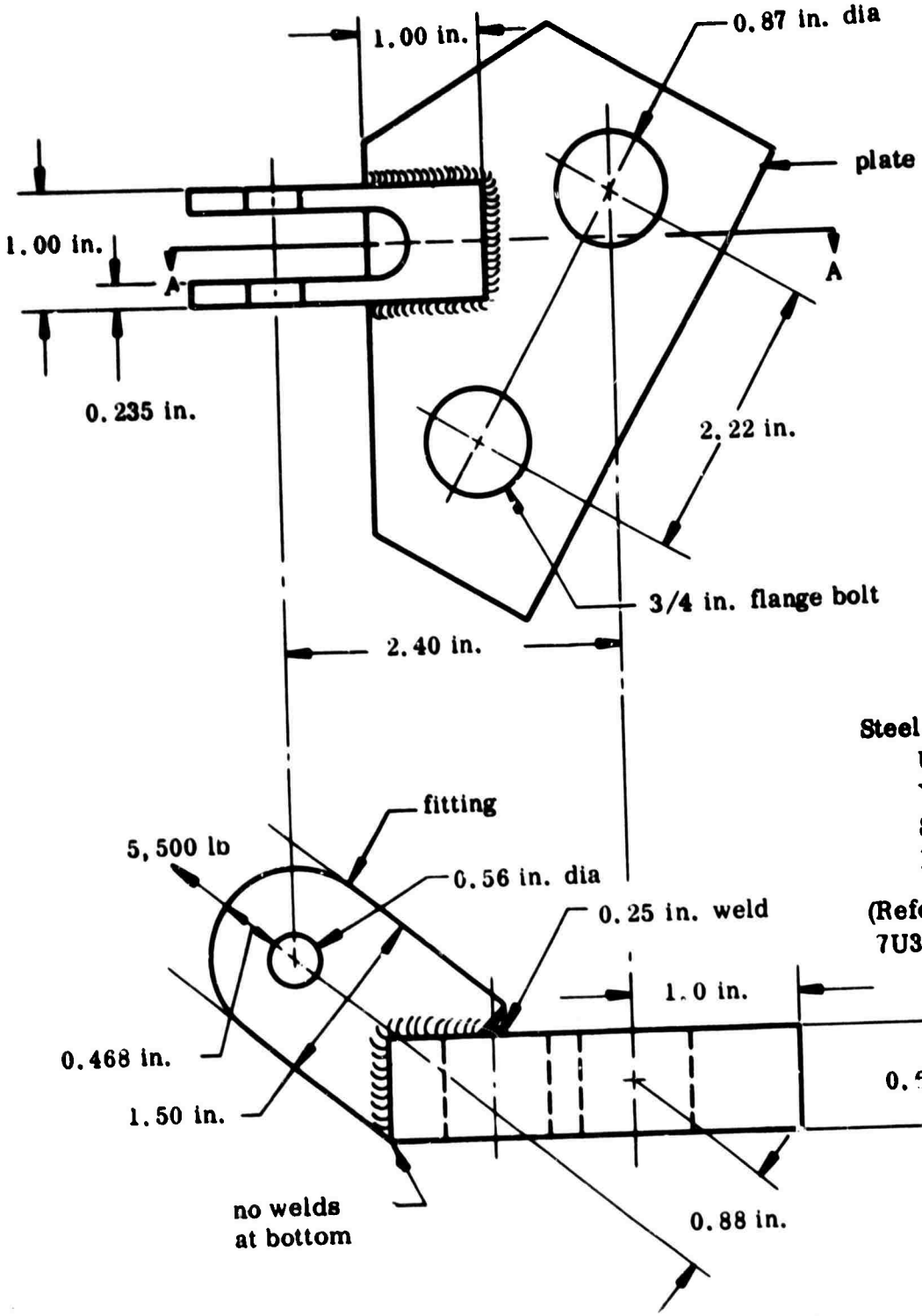

Steel: 4,130 normalized
Ultimate = 90,000 p
Yield = 70,000 p
Shear = 36,000 p
Bearing = 70,000 p

(Reference Thiokol Dwg 7U37801 and 7U37785)

F_{su} = 32,000 psi (Reference 20, p 55)

Welds

$$\text{Weld Line } \sigma = \frac{5,500 \text{ lb}}{4.25\ (0.707)\ (0.25)}$$

$$\sigma = \frac{P}{Lt}$$

$$\sigma_{\text{Shear}} = 7,320 \text{ psi} \qquad \text{F.S.} = \frac{32,000}{7,320} = +4.37$$

Clevis Plate Stress

$$\sigma_{\text{Axial}} = \frac{5,500/2}{1.50\ (0.235)} = 7,830 \text{ psi}$$

$$\text{F.S.} = \frac{70,000}{7,830} = + \text{ high}$$

Support Plate Bending Stress-Use 2 in. Beam Width

$$\sigma_{\text{Stress}} = \frac{P}{A} \pm \frac{MC}{I} = \frac{5,500}{2.0\ (0.625)} \pm \frac{0.88\ (5,500)\ (6)}{2\ (0.625^2)}$$

$$= +4,400 \pm 37,100 = +41,500 \text{ psi}$$

$$-32,700 \text{ psi}$$

$$\text{F.S.} = \frac{70,000}{41,500} = +1.69$$

Plate Stress at Flange Bolt Hole

$$\sigma_{\text{Shear}} = 3,880/2\ (0.50)\ (0.625) = 6,200 \text{ psi}$$

$$\text{F.S.} = \frac{36,000}{6,200} = +5.8$$

$$\sigma_{\text{Bearing}} = 3,880/0.75\ (0.625) = 8,280 \text{ psi}$$

$$\text{F.S.} = \frac{70,000}{8,280} = +8.5$$

Flange Bolt Load-Assume Load is All in One Bolt

$$\text{Shear} = 3,880 \text{ lb}$$

$$\text{Tension} = 3,880 + \frac{5,500\ (0.88)}{1.00} = +\ 3,880 + 4,840 = +\ 8,720 \text{ lb}$$

(Reference Section D3h (4) for factor of safety

Fitting Stress

Bolts and tension, shear, and bearing stress checked out by structures in tank-strut analysis.

$$\sigma_{\text{Bearing}} = \frac{2,750}{0.56\ (0.235)} = 20,900 \text{ psi}$$

$$\text{F.S.} = \frac{70,000}{20,900} = +\ 3.34$$

$$\sigma_{\text{Shear}} = \frac{2,750}{2\ (0.47)\ (0.235)} = 12,450 \text{ psi}$$

$$\text{F.S.} = \frac{36,000}{12,450} = +\ 2.90$$

$$\sigma_{\text{Tension}} = \frac{2,750}{0.90\ (0.235)} = 13,000 \text{ psi}$$

$$\text{F.S.} = \frac{70,000}{13,000} = +\ 5.40$$

(b) Strut AD, Attachment at Injector Torque Box--

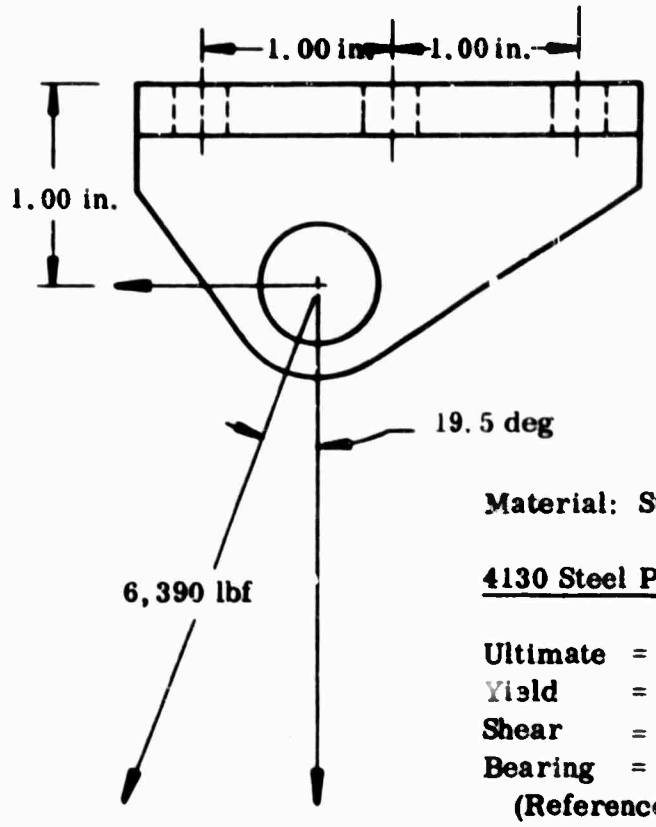

Material: Steel, 4130 normalized

4130 Steel Properties (psi)

Ultimate = 90,000
Yield = 70,000
Shear = 36,000
Bearing = 70,000
(Reference Dwg 7U37784)

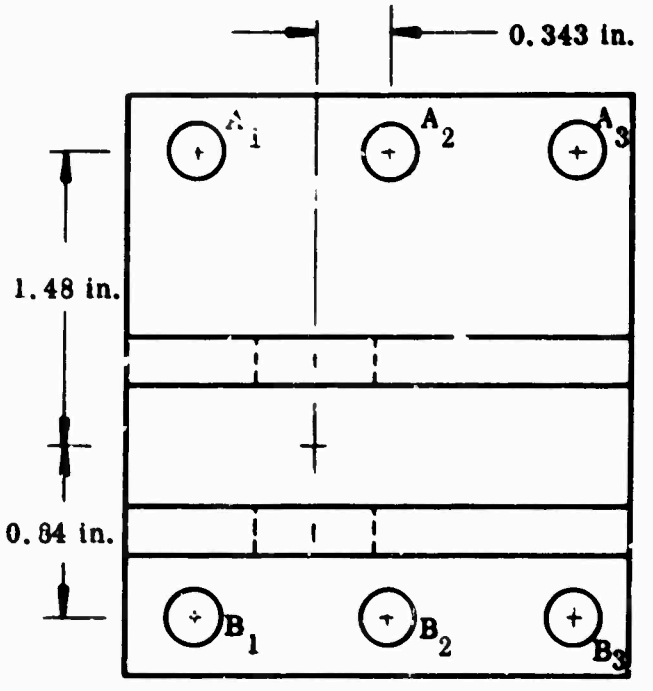

Assuming two brackets:

Bracket No. 1 with bolts A_1, A_2, and A_3 has applied load $\frac{0.84}{0.84 + 1.48}$ of total applied load.

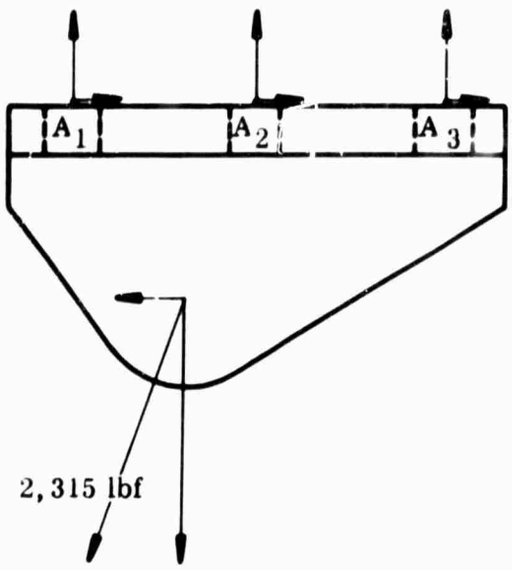

$T_H = 772$

$T_V = 2,180$

$\Sigma Fx = 0$

$$A_1x + A_2x + A_3x = 772$$

$$A_1x = A_2x = A_3x = \frac{772}{3} = 257 \text{ lbf shear}$$

$\Sigma Fy = 0$

$$(1)\quad A_1y + A_2y + A_3y = 2,180$$

$\Sigma M_{A_3} = 0$

$$(2)\quad 2A_1y + A_2y = -772 + (1.343)(2,180)$$

Considering the bolts elongated in tension:

$$A_1y - A_2y - A_2y - A_3y$$

(3) $A_1y + A_3y = 2\,A_2y$

(1) and (3) $A_2y = 727$ lbf tension

(1) and (3) and (2) $A_1y = 716$ lbf tension

Substituting in (1): $A_3y = 737$ lbf tension

Bracket No. 2 with bolts B_1, B_2, and B_3 has applied load $\frac{1.48}{0.84 + 1.48}$ of total applied load.

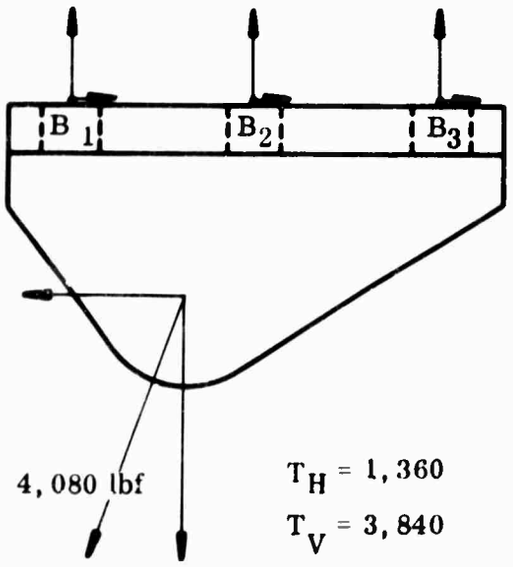

Bracket No. 2 is the same as Bracket No. 1 with all forces multiplied by a factor of $\frac{1.48}{0.84}$.

$\therefore$ $B_1x = B_2x = B_3x = (1.76)\,(257) = 452$ lbf

$B_1y = (1.76)\,(716) = 1,260$ lbf

$B_2y = (1.76)\,(727) = 1,280$ lbf

$B_3y = (1.76)\,(737) = 1,300$ lbf

Summary of Bolt Loads

Bolts used: 5/16 in. Huck Lockbolts with ultimate tensile strength of 7, 190 lbf and ultimate shear strength of 3, 250 lbf.

With member in tension (6, 390 lbf) Max Stress (lbf)			With member in compression (6, 390 lbf) Max Stress (lbf)		
Bolts	Tension	Shear	Bolts	Compression	Shear
A_1	716	257	A_1	716	257
A_2	727	257	A_2	727	257
A_3	737	257	A_3	737	257
B_1	1260	452	B_1	1260	452
B_2	1280	452	B_2	1280	452
B_3	1300	452	B_3	1300	452

Critical Bolt Stress

$$R_2 = R_T = R_{Tension} = \frac{1,300}{3,250} = 0.400$$

$$R_{Shear} = \frac{452}{7,290} = 0.062$$

$$U = \frac{0.400}{0.975} = 0.41$$

Use $R_T + R_S^{10} = 1.0$ curve (Reference 20, Figure 1535)

$$F.S. = \frac{1}{U} = +2.44$$

Bracket Stress Analysis-Not Available

(c) Strut A'D' Attachment at Injector Torque Box--

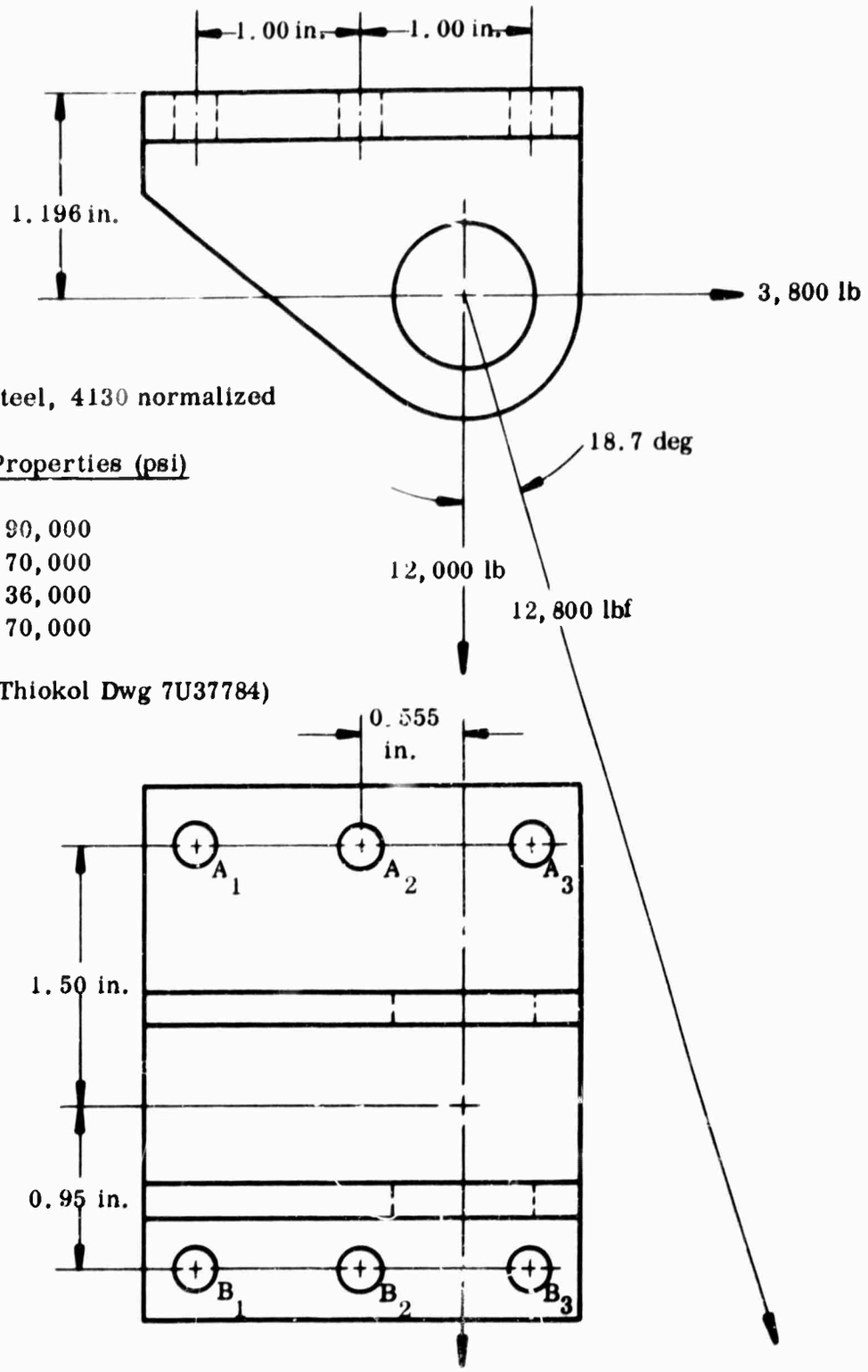

Material: Steel, 4130 normalized

4130 Steel Properties (psi)

Ultimate = 90,000
Yield = 70,000
Shear = 36,000
Bearing = 70,000

(Reference Thiokol Dwg 7U37784)

Assuming two brackets:

Bracket No. 1 with bolts A_1, A_2, and A_3 has applied load $\frac{0.95}{0.95 \quad 1.50}$ of total applied load.

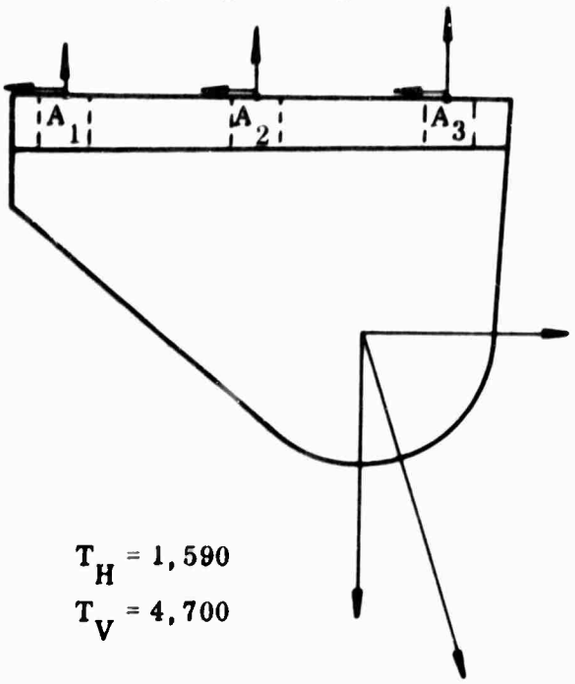

$\Sigma F_x = 0$

$$A_1x + A_2x + A_3x = 1,590$$

$$A_1x = A_2x = A_3x = \frac{1,590}{3} = 530 \text{ lbf shear}$$

$\Sigma F_y = 0$

(1) $A_1y + A_2y + A_3y = 4,700$

$\Sigma MA_3 = 0$

(2) $2A_1y + A_2y = (1.196)(1,590) + (0.445)(4,700)$

Considering the bolts elongated in tension:

$$A_3y - A_2y = A_2y - A_1y$$

(3) $A_1y + A_3y = 2A_2y$

(1) and (3) $A_2y = 1,567$ lbf tension

(1) and (3) and (2) $A_1y = 1,212$ lbf tension

Substituting in (1): $A_3y = 1,921$ lbf tension

Bracket No. 2 with bolts B_1, B_2, and B_3 has applied load $\frac{1.50}{0.95 + 1.50}$ of total applied load.

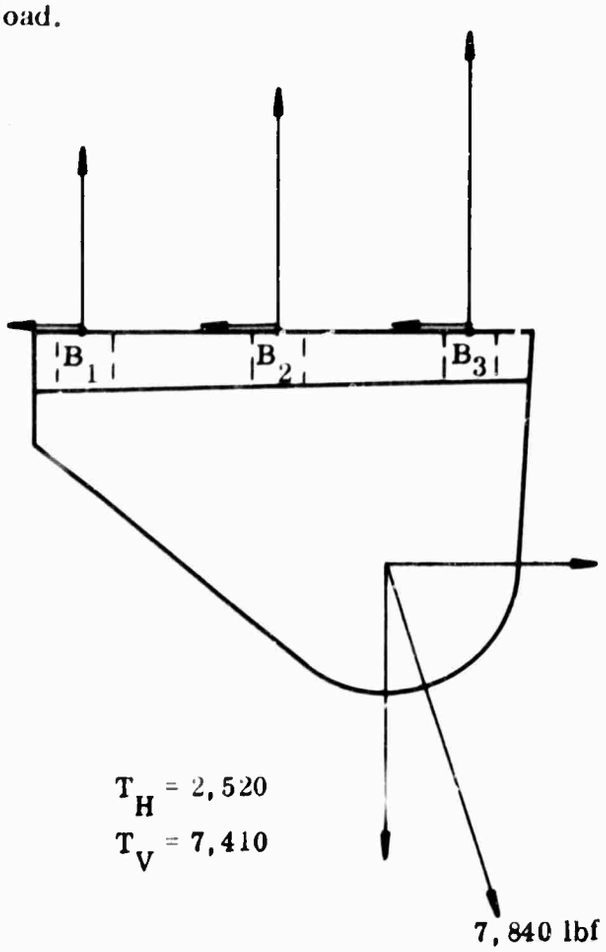

Bracket No. 2 is the same as bracket No. 1 with all forces multiplied by a factor of $\frac{1.50}{0.95}$.

$\therefore$ $B_1x = B_2x = B_3x = (1.58)\ (530) = 836$ lbf

$B_1y = (1.58)\ (1,212) = 1,910$ lbf

$B_2y = (1.58)\ (1,567) = 2,470$ lbf

$B_3y = (1.58)\ (1,921) = 3,030$ lbf

Summary of Bolt Loads

Bolts used: 5/16 in. Huck Lockbolts with ultimate tensile strength of 7, 290 lbf and ultimate shear strength of 3, 250 lbf.

With member in tension* (10, 533 lbf)

Bolts	Max Stress (lbf) Tension	Shear
A_1	995	436
A_2	1, 295	436
A_3	1, 580	436
B_1	1, 570	688
B_2	2, 040	688
B_3	2, 500	688

*Values reduced by $\frac{10,533}{12,800}$ ratio

With member in compression (12, 800 lbf)

Bolts	Max Stress (lbf) Compression	Shear
A_1	1, 210	530
A_2	1, 570	530
A_3	1, 920	530
B_1	1, 910	836
B_2	2, 470	836
B_3	3, 030**	836

**No load on bolt with compression load

Critical Bolt Stress

$$R_2 = R_T = R_{Tension} = \frac{2,500}{3,250} = 0.770$$

$$R_{Shear} = \frac{836}{7,290} = 0.115$$

$$U = \frac{0.770}{0.975} = 0.788$$

Use $R_T + R_S^{10} = 1.0$ curve (Reference 20, Figure 1535)

$$F.S. = \frac{1}{U} = +1.27$$

Bracket Stress Analysis-Not Available

(d) Strut BE and CE Attachment at Injector Torque Box

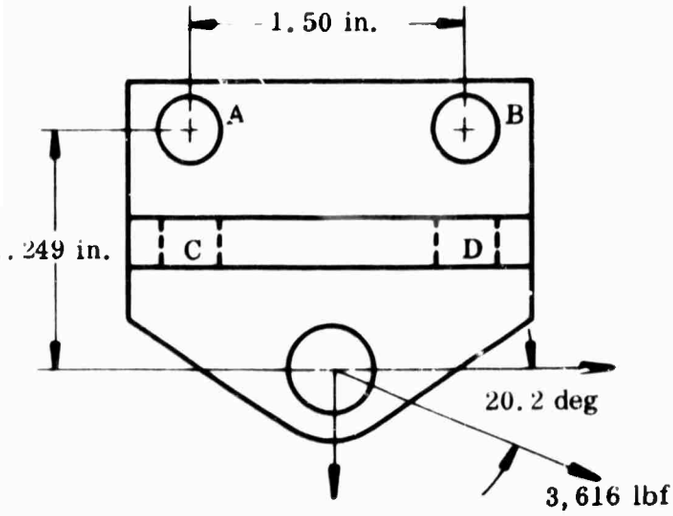

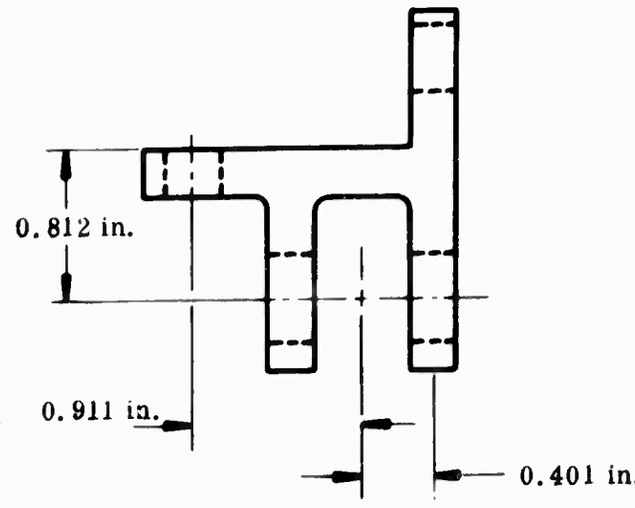

Assuming two brackets:

Bracket No. 1 with bolts A and B has applied load $\frac{0.911}{0.401 + 0.911}$ of total applied load.

Assuming also that load applied to this bracket is carried entirely by bolts.

Bracket No. 2 with bolts C and D has applied load $\frac{0.401}{0.401 + 0.911}$ of total applied load.

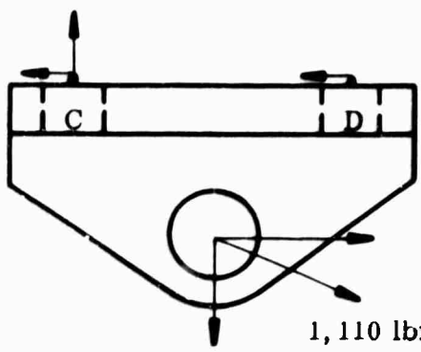

$T_H = 1,040$

$T_V = 380$

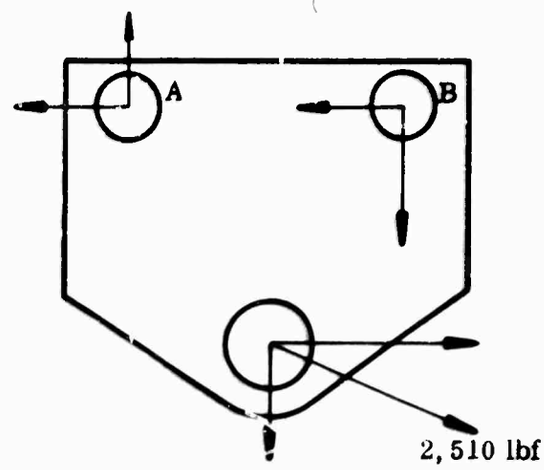

$T_H = 2,350$

$T_V = 860$

(Reference Thiokol Dwg 7U37784)

Material: Steel, 4130 normalized

4130 Steel Material Properties (psi)

Ultimate = 90,000
Yield = 70,000
Shear = 36,000
Bearing = 70,000

Bracket No. 1

$$\text{Vertical shear load on A} = \frac{860}{2} + \frac{(1.249)(2,350)}{1.50} = 2,380 \text{ lbf}$$

$$\text{Horizontal shear load on A} = \frac{2,350}{2} = 1,175 \text{ lbf}$$

$$\text{Total shear load on A} = (2,380^2 + 1,175^2)^{1/2} = 2,650 \text{ lbf}$$

$$\text{Vertical shear load on B} = \frac{860}{2} - \frac{(1.249)(2,350)}{1.50} = 1,520 \text{ lbf}$$

$$\text{Horizontal shear load on B} = \frac{2,350}{2} = 1,175 \text{ lbf}$$

Bracket No. 2

$$\text{Tensile load on C} = \frac{380}{2} + \frac{(0.812)(1,040)}{(1.50)} = 753 \text{ lbf}$$

$$\text{Shear load on C} = \frac{1,040}{2} = 520 \text{ lbf}$$

$$\text{Tensile load on D} = \frac{380}{2} = 190 \text{ lbf}$$

$$\text{Shear load on D} = \frac{1,040}{2} = 520 \text{ lbf}$$

Summary of Bolt Loads

Bolts used: 5/16 in. Huck Lockbolts with ultimate tensile strength of 7, 290 lbf and ultimate shear strength of 3, 250 lbf.

With member in tension (3, 616 lbf) Max Stress (lbf)			With member in compression (3, 616 lbf) Max Stress (lbf)		
Bolts	Tension	Shear	Bolts	Tension	Shear
A	--	2, 650	A	--	2, 650
B	--	1, 920	B	--	1, 920
C	753	520	C	--	520
D	--	520	D	753	520

Where both tension and compression occur, the maximum stresses (used to determine margin of safety) were determined as follows:

$$\text{Max Principal Stress} = \frac{S_T}{2} + \left[\left(\frac{S_T}{2} \right)^2 + S_S^2 \right]^{1/2}$$

$$\text{Max Shear Stress} = \left[\left(\frac{S_T}{2} \right)^2 + S_S^2 \right]^{1/2}$$

Critical Bolt Stress

Bolt A $\qquad F.S. = \frac{7,290}{2,650} = +2.75$ shear

Bracket Stress Analysis-Not Available

(7) Nitrogen Tank Attachments--The nitrogen tank is supported by the same six brackets used in supporting the nitrogen tetroxide tank. Since the nitrogen tank bracket loads are less than the nitrogen tetroxide tank loads, the material and bolt stresses are satisfactory by inspection.

(8) LITVC Injector Attachment--Not Available.

i. Flange Joint (Steel to Plastic)--Several analyses were completed on the nozzle design in an effort to verify the nozzle design confidence level. Subsection (1) below discusses the analysis of the interlaminar shear at the submerged glass cloth to steel connection. Subsection (2) summarizes a study conducted on the hoop compression and tension of the carbon to silica cloth liner, and the bond tension stress due to the rotational and radial movement of the steel flange.

(1) Submerged Nozzle Assembly Shear Analysis--The critical shear stress exists at the base of the submerged assembly, the interface between the glass cloth-phenolic structural cone, and the steel flange shell. In subsection 3.b, Discontinuity Analysis of Flange-Submerged Shell and Case Polar Boss, a discussion is provided on the glass cloth to steel discontinuity analysis for the static firing at MEOP load condition. The following moments and shears exist at the following stations.

Station	Moment (in.-lb/in.)	Shear (lb/in.)	Deflection (in.)
11.0	+1587 Comp Out Face	+845 Outward	+0.072
10.0	-345	+1647	+0.025
9.0	-3912	+3267	-0.010

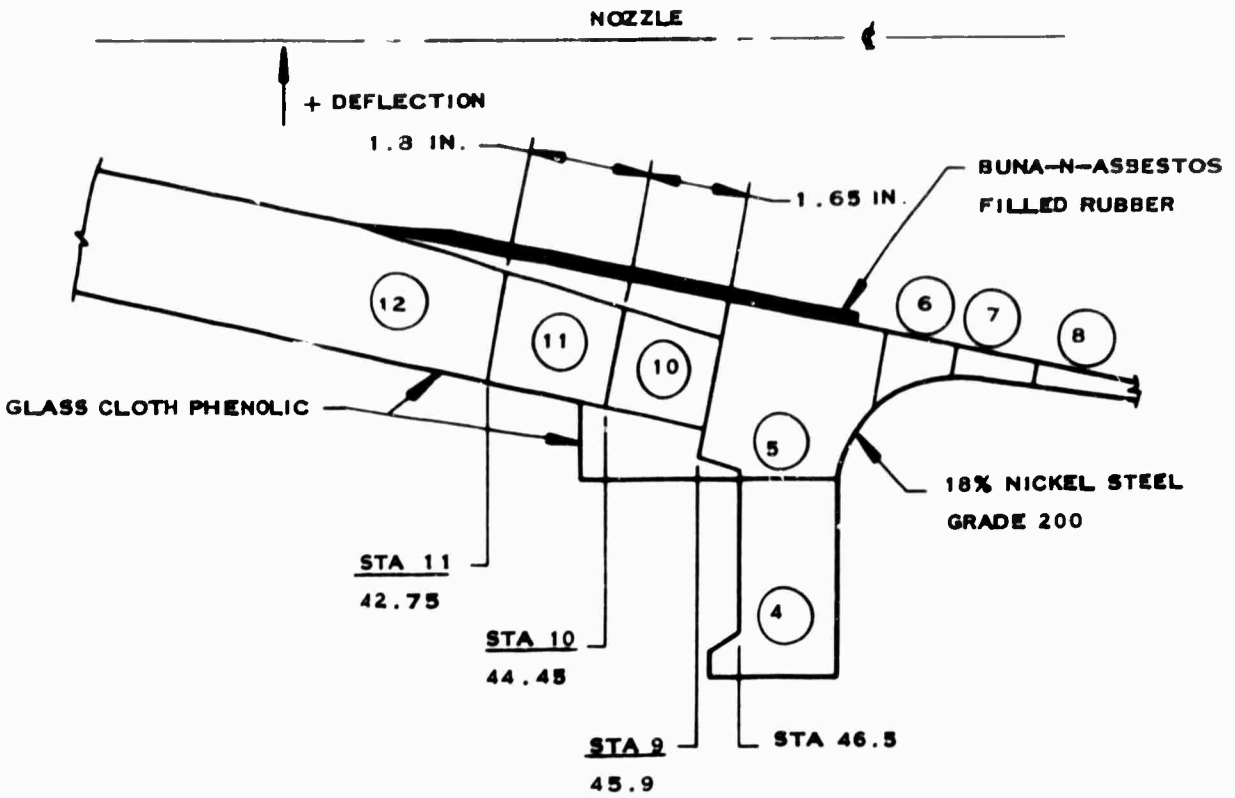

Individual free bodies illustrate the shear and moment distribution.

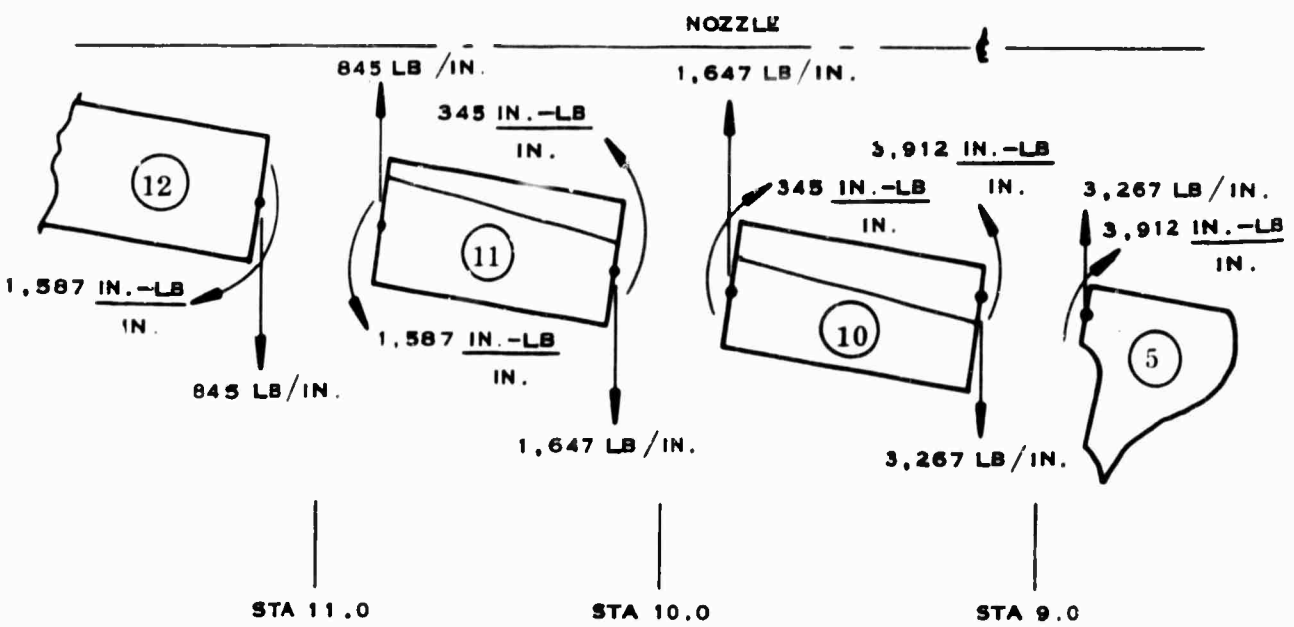

The stress analysis and material factor of safety is indicated in the present TU-393 design analysis report. A shear analysis will be shown for free bodies 12, 11, 10, and 5. The shear stress is limited to the glass cloth for Item 12, to the steel in Item 5, and shared between the glass cloth and steel for Items 11 and 10. The structural adehsive between the glass cloth and 18 percent nickel steel is Epon-913/919, Shell Chemical.

The following tabulation indicates the thickness of steel and glass cloth for each item.

Item	Total Thickness (in.)	Avg Steel Thickness (in.)	Avg Glass Cloth Thickness (in.)
12	1.40	--	1.40
11	1.40	0.25	1.15
10	1.40	0.55	0.85
9	0.85	0.85	--

The shear allowables for the indicated materials are listed below.

Material	Ultimate Axial at Room Temp (Interlaminar Shear) (psi)	Ultimate Transverse at Room Temp (Edge Shear) (psi)
18% Nickel Steel Grade 200	120,000	120,000
Glass Cloth Phenolic	3,700** Beam Shear Test	7,440**
Epon 913/919 Adhesive 82 Parts Epon 913 100 Parts Epon 919	3,200* Cure - 5 hr @ 140°F	3,200

* Ref Shell Chemical Technical Data and Rohr Process Control Tests.

** Ref Mil HDBK-17 and Interlaminar Shear Testing of Filament Winding Materials, 19th Meeting R.F.P. Divisions - Society of Plastics Industry.

(a) **Shear Analysis**

Item 12 - Glass Cloth Reinforced Plastic

$$\sigma_{S\ Max} = \frac{VQ}{It} = \frac{3}{2}\frac{V}{A} \text{ (Rectangular Cross Section)}$$

$$= (1.5)\frac{845.}{dt} = \frac{1,130}{1(1.40)} = 905 \text{ psi}$$

$$\text{Factor of Safety} = \frac{3,700}{905} = +4.08$$

Item 11

Section Properties

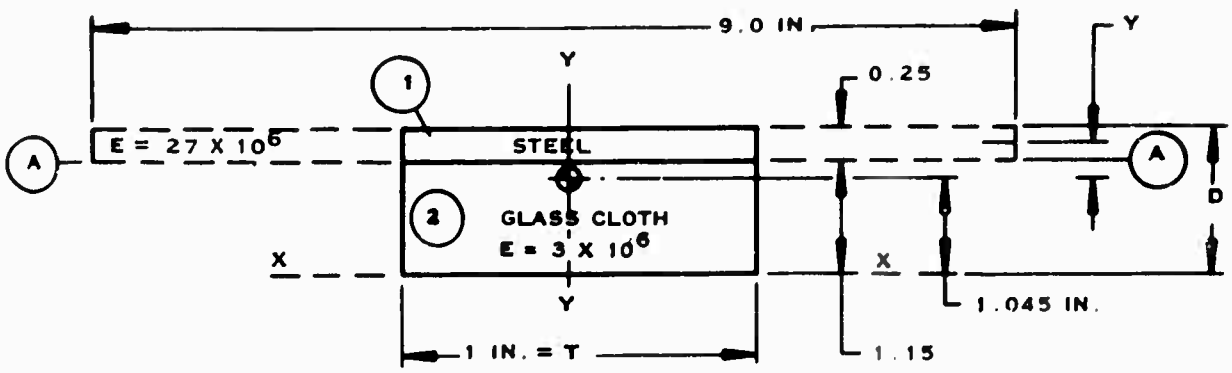

Section	Area	Y	AY	AY^2	Io
1	2.250*	1.275	2.89	3.68	0.046
2	1.150	0.575	0.66	0.37	0.127
	3.400		3.55	4.05	0.163

* Glass cloth area equivalent of steel $= \frac{E_s}{E_c}(As) = \frac{27}{3}(As)$

$$A_1 = 9As$$

$$Y = \frac{3.55}{3.40} = 1.045$$

$$I = (4.05 + 0.163) - 3.4\,(1.045^2) = 4.213 - 3.720 = 0.493 \text{ in.}^4$$

Adhesive Shear Stress

$$\sigma_{S\ A\text{-}A} = \frac{V_{avg}AY}{It} = \frac{1,246\ (2.250)\ (0.230)}{0.493\ (1.0)} = 1,305 \text{ psi}$$

$$V_{avg} = \frac{845 + 1,647}{2} = 1,246 \text{ lb/in.}$$

$$\text{Factor of Safety} = \frac{3,200}{1,305} = +2.45$$

Glass Cloth Shear Stress

$$\sigma_{S \text{ Neutral Axis}} = \frac{VAY}{It} \quad \frac{1,246\ (1.045 \times 1)\ (0.522)}{0.493\ (1)} = 1,375 \text{ psi}$$

$$\text{Factor of Safety} = \frac{3,700}{1,375} = +2.69$$

Item 10

Section Properties - Neglect Assistance of 7U-37734-12 Support Ring

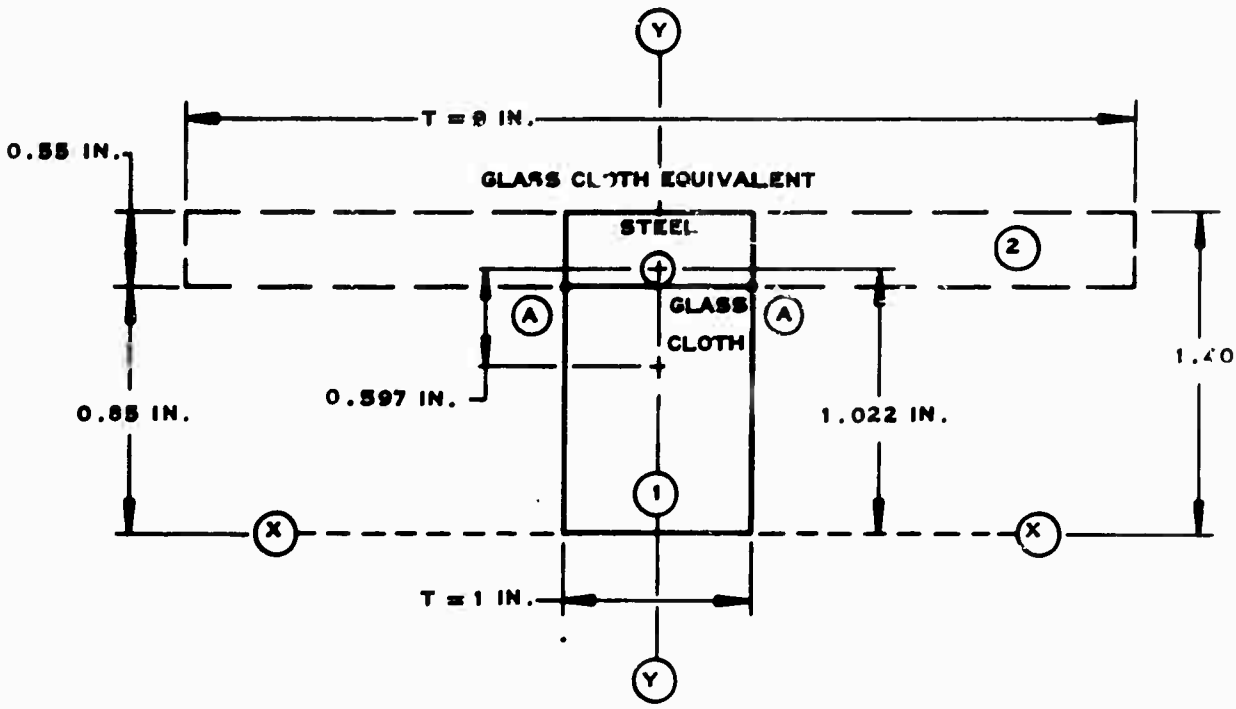

$$\text{Glass Cloth Area Equivalent of Steel} = \frac{E_S}{E_{GC}} (A_S) = \frac{27}{3} (A_S)$$

$$A_2 = 9A_S$$

Section	Area	Y	AY	AY^2	Io
1	0.85	0.425	0.361	0.180	0.051
2	4.95	1.125	5.570	6.260	0.124
	5.80		5.931	6.440	0.175

$$Y = \frac{5.931}{5.80} = 1.022$$

$$I = (6.440 + 0.175) - 5.80\ (1.022)^2 - 6.615 - 6.080$$

$$I = 0.535 \text{ in.}^4$$

Adhesive to Glass Cloth Shear Stress, Sec A-A

$$\sigma S\ A\text{-}A = \frac{VavgAY}{It} = \frac{2,457\ (0.85)\ (0.597)}{0.535\ (1.00)} = 2,320\ psi$$

Adhesive Allowable = 3,200 psi

$$V_{avg} = \frac{3,267 + 1,647}{2} = 2,457\ lb/in.$$

$$\text{Factor of Safety} = \frac{3,200}{2,320} = +1.37$$

Item 5 - Steel - 18 Percent Nickel

$$\sigma S_{Max} = \frac{QV}{It} = \frac{3}{2}\frac{V}{A}\ \text{(Rectangular Cross Section)}$$

$$= 1.5\ \frac{3,267}{1\ (.85)} = 5,770\ psi$$

$$\text{Factor of Safety} = \frac{120,000}{5,770} = +\ High$$

(2) Stress in Nozzle Insulation and Adhesive Bond--In subsection 3.b, Discontinuity Analysis of Flange, Submerged Shell and Case Polar Boss, a discussion is provided on the discontinuity analysis of the submerged glass structural and flange shell. The deflections (radial and rotational) are shown in Figure 72. The materials and design criteria for the nozzle section are shown in Figure 73.

An analysis determines the interface pressure between the liner and the steel. This pressure value can be used to check the adhesive bond and liner for compression or tension.

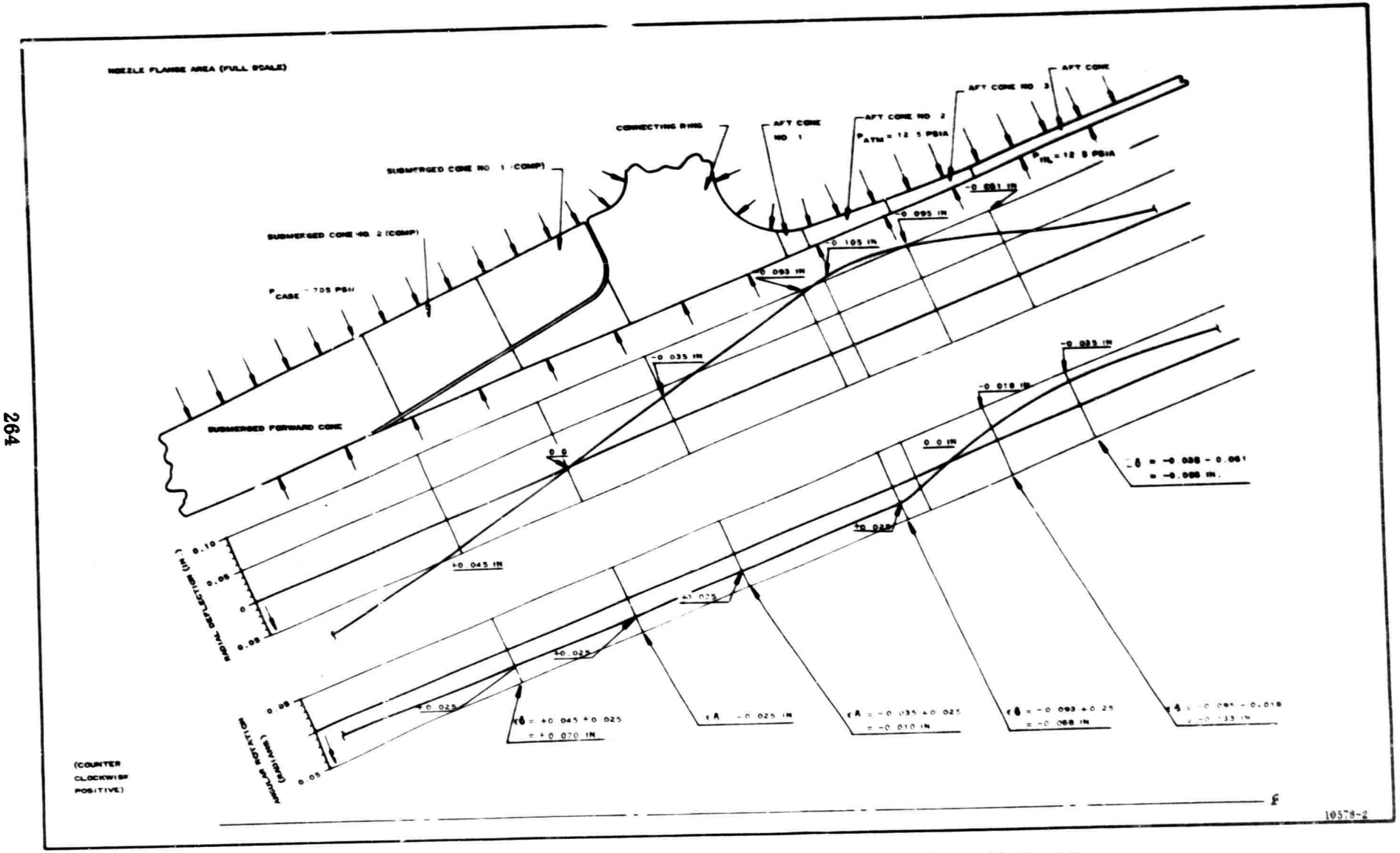

Figure 72. Radial and Rotational Glass Cloth Steel Shell Deflections

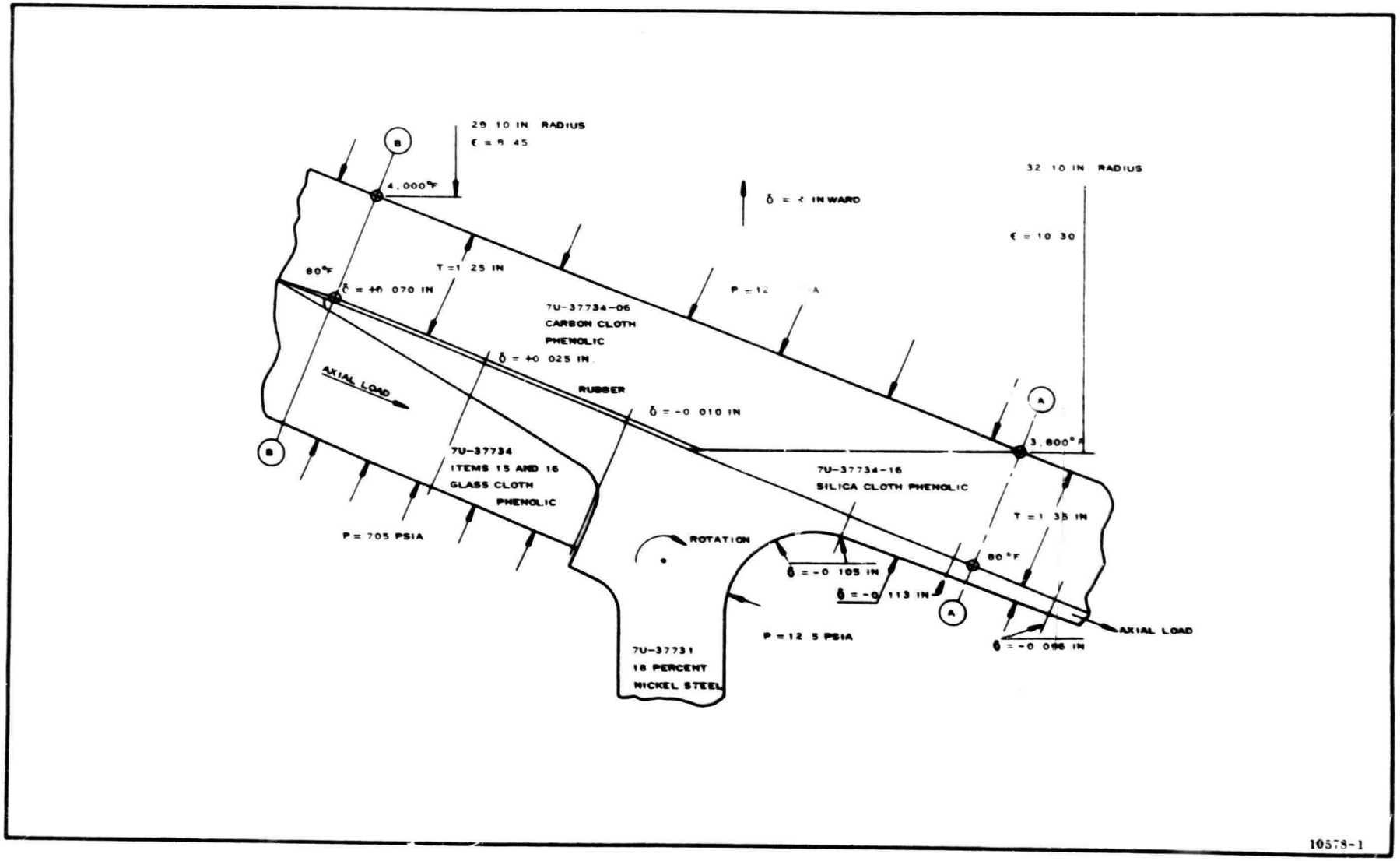

Figure 73. Nozzle Section Materials and Design Criteria

Materials allowables at room and elevated temperatures are listed below.

Material	Section	Average Temperature (°F)	Poisson's Ratio	Modulus (psi x 10^6)	Stress (psi)
Carbon Cloth Phenolic	B-B	2,040 (4,000 / 80)	0	0.375 Compression	7,500 Compression
	B-B	80 (Room Temp)	0.25	2.00 Compression	25,000 Compression
Silica Cloth Phenolic	A-A	1,940 (3,800 / 80)	0	0.250 Tension	1,250 Tension
	A-A	80 (Room Temp)	0.20	2.25 Tension	12,000 Tension

Section A-A - Silica Cloth-Phenolic

At Room Temperature @ t = 0 sec

Interface Pressure

$\delta = \frac{pR^2}{Et}(1-V/2)$ Ref. Timoshenko, Plates and Shells

p = Interface Pressure

R = Radius = 33.28 in.

E = Modulus of Elasticity = 2.25×10^6

t = Thickness = 1.35 in.

V = Poisson's Ratio - 0.20

δ = Deflection = 0.113 in.

$$p = \frac{E t \delta}{R^2(1-V/2)} = \frac{2.25\,(10^6)\,(0.113)\,(1.35)}{(33.28)^2\,(0.90)} = 343 \text{ psi}$$

Bond Stress

σ allowable in tension = 1,000 psi

σ actual = 343 psi

$$\text{Factor of Safety} = \frac{1,000}{343} = +2.92$$

Silica Cloth Hoop Tension Stress

$$\sigma_{H_T} = \frac{pR}{t} = \frac{343\ (33.28)}{1.35} = 8,450$$

$$\text{Factor of Safety} = \frac{12,000}{8,450} = +1.42$$

At Elevated Temperature at t = 110 sec

Interface Pressure

$$p = \frac{E\,t\,\delta}{R^2(1-V/2)} = \frac{0.25\ (10^6)\ (0.113)\ (1.25)}{(33.28)^2\ (1)} = 31.7 \text{ psi}$$

Bond Stress

$$\text{Factor of Safety} = \frac{1,000}{31.7} = + \text{ High}$$

Silica Cloth Hoop Stress

$$\sigma_{Hoop} = \frac{pR}{t} = \frac{31.7\ (33.28)}{1.29} = 845 \text{ psi}$$

$$\text{Factor of Safety} = \frac{1,250}{845} = +1.47$$

Section B-B - Carbon Cloth-Phenolic

At Room Temperature @ t = 0 sec

Interface Pressure

$$p = \frac{E\,t\,\delta}{R^2(1-V/2)} = \frac{2.00\ (1.25)\ (0.070)\ 10^6}{(30.20)^2\ (0.875)} = 219 \text{ psi}$$

Bond Stress Compression — Ok by Inspection

Carbon Cloth Hoop Compression Stress

$$\sigma_{Hc} = \frac{pR}{t} = \frac{219\ (30.20)}{1.25} = 5,300 \text{ psi}$$

$$\text{Factor of Safety} = \frac{25,000}{5,000} = +4.72$$

At Elevated Temperature @ t = 110 sec

Interface Pressure

$$p = \frac{E\,t\,\delta}{R^2(1-V/2)} = \frac{0.375 \times 10^6\,(1.25)\,(0.070)}{(30.20)^2\,(1)} = 35.9 \text{ psi}$$

Bond Stress Ok by Inspection

Carbon Cloth Hoop Stress

$$\sigma_{HT} = \frac{pR}{t} = \frac{35.9\,(30.20)}{1.25} = 866 \text{ psi}$$

$$\text{Factor of Safety} = \frac{7,500}{866} = +8.70$$

SECTION V

WEIGHT ANALYSIS

An accurate weight analysis was required to complete the motor mass fraction, acceleration, and vibration analyses and material and configuration design studies. The analysis included the plane area and mass properties of the components and the total nozzle assembly.

A total nozzle weight of 5,384 lb was reported in Quarterly Progress Report No. 1 October, 1965. Since then the OD insulation Figure 5 Item 18 was changed to silica cloth foam V-44 for a weight increase of 183 pounds.

In addition, a total of 133.11 lb was added with Items 11, 13, and 14 (Figure 9) to accommodate the diffuser attachment. This attachment would not be included in a flightweight nozzle. The present nozzle with gains and decreases is 5,677 pounds.

Without the diffuser attachment the total nozzle weight is 5,544 lb, an increase of 160 lb from the last reported value. Nozzle mass properties data are shown in Figure 72.

	Weight (lb)	Center-of-Gravity			Moment of Inertia		
		Long.	Lat	Vert	Pitch	Roll	Yaw
Total Nozzle	5384.809	232.051	100.000	100.000	2544.685	1601.523	2544.685
Total Graphite Cloth	450.136	171.330	100.000	100.000	13.909	24.128	13.909
Graphite Cloth - Item 1	221.703	169.099	100.000	100.000	8.333	15.603	8.333
Graphite Cloth - Item 2	45.405	168.035	100.000	100.000	1.106	2.195	1.106
Graphite Cloth - Item 3	43.844	170.385	100.000	100.000	0.871	1.730	0.871
Graphite Cloth - Item 4	139.184	176.256	100.000	100.000	2.517	4.600	2.517
Carbon Cloth	485.985	205.598	100.000	100.000	48.466	60.192	48.466
Total Silica Cloth	1747.195	257.112	100.000	100.000	816.186	727.662	816.186
Silica Cloth - Item 6	31.705	174.652	100.000	100.000	0.827	1.484	0.827
Silica Cloth - Item 7	127.009	178.568	100.000	100.000	4.217	7.450	4.217
Silica Cloth - Item 8	1588.481	265.037	100.000	100.000	574.047	718.768	574.047
Structural Wrap Fiberglass	689.157	201.550	100.000	100.000	73.898	93.855	73.898
Support Ring Glass	20.345	222.234	100.000	100.000	2.419	4.835	2.419
V-44	303.593	204.545	100.000	100.000	28.526	43.973	28.526
Structural Steel	1020.178	229.316	100.000	100.000	155.511	289.630	155.511
Forward Glass Cloth End Ring	106.544	243.849	100.000	100.000	18.618	37.487	18.618
Liner - Nozzle Flange	1.964	222.276	100.000	100.000	0.207	0.413	0.207
Doublers	14.855	245.392	100.000	100.000	2.676	5.350	2.676
Facings - Fiberglass	297.395	278.864	100.000	100.000	106.744	166.832	106.744
Hexcell Core	79.629	278.953	100.000	100.000	27.593	44.531	27.593
Total Bolts	35.908	245.379	100.000	100.000	14.383	16.707	14.383
Ht-424 Adhesive	24.163	278.884	100.000	100.000	8.673	13.555	8.673
Packing	0.659	241.320	100.000	100.000	0.115	0.229	0.115
3150 Adhesive	12.326	282.662	100.000	100.000	6.085	7.263	6.085
Glass Cloth Support Block	94.775	310.356	100.000	100.000	34.674	72.860	34.674

Figure 74. 156-7 Nozzle Mass Properties Data

SECTION VI

LIST OF REFERENCES

1. Thiokol Chemical Corporation: 156 Inch Diameter Motor Movable Nozzle TVC Final Test Report SS65SS-1 (TU-402.02) Support Motor Nozzle Evaluation Test. TWR-581, DLB-036-TR, TW-48-4-64. Thiokol Chemical Corporation, Wasatch Division, Brigham City, Utah.

2. Thiokol Chemical Corporation: 156 Inch Diameter Motor Movable Nozzle TVC Final Test Report SS65SS-2 (TU-402.03) Supporting Motor Nozzle Evaluation Test. TWR-615, DLB 041-TR, TW-59-6-64. Thiokol Chemical Corporation, Wasatch Division, Brigham City, Utah.

3. Thickol Chemical Corporation: 156-1 (TU-412.01) Omniaxial Gimbaled Nozzle Design Analysis Report. Vol I, II, and III. TW-690-4-64, DLB-039-DR, TW-691-4-64, DLB-039, DLB-039-DR. Thiokol Chemical Corporation, Wasatch Division, Brigham City, Utah.

4. Thiokol Chemical Corporation: Development of a Lightweight High Performance Composite Structure Nozzle Assembly. EB5-64. Thiokol Chemical Corporation, Elkton Division, Elkton, Maryland.

5. Thiokol Chemical Corporation: Design Report, Semisubmerged Gimbaled Nozzle, IR & D Project No. 64-203. TWR-647. Thiokol Chemical Corporation, Wasatch Division, Brigham City, Utah.

6. Thiokol Chemical Corporation: Final Program Report, Submerged Gimbal Nozzle, IR & D Project No. 64-203. Thiokol Chemical Corporation, Wasatch Division, Brigham City, Utah.

7. Thiokol Chemical Corporation: Parametric Analysis of Lightweight Upper Stage Nozzle Exit Cones for Solid Propellant Rocket Motors. WER-767. Thiokol Chemical Corporation, Wasatch Division, Brigham City, Utah.

8. Thiokol Chemical Corporation: Structural Analysis (TU-412). Report DLB-039-DR-Vol II. Thiokol Chemical Corporation, Wasatch Division, Brigham City, Utah.

9. Thiokol Chemical Corporation: Quarterly Progress Report, Stage I MINUTEMAN (M55A1) Production Support, Project 3045. July thru October 1964. Thiokol Chemical Corporation, Wasatch Division, Brigham City, Utah.

10. Thiokol Chemical Corporation: Design Report, Semisubmerged Gimbal Nozzle. TWR-647. July 1964. Thiokol Chemical Corporation, Wasatch Division, Brigham City, Utah.

11. Zophres, W.: Design Buckling Criteria for Monocoque and Ring Stiffened Cylinders and Truncated Cones. Interoffice Memorandum 62-9712.6.4-58. 8 Oct 1962. Space Technology Laboratories.

12. Plastics for Flight Vehicles - Part I Reinforced Plastics, MIL-HDBK-17. June 1955. Basic Mechanical Properties Section.

13. Roark, R. J.: Formulas for Stress and Strain. Third Edition. 1954.

14. Theory of Plates and Shells, McGraw-Hill-Timoshenko. 1940.

15. Niles and Newell: Aircraft Structures. Third Edition. Vol II, pp 274.

16. Truncated Cone Buckling Coefficient - External Pressure. Douglas Aircraft Structures Manual.

17. Sandwich Construction for Aircraft. ANC-23. May 1951.

18. Design Hand Book - Adhesive Bonding and Sandwich Construction. Rohr Corporation. 1962.

19. Wignot, Combs, Ensrud: Analysis of Circular Shell Supported Frames. NACA TN No. 929. Lockheed Aircraft Corporation. May 1944.

20. Strength of Metal Aircraft Elements. MIL-HDBK-5. March 1955.

21. Bartz, D. R.: "A Simple Equation for Rapid Estimation of Rocket Nozzle Convective Heat Transfer Coefficients," Jet Propulsion. January 1957; page 49.

22. Kurtovich, D. D. and Pinson, G. T.: "How to Find the Exhaust Heat Radiation of Aluminized Solid Rockets," Space/Aeronautics. July 1961.

23. McCuen, Peter A., et al.: A Study of Solid-Propellant Rocket Motor Exposed Materials Behavior. Final Report, Vidya No. 129, AFRPL-TR-65-33, Contract No. AF 04(611)-9073, Vidya Research and Development, Palo Alto, California.

24. A Study of Solid-Propellant Rocket Motor Exposed Materials Behavior, First Quarterly Report. Vidya Research and Development.

25. Elliott, David G., Bartz, Donald R., Silver, Sidney: Calculation of Turbulent Boundary-Layer Growth and Heat Transfer in Axi-Symmetric Nozzles. NASA Contract No. NAS 7-100. Jet Propulsion Laboratory, California Institute of Technology, Pasadena, California, 15 Feb 1963.

26. Test Evaluation Report (Ground Test) XSR 47-UT-1-3 (UA 1205-3). Report No. ER-UTC-64-98. United Technology Center, Sunnyvale, California.

27. Dahn, T. J.: Equations for Optimization of Design Point Performance of Gaseous Secondary Injection Thrust Vector Control Systems. Vidya 9605-1 N-1. July 1964.

28. Preliminary Results, Quadrant Interaction Analytical Study Effort. 63-1942.27-28, Aerospace Corporation. 3 Jun 1963.

29. Roark, Raymond J.: Formulas for Stress and Strain. Second Edition. McGraw-Hill, 1943.

30. Blade, Alexander: Rings and Arcuate Beams. Product Engineering. 7 Jan 1963.

31. Timoshenko: Strength of Materials. Vol II.

32. Bijlaard, P. P.: Buckling of Conical Shells Under External Pressure. Bell Aerospace Company, Buffalo, New York.

33. Singer, J. and Fersht, R.: Buckling of Orthotropic and Stiffened Conical Shells. TAE Report 22. Technion Research and Development Foundation, (Israel) September 1962.

34. Schneider, M. H. and Hofeditz, J. T.: Buckling of Fiberglass Cylinders Under External Pressure. ASME 64-WA/UNT-12. Missile and Space Systems Division, Douglas Aircraft Company, Inc, Santa Monica, California. December 1964.

35. Creszczuk, L. B.: Elastic Constants and Analysis Methods for Filament Wound Shell Structures. Report SM-45849. Missile and Space Systems Division, Douglas Aircraft Company, Inc, Santa Monica, California. January 1964.

36. Plastics for Flight Vehicles, Part I - Reinforced Plastics. Military Handbook MIL-HDBK-17. November 1959.

37. Perry, H. A.: Adhesive Bonding of Reinforced Plastics. McGraw-Hill Book Company, Inc, New York. 1959.

38. Van Den Broek, J. A.: Elastic Energy Theory. Second Edition. John Wiley and Sons, New York. Eighth Printing. April 1960.

39. Zophres, W., Voce, S. J., and Strickler, C. T.: Design Buckling Criteria for Cylinders and Truncated Cones of Small Semi-Vertex Angle in the Low R/t and Z Parameter Ranges. Report 6120-J280-RV000. TRW Space Technology Laboratories, One Space Park, Redondo Beach, California, 29 Nov 1963.

40. Peterson, R. E.: Stress Concentration Design Factors. John Wiley and Sons, New York. Third Printing. September 1962.

41. Cozzone, F. P., Melcon, M. A., and Holbit, F. M.: Analysis of Lugs and Shear Pins Made of Aluminum or Steel Alloys. Product Engineering. May 1950.

DISTRIBUTION LIST

Organization	Copies
U. S. Department of the Interior Bureau of Mines ATTN: M. M. Dolinar, Repts Librarian Explosives Research Center 4800 Forbes Avenue Pittsburgh, Pennsylvania 15213	1
Central Intelligence Agency ATTN: OCD, Standard Dist. 2430 E Street, N.W. Washington, D.C. 20505	1
National Aeronautics and Space Administration Lewis Research Center ATTN: Library 21000 Brookpark Road Cleveland, Ohio 44135	1
John F. Kennedy Space Center NASA ATTN: Library Cocoa Beach, Florida 32931	1
National Aeronautics and Space Administration Manned Spacecraft Center ATTN: Library P. O. Box 1537 Houston, Texas 77001	1
National Aeronautics and Space Administration Langley Research Center ATTN: Library Langley Air Force Base Virginia 23365	3
National Aeronautics and Space Administration ATTN: Office of Technical Information and Educational Programs, Code ETL Washington, D.C. 20546	1
Scientific and Technical Information Facility ATTN: NASA Representative P. O. Box 5700 Bethesda, Maryland 20014	2
National Aeronautics and Space Administration ATTN: R. W. Ziem (RPS) Washington, D.C. 20546	1
National Aeronautics and Space Administration Goddard Space Flight Center ATTN: Library Greenbelt, Maryland 20771	1
Defense Documentation Center Cameron Station Alexandria, Virginia 22314	20
RTD (RTNP) Bolling AFB Washington, D.C. 20332	1
Arnold Engineering Development Center Air Force Systems Command ATTN: AEOIM Tullahoma, Tennessee 37389	1
AFSC (SCTR) Andrews AFB Washington, D.C. 20331	1
AFRPL (RPR) Edwards California 93523	1
AFRPL (RPM) Edwards California 93523	1
AFFTC (FTBPP-2) Technical Library Edwards AFB California 93523	1
Office of Research Analyses (OAR) ATTN: RRRT Holloman AFB, New Mexico 88330	1
Air Force Office of Scientific Research ATTN: SREP, Dr. J. F. Masi Washington, D.C. 20333	1

DISTRIBUTION LIST (Cont)

Organization	Copies
United Aircraft Corporation Corporation Library ATTN: Dr. David Rix 400 Main Street East Hartford, Connecticut 06118	1
United Aircraft Corporation Pratt & Whitney Fla. Res. & Dev. Ctr. ATTN: Library P. O. Box 2691 W. Palm Beach, Florida 33402	1
United Aircraft Corporation United Technology Center ATTN: Librarian P. O. Box 358 Sunnyvale, California	1
General Electric Company Apollo Support Department ATTN: C. Day P. O. Box 2500 Daytona Beach, Florida 32015	1
Naval Ordnance Systems Command Department of the Navy ATTN: ORD-9312 Washington, D.C. 20360	2
Naval Ordnance Systems Command Department of the Navy ATTN: ORD-033 Washington, D.C. 20360	2
Naval Air Systems Command Department of the Navy ATTN: AIR-330 Washington, D.C. 20360	2
Commanding Officer Ammunition Procurement & Supply Agency ATTN: Engr. Library Joliet, Illinois 60400	1
Department of Commerce Office of Export Control ATTN: Chief, Chemistry & Fuels Section Paul M. Terlizzi Washington, D.C. 20230	1
AFRPL (RPCE) Edwards, California 93523	1

Organization	Copies
Callery Chemical Company Research and Development ATTN: Document Control Callery, Pennsylvania 16024	1
Ethyl Corporation P. O. Box 3091 Baton Rouge, Louisiana 70805	1
Hynes Chemical Research Corp 306 Bon Air Avenue Durham, North Carolina 27704	1
California Institute of Technology ATTN: Security Officer 1201 E. California Boulevard Pasadena, California 91109	1
Olin Mathieson Chemical Corporation ATTN: Research Library Box 508 Marion, Illinois 62959	1
Olin Mathieson Chemical Corporation Research Library 1-K-3 ATTN: Mail Control Room Mrs. Laura M. Kajuti 275 Winchester Avenue New Haven, Connecticut 06511	1
Pennsalt Chemicals Corporation Technological Center 900 First Avenue King of Prussia, Pennsylvania 19406	1
Purdue University Lafayette, Indiana 47907	1
North American Aviation Rocketdyne Division McGregor Plant McGregor, Texas 76657	1
Shell Development Company 1400 53rd Street Emeryville, California 94608	1
Thiokol Chemical Corporation Space Booster Division ATTN: Librarian Brunswick, Georgia 31520	1

DISTRIBUTION LIST (Cont)

Organization	Copies
AFRPL (RPC) Edwards California 93524	1
Wright-Patterson AFB ATTN: AFML (MAAE) Ohio 45433	1
Commanding Officer Ballistic Research Laboratories ATTN: AMXBR-I Aberdeen Proving Ground, Maryland 21005	1
Commanding Officer Frankford Arsenal ATTN: Propellant and Explosives Section, 1331 Philadelphia, Pennsylvania 19137	1
Commanding Officer Picatinny Arsenal ATTN: Library Dover New Jersey 07801	1
U.S. Army Missile Command Redstone Scientific Information Center ATTN: Chief, Document Section Redstone Arsenal, Alabama 35808	4
Commanding General White Sands Missile Range ATTN: Technical Library New Mexico 88002	1
Naval Air Systems Command Department of the Navy ATTN: AIR-604 Washington, D.C. 20360	2
Naval Air Systems Command Department of the Navy ATTN: AIR-5367 Washington, D.C. 20360	2
Naval Ordnance Systems Command Department of the Navy ATTN: ORD-0624 Washington, D.C. 20360	1
Naval Air Systems Command Department of the Navy ATTN: AIR-5366 Washington, D.C. 20360	1
Commander U.S. Naval Missile Center ATTN: Technical Library Point Mugu, California 93041	2
Commander U. S. Naval Ordnance Laboratory ATTN: Library White Oak Silver Spring, Maryland 20910	2
Commander (Code 753) U. S. Naval Ordnance Test Station ATTN: Technical Library China Lake, California 93557	6
Superintendent U. S. Naval Postgraduate School Naval Academy Monterey, California 93900	1
Commanding Officer Office of Naval Research 1030 E. Green Street Pasadena, California 91101	1
Director Special Projects Office Department of the Navy Washington, D.C. 20360	1
Commanding Officer U. S. Naval Underwater Ordnance Station ATTN: W. W. Bartlett Newport, Rhode Island 02844	1
Commander U.S. Naval Weapons Laboratory ATTN: Technical Library Dahlgren, Virginia 22448	1
Commanding Officer (AD-2) U.S. Naval Air Development Center Johnsville, Pennsylvania 18974	1
Aerojet-General Corporation ATTN: Librarian P. O. Box 296 Azusa, California 91703	2

DISTRIBUTION LIST (Cont)

Organization	Copies
Aerojet-General Corporation ATTN: F. M. West, Chief Librarian 11711 South Woodruff Avenue Downey, California 90241	1
Aerojet-General Corporation ATTN: Technical Library 2484-2015A P. O. Box 1947 Sacramento, California 95809	4
Aerospace Corporation ATTN: Library-Documents P. O. Box 95085 Los Angeles, California 90045	2
Allied Chemical Corporation ATTN: Security Office P. O. Box 70 Morristown, New Jersey 07960	1
Northrop Carolina, Inc. Box 3049 Asheville, North Carolina 28802	1
American Cyanamid Company ATTN: Security Officer 1937 W. Main Street Stamford, Connecticut 06902	1
IIT Research Institute Technology Center ATTN: C. K. Hersh, Chemistry Division Chicago, Illinois 60616	1
ARO, Inc. Arnold Engineering Development Center ATTN: Dr. B. H. Goethert Chief Scientist Arnold AF Station, Tennessee 37389	1
Atlantic Research Corporation ATTN: Security Office for Library Shirley Highway and Edsall Road Alexandria, Virginia 22314	2
University of Denver Denver Research Institute ATTN: Security Office P. O. Box 10127 Denver, Colorado 80210	1
Battelle Memorial Institute Columbus Laboratories ATTN: Report Library (CPIA) 505 King Avenue Columbus, Ohio 43201	1
The Boeing Company Aero Space Division ATTN: Ruth E. Peerenboom Library Proc. Super. (1190) P. O. Box 3707 Seattle, Washington 98124	1
Chemical Propulsion Information Agency Applied Physics Laboratory 8621 Georgia Avenue Silver Spring, Maryland 20910	2
Douglas Aircraft Co., Inc. Santa Monica Division ATTN: Mr. J. L. Waisman 3000 Ocean Park Boulevard Santa Monica, California 90405	1
The Dow Chemical Company Security Section ATTN: Dr. R. S. Karpiuk 1710 Building Box 31 Midland, Michigan 48641	1
E. I. du Pont de Nemours and Company Eastern Laboratory ATTN: Mrs. Alice R. Steward Gibbstown, New Jersey 08027	1
Esso Research and Engineering Co. Process Research Division ATTN: Dr. J. R. Lovett P. O. Box 8 Linden, New Jersey 07036	1
Ethyl Corporation Research Laboratories ATTN: E. B. Rifkin, Assistant Director, Chemical Research 1600 West Eight Mile Road Ferndale, Michigan 48220	1

DISTRIBUTION LIST (Cont)

Organization	Copies
Allison Division General Motors Corporation ATTN: Plant 8, Tech Library Mr. W. H. Richardson 4700 W. 10th Street Indianapolis, Indiana 46208	1
Hercules Powder Company Allegany Ballistics Laboratory ATTN: Library P. O. Box 210 Cumberland, Maryland 21501	1
Hercules Powder Company Kenvil Works ATTN: Library Kenvil, New Jersey 07847	1
Institute for Defense Analyses ATTN: Classified Library 400 Army-Navy Drive Arlington, Virginia 22202	1
Jet Propulsion Laboratory 4800 Oak Grove Drive Pasadena, California 91103	1
Lockheed Propulsion Company ATTN: Miss Belle Berlad, Librarian P. O. Box 111 Redlands, California 92374	2
Martin Company ATTN: Science - Technology Library - Mail 398 Baltimore, Maryland 21203	1
Martin Company ATTN: Res. Library, 6366 P. O. Box 179 Denver, Colorado 80201	1
Rocket Research Corporation 520 South Portland Street Seattle, Washington 98108	1
Rocketdyne ATTN: Library, Dept. 596-306 6633 Canoga Avenue Canoga Park, California 91304	3
Rohm and Haas Company Redstone Arsenal Research Division ATTN: Librarian Huntsville, Alabama 35808	1
TRW Systems ATTN: STL Tech. Lib. Doc. Acquisitions One Space Park Redondo Beach, California 90200	2
Texaco Experiment Incorporated ATTN: Librarian P. O. Box 1-T Richmond, Virginia 23202	1
Thiokol Chemical Corporation Alpha Division, Huntsville Plant ATTN: Technical Director Huntsville, Alabama 35800	2
Thiokol Chemical Corporation Elkton Division ATTN: Librarian Elkton, Maryland 21921	1
Thiokol Chemical Corporation Reaction Motors Division ATTN: Librarian Denville, New Jersey 07834	1
Thiokol Chemical Corporation Wasatch Division ATTN: Librarian Section P. O. Box 524 Brigham City, Utah 84302	2
Thompson Ramo Wooldridge ATTN: Librarian 2355 Euclid Avenue Cleveland, Ohio 44117	2
Union Carbide Corporation Plastics Co. Division ATTN: Librarian 1 River Road Bound Brook, New Jersey 08805	1

DISTRIBUTION LIST (Cont)

Organization	Copies
Los Alamos Scientific Laboratory University of California P. O. Box 1663 Los Alamos, New Mexico 87544	1
University of Utah College of Engineering ATTN: Professor M. L. Williams 1400 E. Second South Salt Lake City, Utah 84112	1
Defense Metals Information Center Battelle Memorial Institute 505 King Avenue Columbus, Ohio 43201	1
Commanding Officer Picatinny Arsenal Liquid Rocket Propulsion Laboratory ATTN: Technical Library Dover, New Jersey 07801	1

Unclassified
Security Classification

DOCUMENT CONTROL DATA - R&D

(Security classification of title, body of abstract and indexing annotation must be entered when the overall report is classified)

1 ORIGINATING ACTIVITY (Corporate author)
Thiokol Chemical Corporation
Wasatch Division
Brigham City, Utah 84302

2a REPORT SECURITY CLASSIFICATION
Confidential

2b GROUP
IV

3 REPORT TITLE
Final Report
156 Inch Fiberglass Case LITVC Motor Program (U)

4 DESCRIPTIVE NOTES (Type of report and inclusive dates)
Final Technical Report 15 May 1965 thru 30 November 1966

5 AUTHOR(S) (Last name, first name, initial)
Kennedy, Carver G.

6 REPORT DATE	7a. TOTAL NO. OF PAGES	7b. NO. OF REFS
January 1967	1385	66

8a CONTRACT OR GRANT NO.	9a. ORIGINATOR'S REPORT NUMBER(S)
AF 04(695)-773	
b PROJECT NO. PR65-SSD-492	11000-167
c	9b. OTHER REPORT NO(S) (Any other numbers that may be assigned this report)
d	AFRPL-TR-66-331

10 AVAILABILITY/LIMITATION NOTICES IN ADDITION TO SECURITY REQUIREMENTS WHICH MUST BE MET, THIS DOCUMENT IS SUBJECT TO SPECIAL EXPORT CONTROLS AND EACH TRANSMITTAL TO FOREIGN GOVERNMENTS OR FOREIGN NATIONALS MAY BE MADE ONLY WITH PRIOR APPROVAL OF AFRPL (RPPR/STINFO) EDWARDS, CALIFORNIA 93523. FOREIGN ANNOUNCEMENT AND DISSEMINATION OF THIS REPORT BY ODC IS NOT AUTHORIZED.

11 SUPPLEMENTARY NOTES	12. SPONSORING MILITARY ACTIVITY
N/A	Space Systems Division, AFSC Los Angeles Air Force Station, AF Unit P.O. Los Angeles, California 90045

13 ABSTRACT

The 156 in. diameter case LITVC motor program was conducted by the Wasatch Division, Thiokol Chemical Corporation for the Air Force Space Systems Division with technical direction by the Air Force Rocket Propulsion Laboratory. The two major objectives were (1) the design and fabrication of a flightweight 156 in. diameter monolithic solid propellant motor utilizing a fiberglass reinforced plastic monolithic case, a 34 to 1 expansion ratio submerged fixed nozzle, and a N_2O_4 LITVC system; and (2) the demonstration static test of the motor in a simulated altitude environment to provide meaningful LITVC data in a high expansion ratio nozzle. Both objectives were successfully attained. The program was culminated on 13 May 1966 with a static test of the motor utilizing a 10 ft diameter by 82 ft long diffuser for altitude simulation. The motor had a mass fraction in excess of 0.90 and operated for 110 sec at an average thrust level of approximately 325,000 lb. The static test was successful and all motor components were intact and in good condition at the completion of the firing. Two abnormalities occurred during the firing. At approximately 70 sec, a burnthrough occurred in the diffuser tube approximately four feet aft of the nozzle exit plane, apparently due to high localized erosion of the ablative insulation on the inside diameter. The diffuser continued to operate throughout the test although at a lower simulated altitude. A malfunction of the pressure regulating subsystem portion of the LITVC system caused a degradation of injectant pressure during the firing and subsequent degradation of the LITVC performance. Post-test inspection of the motor and components revealed that internal insulation, nozzle design, and case design were satisfactory and the motor had functioned as expected. The static test demonstrated attainment of all program objectives. After post-test analysis of the fired motor and components, the fired case was hydroburst tested to obtain additional data on fiberglass case design. The case burst at 963 psig, very near the design ultimate pressure of 970 psig. This hydroburst, performed under a supplemental agreement to the contract, demonstrated the validity of the design and fabrication techniques used for this case.(U)

DD FORM 1 JAN 64 1473

Unclassified
Security Classification

14 KEY WORDS	LINK A		LINK B		LINK C	
	ROLE	WT	ROLE	WT	ROLE	WT
NONE						

INSTRUCTIONS

1. ORIGINATING ACTIVITY: Enter the name and address of the contractor, subcontractor, grantee, Department of Defense activity or other organization *(corporate author)* issuing the report.

2a. REPORT SECURITY CLASSIFICATION: Enter the overall security classification of the report. Indicate whether "Restricted Data" is included. Marking is to be in accordance with appropriate security regulations.

2b. GROUP: Automatic downgrading is specified in DoD Directive 5200.10 and Armed Forces Industrial Manual. Enter the group number. Also, when applicable, show that optional markings have been used for Group 3 and Group 4 as authorized.

3. REPORT TITLE: Enter the complete report title in all capital letters. Titles in all cases should be unclassified. If a meaningful title cannot be selected without classification, show title classification in all capitals in parenthesis immediately following the title.

4. DESCRIPTIVE NOTES: If appropriate, enter the type of report, e.g., interim, progress, summary, annual, or final. Give the inclusive dates when a specific reporting period is covered.

5. AUTHOR(S): Enter the name(s) of author(s) as shown on or in the report. Enter last name, first name, middle initial. If military, show rank and branch of service. The name of the principal author is an absolute minimum requirement.

6. REPORT DATE: Enter the date of the report as day, month, year; or month, year. If more than one date appears on the report, use date of publication.

7a. TOTAL NUMBER OF PAGES: The total page count should follow normal pagination procedures, i.e., enter the number of pages containing information.

7b. NUMBER OF REFERENCES: Enter the total number of references cited in the report.

8a. CONTRACT OR GRANT NUMBER: If appropriate, enter the applicable number of the contract or grant under which the report was written.

8b, 8c, & 8d. PROJECT NUMBER: Enter the appropriate military department identification, such as project number, subproject number, system numbers, task number, etc.

9a. ORIGINATOR'S REPORT NUMBER(S): Enter the official report number by which the document will be identified and controlled by the originating activity. This number must be unique to this report.

9b. OTHER REPORT NUMBER(S): If the report has been assigned any other report numbers *(either by the originator or by the sponsor)*, also enter this number(s).

10. AVAILABILITY/LIMITATION NOTICES: Enter any limitations on further dissemination of the report, other than those imposed by security classification, using standard statements such as:

(1) "Qualified requesters may obtain copies of this report from DDC."

(2) "Foreign announcement and dissemination of this report by DDC is not authorized."

(3) "U. S. Government agencies may obtain copies of this report directly from DDC. Other qualified DDC users shall request through _____."

(4) "U. S. military agencies may obtain copies of this report directly from DDC. Other qualified users shall request through _____."

(5) "All distribution of this report is controlled. Qualified DDC users shall request through _____."

If the report has been furnished to the Office of Technical Services, Department of Commerce, for sale to the public, indicate this fact and enter the price, if known.

11. SUPPLEMENTARY NOTES: Use for additional explanatory notes.

12. SPONSORING MILITARY ACTIVITY: Enter the name of the departmental project office or laboratory sponsoring *(paying for)* the research and development. Include address.

13. ABSTRACT: Enter an abstract giving a brief and factual summary of the document indicative of the report, even though it may also appear elsewhere in the body of the technical report. If additional space is required, a continuation sheet shall be attached.

It is highly desirable that the abstract of classified reports be unclassified. Each paragraph of the abstract shall end with an indication of the military security classification of the information in the paragraph, represented as *(TS), (S), (C), or (U)*.

There is no limitation on the length of the abstract. However, the suggested length is from 150 to 225 words.

14. KEY WORDS: Key words are technically meaningful terms or short phrases that characterize a report and may be used as index entries for cataloging the report. Key words must be selected so that no security classification is required. Identifiers, such as equipment model designation, trade name, military project code name, geographic location, may be used as key words but will be followed by an indication of technical context. The assignment of links, rules, and weights is optional.